Antascomicin B stabilizes FK506-binding protein 51-kinase protein complexes as a molecular glue

TECHNISCHE UNIVERSITÄT DARMSTADT

Antascomicin B stabilisiert
FKBP51-Kinase Protein Komplexe
als molekularer Kleber

Vom Fachbereich Chemie
der Technischen Universität Darmstadt

zur Erlangung des Grades
Doctor rerum naturalium (Dr. rer. nat.)

Genehmigte Dissertation von
Sabine Claudia Schäfer, M. Sc.
aus Bad Hersfeld

Erstgutachter: Prof. Dr. Felix Hausch
Zweitgutachter: Prof. Dr. Katja Schmitz

Darmstadt 2024

Schäfer, Sabine Claudia: Antascomicin B stabilizes FK506-binding protein 51-kinase protein complexes as a molecular glue
Darmstadt, Technische Universität Darmstadt
Jahr der Veröffentlichtung der Dissertation auf Tuprints: 2024
Tag der mündlichen Prüfung 12.03.2024

Tag der Einreichung: 25.01.2024

Tag der mündlichen Prüfung: 12.03.2024

Erklärung laut Promotionsordnung

§8 Abs. 1 lit. c PromO

Ich versichere hiermit, dass die elektronische Version meiner Dissertation mit der schriftlichen Version übereinstimmt und für die Durchführung des Promotionsverfahren vorliegt.

§8 Abs. 1 lit. d PromO

Ich versichere hiermit, dass zu einem vorherigen Zeitpunkt noch keine Promotion versucht wurde und zu keinem früheren Zeitpunkt an einer in- oder ausländischen Hochschule eingereicht wurde. In diesem Fall sind nähere Angaben über Zeitpunkt, Hochschule, Dissertationsthema und Ergebnis dieses Versuchs mitzuteilen.

§9 Abs. 1 PromO

Ich versichere hiermit, dass die vorliegende Dissertation selbstständig und nur unter der Verwendung der angegebenen Quellen verfasst wurde.

§9 Abs. 2 PromO

Die Arbeit hat bisher noch nicht zu Prüfungszwecken gedient.

Darmstadt, den 25.01.2024

Sabine Claudia Schäfer

Table of Contents

1 Abstract

Rapamycin and FK506 are natural products with a highly conserved macrolide structure and a pipecolate moiety allowing them to interact with the PPIase domain of FK506-binding proteins (FKBPs). This leads to a chemically induced dimerization of the FKBP:glue complex with either the mammalian target of Rapamycin (mTOR) or the calcineurin phosphatase B (CaN) resulting in an inhibition of genes involved in the immune response. These molecular glues were found serendipitously. In biochemical assays, other natural products like Antascomicin B, Meridamycin and 3-Normeridamycin were found to bind to the PPIase domain of FKBP12 by a highly conserved pipecolate core in the same nanomolar range as Rapamycin and FK506. Compared to Rapamycin and FK506, Antascomicin B showed no immunosuppressive effects. As no ternary complex formation of Antascomicin B and a protein of interest is described far, the natural product can therefore be referred for as 'orphan' molecular glue.

To create a reliable method for the investigation of potential target proteins of Antascomicin B an affinity chromatography approach utilizing covalent immobilized FKBP12 or FKBP51 FK1 was applied. While recombinant FKBPs and GST-FRB were complexed upon Rapamycin, no endogenous level of mTOR was identified when HEK293T cell lysate was utilized. When HEK293T cells were transfected with FKBPs containing a FLAG tag and treated with Rapamycin, mTOR was visualized after co-immunoprecipitation indicating, that an *in-cell* approach is suitable for the detection potential protein-protein interactions. Therefore, the unnatural photo-crosslinker 4-*para*-benzoyl-phenylalanine (pBpa) was introduced by amber suppression in FKBP51 and FKBP12 mutants. When HEK293T cells were treated with Antascomicin B, incorporation of pBpa at positions K52 and P120 were found to enhance a photo-crosslink at 120/125 kDa. Further investigation *via* mass spectrometry and western blot supported the hypothesis, that Antascomicin B promotes the interaction of FKBP51 and Akt1. Additionally, the checkpoint kinase 1 (Chk1) was identified after MS. Utilizing Akt1 constructs mimicking the active and inactive conformation on Thr308 and Ser473 of the kinase had no influence on the ternary complex formation of $FKBP51^{K52pBpa}$ or $FKBP51^{P120pBpa}$ after treatment with Antascomicin B and UV irradiation.

When studying the smaller homolog FKBP12 by in-cell photo-crosslinking a prominent 35 kDa photo-crosslink was observed upon treatment with Rapamycin. Rapamycin was found to induce the ternary complex between FKBP12 mutants and mTOR, while no photo-crosslinks were observed. In addition, Rapamycin induced a ternary complex between overexpressed pBpa containing FKBP12 mutants and the overexpressed FRB domain of mTOR as observed by Rapamycin induced photo-crosslinks. Collectively, the results suggest site-specific in-cell photo-crosslinking as a new method to investigate molecular glues.

2 Zusammenfassung

Rapamycin und FK506 sind Naturstoffe, die eine hoch konservierte Macrolidstruktur und einen Pipecolat-Kern besitzen, die es Ihnen ermöglichen, mit der PPIase-Domäne von FK506-bindenden Proteinen (FKBPs) zu interagieren. In einem ersten Schritt führt das zu einer chemisch induzierten Dimerisierung des FKBP:glue Komplexes mit entweder dem mammalian target of Rapamycin (mTOR) oder der Phosphatase Calcineurin (CaN). Diese werden dadurch inhibiert was die Immunantwort supprimiert. Diese molekularen Kleber werden zufällig entdeckt. In pulldown assays wurden andere Naturstoffe wie Antascomicin B, Meridamycin und 3-Normeridamycin identifiziert, die durch ihren hoch konservierten Pipecolat-Kern an die PPIase-Domäne von FKBP12 in derselben nanomolaren Reichweite wie Rapamycin und FK506 binden. Antascomicin B zeigte im Vergleich zu Rapamycin und FK506 keine Immunsupprimierenden Eigenschaften. Bisher wurde keine ternäre Komplex Formation von Antascomicin B mit einem Protein von Interesse beschrieben, weshalb sich der Naturstoff auch als ‚orphan' molecular glue bezeichnen lässt.

Um eine zuverlässige Methode für die Entdeckung von potenziellen ternären Zielproteinen von Antascomicin B zu entwickeln, wurde eine Affinitätschromatographie mittels immobilisiertem FKBP12 oder FKBP51 FK1 angewendet. Während die rekombinanten FKBPs mit Rapamycin und GST-FRB einen Komplex bildeten, wurde nach Anwendung in HEK293T-Lysaten keine endogene mTOR-Kinase nachgewiesen. Wenn HEK293T Zellen mit FKBPs mit zusätzlichem FLAG tag transfiziert und mit Rapamycin behandelt wurden, konnte mTOR nach einem Affinitäts Pulldown nachgewiesen werden. Dies führte dem Schluss, dass ein in-cell Ansatz für die Detektion von potenziellen Protein-Protein Interaktionen geeigneter ist. Die unnatürliche Aminosäure 4-*para*-benzoyl-phenylalanine (pBpa) wurde als Photo-crosslinker mittels „amber suppression" in FKBP51- and FKBP12-Mutanten eingeführt. Der Einbau von pBpa an Positionen K52 und P120 in FKBP51 führte nach Transfektion in HEK293T Zellen und Behandlung mit Antascomicin B und UV-Licht zu einer Verstärkung eines Photo-Crosslinks mit einem molekularen Gewicht von 120/125 kDa. Weitere Untersuchungen mittels Massenspektrometrie und Western Blot unterstrichen die Hypothese, dass Antascomicin B die Interaktion von FKBP51 und Akt1 unterstützt. Zusätzlich wurde in der Massenspektrometrie die Checkpoint Kinase 1 (Chk1) als potenzieller Interaktionspartner identifiziert. Die Stabilisierung der aktiven und inaktiven Konformation an den Positionen Thr308 und Ser473 mittels Akt1-Konstrukten hatte keinen Einfluss auf die ternäre Komplexbildung von Antascomicin B und FKBP51^{K52pBpa} oder FKBP51^{P120pBPa} nach UV-Bestrahlung.

Als das kleinere homolog FKBP12 durch ortsspezifische in-cell photo-crosslinking untersucht wurde, zeigte sich nach Behandlung mit Rapamycin und UV-Bestrahlung ein starker Photo-Crosslink bei 35 kDa. Photo-Crosslinks, die die ternäre Komplex Formation von FKBP12:Rapamycin:mTOR zeigten, wurden

nicht gefunden, obwohl die FKBP12-Mutanten einen ternären Komplex imitierten. Jedoch konnte die überexprimierte FRB-Domäne von mTOR nach Behandlung mit Rapamycin und UV-Bestrahlung in co-transfizierten HEK293T Zellen durch Photo-Crosslinking quervernetzt werden. Zusammengenommen zeigen die Daten, dass ortsspezifisches Photo-Crosslinking in lebenden Zellen eine geeignete Methode ist, um molekulare Kleber zu untersuchen.

3 Introduction

3.1 The FK506-binding protein family and their versatile biological functions

FK506-binding proteins (FKBPs) are a highly conserved immunophilin family in eukaryotes and named after their molecular weight [1]. The archetype FKBP12 was discovered in the early 90's with a protein sequence of 108 amino acids, which is the minimal sequence for the Peptidyl-Prolyl Isomerase (PPIase) domain of FKBPs [2; 3]. The PPIase (FK1) domain consists of a central α-helix, which wraps around an antiparallel five-stranded β-sheet [4; 5]. The closest homolog to FKBP12 is FKBP12.6 displaying 83 % sequence identity [6]. These two FKBPs only possesses the PPIase domain, which accelerates the conformational change between *cis* and *trans* of Xaa-Pro bonds (**Figure 1**) [7]. The majority (~ 99.7 %) of peptide bonds found in proteins are in *trans* conformation which is energetically advantageous [8; 9]. Only up to 6 % of all Xaa-Pro peptide bonds are in *cis* conformation. The PPIase domain of FKBPs stabilizes the transition state by hydrogen bonds facilitating out-of-plane conformational isomerization of Xaa-Pro bonds [10; 11].

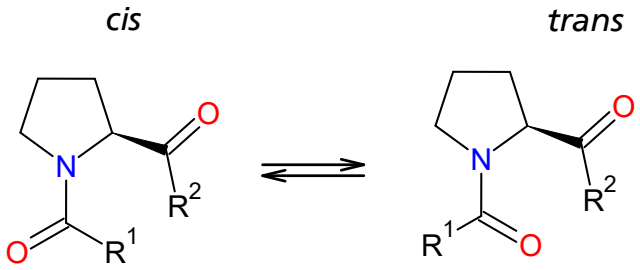

Figure 1: The PPIase domain of FK506-binding proteins possesses Peptidyl-Prolyl-Isomerase activity, which converts Xaa-Pro bonds from *cis* to *trans* conformation. The N-terminus of proline is described as R^1 while the C-terminus is described as R^2.

Besides their function as PPIase, some FKBPs are also acting as chaperones in protein folding of non-native proteins preventing unwanted inter- or intramolecular interactions monitoring the partitioning between the productive and unproductive folding steps [11; 12]. Often, the activity of chaperoning is not influenced upon binding of FKBP ligands like FK506 or Rapamycin, indicating that the PPIase domain is not involved in protein folding [11]. To date, 18 FKBPs were identified in humans while plants like *Arabidopsis*, *Chlamydomonas* or *Oryza sativa* (rice) have 23 to 29 FKBPs [13–15]. Unlike FKBP12 and FKBP12.6, larger FKBPs contain additional functional domains. FKBP51 and FKBP52 possesses tetratricopeptide (TPR) domains, while FKBP38 and FKBP19 additionally contain a Ca^{2+}/calmodulin binding domain (CaM) for a transmembrane domain. Other FKBPs possesses an EF-hand (endoplasmic reticulum), ER targeting and retention motif (**Figure 2**) [16–18]. A single TPR unit possesses two consecutive α-helices of 12-15 residues which, cross each other by an angle of ~ 20°. The putative CaM binding site is an additional seventh helix of FKBP38, FKBP51 and FKBP52 [19–21].

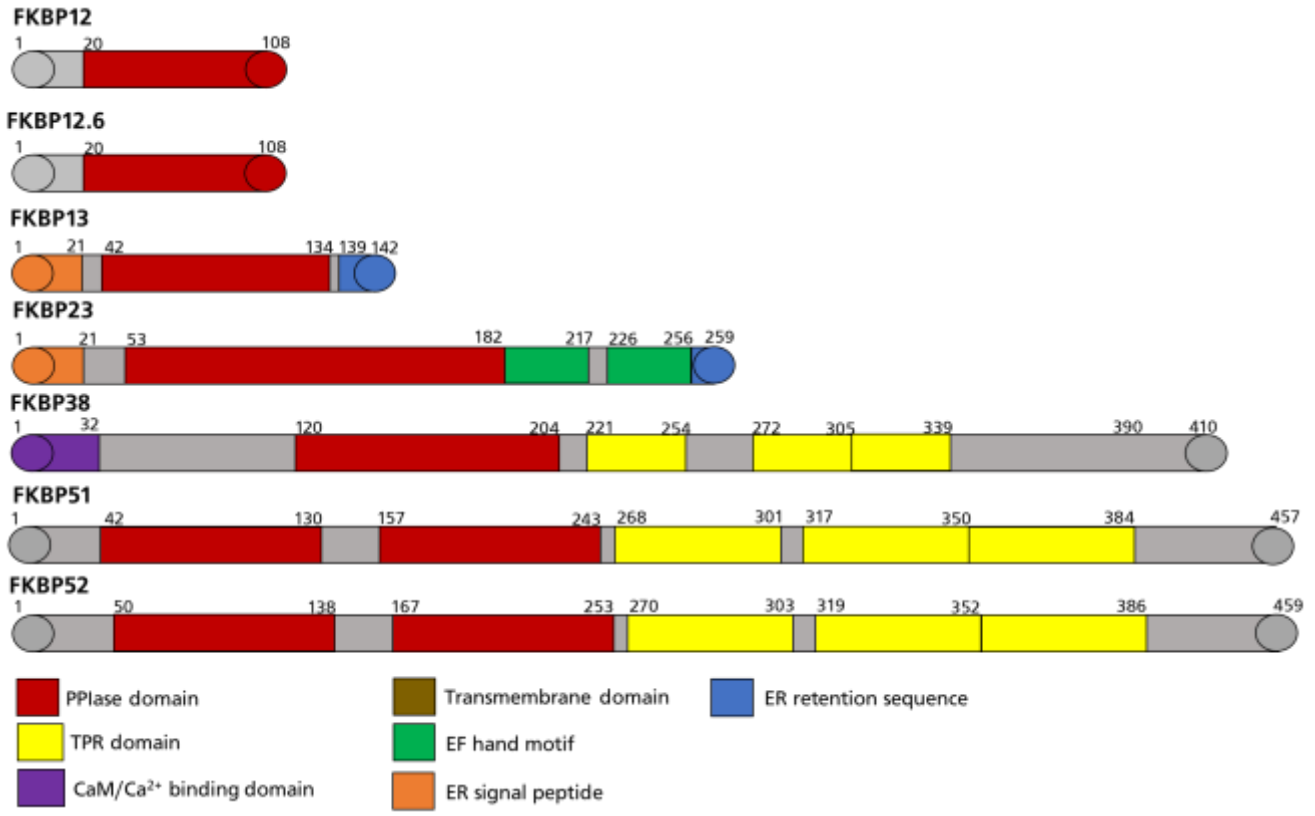

Figure 2: FKBPs often possesses domains in addition to the PPIase (FK1) domain. While FKBP12 and FKBP12.6 only possesses the FK1 domain, large FKBPs like FKBP38, FKBP51 and FKBP52 possess additional TPR domains and CaM binding sites. Figure adapted from Tong & Jiang [16].

3.1.1 FKBP12 and FKBP12.6 – small, but important

FKBP12 is a 12 kDa cytosolic protein which is abundantly expressed in all tissues, it possesses a PPIase (FK1) domain. The protein was identified as an immunophilin targeted by FK506 (Kd 0.4 nM) and Rapamycin (Kd 0.2 nM), which inhibit its PPIase activity [3; 2; 22]. The inhibition of the FK1 domain does not contribute to the immunosuppressive activity as Rapamycin and FK506 chemically induce dimerization of FKBP12 and its target proteins calcineurin (CaN) or the mechanical target of Rapamycin (mTOR) [23–26]. Besides the role as immunophilin, FKBP12 associates with the skeletal muscle ryanodine receptors (RyRs), which are the major Ca^{2+} release channels of the sarcoplasmic reticulum [27–31]. While FKBP12 selectively was report to bind to RyR1 in skeletal muscle, FKBP12.6 binds to the RyR2 in cardiac muscle cells [32; 33]. By binding four FKBP12 proteins, the tetrameric receptors mediate Ca^{2+} release into the cytoplasm during muscle contraction. Upon treatment with FK506 or Rapamycin the channels were found to be 'leaky' as FKBP12 is displaced from the receptors and consequently depletion of Ca^{2+} leads to reduction in muscle contractility [16; 34]. Moreover, FKBP12 was reported to interact with the inositol-1,4,5-triphosphate receptors (IP_3R) of the endoplasmic reticulum, which are structurally and functionally related to RyRs [35; 36]. The mechanism of action upon Rapamycin and FK506 is thought to be similar to RyRs.

Additionally, FKBP12 interacts with type I receptor for transforming growth factor-β (TGF-β) serving as a natural ligand by binding to a glycine- and serine-rich (GS) domain of ligand-free TGF-βR1. The interaction blocks phosphorylation of TGF-βR2, which keeps the receptor in an inactive state this can be reversed by Rapamycin and FK506 [37; 38]. The most validated subgroup of the TGF-β-family type I receptors is the bone morphogenic protein (BMP) type I receptor activin-like kinase 2 (ALK2) [39; 40]. In multiple myeloma cancer of the bone marrow, BMP type I receptors ALK2 and ALK3 can induce growth arrest and apoptosis *in-vitro* [41–43]. As FKBP12 competes the activation of type I receptors with type II receptors, the presence of FK506 leads to ligand-induced SMAD-activation and apoptosis in multiple myeloma cells, as FKBP12 is sequestered by FK506 [43; 44]. The ALK3 ligands BMP2, BMP4 and BMP10 did not induce apoptosis but gained activity in ALK2 induced apoptosis when FK506 was present, indicating that FK506 can switch a non-signalling complex (NSC) into an active complex in myeloma cells [45].

FKBP12 was reported to associate with the Tau protein and the intracellular domain of the Amyloid Precursor protein (APP) in Alzheimer's disease [46; 47]. The microtubule-associated protein tau is a major constituent of the intracellular neurofibrillary tangles that are a pathological hallmark of Alzheimer's disease [48]. The PPIase activity of FKBP12 and Pin1 has been implicated in regulating tau misfolding [49]. FKBP12 does not require a specific phosphorylation state or hyperactivation of tau for its oligomerization [47; 50–52]. While the smallest member of the FKBP family is involved in tau aggregation, FKBP51 and FKBP52 were found to regulate the turnover of the native proteins, while affecting the levels of tau in neurons [53; 54].

3.1.2 FKBP51 and FKBP52 – antagonists in the regulation of steroid receptors

FKBP51 (51 kDa) and **FKBP52** (52 kDa) were first identified as subunits of the Hsp90-progesterone complex and later intensively studied in context with androgen (AR), glucocorticoid (GR), estrogen and mineralocorticoid receptors [55; 56]. FKBP51 is an antagonist to FKBP52 on steroid hormone receptor (SHR) signalling displaying 60 % sequence homology (48 % sequence homology of the FK1 domain) [19; 57]. Both proteins possesses a Ca^{2+}/CaM binding motif and three C-terminal TPR domains, which bind to Hsp90 [19; 58]. The PPIase active site (FK1) domain of both FKBPs bind to FK506 and Rapamycin, while an additional FK2 domain possesses no enzymatic activity and neither binds the natural products [19; 59; 58]. FKBP51 acts as a negative regulator on receptor transcriptional activity of the glucocorticoid receptor (GR) compared to FKBP52, but it was found that the PPIase is required for optimal androgen receptor activity [56; 60–63]. In contrast, FKBP52 positively stimulates glucocorticoid, progesterone, and androgen receptors but not estrogen and mineralocorticoid receptors [64–66]. Interestingly, androgen receptors regulate the expression of FKBP51, which induces a positive

feedback loop that might lead to prostate cancer development [60; 67; 68]. The mode of action of FKBP51 and FKBP52 in AR signalling is still elusive as it was demonstrated that both FKBPs can promote AR activation upon dimerization but have no influence on AR level or localization. Overexpression of PPIase-dead FKBP52 to compensate FKBP52 knock out led to the hypothesis, that the PPIase domain of FKBP51 but not FKBP52 leads to AR activation [69].

The best characterized properties of both PPIases are their function as co-chaperones of the heat-shock protein 90 (Hsp90) [70; 71]. In general, maturation and activation of SHRs is conducted by the Hsp90 chaperone machinery. SHRs like the GR reside in the cytosol in complex with Hsp90 while steroid binding triggers conformational changes exposing nuclear localization signals and attachment of cofactors resulting in SHRs acting as transcription factors [72; 73]. FKBP52 acts as positive regulator on the GR which, has been associated with the recruitment of dynein as well as increased nuclear translocation of the GR [56; 74; 75]. While both FKBPs have a fold similar fold, the orientation of the FK1 and FK2 domain as well as the hinge regions and C-terminal domain may differ (**Figure 3A**) [21; 76].

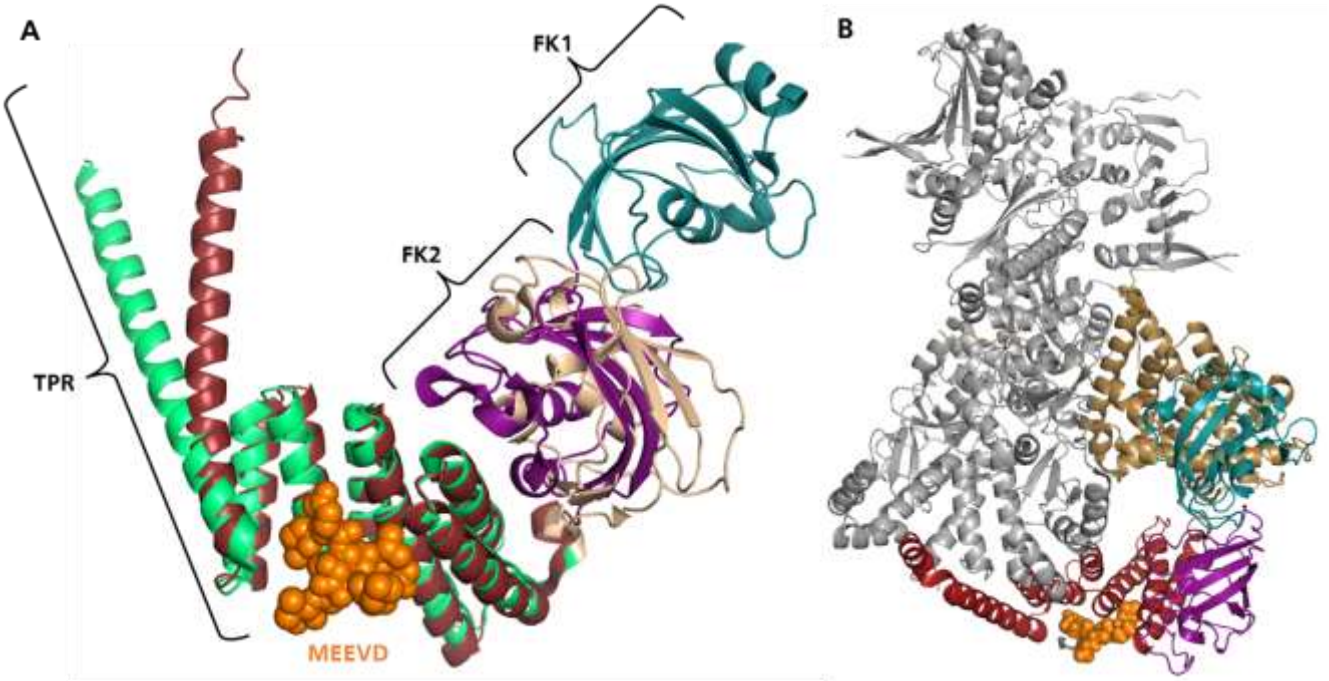

Figure 3: The secondary structure of FKBP51 and FKBP52 (A) The orientation of the domains of FKBP51 (**PDB: 5NJX**) and FKBP52 (**PDB: 1QZ2**) can differ. The FKBP51 FK1 domain is highlighted in marine blue while the FK2 domain is coloured in purple. In contrast, the FK2 domain of FKBP52 (wheat) possess a different orientation. The C-terminal TPR domain of FKBP52 (pale green) distinguishes from the C-terminal TPR domain of FKBP51 (dark red) while both FKBPs are capable to bind to the MEEDV motif of Hsp90 as the six TPR domains are highly conserved upon Hsp90 binding proteins. **(B)** Cryo-EM structure of the closed state of Hsp90 (grey) in complex with FKBP51 (coloured as in A) and the GR (brown) (**PDB: 8FFW**).

The role of FKBP51 on GR activity was first examined in squirrel monkeys indicating that the PPIase domain is not necessary for the inhibitory effect on the GR binding affinity to Hsp90 [77]. The activation and maturation of the GR requires a complex of Hsp90, Hsp70, Hop, Hsp40 and p23 [78; 79]. Corticosteroids increase the expression of FKBP51 indicating that the cortisol response in hormone-conditioned tissues can be diminished by a negative feedback loop mechanism [80–82]. The activation and maturation of the GR is inhibited by FKBP51 during the Hsp90 maturation cycle, and the complex was recently first described in a cryo EM structure (**Figure 3B**) [83]. Utilizing FKBP51 in photo probing with an unnatural amino acid corroborates the structure with the GR in complex with Hsp90 on a molecular level [84]. A direct negative feedback loop is induced upon inhibition of GR by FKBP51, which induces transcription of the *fkbp5* gene [77; 85; 86]. The gene is linked to single nucleotide polymorphisms, which has been associated with an increased recurrence of depressive episodes and improved patient's response to antidepressive medication [87–89]. Moreover, FKBP51 is a major player in depression, post-traumatic stress disorders, diabetes, and chronic pain in endocrine stress responses [90–92]. The mammalian stress response is regulated within the feedback control of the hypothalamus-pituitary-adrenal axis (HPA) [93–95] based on findings that FKBP51$^{-/-}$ mice showed an improved sleep profile [96] and enhanced glucose tolerance and resistance to diet-induced obesity [90; 97]. The number of GR targets was unaffected upon FKBP51 knock out [98]. Additional substrates of FKBP51 emerged within the last decades, reviewed from Hähle *et.* al [99]. Notably, FKBP51 is suggested as safe drug target in several pharmacological studies with SAFit2, a ligand, which co-applied with the antidepressant escitalopram improved stress-coping behaviour [100; 101]. FKBP51 is described as a regulator of the nuclear factor κ-light-chain-enhancer of activated B-cells (NF-κB). The NF-kB transcription factors mediate the innate and adaptive immune response resulting in inflammation and other cellular processes, e.g., proliferation, survival and apoptosis [102–104]. The PPIase was identified as interaction partner of the IKK complex (inhibitor of nuclear factor kappa-B kinase subunits α-γ), by which FKBP51 became an interesting drug target in the treatment of inflammation and cancer [105; 106]. The influence of FKBP51 on the stability of the IKK complex is still a widely discussed field as the effect might be tissue- or cell line-specific [99]. Moreover, FKBP51 is thought to modulate the interaction of the AGC kinase Akt and PH domain and leucine-rich repeat protein phosphatases (PHLPP) [107; 108]. It is thought that the FK1 domain of FKBP51 recruits Akt [109], while the TPR domain is responsible for the interaction with PHLPP [108]. FKBP51 is believed to recruit PHLPP to Akt as a scaffolding protein, which induces dephosphorylation of the kinase resulting in downregulation of downstream targets glycogen synthase kinase 3 beta (GSK3β) and Forkhead box protein O1 (FOXO1). On one hand, a knockout of FKBP51 was found to enhance the phosphorylation of Akt at Ser473 [107; 108; 110]. On the other hand, overexpression of FKBP51 led to enhanced GSK3β phosphorylation in HEK293T cells [111]. Moreover, Beclin1 and ubiquitin-specific peptidase 49 (USP49) are substrates for Akt, which may stabilize the interaction of Akt and FKBP51 [107; 111].

3.2 Molecular glues from nature as chemical inducers of protein-protein complexes

Molecular glues can interact with two protein surfaces, inducing or enhancing the affinity of the proteins. In the early nineties the mode of action of the natural products cyclosporine, Rapamycin and FK506 were first identified. To trigger chemically induced dimerization (CID) of two proteins, the natural products require an accessory protein and a protein-of-interest (POI). By binding to the accessory protein, the protein possesses an enlarged composite binding surface, which allows direct contacts with the POI allowing CID with small molecule drug-inaccessible targets. Immunophilins such as cyclophilins (Cyps) or FK506-binding proteins (FKBPs) can serve as accessory proteins. In 1984, cyclophilin 18 was discovered as the target of cyclosporine A (CsA) [112]. Cyclosporine A was first isolated in an antibiotic screening program [113] and Liu *et.* al discovered that the Cyp18-CsA complex interferes with the Ca^{2+}/calmodulin dependent serine/threonine protein phosphatase calcineurin (CaN) by allosteric inhibition, while transcription of cytokine genes IL-2 and IL-4 were inhibited [114; 115]. While Cyps serve as accessory protein for CsA or Sanglifehrin A (SfA), the natural products Rapamycin, FK506 and ascomycin (FK520) were found to interact with FKBP12 [2; 3]. FK506 and FK520 in complex with FKBP12 allosterically inhibit CaN as the Cyp18-CsA complex. The FKBP12:Rapamycin complex targets the mammalian target of Rapamycin (mTOR) [23–26]. CsA, FK506 and Rapamycin therefore possesses immunosuppressive effects, while so called 'orphan molecular' glues like Antascomicin B, Meridamycin or 3-Normeridamycin were discovered, which do not display immunosuppressive properties (**Figure 4**) [116–118].

CsA is an FDA approved drug (Sandimmune®) for prevention of allograft rejections in humans. Its also effective in human autoimmune diseases like psoriasis, nephrotic syndrome, type I diabetes, and sight-threatening uveitis [119]. FK506 (Tacrolimus®), first isolated from *Streptomyces tsucubaensis* is approved as medication after organ transplantation to prevent allograft rejections and utilized for treatment of inflammatory diseases as psoriasis, contact eczema and hand dermatitis [120]. In the 1970's Rapamycin (Sirolimus or Rapamune®) was isolated from *Streptomyces hygroscopius* and named after the Easter island (Rapa Nui) [121]. The natural product possesses antifungal activity and was found to be effective against transplanted tumours and was found to have immunosuppressive actions [122–125].

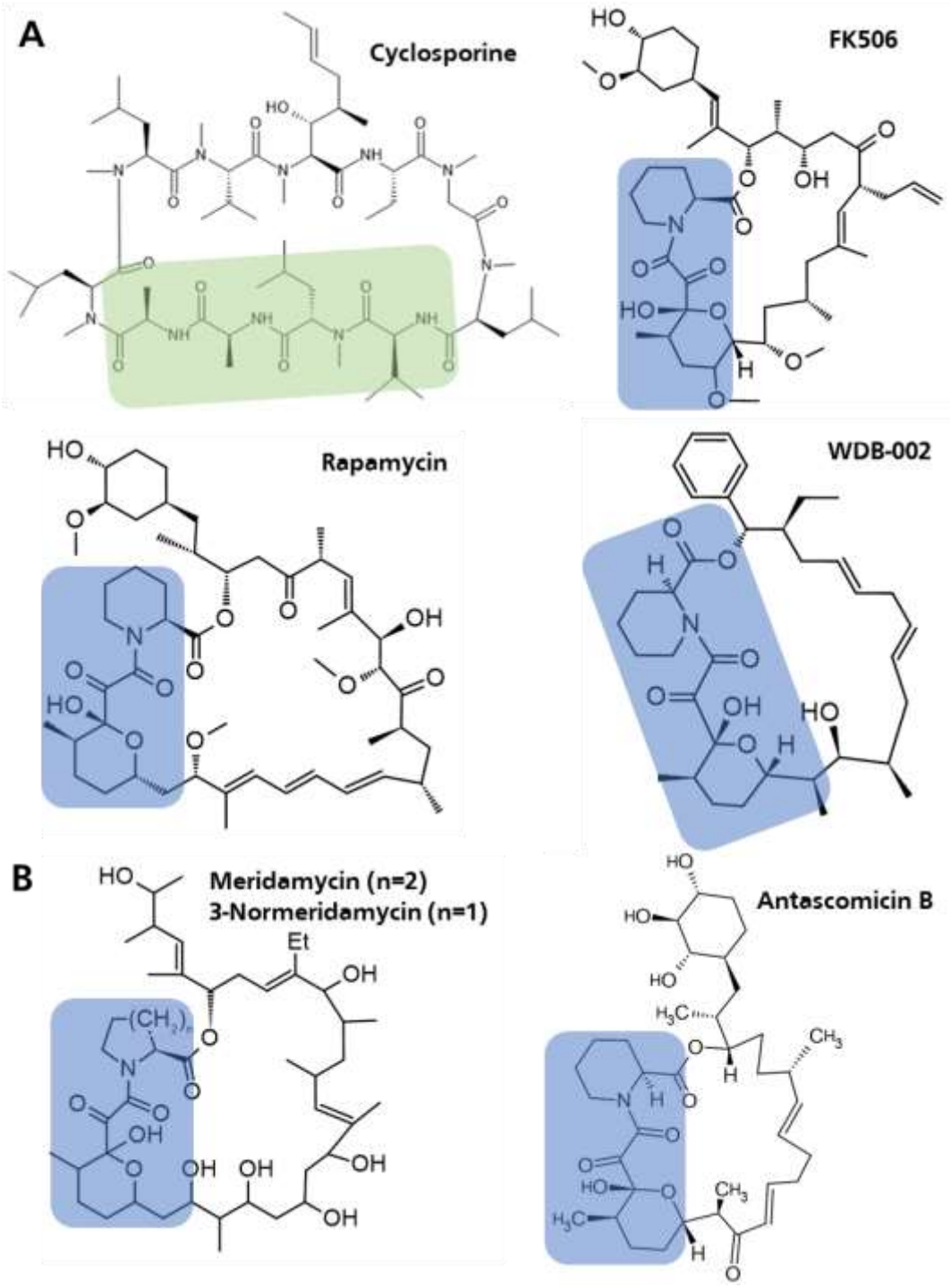

Figure 4: Schematic presentation of natural products which act as a molecular binder for cyclophilins (binding site highlighted in green) and FKBPs (binding site highlighted in blue). (A) identified molecular glues cyclosporine A (target calcineurin), FK506 (target calcineurin), Rapamycin (target mTOR), WDB-002 (target CEP250). **(B)** 'Orphan' molecular glues and 3-Normeridamycin and Antascomicin B are illustrated with no POI known to date.

3.2.1 The immunosuppressants FK506 and Rapamycin can bind to multiple FKBPs

Like CsA, FK506 and its derivate FK520 allosterically inhibit the phosphatase activity of Calcineurin (CaN). First, FK506 or FK520 is interacting with FKBP12, while the complex then binds to CaN forming contacts with two distinct areas on CaN in a similar mechanism of action as CsA-Cyp18 (**Figure 5A**) [23; 24]. In comparison, the interaction of Rapamycin to FKBP12 results in an alternative binding surface of the immunophilin resulting in targeting the FKBP12-Rapamycin-binding domain (FRB) of the mammalian target of Rapamycin, the kinase TOR (mTOR) [126]. The molecular glue binds tightly to FKBP12 while the interaction to FRB is weak. No direct interaction of FKBP12 and FRB could be detected (**Figure 5B**) [127; 128]. mTOR is an atypical serine-threonine kinase (289 kDa) functioning in two distinct signalling complexes, namely mTORC1 and mTORC2. By allosterically blocking the active site of mTOR in mTORC1 the phosphorylation of its substrates p70 S6K and 4E-BP1 is inhibited resulting in a reduced immune response, while mTORC2 is unaffected by Rapamycin [129]. Rapaloga like DL001 or bi-functional Rapamycin-ATP-competitive mTOR kinase inhibitors improve the selectivity to mTORC1 up to 40-fold, while inhibiting 4E-BP1 [130–132]. Recent studies showed that CNS-specific mTORC1 inhibition by RapaLink-1 can reduce alcohol intake in a mouse model, while undesirable periphery-mediated effects could be reduced [133; 134].

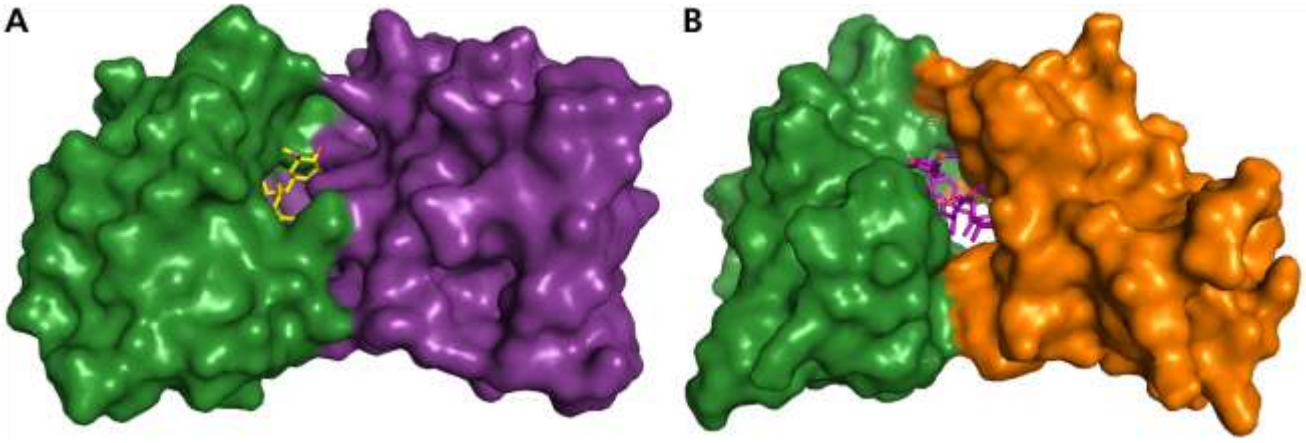

Figure 5: The natural products FK520 and Rapamycin induce ternary complex formation of FKBP12 and either Calcineurin (CaN) or with the FRB domain of the mammalian target of Rapamycin (mTOR). (A) FKBP12 (green) in complex with FK520 (yellow) and Calcineurin subunit B (**PDB: 7U0T**) [135]. **(B)** FKBP12 (green) in complex with Rapamycin (purple) and the FRB domain of mTOR (orange) **(PDB: 1FAP)** [127].

FK506 and Rapamycin can also affect the PPIase (FK1) domain of other FKBPs. The FK1 domain of FKBP51 shares a sequence similarity of 50 % with FKBP12 consisting of a comparable structure of a central α-helix which is surrounded by five antiparallel β-sheets. FK506 interacts with the FK1 domain forming hydrogen bonds to the amino acid residues D68, Q85, I87, and Y113 [76]. The natural compound can weakly inhibit CaN *in vitro* but the relevance is missing [86]. On the level of FKBP51 FK506 is thought to modulate GR binding [63; 136; 137]. While FK506 does not alter Dexamethasone-induced translocation of GRα, the ligand may increase the association of FKBP51 and GRβ in TM

(trabecular meshwork) cells [138]. Rapamycin was found to inhibit the activity of mTOR utilizing numerous FKBPs. This revealed that large FKBP homologs can functionally substitute the effect of FKBP12 to mTOR *in vitro*. The large FKBP51 and FKBP52 were capable to abolish the phosphorylation of the S6K and 4E-BP1. In an *in vitro* kinase assay numerous FKBPs showed an inhibitory effect on mTOR kinase activity. GST-FRB/Rapamycin/EGFP-FKBP complex was determined with an EC_{50} of 3.8 nM for FKBP12 and 25 nM for FKBP51 confirming that larger FKBPs can contribute to the effects of Rapamycin [128; 139]. As FKBP51 is known as a biomarker for tumour progression and target for cancer therapy which is differently expressed among specific cell or tissue types, these findings led to the hypothesis, that natural products may trigger alternative PPIs than their primary role with FKBP12.

3.2.2 'Orphan' molecular glues as potential molecular binders of FKBPs

Next to CsA, FK506 and Rapamycin, the additional natural molecular products Meridamycin [117], 3-Normeridamycin [118] and Antascomicin [116] were discovered in the early 90's as FKBP12-binding compounds (**Figure 4**). Antascomicin and Meridamycin compete the effect of Rapamycin and FK506 on FKBP12, which reversed the immunosuppressive effects of FK506 and Rapamycin [117; 140]. Except Antascomicin D (5~10 times less) all Antascomicins were reported to bind with the same nanomolar affinity to FKBP12 as Rapamycin [116]. The total synthesis of Antascomicin B required 52 steps in total while the stereoselective synthesis of the C22-C34 fragment was studied intensively [141–143]. Meridamycin was isolated from *streptomyces sp.* NRRL 30748 and was utilized as steroid potentiator in the treatment of inflammatory/hyperproliferative skin diseases and anti-infective agent for infectious diseases [144]. While the gene cluster of Meridamycin was revealed by He *et.* al [140] no information on the gene synthesis of Antascomicin is known so far. The natural product was first isolated from a *micromonospora spp.* strain [116]. All 'orphan' molecular glues possesses a conserved pipecolate ester domain and a cyclic hemiketal moiety, which is presumed as FKBP12-binding motif, while the remaining portion of the molecules differs [145]. The chemical synthesis of the natural by-products of bacterial metabolism cannot be easily achieved, while genetic engineering of the entire biosynthetic gene clusters is required to receive higher yields of those molecules [146]. Recently, the centrosomal protein 250 (CEP250) was identified as binding partner of the 'orphan' molecular glue WDB002 in a screening of WarpDrive Bio [147]. CEP250 is linked to Cone-Rod Dystrophy and hearing loss 2 and Usher syndrome. The centrosomal protein is required for centriole-centriole cohesion during the interphase of the cell cycle [148]. The 'deorphanization' of molecular glues and the identification of their binding partners can therefore be a milestone in finding ligands for otherwise undruggable proteins.

3.3 Kinases – highly conserved and key role player in cellular signalling

About 2 % of the human genome encodes the kinome, which is one of the largest superfamilies in humans consisting of 538 kinases [149]. The first kinase and their role in protein phosphorylation in oncogenesis was discovered in 1980 in the Rous sarcoma virus [150]. Kinases catalyse the transfer of the γ-phosphate of ATP to the alcohol groups on Serine (Ser) and Threonine (Thr) of phenolic groups on Tyrosine (Tyr) of proteins generating monoesters [151]. The phosphorylation of proteins is described as molecular switch, which is essential in whole cellular activities such as subcellular localization or interacting with other proteins [152; 153]. Kinases are divided in nine major groups of typical kinases (AGC, CAMK, CK1, CMGC, Other, RGC, STE, TK, TKL) and one group of atypical kinases (**Figure 6**) [151]. In an open source project called 'KinMap' the kinome tree can be represented with the number of entries in the protein data base (PDB) [154]. Green dots represent the amount of pdb entries while red dots represent key targets of approved drugs. CDK2 and p38a share the highest pdb entries while CDK2 is an approved target for kinase inhibitors. In general, the most drug targets were found within the TK (tyrosine kinase) family while no approved drug for Akt and Chk are known up to date (**Figure 6**).

Notably, the majority of the kinases reside in the cytoplasm (50.2 %) which are 229 proteins in total. 16.4 % of kinases reside in the nucleus, while other kinases populate other cellular compartments [151]. Kinases are highly conserved and homologous in their secondary structure. The structure of all kinases is named after the first crystal structure of the protein kinase A (PKA), which was identified 30 years ago [155]. The conserved core of the N-lobe is a five-stranded β-sheet (β1-β5), while the C-lobe contains α-helices. The two domains are connected with a linker of three to five amino acids which form a small β-sheet. The cleft is called the hinge region and ATP as substrate can interfere at the interface between both lobes [155; 156]. The phosphates of the ATP molecule are sandwiched under the Gly-rich loop which connects β1 and β2 while interacting with a conserved Lysine (Lys) residue on β3. Moreover, the phosphates are connected with the C-lobe via a divalent cation, usually Mg^{2+} (**Figure 7**) [157].

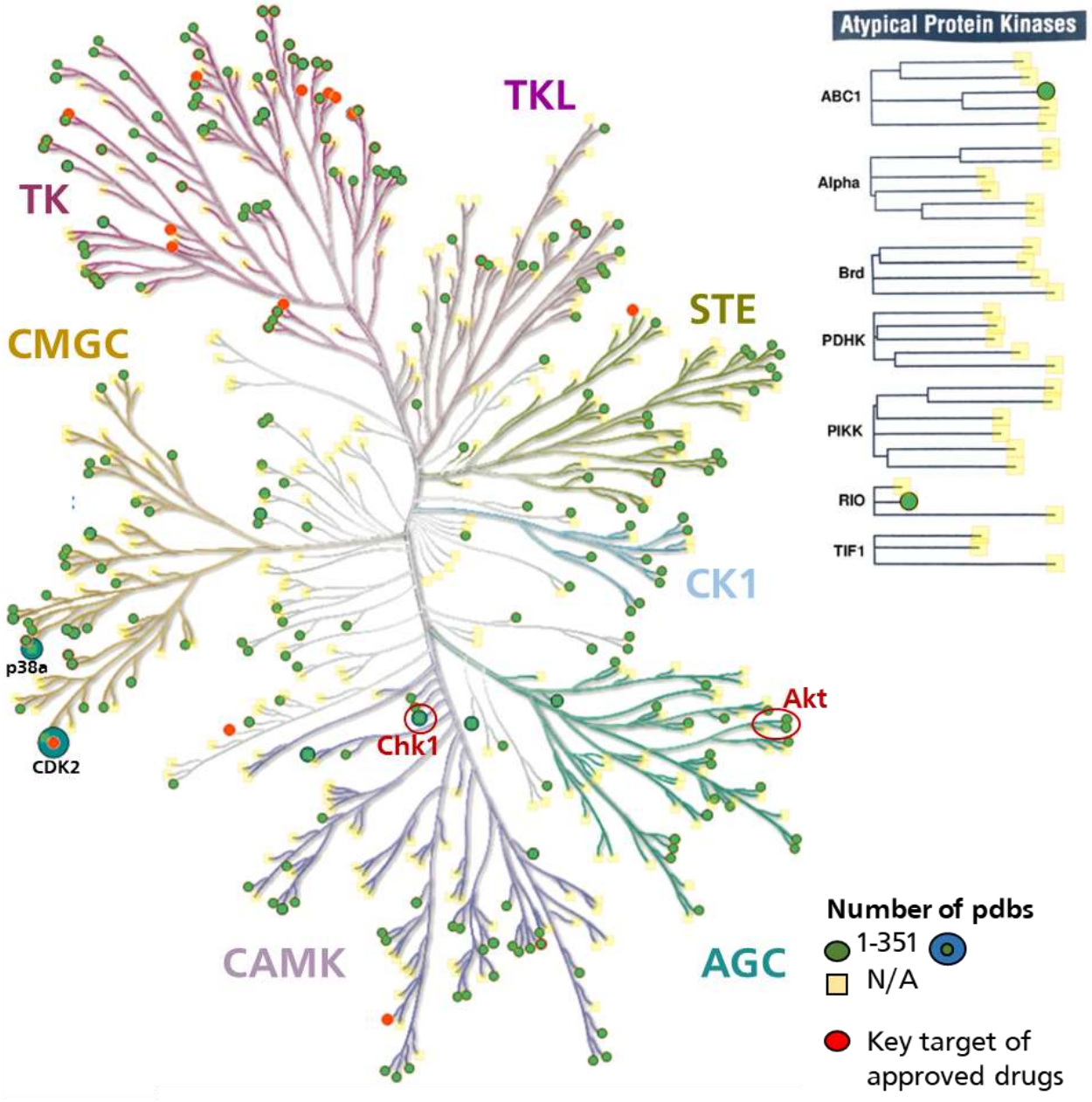

Figure 6: The kinome tree and relationship and homology of the best characterized Kinase superfamilies. Kinome tree of AGC, CAMK, CMGC, CK1, STE, TK and TKL and a subset of atypical kinases with dots representing a kinase and its localization. No pdb entries were observed for kinases represented as yellow square while the amount of pdb entries is highlighted in green. The most established kinases are CDK2 and p38a with up to 351 pdb entries (green dots with blue circles). Moreover, key targets of approved drugs can be identified with the web based 'KinMap'. The most prominent target is CDK2, while the TK family exhibits the most druggable kinases. Akt and Chk are surrounded by a red circle. Figure was prepared utilizing the open source 'KinMap' from Eid *et.* al, [154].

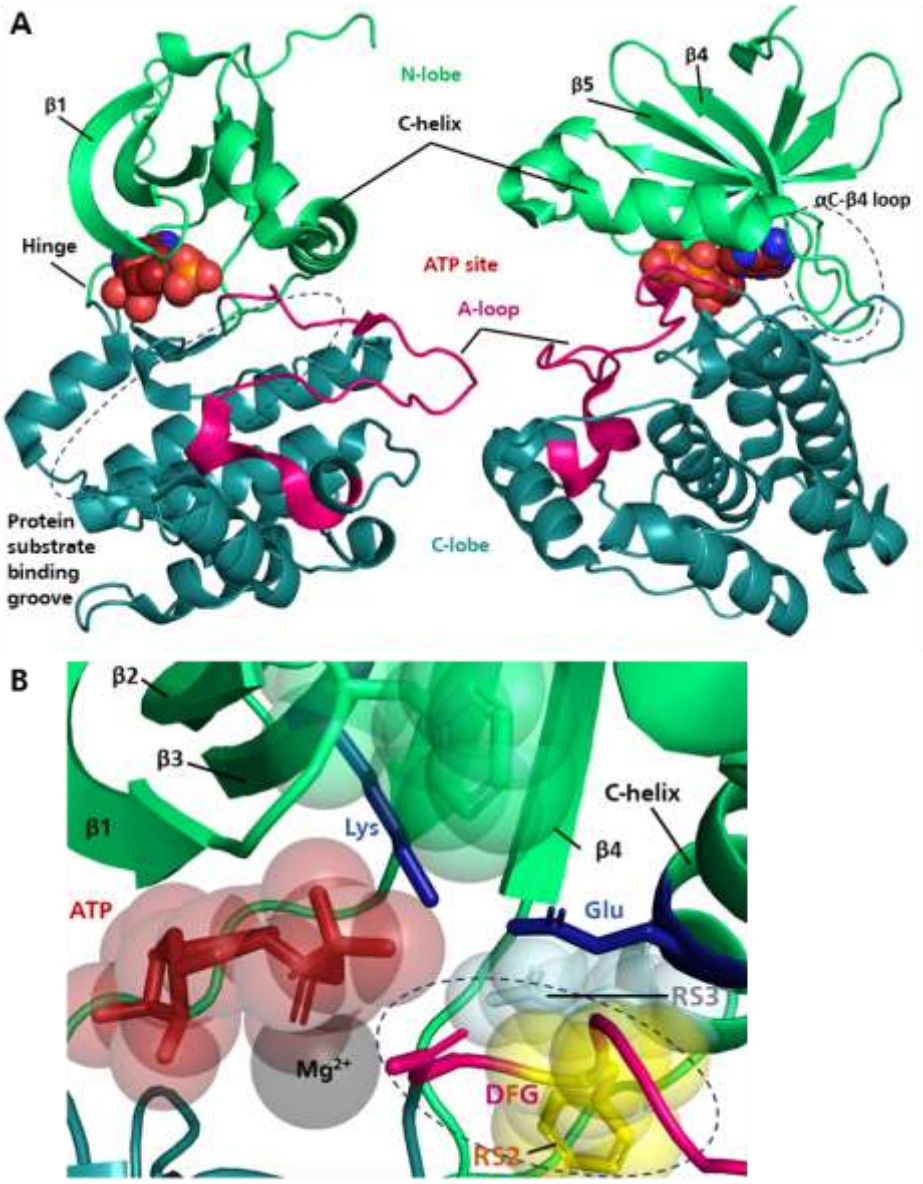

Figure 7: Key structural features of a kinase domain. A) The N-lobe (orange) and C-lobe (green) are connected by the hinge region. The ATP binding site (red) is close to the hinge region. The C-helix and A-loop is a critical regulatory feature. **B)** critical interactions of β3 Lys and Glu residue of the C-helix. The R-spine residue (RS3) and RS2 are crucial contacts at the interface of both lobes. RS2 interferes with the DFG motif located at the A-loop (yellow, activation loop). Figure adapted from Arter *et.* al [157].

The C-helix and the activation loop (A-loop) are critical features for regulation of the kinase activity. The A-loop is involved in recognizing protein substrates forming a groove along the front of the C-lobe. The R-spines possesses hydrophobic characters and together with the catalytic spine (C-spine) both spines form a hydrophobic core connection between both lobes [157]. The stabilization of the activation loop (A-loop) is regulated upon phosphorylation and/or protein-protein interactions resulting in a platform to support the binding of protein substrates [158; 159]. The C-helix drives the allosteric behaviour of protein kinases as it forms a salt bridge with its conserved Glu with the Lys of the β3 sheet in the active state (**Figure 7B**). Moreover, the C-helix directly interacts with the A-loop which is contributed by an

activated phosphate group, while the adenine moiety of ATP interacts with the C-helix [157; 158]. Some kinases like tyrosine kinases possesses a looser attachment of the C-helix in an autoinhibitory inactive state referred as C-helix out/C-helix in mechanism [160]. To reverse the inactive state kinases like the cyclin-dependent kinase 2 (CDK2), they bind Cyclin A resulting in a substantial conformational change. While the A-loop occupies the space between the Lys and Glu in the inactive state, binding of Cyclin A results in the displacement of the A-loop from the active site, while trapped under the C-helix, which possess now the C-helix in state. The displacement is stabilized by a phosphorylation on Thr160 which forms a salt bridge to Arg50 of the C-helix. [157; 161]. Importantly, mutations in the A-loop can cause constitutive kinase activity, which is linked to various cancers, which led to an increasing interest for the role of kinases in cellular signalling and therapeutic invention. The R-spine residues (RS3 and RS4) are interacting with the αC-β4 loop which minimal consist of 8 amino acids. The loop has the conserved sequence motif "Φ-X-H-X-N-Φ-Φ-X" (Φ is hydrophobic, X any amino acid) and is highly ordered, while forming extensive interactions with the C-lobe [162]. In RTKs the αC-β4 loop stabilizes the inactive state forming additional interaction within the loop, which is called a 'molecular brake'. Mutations in the loop result in the disruption of that molecular brake leading to an active state and therefore disease-associated mutations. Moreover, the loop is also involved in the regulation of protein-protein interactions [162; 163]. The tripeptide motif Asp-Phe-Gly (DFG) is located at the N-terminal end of the A-loop and acts as a pivot point for the conformation (**Figure 7B**). This motif regulates the conformation of the A-loop. In the active conformation (DFG-in) and C-in, the Phenylalanine (RS2 residue) is packed against the RS3 residue from the C-helix formatting the central interaction of the R-spine [164]. The Asp-Phe peptide possesses eight distinct conformations resulting in six subclasses of DFG-in, one DFG-out and DFG-inter states. The Asp in the DFG-in conformation is pointing towards the ATP-binding site interacting with the Mg^{2+} while the Phe is pointing into the hydrophobic core of the kinase [157]. The understanding of the dynamics of the kinase motifs can be further utilized in the development of useful kinase inhibitors as only 8 % of the human kinome can be targeted for cancer therapeutic exploration described as Illuminating the Druggable Genome (IDG) [165]. This thesis will focus on kinases of the AGC and CAMK family.

3.3.1 Akt – Member of the AGC kinase superfamily and game changer in cancer and diseases

The AGC kinase family is named after the protein kinase A, G, and C families and is divided into 14 families and 21 subfamilies [149]. There are 63 AGC serine/threonine protein kinases in total with the popular members PDK1, Protein kinase B (PKB/Akt), Serum-glucocorticoid kinase (SGK), p70 S6 kinase (S6K) and the most closely related families of Aurora and PLK kinases. Most of AGC kinases are basophilic, interacting with positively charged amino acids when recognizing their substrate [166]. Akt,

S6K and SGK possesses three isoforms with conserved Threonine and Serine for phosphorylation (**Figure 8**).

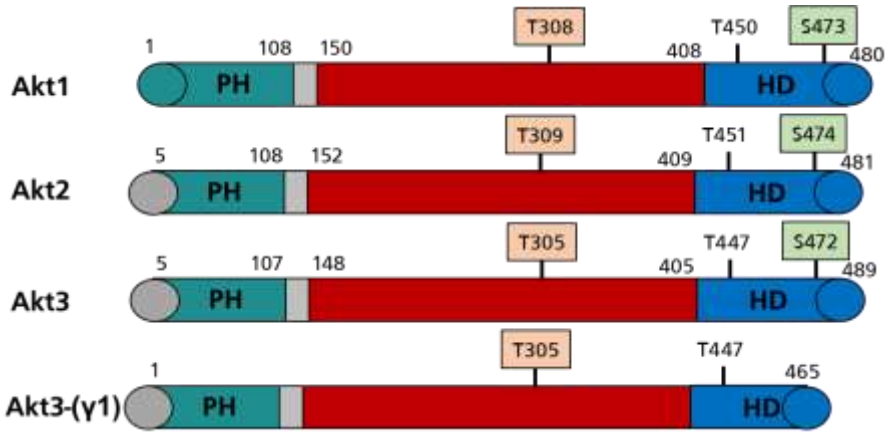

Figure 8: The human Akt isoforms possesses a PH, a kinase, and a hydrophobic domain (HD). Activation of Akt requires phosphorylation at T308 (Akt1), T309 (Akt2) or T305 (Akt3). The alternative splice variant of Akt3 possesses a truncated hydrophobic domain. Each isoforms contains a N-terminal PH domain and a C-terminal hydrophobic domain (HD). The catalytic domain contains S473 (Akt1), S474 (Akt2) or S472 (Akt3), while the truncated version is missing the domain. Hyperactivation of Akt1 is mediated by mTORC2 via phosphorylation on T440 (Akt1), T451 (Akt2) or T447 (Akt3). Figure adapted from [167].

Initially, 3-phosphoinositide-dependent protein kinase-1 (PDK1) phosphorylates and therefore activates Akt1 on Thr308 in the T-loop residue [168]. The hyperactivation of Akt1 requires phosphorylation of Ser473 in the hydrophobic motif [169]. PDK1 and Akt possess a pleckstrin homology (PH) domain, which binds the second messenger of the PI3K (phosphoinositide 3-kinase) PtdIns(3,4,5)P_3. Binding of the second messenger promotes the interaction of both kinases at the plasma membrane, whereas Akt undergo a conformational change which facilitates the phosphorylation on Thr308 by PDK1 [169–173]. The kinases S6K and SGK do not possess a 3-phosphoinositide-binding pleckstrin homology (PH) domain. Their activation is triggered through phosphorylation of their hydrophobic motif by mTORC1 and mTORC2 [174; 175]. Moreover, mTORC2 phosphorylates the hydrophobic motif of Akt [175]. Akt1 is a key regulator of the PI3K/Akt1 signalling pathway controlling cell growth and survival. Notably, it was found that in more than 50 % of human tumours Akt is hyperactivated, which makes the kinase an attractive target for cancer drug therapeutics [176]. The intense studies of Akt activation led to the discovery of negative regulators, namely protein phosphatase 2 (PP2A), phosphatase and tensin homolog (PTEN), and the PH-domain leucine-rich-repeat-containing protein phosphatases (PHLPP1/2) [177]. The activation of Akt is a multistep event which starts with the response to growth factor stimuli like insulin (**Figure 9**). Activated receptor tyrosine kinases (RTKs) initially phosphorylates the PI3K which then phosphorylates the lipid second messenger phosphatidylinositol-4,5-biphosphate (PIP2) triggering conversion in phosphatidylinositol-3,4,5-triphosphate (PIP_3) [176]. Akt1 then interacts with the membrane-anchored PIP3 via its PH domain, which triggers the PDK1 phosphorylation on Thr308 [178]. Phosphorylation on Thr308 is sufficient to activate mTORC1 by inactivating the proline-rich Akt

substrate of 40 kDa (PRAS40) and tuberous sclerosis protein 2 (TSC2), which triggers events in protein synthesis and cellular proliferation [179]. Hyperactivation of Akt facilitates additional substrate-specific events in the cytoplasm and nucleus modulating numerous cellular functions like angiogenesis, metabolism, growth, proliferation, survival, protein synthesis, transcription, and apoptosis (**Figure 9**), see [177].

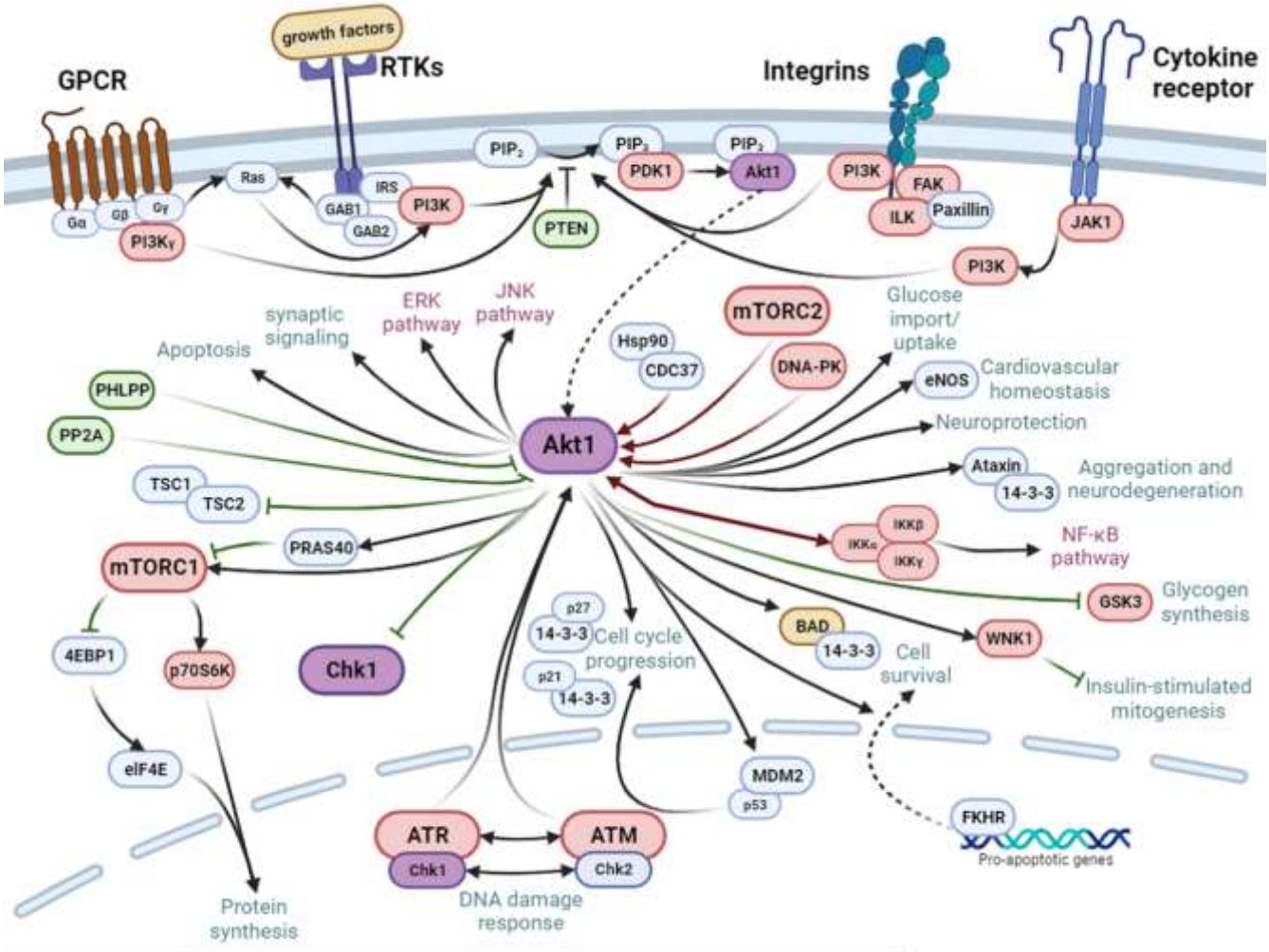

Figure 9: Akt1 plays an essential and pivotal role in cellular events. The activation is triggered upon growth factor stimuli by help of different receptors (GPCR, RTKs, Integrins, Cytokine receptors) and subsequent phosphorylation events of PI3K and PIP2 into PIP_3 which serves as initial factor upon activation of Ak1t. Phosphorylation on Thr308 is a PDK1-mediated event while hyperactivation of Akt is triggered by mTORC2. While PHLPP and PP2A can serve as inhibitor of Akt1, the kinase promotes phosphorylation of various protein substrates and cellular signalling cascades. Figure adapted from Hemmings and Restuccia [177] and prepared by Biorender.com.

FKBP51 is known to act as a scaffolding protein which may facilitate the Akt-PHLPP protein complex. The interaction of FKBP51 and Akt was either described with an enhanced de-phosphorylation of Akt in pancreatic cancer context or the interaction was described in an upregulation of Akt activation [108; 109]. Treatment with FKBP51siRNA decreased the phosphorylation of Akt at S473 in cancerous tissues of locoregional lymph nodes or xenografts [180]. Eventually Akt directly binds to FKBP51 via the FK1

domain or indirectly via the TPR domain through Hsp90 [109], while FKBP51 probably does not assist in the de-phosphorylation of Akt which might depends on the acetylation status of FKBP51 [181]. Recent studies demonstrated, that the FKBP51-Akt-PHLPP complex contributes in the K63-ubiquitination of Akt, whereas overexpression of FKBP51 and low expression levels of PHLPP could not support Akt activation [182].

3.3.2 CAMK kinases - CHEKing cell cycle progression

The checkpoint kinase 1 (Chk1/CHEK1) is a serine/threonine protein kinase and classified as a member of the Ca^{2+}/calmodulin-depended protein kinase (CAMK). The kinase was identified as a 'druggable' target and is triggered by upstream events *inter alia* of Akt (**Figure 9**) [183]. Chk1 is responsible for the evolutionary conserved DNA damage response (DDR) and cell cycle progression to preserve the genomic integrity. DNA damage induces the activation of Chk1, which triggers checkpoint signals for cell cycle arrest and DNA damage repair. The event requires the canonical ATR-Chk1 and ATM-Chk2 pathways. The ATR-Chk1 pathway is triggered upon several DNA abnormalities, e.g., single strand breaks, while the ATR-Chk2 pathway primarily responds of double-strand breaks (DSB) (**Figure 10**) [184; 185].

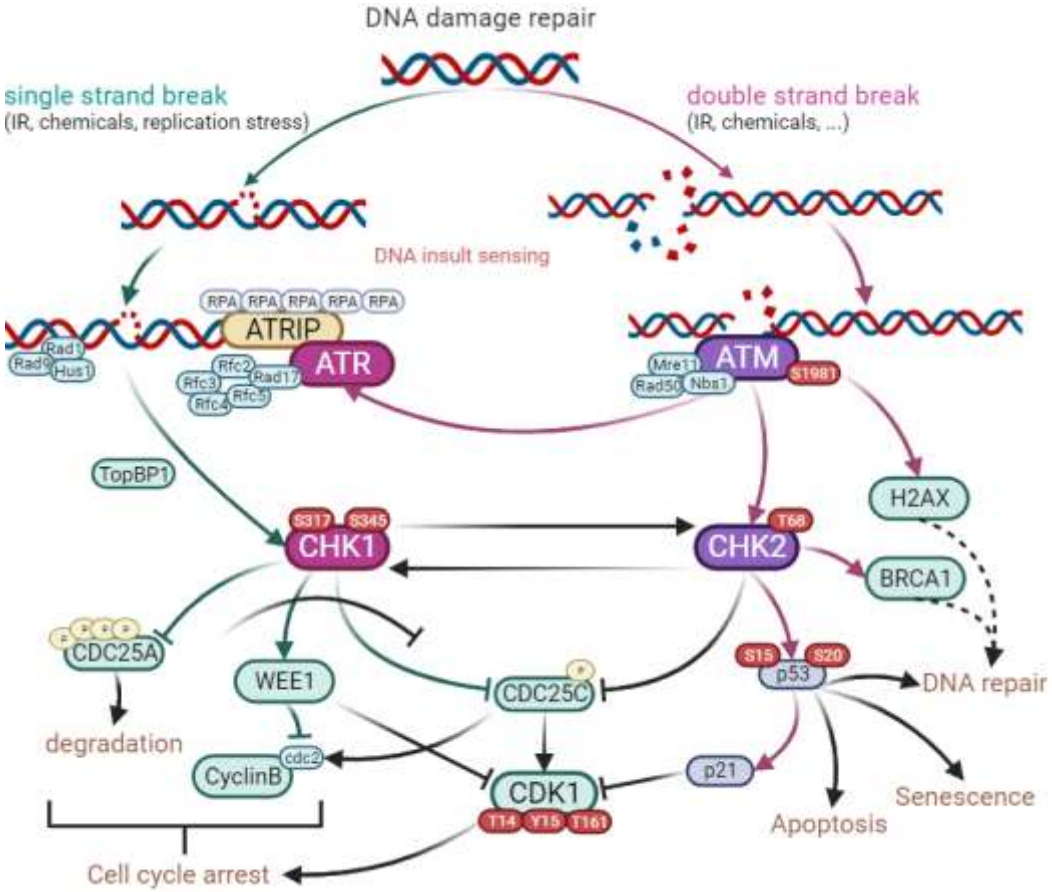

Figure 10: DNA damage response (DDR) and cell cycle progression involves the two canonical pathways ATR-Chk1 and ATM-Chk2. Single strand DNA breaks primarily involves the ATR-Chk1 pathway while double strand breaks involve the ATM-Chk2 pathway. Chk1 and Chk2 can regulate themselves. Chk1 is responsible for degradation and cell cycle arrest while Chk2 participates in apoptosis, senescence, and DNA repair. Figure adopted from [185]. Figure prepared with Biorender.com.

The ATR-Chk1 and ATM-Chk2 are interconnected pathways, and their involvement depends on the type of lesion. Double strand breaks are rapidly sensed by the Mre11-Rad50-NBS1 (MNR) complex which interacts with chromatin promoting the autophosphorylation and therefore activation of Ataxia Telangiectasia Mutated (ATM) kinase. ATM activates Chk2 and p53, while other DNA lesions like single strand breaks are sensed by the Rad9-Hus1-Rad1 complex. For the activation of the Ataxia Telangiectasia and Rad3-Related kinase (ATR) the additional factors Rad17 and Rfc2-5 are required. ATR is directed by its subunit ATR interacting protein (ATRIP) to RPA (Replication Protein A). Subsequently, Rad9 interacts with TopBP1 resulting in the ATR-mediated phosphorylation of Chk1 (**Figure 10**) [185]. Chk1 activation leads to the initiation of cell cycle checkpoints (G2/M) resulting in cell cycle arrest, DNA repair and cell death as the kinase mediates the degradation of the Cell-Division Cycle 25A (CDC25A) phosphatase via phosphorylation slowing down the progression of DNA replication The phosphorylation prevents the activation of the cyclin-dependent kinase 1 (CDK1) [186; 187]. In order of its regulatory role, Chk1 complexes with Claspin initiating a phosphorylation at S345 and S317 by ATR whereas substrates of Chk1 mostly reside in the nucleoplasm. The phosphorylation of the two serines results in binding of 14-3-3 proteins facilitating nuclear retention of Chk1 leading to autoactivation of S296 which then targets CDC25A. On the other hand ATR-dependent phosphorylation can be induced by metalloproteases cleaving the inhibitory C-terminal domain allowing the kinase active N-terminal domain facilitating downstream signalling [188]. Full activation of Chk1 requires the assembly with the Hsp90 complex [189], while Akt directly phosphorylates Chk1 on S280 [190]. The phosphorylation was enhanced upon overexpression of Akt in HEK293 cells [191]. The interplay of Chk1 and Akt influences the induced G2 cell cycle arrest as it is thought that activated Akt abrogates the effect of DNA damage [192]. Moreover, Chk1 was found to possess reduced electrophoretic mobility in Akt-null cells indicating, that the phosphorylation on S280 is a specific phosphorylation site of Akt [191]. Other studies identified novel auto-phosphorylation sites T378, T382. Chk1 phosphorylation is highly dependent on the upstream kinase, cell type and growth conditions. Its regulatory role in DNA damage response as checkpoint in the cell cycle of the Intra-S and G2/M mitotic exit is reviewed in [188].

3.3.3 Inhibitors of Kinases – the difficulty to target a specific kinase

To date, it is not known if FKBP51 might also function as a scaffolding protein in the Chk1-Akt interaction. Both kinases are biomarkers in cancer. The first developed small molecule kinase inhibitor Imatinib inhibits the Abelson (ABL) tyrosine kinase in chronic myeloid leukaemia (CML). Its successors are precisely reviewed from Cohen *et.* al [193]. Notably, most of kinase inhibitors are small molecules which directly inhibits the catalytic activity of kinases by blocking the binding of ATP [194]. As the structure of the ATP binding site is highly conserved, kinase inhibitors inhibit a wide range of protein kinases, affecting multiple signalling pathways [195–197]. However, kinase inhibitors have important side effects, which leads to a cytotoxic profile resulting in abnormalities in thyroid function, bone metabolism, linear growth, gonadal function, fetal development, adrenal function, and glucose metabolism [198]. The improvement of kinase inhibitors is an ongoing field to reduce the cytotoxic side effects among other cellular signalling pathways except the preferred kinase. 64 of out of 72 FDA approved kinase inhibitors (Type I and Type II inhibitors) target the ATP-binding site utilizing heterocyclic cores or recapitulating elements of the adenine core of ATP [199–201]. Another FDA approved class of kinase inhibitors are allosteric inhibitors (Type III inhibitors), whereas Rapamycin was the first identified compound for the kinase mTOR [202]. Moreover, covalent inhibitors (Type V) forming irreversible bonds with an active site cysteine residue. Prominent representatives are the compounds Afatinib (2013) and Ibrutinib [203]. The number of FDA approved kinase inhibitors is continuously rising indicating kinases are druggable targets [204] (**Figure 6**, see red dots).

Only up to 8 % of the human kinome are suggested as ‘druggable’ targets. In case of Rapamycin, allosteric inhibition of mTOR led to further inhibition of downstream signalling in the PI3K/Akt/mTOR signalling pathway. While small molecule inhibitors are easier to be synthesised but requires precise mechanism for e.g., the ATP binding site, macrolides like Rapamycin can modulate the binding surface of their accessory proteins by acting as a molecular glue.

4 Aim

So far, the glue effects of natural products were discovered serendipitously. This led to the question, if the ‘orphan’ natural product Antascomicin B induces chemically ternary complex formation with a protein of interest. It is known that the natural product interacts with the PPIase domain of FKBP12 similar to the established molecular glues FK506 and Rapamycin. As FKBP51 is an important player in several diseases and highly conserved compared to FKBP12, it was suggested that Antascomicin B might interact with the FK1 domain of the large immunophilin. The overall goal of this thesis is the evaluation of Antascomicin B as a molecular binder for FKBP51 and FKBP12 as well as its role as a molecular glue on potential interaction partners indicating in a Rapamycin-like binding mode.

5 Materials

5.1 Oligonucleotide Primers

Table 1: Oligonucleotide primers for mammalian expression vectors of wildtype proteins.

Name	Sequence (5'-3')	Details
HP16_CSF_*EcoR*I fwd	caga **GAATTC** ATGGGAGTGCAGGTGGAAACCA	Amplification of FKBP12 WT protein sequence with restriction sites for implementation in MCS of C-SF-TAP plasmid
HP16_CSF_*Not*I rev	catc **GCGGCCGC** TTCCAGTTTTAGAAGCTCCACATCG	
HP16_NSF_*Nhe*I fwd	caga **GCTAGC** ATGGGAGTGCAGGTGGAAA	Amplification of FKBP12 WT protein sequence with restriction sites for implementation in MCS of C-SF-TAP plasmid
HP16_NSF_*Xho*I rev	catc **CTCGAG** TTCCAGTTTTAGAAGCTCCACATCG	
HP41fwd_CSF_*EcoR*I	caga **GAATTC** ATGACTACTGATGAAGGTGC	Amplification of FKBP51 FK1 domain WT protein sequence with restriction sites for implementation in MCS of C-SF-TAP plasmid
HP41rev_CSF_*Not*I	catc **GCGGCCGC** CTCTCCTTTGAAATCAAGGAGC	
HP41fwd_NSF_*Nhe*I	caga **GCTAGC** ATGACTACTGATGAAGGTGC	Amplification of FKBP51 FK1 domain WT protein sequence with restriction sites for implementation in MCS of C-SF-TAP plasmid
HP41rev_NSF_*Xho*I	catc **CTCGAG** CTCTCCTTTGAAATCAAGGAGC	
SFC-Akt fwd	aaa **GGTACC** ATGAGCGACGTGGCTATT	Amplification of Akt1 WT protein sequence with restriction sites for implementation in MCS of C-SF-TAP plasmid with *Kpn*I and *EcoR*I
SFC-Akt rev	aaa **GAATTC** GGCCGTGCCGCTG	

Table 2: Oligonucleotide primers for mammalian expression vectors of FKBP12 and FKBP12Δmutants.

Name	Sequence (5'-3')	Details
HP16fwd_CSF_EcoRI	CAGA **GAATTC** ATGGGAGTGCAGGTGGAAACCA	Amplification of FKBP12/ FKBP12Δmut for destination vector C-SF-TAP or N-SF-TAP
HP16rev_CSF_NotI	CAT **CGCGGCC** GCTTCCAGTTTTAGAAGCTCCACATCG	
FKBP12_14TAGfwd	GAGACGGGCGC **TAG** TTCCCCAAGCG	Replacement of codon T14 by TAG codon for pBpa translation
FKBP12_14TAGrev	CGCTTGGGGAA **CTA** GCGCCCGTCTC	
FKBP12_17TAGfwd	ACCTTCCCC **TAG** CGC GGCCAGACCT	Replacement of codon K17 by TAG codon for pBpa translation
FKBP12_17TAGrev	AGGTCTGGCCGCG **CTA** GGGGAAGGT	
FKBP12_18TAGfwd	ACCTTCCCCAAG **TAG** GGCCAGACCTGC	Replacement of codon R18 by TAG codon for pBpa translation
FKBP12_18TAGrev	GCAGGTCTGGCC **CTA** CTTGGGGAAGGT	
FKBP12_21TAGfwd	AAGCGCGGCCAG **TAG** TGCGTGGTGCACTA	Replacement of codon T21 by TAG codon for pBpa translation
FKBP12_21TAGrev	TAGTGCACCACGCA **CTA** CTGGCCGCGCTT	
FKBP12_31TAGfwd	ACACCGGGATGCTT **TAG** GATGGAAAGAAATT	Replacement of codon E31 by TAG codon for pBpa translation
FKBP12_31TAGrev	AATTTCTTTCCATC **CTA** AAGCATCCCGGTGT	
FKBP12_34TAGfwd	ATGCTTGAAGATGGA **TAG** AAATTTGATTCCTCCC	Replacement of codon K34 by TAG codon for pBpa translation
FKBP12_34TAGrev	GGGAGGAATCAAATTT **CTA** TCCATCTTCAAGCAT	
FKBP12_35TAGfwd	CTTGAAGATGGAAAG **TAG** TTTGATTCCTCC	Replacement of codon K35 by TAG codon for pBpa translation
FKBP12_35TAGrev	GGAGGAATCAAA **CTA** CTTTCATCTTCAAG	
FKBP12_41TAGfwd	ATTCCTCCCGG **TAG** AGAAACAAGCC	Replacement of codon D41 by TAG codon for pBpa translation
FKBP12_41TAGrev	GGCTTGTTTCT **CTA** CCGGGAGGAAT	
FKBP12_43TAGfwd	CCGGGACAGA **TAG** AAGCCCTTTAAGTTTAT	Replacement of codon N43 by TAG codon for pBpa translation
FKBP12_43TAGrev	ATAAACTTAAAGGGCTT **CTA** TCTGTCCCGG	
FKBP12_44TAGfwd	GGACAGAAAC **TAG** CCCTTTAAGTTTATGCT	Replacement of codon K44 by TAG codon for pBpa translation
FKBP12_44TAGrev	AGCATAAACTTAAAGGG **CTA** GTTTCTGTCC	
FKBP12_47TAGfwd	AACAAGCCCTTT **TAG** TTTATGCTAGGCAAG	Replacement of codon K47 by TAG codon for pBpa translation
FKBP12_47TAGrev	CTTGCCTAGCATAAA **CTA** AAAGGGCTTGTT	

FKBP12_49TAGfwd	CTTTAAGTTT **TAG** CTAGGCAAGCAGGAGG	Replacement of codon M49 by TAG codon for pBpa translation
FKBP12_49TAGrev	CCTCCTGCTTGCCTAG **CTA** AAACTTAAAG	
FKBP12_52TAGfwd	TTTATGCTAGGC **TAG** CAGGAGGTGAT	Replacement of codon K52 by TAG codon for pBpa translation
FKBP12_52TAGrev	ATCACCTCCTG **CTA** GCCTAGCATAAA	
FKBP12_53TAGfwd	TTATGCTAGGCAAG **TAG** GAGGTGATCCGA	Replacement of codon Q53 by TAG codon for pBpa translation
FKBP12_53TAGrev	TCGGATCACCTC **CTA** CTTGCCTAGCATAA	
FKBP12_57TAGfwd	AAGCAGGAGGTGATC **TAG** GGCTGGGAAGAA	Replacement of codon R57 by TAG codon for pBpa translation
FKBP12_57TAGrev	TTCTTCCCAGCC **CTA** GATCACCTCCTGCTT	
FKBP12_61TAGfwd	CGAGGCTGGGAA **TAG** GGGGTTGCCCAGAT	Replacement of codon E61 by TAG codon for pBpa translation
FKBP12_61TAGrev	ATCTGGGCAACCCC **CTA** TTCCCAGCCTCG	
FKBP12_73TAGfwd	TGGGTCAGAGAGCC **TAG** CTGACTATATCTCCA	Replacement of codon K73 by TAG codon for pBpa translation
FKBP12_73TAGrev	TGGAGATATAGTCAG **CTA** GGCTCTCTGACCCA	
FKBP12_79TAGfwd	TGACTATATCTCCA **TAG** TATGCCTATGGTGC	Replacement of codon D79 by TAG codon for pBpa translation
FKBP12_79TAGrev	GCACCATAGGCATA **CTA** TGGAGATATAGTCA	
FKBP12_84TAGfwd	TTATGCCTATGGT **TAG** ACTGGGCAC	Replacement of codon A84 by TAG codon for pBpa translation
FKBP12_84TAGrev	GTGCCCAGT **CTA** ACCATAGGCATAA	
FKBP12_85TAGfwd	TATGGTGCC **TAG** GGGCACCCA	Replacement of codon T85 by TAG codon for pBpa translation
FKBP12_85TAGrev	TGGGTGCCC **CTA** GGCACCATA	
FKBP12_87TAGfwd	ATGGTGCCACTGGG**TAG**CCAGGCATCATCC	Replacement of codon H87 by TAG codon for pBpa translation
FKBP12_87TAGrev	GGATGATGCCTGG**CTA**CCCAGTGGCACCAT	
FKBP12_88TAGfwd	TGCCACTGGGCAC**TAG**GGCATCATCCCAC	Replacement of codon P88 by TAG codon for pBpa translation
FKBP12_88TAGrev	GTGGGATGATGCC**CTA**GTGCCCAGTGGCA	
FKBP12_89TAGfwd	CACTGGGCACCCA**TAG**ATCATCCCACCA	Replacement of codon G89 by TAG codon for pBpa translation
FKBP12_89TAGrev	TGGTGGGATGAT**CTA**TGGGTGCCCAGTG	
FKBP12_93TAGfwd	CAGGCATCATCCCA **TAG** CATGCCACTCTCGT	Replacement of codon P93 by TAG codon for pBpa translation
FKBP12_93TAGrev	ACGAGAGTGGCATG **CTA** TGGGATGATGCCTG	
FKBP12_94TAGfwd	CATCATCCCACCA **TAG** GCCACTCTCGTCTT	Replacement of codon H94 by TAG codon for pBpa translation
FKBP12_94TAGrev	AAGACGAGAGTGGC **CTA** TGGTGGGATGATG	

5.2 Expression vectors

Table 3: Vectors for expression in bacteria strains of e. Coli

Name	Resistance	Expression	Provider
pET30b_FKBP12monoCys (FKBP12mCys)	Kanamycin	Vector containing protein sequence of FKBP12 with His- and TEV cleavage site (mutations: C22V/E108C)	Biocat (Heidelberg, Ger)
pET30b_FKBP51FK1monoCys (FKBP51FK1mCys)	Kanamycin	Vector containing protein sequence of FKBP51 FK1 domain (1-140) with His- and Tev cleavage site (mutations: C103A / C107I / E140C)	RG Hausch (TUD, Ger)
pGEX-4T-2-FRB	Ampicillin	Vector containing protein sequence of FRB domain of mTOR with a GST-tag	[139]
pProExHTa-FKBP12-His	Ampicillin	Human FKBP12 WT with N-terminal 6xHis tag	RG Hausch (TUD, Ger)

Table 4: Vectors for expression in mammalian cell lines HEK293T and HEK293T FKBP12 knock-out.

Name	Resistance	Expression	Provider
pCDNA3.1	Ampicillin	Empty backbone vector with MCS	RG Hausch (TUD. Ger)
pCDNA3.1_HA_FKBP51	Ampicillin	Human FKBP51 wildtype with V67F mutation an N-terminal HA tag	RG Hausch
pCDNA3.1_HA_Akt1	Ampicillin	Human kinase Akt1 wildtype with N-terminal HA tag	Addgene (Cambridge, MA, USA, #73408)
pcDNA3.0-C-SF-TAP MCS	Ampicillin	Empty backbone vector with MCS and C-terminal Twin StrepII FLAG tag	[205]
pcDNA3.0-N-SF-TAP MCS	Ampicillin	Empty backbone vector with MCS and N-terminal Twin StrepII FLAG tag	[205]

pcDNA3.0-C-SF-TAP_Akt1_WT	Ampicillin	Human kinase Akt1 wildtype with C-terminal Twin StrepII FLAG tag	Sabine C. Schäfer
pcDNA3.0-C-SF-TAP_FKBP12_WT	Ampicillin	Human FKBP12 wildtype with C-terminal Twin StrepII FLAG tag	Sabine C. Schäfer
pcDNA3.0-C-SF-TAP_FKBP51FK1 WT	Ampicillin	Human FKBP51 FK1 domain with C-terminal Twin StrepII FLAG tag	Sabine C. Schäfer
pcDNA3.0-N-SF-TAP_FKBP12_WT	Ampicillin	Human FKBP12 wildtype with N-terminal Twin StrepII FLAG tag	Sabine C. Schäfer
pcDNA3.0-N-SF-TAP_FKBP51FK1_WT	Ampicillin	Human FKBP51 FK1 domain with N-terminal Twin StrepII FLAG tag	Sabine C. Schäfer
pcDNA3.0_HA_FRB	Ampicillin	Human FRB domain (of mTOR) with N-terminal HA tag	Biocat (Heidelberg, Ger)
pcDNA3.0_HA_Chk1	Ampicillin	Human Chk1 wildtype with N-terminal HA tag	Biocat (Heidelberg, Ger)
pRK5_MCS	Ampicillin	Empty backbone vector with MCS	[206; 207]
pRK5_FKBP51_FLAG	Ampicillin	Human FKBP51 with C-terminal FLAG tag	[206; 207]
pRK5_FKBP51ΔTPR_FLAG	Ampicillin	Human FKBP51K352A/R356A wit C-terminal FLAG tag (to prevent Hsp90 interaction)	[206; 207]
pRK5_FKBP51_HA	Ampicillin	Human FKBP51 with C-terminal HA tag	Biocat (Heidelberg, Ger)
pRK5_HA_GR	Ampicillin	Human GR with N-terminal HA tag	[206; 207]
pCMV5.HA-PKBα	Ampicillin	Human kinase Akt1 wildtype with N-terminal HA tag	P. Cron/B. Hemmings (FMI, Basel, CHE)
pCMV5.HA-PKBα^{S473A}	Ampicillin	Human kinase Akt1 with S473A exchange and N-terminal HA tag	[139; 208]
pCMV5.HA-PKBα^{S473D}	Ampicillin	Human kinase Akt1 with S473D exchange and N-terminal HA tag	[139; 208]
pCMV5.HA-PKBα^{T308A}	Ampicillin	Human kinase Akt1 with T308A exchange and N-terminal HA tag	[139; 208]
pCMV5.HA-PKBα^{T308D}	Ampicillin	Human kinase Akt1 with T308D exchange and N-terminal HA tag	[139; 208]
pCMV5.HA-PKBα^{T450A}	Ampicillin	Human kinase Akt1 with T450A exchange and N-terminal HA tag	[139; 208]
pCMV5.HA-PKBα^{T450D}	Ampicillin	Human kinase Akt1 with T450D exchange and N-terminal HA tag	[139; 208]
pCMV5.HA-PKBα$^{T308A/S473A}$	Ampicillin	Human kinase Akt1 with T308A/S473A exchange and N-terminal HA tag	[139; 208]
pCMV5.HA-PKBα$^{T308A/S473D}$	Ampicillin	Human kinase Akt1 with T308A/S473D exchange and N-terminal HA tag	[139; 208]
pCMV5.HA-PKBα$^{T308D/S473A}$	Ampicillin	Human kinase Akt1 with T308D/S473A exchange and N-terminal HA tag	[139; 208]
pCMV5.HA-PKBα$^{T308D/S473D}$	Ampicillin	Human kinase Akt1 with T308D/S473D exchange and N-terminal HA tag	[139; 208]
pCMV5.HA-PKBα$^{T450A/S473A}$	Ampicillin	Human kinase Akt1 with T450A/S473A exchange and N-terminal HA tag	[139; 208]
pCMV5.HA-PKBα$^{T450A/S473D}$	Ampicillin	Human kinase Akt1 with T450A/S473D exchange and N-terminal HA tag	[139; 208]
pCMV5.HA-PKBα$^{T450D/S473A}$	Ampicillin	Human kinase Akt1 with T450D/S473A exchange and N-terminal HA tag	[139; 208]
pCMV5.HA-PKBα$^{T450D/S473D}$	Ampicillin	Human kinase Akt1 with T450D/S473D exchange and N-terminal HA tag	[139; 208]
HA_Akt2	Ampicillin	Human kinase Akt2 wildtype with N-terminal HA tag	[209]
pcDNA3.0-pBpa-RS	Kanamycin	pBpa Synthetase and tRNA cassette	Coin Lab, Uni Leipzig
Pyl-tRNA-synthetase-FLAG	Ampicillin	optimized Pyl tRNA Synthetase D171 (*Methanosarcina barkeri*)	K. Lang, TUM, Ger

5.2.1 Expression vectors for incorporation of unnatural amino acids in HEK293T cells

Table 5: Vectors for expression of FKBP51Δmutants in mammalian cell lines to incorporate unnatural amino acids (unAA)

Name	Resistance	Expression	Provider
pCAG_FKBP51 WT_FLAG	Ampicillin	Vector containing sequence of human FKBP51 WT with C-terminal FLAG tag	[84; 210]
pCAG_FKBP51^{K28TAG}	Ampicillin	Replacement of codon K28 of human FKBP51 by TAG codon for pBpa translation with C-terminal FLAG tag	[84; 210]
pCAG_FKBP51^{M48TAG}	Ampicillin	Replacement of codon M48 of human FKBP51 by TAG codon for pBpa translation with C-terminal FLAG tag	[84; 210]
pCAG_FKBP51^{K52TAG}	Ampicillin	Replacement of codon K52 of human FKBP51 by TAG codon for pBpa translation with C-terminal FLAG tag	[84; 210]
pCAG_FKBP51^{K65TAG}	Ampicillin	Replacement of codon K65 of human FKBP51 by TAG codon for pBpa translation with C-terminal FLAG tag	[84; 210]
pCAG_FKBP51^{S70TAG}	Ampicillin	Replacement of codon S70 of human FKBP51 by TAG codon for pBpa translation with C-terminal FLAG tag	[84; 210]
pCAG_FKBP51^{D72TAG}	Ampicillin	Replacement of codon D72 of human FKBP51 by TAG codon for pBpa translation with C-terminal FLAG tag	[84; 210]
pCAG_FKBP51^{N74TAG}	Ampicillin	Replacement of codon N74 of human FKBP51 by TAG codon for pBpa translation with C-terminal FLAG tag	[84; 210]
pCAG_FKBP51^{E75TAG}	Ampicillin	Replacement of codon E75 of human FKBP51 by TAG codon for pBpa translation with C-terminal FLAG tag	[84; 210]
pCAG_FKBP51^{V78TAG}	Ampicillin	Replacement of codon V78 of human FKBP51 by TAG codon for pBpa translation with C-terminal FLAG tag	[84; 210]
pCAG_FKBP51^{K83TAG}	Ampicillin	Replacement of codon K83 of human FKBP51 by TAG codon for pBpa translation with C-terminal FLAG tag	[84; 210]
pCAG_FKBP51^{G84TAG}	Ampicillin	Replacement of codon G84 of human FKBP51 by TAG codon for pBpa translation with C-terminal FLAG tag	[84; 210]
pCAG_FKBP51^{K88TAG}	Ampicillin	Replacement of codon K88 of human FKBP51 by TAG codon for pBpa translation with C-terminal FLAG tag	[84; 210]
pCAG_FKBP51^{E110TAG}	Ampicillin	Replacement of codon E110 of human FKBP51 by TAG codon for pBpa translation with C-terminal FLAG tag	[84; 210]
pCAG_FKBP51^{S115TAG}	Ampicillin	Replacement of codon S115 of human FKBP51 by TAG codon for pBpa translation with C-terminal FLAG tag	[84; 210]
pCAG_FKBP51^{A116TAG}	Ampicillin	Replacement of codon A116 of human FKBP51 by TAG codon for pBpa translation with C-terminal FLAG tag	[84; 210]
pCAG_FKBP51^{G117TAG}	Ampicillin	Replacement of codon G117 of human FKBP51 by TAG codon for pBpa translation with C-terminal FLAG tag	[84; 210]
pCAG_FKBP51^{S118TAG}	Ampicillin	Replacement of codon S118 of human FKBP51 by TAG codon for pBpa translation with C-terminal FLAG tag	[84; 210]
pCAG_FKBP51^{L119TAG}	Ampicillin	Replacement of codon L119 of human FKBP51 by TAG codon for pBpa translation with C-terminal FLAG tag	[84; 210]
pCAG_FKBP51^{P120TAG}	Ampicillin	Replacement of codon P120 of human FKBP51 by TAG codon for pBpa translation with C-terminal FLAG tag	[84; 210]
pCAG_FKBP51^{I121TAG}	Ampicillin	Replacement of codon I121 of human FKBP51 by TAG codon for pBpa translation with C-terminal FLAG tag	[84; 210]
pCAG_FKBP51^{E136TAG}	Ampicillin	Replacement of codon E136 of human FKBP51 by TAG codon for pBpa translation with C-terminal FLAG tag	[84; 210]
pCAG_FKBP51^{Y159TAG}	Ampicillin	Replacement of codon Y159 of human FKBP51 by TAG codon for pBpa translation with C-terminal FLAG tag	[84; 210]

Table 6: Vectors for expression of FKBP12Δmutants in mammalian cell lines to incorporate unnatural amino acids (unAA)

Name	Resistance	Expression	Provider
C-SF-TAP-FKBP12 WT	Ampicillin	Vector expression FKBP12 with C-terminal Twin-Strep-Flag Tag (hereinafter all FKBP12 mutants)	Sabine C. Schäfer
C-SF-TAP-FKBP12^{T14TAG}	Ampicillin	Replacement of codon T14 of human FKBP12 by TAG codon for pBpa translation	Sabine C. Schäfer
C-SF-TAP-FKBP12^{R18TAG}	Ampicillin	Replacement of codon R18 of human FKBP12 by TAG codon for pBpa translation	Sabine C. Schäfer
C-SF-TAP-FKBP12^{T21TAG}	Ampicillin	Replacement of codon T21 of human FKBP12 by TAG codon for pBpa translation	Sabine C. Schäfer
C-SF-TAP-FKBP12^{E31TAG}	Ampicillin	Replacement of codon E31 of human FKBP12 by TAG codon for pBpa translation	Sabine C. Schäfer
C-SF-TAP-FKBP12^{K34TAG}	Ampicillin	Replacement of codon K34 of human FKBP12 by TAG codon for pBpa translation	Sabine C. Schäfer
C-SF-TAP-FKBP12^{K35TAG}	Ampicillin	Replacement of codon K35 of human FKBP12 by TAG codon for pBpa translation	Sabine C. Schäfer
C-SF-TAP-FKBP12^{D41TAG}	Ampicillin	Replacement of codon D41 of human FKBP12 by TAG codon for pBpa translation	Sabine C. Schäfer
C-SF-TAP-FKBP12^{N43TAG}	Ampicillin	Replacement of codon N43 of human FKBP12 by TAG codon for pBpa translation	Sabine C. Schäfer
C-SF-TAP-FKBP12^{K44TAG}	Ampicillin	Replacement of codon K44 of human FKBP12 by TAG codon for pBpa translation	Sabine C. Schäfer
C-SF-TAP-FKBP12^{K47TAG}	Ampicillin	Replacement of codon K47 of human FKBP12 by TAG codon for pBpa translation	Sabine C. Schäfer
C-SF-TAP-FKBP12^{M49TAG}	Ampicillin	Replacement of codon M49 of human FKBP12 by TAG codon for pBpa translation	Sabine C. Schäfer
C-SF-TAP-FKBP12^{K52TAG}	Ampicillin	Replacement of codon K52 of human FKBP12 by TAG codon for pBpa translation	Sabine C. Schäfer
C-SF-TAP-FKBP12^{Q53TAG}	Ampicillin	Replacement of codon Q53 of human FKBP12 by TAG codon for pBpa translation	Sabine C. Schäfer
C-SF-TAP-FKBP12^{R57TAG}	Ampicillin	Replacement of codon R57 of human FKBP12 by TAG codon for pBpa translation	Sabine C. Schäfer
C-SF-TAP-FKBP12^{K73TAG}	Ampicillin	Replacement of codon K73 of human FKBP12 by TAG codon for pBpa translation	Sabine C. Schäfer
C-SF-TAP-FKBP12^{D79TAG}	Ampicillin	Replacement of codon D79 of human FKBP12 by TAG codon for pBpa translation	Sabine C. Schäfer
C-SF-TAP-FKBP12^{A84TAG}	Ampicillin	Replacement of codon A84 of human FKBP12 by TAG codon for pBpa translation	Sabine C. Schäfer
C-SF-TAP-FKBP12^{T85TAG}	Ampicillin	Replacement of codon T85 of human FKBP12 by TAG codon for pBpa translation	Sabine C. Schäfer
C-SF-TAP-FKBP12^{H87TAG}	Ampicillin	Replacement of codon H87 of human FKBP12 by TAG codon for pBpa translation	Sabine C. Schäfer
C-SF-TAP-FKBP12^{P88TAG}	Ampicillin	Replacement of codon P88 of human FKBP12 by TAG codon for pBpa translation	Sabine C. Schäfer
C-SF-TAP-FKBP12^{G89TAG}	Ampicillin	Replacement of codon G89 of human FKBP12 by TAG codon for pBpa translation	Sabine C. Schäfer
C-SF-TAP-FKBP12^{P93TAG}	Ampicillin	Replacement of codon P93 of human FKBP12 by TAG codon for pBpa translation	Sabine C. Schäfer
C-SF-TAP-FKBP12^{H94TAG}	Ampicillin	Replacement of codon H94 of human FKBP12 by TAG codon for pBpa translation	Sabine C. Schäfer

5.3 Antibodies

Table 7: Primary antibodies for detection of total protein levels.

Name	Antigene/ref.	Species	Dilution factor	Manufacturer, cat#
αFLAG-HRP	DYKDDDDK	IgG, polyclonal, rabbit	1:5000 in 5 % (w/v) BSA in 1x TBS	Sigma Aldrich (St. Louis, MO, USA)
αHA-HRP	YPYDVPDYA	IgG1, monoclonal, rat	1:5000 in 5 % (w/v) BSA in 1x TBS	Sigma Aldrich (St. Louis, MO, USA)
αHA-HRP	YPYDVPDYA	IgG1, (6E2) mAb, mouse	1:3.500 in 5 % (w/v) BSA in 1x TBS	Cell signaling Technology (Denver, MA, USA)
αGR-HRP	aa 121-420 (#sc-393232)	IgG1, mAb, mouse (G-5)	1:2000 in 5 % (w/v) BSA in 1x TBS	Santa Cruz biotechnology (Santa Cruz, CA, USA)
αStrep-Tactin®-HRP	Strep-tag® II, Twin-Strep-Tag®	synthetic	1:2000 in 5 % (w/v) BSA in 1x TBS	IBA Lifesciences (Göttingen, Ger)
αAkt (pan)	Full length protein	IgG1, Rabbit mAb (11E7, #4685)	1:1000 in 5 % (w/v) BSA in 1x TBS	Cell signaling Technology (Denver, MA, USA)
αChk1	aa 1-476 (#sc-8408)	IgG1, mouse mAb (G-4)	1:1000 in 5 % (w/v) BSA in 1x TBS	Santa Cruz biotechnology (Santa Cruz, CA, USA)
αGAPDH	aa 250-300 (#A300-641A)	IgG1, polyclonal, rabbit	1:1000 in 5 % (w/v) milk powder in 1x TBS	Bethyl Laboratories, Inc (Montgomery, TX, USA)
αFKBP12	aa 1-108 (#sc-136962)	IgG1, mAb, mouse (G-4)	1:1000 in 5 % (w/v) BSA in 1x TBS	Santa Cruz biotechnology (Santa Cruz, CA, USA)
αFKBP51	aa 358-457 (#sc-271547)	IgG1, mAb, mouse (D-4)	1:1000 in 5 % (w/v) milk powder in 1x TBS	Santa Cruz biotechnology (Santa Cruz, CA, USA)
α mTOR kinase	aa residues surrounding Ser2481	IgG1, Rabbit mAb (7C10, #2983)	1:1000 in 5 % (w/v) BSA in 1x TBS	Cell signaling Technology (Denver, MA, USA)
α p70 S6K	Total protein, also recognizes p85 S6 kinase	IgG1, Rabbit, polyclonal	1:1000 in 5 % (w/v) BSA in 1x TBS	Cell signaling Technology (Denver, MA, USA)
α p70 S6K (Thr389)	C-terminus with phosphorylation on Thr389	IgG1, rabbit, polyclonal (#07-018-I)	1:1000 in 5 % (w/v) BSA in 1x TBS	Merck Millipore (Burlington, MA, USA)
αRaptor	Total protein	IgG1, Rabbit mAb (24C12, #2280)	1:1000 in 5 % (w/v) milk powder in 1x TBS	Cell signaling Technology (Denver, MA, USA)
αSgk1	aa 300-400	IgG1, rabbit, polyclonal (#ab43606)	1:1000 in 5 % (w/v) milk powder in 1x TBS	Abcam (Cambridge, UK)
αlactoferrin	Full length protein	IgG1, mouse mAb (#sc-53498)	1:1000 in 5 % (w/v) BSA in 1x TBS	Santa Cruz biotechnology (Santa Cruz, CA, USA)

Table 8: Secondary antibodies conjugated to horseradish peroxidase (HRP) for visualization by ECL signaling.

Name	Conjugation	IgG Species Subtype	Dilution factor	Manufacturer, cat#
Mouse IgG	HRP	Horse anti-mouse IgG, (#7076)	1:1000 in 5 % (w/v) BSA in 1x TBS	Cell signaling Technology (Denver, MA, USA)
Rabbit IgG	HRP	Goat anti-Rabbit IgG-Fc Fragment (#A120-111P)	1:1000 in 5 % (w/v) BSA in 1x TBS	Bethyl Laboratories, Inc (Montgomery, TX, USA)
Goat IgG	HRP	Donkey Anti-Goat IgG H&L (#ab6885)	1:1000 in 5 % (w/v) BSA in 1x TBS	Abcam (Cambridge, UK)

5.4 Bacterial strains

Table 9: Bacterial strains for production of either plasmid DNA or expression of recombinant proteins.

Name	Genotype
e. coli DH5α	F' Phi80dlacZ ΔM15 Δ(lacZYA-argF)U169 deoR recA1 end A1 hsdR17(rK-mK+)phoA supE44 lambda- thi-1
e. coli BL21 Gold(DE3)pLysS	F-, ompT, hsdSb (rb-, mb-), dcm, gal, λ(DE3), pLysS, CM'

5.5 Mammalian cell lines

Table 10: Mammalian cell lines utilized for transfection and treatment of compounds and UV irradiation.

Name	Description	Origin	Provided by	ATCC No.
HEK293T	Embryonic kidney cells, transfected with SV40 T-antigen	H. sapiens	Dr. T. Rein	CRL-11268
HEK293T-12KO	Embryonic kidney cells, transfected with SV40 T-antigen, FKBP12 knock-out variant	H. sapiens	[211]	

5.6 Media and additives for cell culture

Table 11: Materials and additives for cell culture and passaging of mammalian cells. All Media are filtered sterile.

Name	Additives	Manufacturer/Provider
0.25 % Trypsin-EDTA	EDTA, phenol red (#25200056)	Gibco-Invitrogen (Karlsruhe, Ger)
Dulbecco's modified eagle medium (DMEM)	4.5 g/L glucose, HEPES, L-glutamine, sodium pyruvate, phenol red (#41966029)	Gibco-Invitrogen (Karlsruhe, Ger)
Dulbecco's Phosphate Buffered Saline (DPBS)	No calcium, no magnesium, without phenol red (#14190169)	Gibco-Invitrogen (Karlsruhe, Ger)
Fetal Bovine Serum (FBS)	Heat inactivated, qualified, origin: Brazil (#10500064)	Gibco-Invitrogen (Karlsruhe, Ger)
Opti-MEM reduced serum medium	L-glutamine, without phenol red (#11058021)	Gibco-Invitrogen (Karlsruhe, Ger)
Penicillin-Streptomycin	Penicillin 10.000 U/mL Streptomycin 10.000 µg/ml (#15140122)	Gibco-Invitrogen (Karlsruhe, Ger)
Poly-D-Lysin solution	0.1 mg/mL (#Gibco™ A3890401)	Thermo Fisher Scientific (Waltham, MA, USA)
Poly-L-Lysin solution	0.01 % (w/v) in H_2O 0.02 (#P8920)	Sigma Aldrich (St. Louis, MO, USA)
Sterile Water	MQ H_2O, autoclaved	In house, RG Hausch
Trypan blue stain (0.4 %)	0.4 % (w/v) in H_2O (#15250061)	Thermo Fisher Scientific (Waltham, MA, USA)

5.7 Chemicals

Table 12: Commercially available chemicals and resins.

Chemical	Manufacturer
1,4-Dithiothreitol (DTT) ≥ 99% p.a.	Carl Roth GmbH & Co. Kg (Karlsruhe, Ger)
2-Mercaptoethanol (β-Mercapto ethanol)	Sigma Aldrich (St. Louis, MO, USA)
2-propanol for molecular biology (Assay (GC): min. 99.8 %)	AppliChem (Darmstadt, Ger)
2-propanol (≥99,5 %, Ph. Eur., extra pure)	Carl Roth GmbH & Co. Kg (Karlsruhe, Ger)
3'-azibutyl-N-carbamoyl-lysine (Abk)	In house (Dr. Tim Heymann)
3-(*N*-Morpholino)-propane sulphonic acid (MOPS), PUFFERAN® ≥99,5%	Carl Roth GmbH & Co. Kg (Karlsruhe, Ger)
4-Benzoyl-L-phenylalanine, 95%	Alfa Aesar (Haverhill, MA, USA)
Acetic acid 99-100 %	Carl Roth GmbH & Co. Kg (Karlsruhe, Ger)
Acetonitrile (ACN) ≥99.9%, HiPerSolv CHROMANORM® for LC-MS	VWR Life sciences (Darmstadt, Ger)
Agar-Agar Kobe I, powder, for Microbiology	Carl Roth GmbH & Co. Kg (Karlsruhe, Ger)
Anti-FLAG M2 magnetic beads	Sigma Aldrich (St. Louis, MO, USA)
Agarose, universal	VWR Life sciences (Darmstadt, Ger)
Ammonium bicarbonate (ABC) BioUltra ≥ 99.5 %	Sigma Aldrich (St. Louis, MO, USA)
Ammonium hydroxide (NH_4OH)	Carl Roth GmbH & Co. Kg (Karlsruhe, Ger)
Ammonium peroxydisulfate (APS)	Carl Roth GmbH & Co. Kg (Karlsruhe, Ger)
Ampicillin sodium salt ≥ 99 %, for molecular biology and biochemistry	Carl Roth GmbH & Co. Kg (Karlsruhe, Ger)
Antascomicin B (synthetic)	Stephen Ley (Cambridge University, UK)
Antascomicin B (biosynthetic)	In house (B. Ritter, Bachelor thesis)
Bovine serum albumin (BSA) lyophilized powder, Protease, essentially free, ≥98%	Sigma Aldrich (St. Louis, MO, USA)
Brom phenol blue	Sigma Aldrich (St. Louis, MO, USA)
Calcium chloride dihydrate ($CaCl_2 \cdot 2\ H_2O$) ≥99 %, p.a., ACS	Carl Roth GmbH & Co. Kg (Karlsruhe, Ger)
Calcium carbonate (K_2CO_3) ≥98,5 %, powdered	Carl Roth GmbH & Co. Kg (Karlsruhe, Ger)
Coomassie Brilliant Blue R250	Carl Roth GmbH & Co. Kg (Karlsruhe, Ger)
cOmplete, Mini, EDTA-free Protease Inhibitor Cocktail Tablets	Sigma Aldrich (St. Louis, MO, USA)
Dimethyl sulfoxide (DMSO), ROTIPURAN®≥ 99.8% p.a	Carl Roth GmbH & Co. Kg (Karlsruhe, Ger)
Di-potassium hydrogen phosphate (K_2HPO_4)	Carl Roth GmbH & Co. Kg (Karlsruhe, Ger)
Di-sodium hydrogen phosphate (Na_2HPO_4), ≥98 %, p.a., ACS	Carl Roth GmbH & Co. Kg (Karlsruhe, Ger)
Deoxyribonucleotide mix (dNTPs)	New England Biolabs (Frankfurt am Main, Ger)
DNAseI, Deoxyribonuclease I from bovine pancreas, lyophilized powder, protein ≥ 85%, ≥ 400 Kunitz units/mg	Sigma Aldrich (St. Louis, MO, USA)
Ethylenediaminetetraacetic acid (EDTA) 99.4-100.6%, powder	Sigma Aldrich (St. Louis, MO, USA)
Ethanol, ROTIPURAN® ≥ 99.8% p.a.	Carl Roth GmbH & Co. Kg (Karlsruhe, Ger)
Ethanol ≥ 99,8 %, denatured	Carl Roth GmbH & Co. Kg (Karlsruhe, Ger)
Ethanol 70 % DAB	Carl Roth GmbH & Co. Kg (Karlsruhe, Ger)
Ethylenediaminetetraacetic acid disodium salt dehydrated (EDTA $2Na^+ \cdot 2H_2O$)	Sigma Aldrich (St. Louis, MO, USA)
FK506 (Tacrolimus)	Betapharm (Augsburg, Ger)
FLAG peptide (3x)	Sigma Aldrich (St. Louis, MO, USA)
Formaldehyde 37 %	Carl Roth GmbH & Co. Kg (Karlsruhe, Ger)
Glutathione Sepharose 4 Fast Flow	GE Healthcare GmbH (Frankfurt am Main, Ger)
Glycerol 86 % (v/v)	Carl Roth GmbH & Co. Kg (Karlsruhe, Ger)
Glycine	Carl Roth GmbH & Co. Kg (Karlsruhe, Ger)
Hydrochloric acid (HCl)	Carl Roth GmbH & Co. Kg (Karlsruhe, Ger)
HEPES PUFFERAN® ≥ 99.5 % p.a.	Carl Roth GmbH & Co. Kg (Karlsruhe, Ger)
Immobilon Western Chemiluminescent HRP Substrate	Sigma Aldrich (St. Louis, MO, USA)
Imidazole	Carl Roth GmbH & Co. Kg (Karlsruhe, Ger)
Insulin from bovine pancreas, ≥25 USP units/mg (HPLC), powder	Sigma Aldrich (St. Louis, MO, USA)
Isopropyl-β-D-1-thiogalactopyranosid (IPTG) ≥ 99% for Biochemistry	Carl Roth GmbH & Co. Kg (Karlsruhe)
Kanamycin Sulfate ≥ 750 I.U./mg	Carl Roth GmbH & Co. Kg (Karlsruhe)
LB-Agar (Luria/Miller), pH 7.0 ± 0.2: 10 g/L Tryptone, 5 g/L Yeast extract, 10 g/L NaCl, granulated, for molecular biology	Carl Roth GmbH & Co. Kg (Karlsruhe, Ger)

LB Broth (Luria/Miller), pH 7.0 ± 0.2: 10 g/L Tryptone, 5 g/L Yeast extract, 10 g/L NaCl, granulated, for microbiology	Carl Roth GmbH & Co. Kg (Karlsruhe, Ger)
L-Glutathione reduced, ≥98 %, for biochemistry	Carl Roth GmbH & Co. Kg (Karlsruhe, Ger)
Lipofectamine™ 2000 Transfectionreagent	Thermo Fisher Scientific (Waltham, MA, USA)
Lysozyme ≥ 35000 FIP U/mg Bioscience-Grade, Lyophilized, M=14 kDa	Carl Roth GmbH & Co. Kg (Karlsruhe, Ger)
Magnesium chloride hexahydrate ($MgCl_2 \cdot 6\ H_2O$), ≥99 %, p.a., ACS	Carl Roth GmbH & Co. Kg (Karlsruhe, Ger)
Magnesium sulfate Heptahydrate ($MgSO_4 \cdot 7\ H_2O$), ≥99 %, p.a., ACS	Carl Roth GmbH & Co. Kg (Karlsruhe, Ger)
Manganese(II) chloride tetrahydrate ($MnCl_2 \cdot 4\ H_2O$), ≥99 %, p.a.	Carl Roth GmbH & Co. Kg (Karlsruhe, Ger)
MIDORI Green Advance (Safe DNA/RNA stain)	Nippon Genetics Europe GmbH (Düren, Ger)
Nonidet® P40 substitute	Sigma Aldrich (St. Louis, MO, USA)
Octoxinol 9 (Triton® X-100)	Carl Roth GmbH & Co. Kg (Karlsruhe, Ger)
PEI Prime™ linear polyethylenimine	Sigma Aldrich (St. Louis, MO, USA)
Phenyl methylsulfonyl fluoride (PMSF) ≥ 99% for Biochemistry	Carl Roth GmbH & Co. Kg (Karlsruhe, Ger)
Pierce™ Phosphatase Inhibitor Mini Tablets	Thermo Fisher Scientific (Waltham, MA, USA)
Pierce™ Protease- und Phosphatase inhibitor-Minitabletten	Thermo Fisher Scientific (Waltham, MA, USA)
Pierce™ Protease Inhibitor Tablets	Thermo Fisher Scientific (Waltham, MA, USA)
Pierce™ Trypsin/Lys-C Protease-Mix, > 90 %, MS grade	Thermo Fisher Scientific (Waltham, MA, USA)
Ponceau S (C.I. 27195), for histology and electrophoresis	Carl Roth GmbH & Co. Kg (Karlsruhe, Ger)
Poly(ethyleneimine) solution, analytical standard, 50 % (w/v) in H_2O	Sigma Aldrich (St. Louis, MO, USA)
Potassium acetate $K(CH_3COO)$ CELLPURE® ≥99 %	Carl Roth GmbH & Co. Kg (Karlsruhe, Ger)
Potassium carbonate (K_2CO_3) ≥99 %, Ph. Eur.	Carl Roth GmbH & Co. Kg (Karlsruhe, Ger)
Potassium chloride (KCl) ≥99 %, Ph. Eur., USP, BP	Carl Roth GmbH & Co. Kg (Karlsruhe, Ger)
Potassium hydroxide (KOH) ≥85 %, p.a., in pellets	Carl Roth GmbH & Co. Kg (Karlsruhe, Ger)
Powdered milk, Blotting Grade, powdered, low in fat	Carl Roth GmbH & Co. Kg (Karlsruhe, Ger)
Protino® Ni-NTA Agarose (50% (v/v) aqueous suspension, containing 30% (v/v) ethanol)	Macherey-Nagel (Düren, Ger)
Rapamycin (Sirolimus)	Alfa Aesar (Haverhill, MA, USA)
Ribonuclease A, 90 U/mg (Kunitz), BioScience Grade, salt-free	Carl Roth GmbH & Co. Kg (Karlsruhe, Ger)
Rotiphorese® Gel 30 (37.5:1, 30% Acrylamide, 0.8% Bisacrylamide)	Carl Roth GmbH & Co. Kg (Karlsruhe, Ger)
Silver nitrate ($AgNO_3$)	Carl Roth GmbH & Co. Kg (Karlsruhe, Ger)
Sodium chloride (NaCl) ≥ 99.5% p.a.ACS, ISO	Carl Roth GmbH & Co. Kg (Karlsruhe, Ger)
Sodium hydrochloride (NaOH) ≥98 %, p.a., ISO, in pellets	Carl Roth GmbH & Co. Kg (Karlsruhe, Ger)
Sodium dodecyl sulfate (SDS) ≥99,5 %, ROTIPHORESE® Grade, pellets	Carl Roth GmbH & Co. Kg (Karlsruhe, Ger)
Sodium thiosulfate ($Na_2S_2O_2$) ≥99 %, p.a., anhydrous	Sigma Aldrich (St. Louis, MO, USA)
SulfoLink® Coupling Resin	Thermo Fisher Scientific (Waltham, MA, USA)
TEMED (N,N,',N'-Tetramethyl ethylenediamine)	Carl Roth GmbH & Co. Kg (Karlsruhe, Ger)
Terrific-Broth (TB) medium for molecular biology	Carl Roth GmbH & Co. Kg (Karlsruhe, Ger)
Trichloroacetic acid (TCA), ≥99 %, p.a.	Carl Roth GmbH & Co. Kg (Karlsruhe, Ger)
Tris-(2-carboxyethyl)-phosphine hydrochloride (TCEP) ≥98 %, for biochemistry	Carl Roth GmbH & Co. Kg (Karlsruhe, Ger)
Tris-(hydroxymethyl)-amino methane, PUFFERAN® ≥99,9 %, p.a.	Carl Roth GmbH & Co. Kg (Karlsruhe, Ger)
Tris-HCl, Tris-(hydroxymethyl)-aminomethane hydrochloride, PUFFERAN® ≥99 %, p.a.	Carl Roth GmbH & Co. Kg (Karlsruhe, Ger)
Trifluoroacetic acid (TFA), suitable for HPLC, ≥99.0%	Sigma Aldrich (St. Louis, MO, USA)
Trypton/Pepton	Carl Roth GmbH & Co. Kg (Karlsruhe, Ger)
Tween20 (Polysorbate, Polyoxyethylene-20-sorbitan monolaurate), Ph. Eur.	Carl Roth GmbH & Co. Kg (Karlsruhe, Ger)
WesternBright Chemiluminescent Substrate Sirius	Advansta (San Jose, CA, USA)
Yeast extract (for technical purposes (in fermentation))	Sigma Aldrich (St. Louis, MO, USA)

5.8 Enzymes and Proteins

Table 13: Enzymes utilized for cloning steps and PCR reactions for generation of dsDNA plasmids.

Enzyme	Additional Information	Manufacturer/Provider
Gibson Assembly® Master Mix	Easily adapted for multiple DNA manipulations, including SDM	New England Biolabs (NEB, Ipswich, MA, USA)
OneTaq® DNA polymerase	5.000 U/ml, with Quick-Load® Buffer	New England Biolabs (NEB, Ipswich, MA, USA)
Q5® High-Fidelity DNA polymerase	2.000 U/ml, Q5® with Reaction Buffer	New England Biolabs (NEB, Ipswich, MA, USA)
Taq DNA polymerase	5.000 U/ml, with ThermoPol® Buffer	New England Biolabs (NEB, Ipswich, MA, USA)
T4 DNA Ligase	400.000U/ml	New England Biolabs (NEB, Ipswich, MA, USA)

Table 14: Restriction enzymes utilized according to the manufacturer's protocol for restriction and insertion of dsDNA in vectors.

Restriction enzyme	Cleavage site	Manufacturer/Provider
BamHI-HF®	GGATCC	New England Biolabs (NEB, Ipswich, MA, USA)
EcoRI-HF®	GAATTC	New England Biolabs (NEB, Ipswich, MA, USA)
HindIII-HF®	AAGCTT	New England Biolabs (NEB, Ipswich, MA, USA)
KpnI-HF®	GGTACC	New England Biolabs (NEB, Ipswich, MA, USA)
NheI-HF®	GCTAGC	New England Biolabs (NEB, Ipswich, MA, USA)
NotI-HF®	GCGGCCGC	New England Biolabs (NEB, Ipswich, MA, USA)
XbaI	TCTAGA	New England Biolabs (NEB, Ipswich, MA, USA)
XhoI	CTCGAG	New England Biolabs (NEB, Ipswich, MA, USA)

5.9 Kits

Table 15: Kits were utilized according to the manufacturer's protocol.

Name	Application	Manufacturer /Provider
FastGene Gel/PCR Extraction Kit	Purification of PCR Fragments	Nippon Genetics Europe GmbH (Düren, Ger)
FastGene Plasmid Mini Kit	Purification of dsDNA plasmids from e. coli DH5α	Nippon Genetics Europe GmbH (Düren, Ger)
Phospho-P70S6K (Thr389) cellular kit	Assay for determination of endogenous level of p70 S6K kinase and p70 S6K kinase (Thr389)	Perkin Elmer (Waltham, MA, USA)
Pierce™ BCA Protein Assay Kit	Determination of total protein in cell lysate	Thermo Fisher Scientific (Waltham, MA, USA)
Pierce™ Rapid Gold BCA Protein Assay Kit	Determination of total protein in cell lysate	Thermo Fisher Scientific (Waltham, MA, USA)
PureLink™ HiPure Plasmid Midiprep Kit	Purification of dsDNA plasmids from e. coli DH5α	Thermo Fisher Scientific (Waltham, MA, USA)

5.10 Markers

Table 16: DNA and protein standards utilized for agarose gel electrophoresis and SDS PAGE.

Name	Manufacturer/Provider
1 kb DNA ladder (#B7025)	New England Biolabs (NEB, Ipswich, MA, USA)
Hi Mark pre-stained protein Standard (#LC5699)	Thermo Fisher Scientific (Waltham, MA, USA)
PageRuler™ Prestained Protein Ladder (#26616)	Thermo Fisher Scientific (Waltham, MA, USA)
PageRuler™ Plus Prestained Protein Ladder (#26619)	Thermo Fisher Scientific (Waltham, MA, USA)
PageRuler™ Unstained High Range Protein Ladder (#26637)	Thermo Fisher Scientific (Waltham, MA, USA)
Spectra Multicolor High Range Protein Ladder (#26625)	Thermo Fisher Scientific (Waltham, MA, USA)

5.11 Instruments and Equipment

Table 17: Instruments and Equipment utilized for experimental set ups.

Device	Manufacturer
Balance, 2.2 kg/ 1g	Kern & Sohn (Balingen, Ger)
Branson 450 Analog Sonifier with 1/2" Horn, 400 W, 240 VAC	New Balance Branson (Branson, MO, USA)
Biofuge Pico	Heraeus Deutschland GmbH & Co. KG (Hanau, Ger)
Biofuge Primo R refrigerated centrifuge	Heraeus Deutschland GmbH & Co. KG (Hanau, Ger)
Biometra TAdvanced Twin 48, 230 V	Analytik Jena GmbH+Co. KG (Jena, Ger)
Bio-rad power pac 300 biorad POWER SUPPLY electrophoresis 300v 195VA	Bio-Rad Laboratories, Inc (Hercules, CA, USA)
Bio-Rad Powerpac 3000 Power Supply	Bio-Rad Laboratories, Inc (Hercules, CA, USA)
BioWizard Silver Line Biosafety cabinet	Kojair Tech Oy (Mäntta-Vilppula, Fin)
CellXpert™ C170i, Segmented Inner Door, Oxygen Control	Eppendorf SE (Hamburg, Ger)
Centrifuge 5804 R, refrigerated 230V/50-60 Hz	Eppendorf SE (Hamburg, Ger)
CONC/VACUF, 48x2 ml ROTOR, 230V	Eppendorf SE (Hamburg, Ger)
Corning® LSE™ High Speed Microcentrifuge, 230V, UK Plug	Corning, Inc. (Corning, NY, USA)
CVC 3000 Vacuum pump	VACUUBRAND GMBH + CO KG (Wertheim, Ger)
DeNovix Nanodrop (DS-11+ µVolume Spectrophotometer with Cuvette)	Biozym Scientific GmbH (Hessisch Oldendorf, Ger)
Duomax 13030 shaker	Heidolph Instruments GmbH & Co. KG (Schwabach, Ger)
Electrophorese Power supply (EPS series)	Amersham Biosciences Europe GmbH (Freiburg, Ger)
GFL 3016 shaker	GFL Gesellschaft für Labortechnik mbH (Burgwedel, Ger)
Heracell™ VIOS 160i CO2 Incubator, 165 L	Thermo Fisher Scientific (Waltham, MA, USA)
HI 221 Benchtop pH-Meter w/ Calibration Check & mV / °C + electrode holder	HANNA instruments (Woonsocket, Rhode Island, USA)
Horizontal incubator shaker	Labwit Scientific (Melbourne, Australia)
Hybaid PCR Sprint Thermal Cycler SPRT001 Lab	Qiagen GmbH (Hilden, Ger)
Innova 4000 Benchtop Incubator Shaker	Eppendorf SE (Hamburg, Ger)
LAS3000 Imaging System	Fujifilm (Tokio, Japan)
Light Microscope WILOVERT S	Helmut Hund GmbH (Wetzlar, Ger)
LLG-uniVACUUSYS	LLG labware (Meckenheim, Ger)
Micro Plate Centrifuge, EU Version	Greiner Bio-One GmbH (Frickenhausen, Ger)
Microplate shakers, Variomag Monoshake and Teleshake	Thermo Fisher Scientific (Waltham, MA, USA)
Microwave	Samsung Electronics (Suwon-si, southern Corea)
Mixing Block MB-102	Bioer technology (Hangzhou, Japan)
Multichannel Pipette 8 – 100 µL	Eppendorf SE (Hamburg, Ger)
Ninolaf safety cabinet	biomedis Laborservice GmbH (Gießen, Ger)
Precision Balance scale A210P	Sartorius AG (Göttingen, Ger)
Pipetboy acu 2	INTEGRA Biosciences Deutschland GmbH (Biebertal, Ger)
Pipette Matrix Multichannel 16 – 125 µL	Thermo Fisher Scientific (Waltham, MA, USA)
Pipettes (1000 µl- 2.5 µl)	Eppendorf SE (Hamburg, Ger)
Protean Tetra Vertical Electrophoresis Cell	Bio-Rad Laboratories, Inc (Hercules, CA, USA)
Research Plus Multipipette M4	Eppendorf SE (Hamburg, Ger)
Simplicity® UV water purification system	Merck Millipore (Darmstadt, Ger)
Sprout Minifuge	Biozym Scientific GmbH (Hessisch Oldendorf, Ger)
Tecan (GENiosPro or SPARK)	Tecan group Ltd. (Männedorf, CHE)
Tilt/roller mixer RS-TR series model RS-TR 05	Phoenix Instrument GmbH (Garbsen, Ger)
Turboblot Trans-Blot	Bio-Rad Laboratories, Inc (Hercules, CA, USA)
VL-215.L UV lamp (wavelength 365 nm, 2x 15 W)	Vilber Lourmat Deutschland GmbH (Eberhardzell, Ger)
VWB2, Water Bath	VWR Life sciences (Darmstadt, Ger)

5.12 Consumables

Table 18: Consumables for experimental set ups.

Consumables	Manufacturer
12-Well empty cassettes	Bio-Rad Laboratories, Inc (Hercules, CA, USA)
96-well plates, transparent, flat bottom	Greiner Bio-One (Kremsmünster, Austria)
Amersham Protran® Nitrocellulose western blotting membrane (0.45 µm/ 0.2 µm)	Sigma Aldrich (St. Louis, MO, USA)
Amicon® Ultra-0.5ml centrifugal filter devices, 3K device	Merck Millipore (Darmstadt, Ger)
Amicon® Ultra-2ml centrifugal filter device, 10K device	Merck Millipore (Darmstadt, Ger)
Biosphere® Plus Pipette Tips (1000 µL/200 µL/10 µL)	Sarstedt Inc. (Nümbrecht, Germany)
Cell culture plate, 10 cm dish	Sarstedt Inc. (Nümbrecht, Germany)
Cell culture plate, 15 cm dish	Sarstedt Inc. (Nümbrecht, Germany)
Cell culture plate, 6 well, PS, flat bottom	Greiner Bio-One (Kremsmünster, Austria) Sarstedt Inc. (Nümbrecht, Germany)
Cell culture plate, 12 well, PS, flat bottom	Greiner Bio-One (Kremsmünster, Austria) Sarstedt Inc. (Nümbrecht, Germany)
Cell culture plate, 24 well, PS, flat bottom	Greiner Bio-One (Kremsmünster, Austria) Sarstedt Inc. (Nümbrecht, Germany)
Cell culture plate, 48 well, PS, flat bottom	Greiner Bio-One (Kremsmünster, Austria) Sarstedt Inc. (Nümbrecht, Germany)
Cell culture plate, 96 well, PS, flat bottom	Greiner Bio-One (Kremsmünster, Austria) Sarstedt Inc. (Nümbrecht, Germany)
Combi Tips advanced 0.5 mL	Eppendorf (Hamburg, Germany)
Combi Tips advanced 1 mL	Eppendorf (Hamburg, Germany)
Combi Tips advanced 1 mL (sterile, single blistered)	Eppendorf (Hamburg, Germany)
Combi Tips advanced 2.5 mL (sterile, single blistered)	Eppendorf (Hamburg, Germany)
Combi Tips advanced 5 mL	Eppendorf (Hamburg, Germany)
Combi Tips advanced 5 mL (sterile, single blistered)	Eppendorf (Hamburg, Germany)
Combi Tips advanced 10 mL	Eppendorf (Hamburg, Germany)
Combi Tips advanced 10 mL (sterile, single blistered)	Eppendorf (Hamburg, Germany)
Corning® 384-well Low Flange Black Flat Bottom Polystyrene NBS Microplate, 10 per Bag, without Lid, Nonsterile	Corning Inc. (Corning, NY, USA)
Gelloader pipette Tips 200 µL	Sarstedt Inc. (Nümbrecht, Germany)
Mobi Spin column "F" with fixed outlet plug, inserted 10 µm filter, 1 ml (#M105010S)	MoBiTec Molecular Biotechnology (Göttingen, Ger)
Mobi Spin column "F" with fixed outlet plug, inserted 35 µm filter, 1 ml (#M105035F)	MoBiTec Molecular Biotechnology (Göttingen, Ger)
Mobi Spin column "F" with fixed outlet plug, inserted 35 µm filter, 10 ml (#S10141)	MoBiTec Molecular Biotechnology (Göttingen, Ger)
Nitrocellulose membrane (40 and 20 dings)	Amersham Biosciences Europe GmbH (Freiburg, Ger)
Novex® Wedge well 4-20 % TRIS glycine	Bio-Rad Laboratories, Inc (Hercules, CA, USA)
Lo Binding conical tubes (15/50 mL)	Eppendorf (Hamburg, Germany)
Lo Binding reaction tubes (1.5 mL, 2 mL)	Eppendorf (Hamburg, Germany)
Pipette, Graduated 1/10 ML, Sterile (5 mL, 10 mL, 25 mL, 50 mL)	Greiner Bio-One (Kremsmünster, Austria) Sarstedt Inc. (Nümbrecht, Germany)
Pipette Tips (1000 µL/200 µL/10 µL) without filter	Sarstedt Inc. (Nümbrecht, Germany)
Protein LoBind® tubes (1.5 ml, 2 ml, 15 ml, 50 ml); conical	Eppendorf (Hamburg, Germany)
ProxiPlate-384 Plus, White 384-shallow well Microplate	Perkin Elmer (Waltham, MA, USA)
Reaction tubes (1.5 mL, 2 mL)	Sarstedt Inc. (Nümbrecht, Germany)
Serological pipettes (1 ml/5 ml/ 10 ml/25 ml/50 ml)	Greiner Bio-One (Kremsmünster, Austria) Sarstedt Inc. (Nümbrecht, Germany)
Trans-Blot Turbo Mini 0.2 µm Nitrocellulose Transfer Packs #1704158	Bio-Rad Laboratories, Inc (Hercules, CA, USA)
Whatman® Blotting paper 20x20 cm, extra thick (#88620)	Thermo Fisher Scientific (Waltham, MA, USA)

5.13 Software and databases

Table 19: Software and databases for data analysis and graphic presentation

Software	Application
ACD/ChemSketch (Freeware)	Drawing chemical structures
Biorender (https://www.biorender.com/)	Graphic presentation
ChemDraw Ultra12.0	Drawing chemical structures
Citavi 6.8.0.0	Reference management software
Expasy (https://www.expasy.org/)	Open source for calculation of chemical and physical parameters of proteins based on the amino acid sequence
GraphPad Prism 9.3.1	Data analysis, Graphic presentation
GO annotations (https://geneontology.org/)	Computational database to compare phosphoproteomic results with published literature in signalling pathways
Image-Reader 3000	Detection of ECL signalling of LAS-3000 imager (Fujifilm)
KEGG; Kyoto encyclopedia of genes and genomes (https://www.genome.jp/kegg/)	Computational database to compare phosphoproteomic results with published literature in signalling pathways
MaxQuant (Version 2.4.2.0)	MSMS Calculation
Microsoft Office 360	Data analysis, calculation, writing and figure editing
Perseus (Version 2.0.10.0)	MSMS Calculation and graphic presentation
PhosphoSitePlus® (https://www.phosphosite.org/homeAction.action)	Cell signaling technology, reference database of identified phosphosites
Pymol (Version 2.5.4.)	Graphic presentation and editing of protein structures
Serial Cloner	Editing of plasmid DNA, Tool for primer Design
SnapGene	Editing of plasmid DNA, Tool for primer Design
Uniprot (https://www.uniprot.org/)	Sequence analysis of secondary protein structures as well as database for crystal structures of proteins

6 Methods

6.1 Molecular biological methods

6.1.1 Preparation of competent E. coli BL21 DE3 and DH5α

5 mL sterile TYM medium were inoculated with a small amount of a glycerol stock containing e. *coli* BL21 DE3 or e. *coli* BL21 DH5a to prepare transformation-competent e. *coli*. TYM medium were incubated over night at 37 °C on a shaking platform at 250 rpm. On the next day, 250 mL TYM medium were inoculated with the overnight culture with a starting OD_{600} of 0.01. Cells were grown until OD_{600} reached 0.5-0.6 to harvest cells in the log phase. Cells were centrifuged at 2000 rpm for 15 min at 4 °C. Subsequently, the supernatant was removed, and the cell pellet was carefully resuspended in 50 ml ice cold TFB1 buffer. Afterwards, centrifugation was repeated. After the supernatant was removed, cells were resuspended in 15 ml TFB2 buffer and aliquoted (50 μL per transformation) and subsequently freeze in liquid nitrogen. Aliquots were stored at -80 °C in a freezer. Buffer conditions are listed in **Table 20**.

Table 20: Required medium and buffer for competent E. coli. All medium and buffer must be autoclaved prior utilization.

TYM medium	TFB1 buffer pH 5.0-6.0	TFB2 buffer pH 7.0
20 g/L tryptone 5 g/L yeast extract 0.1 M NaCl 10 mM $MgSO_4$ * 7 H2O	30 mM potassium acetate 0.1 M KCl 10 mM CaCl2 15 % (v/v) glycerine after autoclavation and sterile filtration 50 mM $MnCl_2$ * 4 H2O	10 mM MOPS 75 mM $CaCl_2$ 10 mM KCl 15 % (v/v) glycerine

6.1.2 Transformation

50 μL aliquots of competent e. *coli* were thawed on ice and 2 μL plasmid DNA were added and resuspended carefully. Cells were incubated on ice for 20 min and directly heat shocked at 42 °C for 45 sec. Cells were stored for 2 min on ice and 750 μL LB medium were added for regeneration. Cells were incubated at 37 °C for 1 h on a thermo shaker slightly shaking (500 rpm). Next, cells were harvested by short centrifugation (2min, 8000g) and resuspended in 200 μL LB medium to plate cells on agar plates containing corresponding antibiotics (e.g., 100 μg/ml ampicillin). Agar plates were incubated upside down at 37 °C overnight until single colonies were grown which then can be picked for further analysis.

6.1.3 Bacterial culture

5 ml LB medium were inoculated with single colonies after transformation and cultivated at 37 °C overnight. After incubation, 750 μL of cell culture were mixed with 750 μL 50 % (v/v) glycerol to receive bacterial glycerol stocks which were stored at –80 °C. Small amounts of bacterial glycerol stocks could be then further utilized to inoculate new bacterial cultures for e.g., plasmid DNA preparation.

6.1.4 DNA preparation and quantification

Plasmid DNA was prepared and purified utilizing either the FastGene Plasmid Mini Kit (Nippon®), Nucleobond AX Mega columns or Qiagen Plasmid Midi Kit according to the manufacturer's protocols. DNA which was generated during polymerase chain reaction (PCR) was purified utilizing FastGene Gel/PCR Extraction Kit. The DNA concentration was determined by DeNovix Nanodrop at 260 nm. At this wavelength, an OD=1 corresponds to 50 μg/ml double stranded DNA at pH 7.0. The ratio of A_{260}/A_{280} indicated protein contamination and the ratio of A_{260}/A_{230} indicated nucleotide contamination, ideally ranging from 1.8-2.0.

6.1.5 Polymerase chain reaction (PCR)

Polymerase chain reaction (PCR) is used to amplify defined DNA sections utilizing specific primers. Primers can contain either new restriction sites at 5' or 3'-ends. Moreover, they can be used to insert or delete nucleotides for mutagenesis. PCR can also be used to identify if ligation of plasmid DNA and inserts were successful in E. coli by utilizing specific primers for sequencing for 'colony' PCR. For PCR, Q5 Polymerase, and ingredients from New England Biolabs (NEB) were used following the manufacturer's protocol.

Table 21: PCR reaction components and running conditions standardized of New England Biolabs (NEB) protocol (2023)

PCR reaction components	PCR running conditions (standardized)		
	Step	Temperature	Time
5x Q5 reaction buffer 5 µL (in total 1x)	Initial Denaturation	98 °C	30s
5x Q5 High GC Enhancer 5 µL (optional, in total 1x)	25-35 cycles	98 °C	5-10s
10 mM dNTPs 0.5 µL (in total 200 µM)		50-72 °C	10-30s
10 µM Forward Primer (in total 0.5 µM)		72 °C	20-30 s/kb
Template DNA variable (< 1000 ng)	Final Extension	72 °C	2 min
Q5 High-Fidelity DNA Polymerase 0.25 µl (in total 0.02 U/µL)	Hold	4-10 °C	infinite
Fill up with Nuclease-Free Water up to 25 µL			

6.1.6 Agarose gel electrophoresis

To obtain, if amplification during PCR was successful, agarose gel electrophoresis was performed. To prepare an agarose gel, 1 % (w/v) Agarose was mixed with in an appropriate volume of 1x TBS buffer and boiled in a microwave until agarose is dissolved completely. The agarose solution is cooled down and 5 μl Midori Green® is added in 50 ml solution. Subsequently, the solution is casted in a tray for gel electrophoresis chamber and a comb was inserted. When the gel was cooled down, 5 μL of DNA samples were mixed with 5x purple loading dye (NEB) and filled into the gel wells when the comb was removed. In general, gel electrophoresis was performed at 120 V for 30 min to separate DNA fragments in the mix. For visualization of DNA fragments dyed with Midori Green, Agarosegel was irradiated by UV light (365 nm) in LAS3000 Imaging system.

6.1.7 Site directed mutagenesis (SDM) for SFC-FKBP12 mutant library

To examine the importance of specific residues in protein structure and function site directed mutagenesis (SDM) can be utilized to insert or delete mutations in double stranded DNA plasmids. For Mutagenesis, custom designed oligonucleotide primers were used. For amber suppression-mediated photo cross linkable FKBP mutants, triplets of nucleic acids were exchanged by TAG amber codon. Initially, e. *coli* expression plasmids were utilized to introduce TAG amber codon in the DNA sequence of FKBP12.

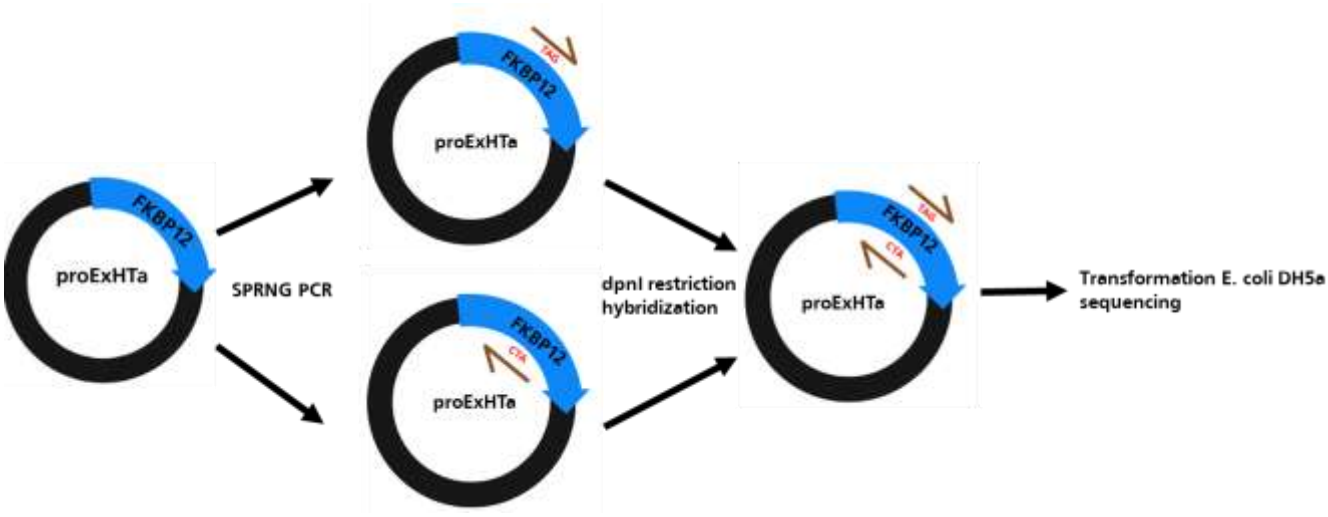

Figure 11: Scheme of site directed mutagenesis utilizing SPRINP PCR (single primer reaction in parallel) [212]. Bacterial modified expression vector pET (proExHTa) is utilized as template containing the sequence of FKBP12. (scheme by biorender.com)

SDM mutagenesis was performed utilizing the method of single primer reaction in parallel for PCR [212]. pET3.0b modified vector containing FKBP12 WT sequence was utilized in two reaction mixes whereas only the forward or reverse primer was added for PCR reaction mix (**Figure 11**). PCR was performed according to the protocol in **Table 22**. After PCR, the reaction mix was mixed in a ratio of 1:1 for

hybridization of both ssDNA plasmids. To start hybridization temperature is set to 95 °C. As hybridization continues, temperature is lowered to 37 °C over time to ensure, that both ssDNA plasmid fragments combine to one dsDNA plasmid. After hybridization, 1 μl dpnI was added at 37 °C for 5 hours to ensure restriction of template plasmid DNA as the enzyme recognizes methylation sites when plasmids are copied in e. coli DH5a. 5 μl of the reaction mix was further utilized for transformation of generated dsDNA plasmids in e. coli DH5a and plated on agar plates with the corresponding antibiotics and incubated overnight at 37 °C upside down. On the next day, colonies were picked and send to Microsynth for further sequencing to identify, if SDM has taken place.

Table 22: PCR reaction mix and protocol for site directed mutagenesis of FKBP12 mutant library.

PCR reaction mix		PCR protocol		
5x Q5 reaction buffer	5 µL (in total 1x)	1 initial denaturation	95 °C	5 min
10 mM dNTPs	2.5 µl	2 denaturation	95 °C	30 s
10 µM Primer (fwd/rev)	2.5 µl	3 annealing	60 °C	1 min
Template DNA variable	(< 1000 ng)	4 elongation	72 °C	5 min
Q5 High-Fidelity DNA Polymerase	0.5 µl	5 Hold	4 °C	infinite
Fill up with Nuclease-Free Water up to	50 µL			

6.1.8 Gibson Assembly

Gibson assembly is described as a robust exonuclease-based method under isothermal conditions to assemble DNA inserts into a linearized vector via 15-20 bp overlapping ends. The reaction takes place in a single-tube reaction mix according to the NEB Gibson Assembly Workflow (see https://international.neb.com/applications/cloning-and-synthetic-biology/dna-assembly-and-cloning/gibson-assembly; 09/08/2023).

6.1.9 DNA restriction

DNA can be cleaved at specific recognition sites into fragments by help of so-called restriction enzymes. Restriction enzymes are classified in five types, e.g., single site cutter or multiple site cutter. One unit of restriction enzyme can cut 50 μg of plasmid DNA in one hour in optimal conditions. Restriction enzymes and reaction buffers which were utilized in this thesis are provided by New England Biolabs (NEB®) and applied according to the manufacturer's protocol.

6.1.10 DNA ligation

To assemble DNA fragments into desired plasmids, T4 ligase with corresponding ligation buffers was utilized from NEB. Plasmid DNA and combining DNA fragments were previously digested by restriction enzymes to receive corresponding ligation sites at 5' and 3' ends. For Ligation, plasmid DNA and insert DNA were mixed in a ratio of 1:3 or 1:5. The reaction mix was mixed according to the manufacturer's protocol and the mix was either incubated at 25 °C for 20 min or incubated at 4 °C overnight.

6.1.11 DNA sequencing

To investigate successful transformation of plasmids which were utilized in SDM or restriction cloning, either bacteria colonies or purified plasmid DNA were prepared and send to Microsynth. The facility provides sequencing services with standardized primer sources or custom primers. The obtained results were compared to corresponding DNA sequences of desired proteins.

6.2 Protein biochemical Methods

6.2.1 Expression of proteins in e. *coli* BL21 DE3 by induction with IPTG

50 mL LB medium were inoculated with E. coli BL21 DE3 containing a bacterial expression plasmid and incubated on a shaking device at 37 °C overnight. For expression of proteins in e. *coli*, 3 litres of LB medium were inoculated with the overnight culture at $OD_{600} = 0.01$ and incubated at 37 °C on a shaking device (250 rpm). When OD600 reached 0.5-0.7 expression of proteins was induced by a concentration of 600 μM IPTG and either incubated at 37 °C for 3-4 hours or overnight at 25 °C. IPTG is an inducer by binding to a repressor and therefore triggers the transcription of the desired genes for protein expression. After incubation, cells were harvested by centrifugation at 4 °C for 15 min at 4.000g.

6.2.2 Purification of proteins from e. *coli* BL21 DE3 with different tags

After cells were harvest, cells were resuspended in lysis buffer (**Table 23**) at 4 °C on ice to ensure, that proteins will not degenerate. The lysate was incubated on ice for 30 min and treated with an ultrasound sonifier three times for 3 mins to break up membranes of e. *coli*. After sonification and inversion, cell lysate was centrifuged at 4 °C and 10.000 g for 30 min.

Recombinant Proteins which are expressed with a 6x Histidine-tag (His tag) were purified by Ni-NTA affinity chromatography. For purification 2 mL slurry can be utilized for 100 mg protein and the beads were equilibrated with lysis buffer. The lysate was added onto the column, allowing to flow through. Next, the resin bed was washed with washing buffer already containing imidazole to remove weak interaction with Ni-agarose beads (e.g., nucleic acids). Higher concentrations of imidazole help to elute desired proteins from the column as small volumes (1 ml) of elution buffer was added little by little and collected in 1.5 ml reaction tubes.

For recombinant proteins with a mono cysteine (FKBP12 and FKBP51 FK1) residue, 1 mM DTT was added in all buffers utilized for purification to ensure, that no oxidation took place at free cysteine residues.

For recombinant proteins which owned a GST-tag, GST ProCatch Sepharose beads were utilized for purification. For elution, 10 mM L-glutathione (reduced) was added freshly to replace recombinant proteins from Sepharose beads.

Samples of the flow through of each fraction as well as elution fractions were boiled in 4x Lämmli buffer and utilized for SDS PAGE gel and Coomassie staining to obtain, if purification and expression of proteins was successful. Elution fractions with the highest number of proteins were collected in 50 ml Dialyse Tubes and incubated on a stirrer overnight in dialysis buffer. The buffer was replaced frequently to remove e.g., imidazole. After two days, concentration of the protein solution was measured at the DeNovix Nanodrop by a defined extinction coefficient. Aliquots were prepared and frozen in liquid nitrogen for storage at – 80 °C.

Table 23: Buffers for purification of His- or GST- tagged recombinant proteins.

Lysis buffer	Washing buffer	Elution buffer	Storage/dialysis buffer
20 mM HEPES 300 mM NaCl 1x DNAse (20 mg/ml) 1x Lysozyme (20 mg/ml) 1 mM PMSF	20 mM HEPES 20 mM NaCl 40 mM Imidazole	His-elution buffer: 20 mM HEPES 20 mM NaCl 300 mM Imidazole Elution GST-buffer: 50 mM TRIS HCl pH 8.0 10 mM L-glutathione, reduced (fresh)	20 mM HEPES 20 mM NaCl For mono cysteine FKBPs add 1 mM TCEP (fresh prepared) 1 mM DTT (fresh prepared)

6.2.3 Immobilization of mono cysteine FKBPs on SulfoLink™ coupling resin

Recombinant proteins FKBP12 or FKBP51 FK1 possessing a mono cysteine residue on the surface on the opposite of the FK506-binding pocket were expressed and purified as described in **6.2.1** and **6.2.2**. As DTT was added in all buffers required for purification and storage, mono cysteine residues are presented in a reduced state. Thermo Scientific SulfoLink™ Coupling Resin was utilized which allows covalent immobilization of proteins with a sulfhydryl residue to the iodacetyl group of agarose beads (**Figure 12**). The 12-atom spacer arm should minimize steric hindrance and should ensure efficient binding interaction with the coupled proteins and interaction partners. As the mono cysteine resides on the back of the FK506-binding pocket, the covalent immobilization of FKBPs is site directed to ensure, that the binding pocket is available.

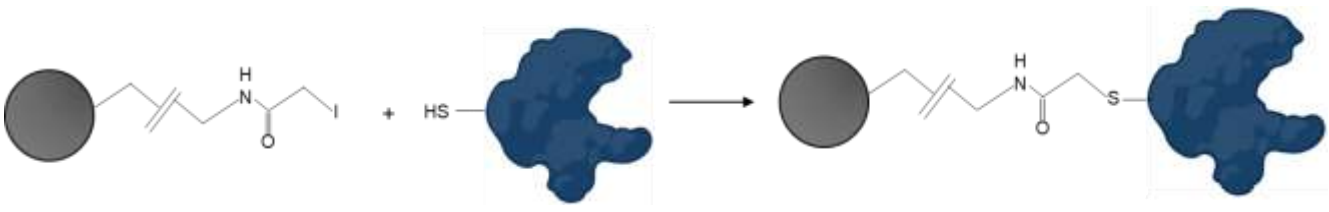

Figure 12: General scheme and structure of the coupling reaction of FKBP proteins (depicted in blue) by surface mono-exposed cysteine residue and Thermo scientific SulfoLink™ Coupling Resin (modified Manual Thermo fisher scientific (20402, 0527.3), Protein by Biorender.com

Initially, the volume of resin bed for coupling reaction was calculated by free iodacetyl groups of the agarose beads. In total, 19 μM free iodacetyl groups per ml resin were calculated which were required for one cysteine residue. For preparation, the column was washed with Millipore H_2O to prewet the filter. The resin bed was transferred (50 % slurry) onto the column and the flow through was discarded. The resin bed was equilibrated with coupling buffer pH 8.0 (10 CV).

For immobilization, mono cysteine FKBP12 or FKBP51 FK1 were added onto the resin bed in an appropriate amount, calculated by free iodacetyl groups and concentration of protein solution. The column is mixed by inverting or flipping, and the resin bed is allowed to settle for 5-10 min at room temperature. A sample is taken for further analysis of the immobilization process. Subsequently, the column is incubated for 1 hour on a rolling device. The resin bed is allowed to settle for 5 min and sample (1 h) is taken. The flow-through is allowed to pass the resin bed and the resin bed was washed four times with coupling buffer. For mock column, 1 mM β-mercaptoethanol was added to block the beads. To block the remaining free iodoacetyl groups coupling buffer prepared with β-Mercaptoethanol was added onto the resin bed and mixed by inversion. The column was incubated for 15 min at room temperature on a rolling device for 15-20 CV. Afterwards, the column was washed with coupling buffer (15-20 CV) and aliquots were prepared in protein low binding reaction tubes and stored at 4 °C.

6.2.4 Affinity Chromatography with immobilized FKBP proteins

The successful coupled recombinant FKBPs were utilized for site-directed affinity chromatography to investigate if ternary complexes of FKBPs chemically induced by molecular glues can be determined and evaluated. First, the column was washed with Millipore H_2O and the resin bed (either immobilized FKBPs or mock control) were added onto the column. The flow through was collected (sample storage buffer) to investigate loss of protein of the agarose beads. Equilibration buffer (2 CV) is added to equilibrate agarose beads. In the first step, natural molecular glues like Rapamycin were added onto the column in a 10-fold ratio compared to the resin bed to ensure equilibration of FKBPs and the molecular glue. Rapamycin, which was not interacting with the bait proteins was removed by rinsing the column (1.5 CV) with equilibration buffer. For affinity chromatography with purified proteins like GST-FRB, proteins were added onto the column in a ratio of 1:10 allowing the flow through to pass the resin bed. The flow through (sample flow through I) was collected and added onto the column twice (sample flow through II). To remove unbound GST-FRB, the columns were washed with equilibration buffer (5 CV) and samples were taken (samples wash fraction 1-5). The resin bed was subsequently removed and transferred to a 1.5 ml reaction tube and boiled with 4x Lämmli buffer to crack covalent binding of the potential ternary complex from Agarose beads (sample boiled beads). Samples were analysed by SDS PAGE gel and Coomassie staining. When HEK293T cell lysate was utilized for affinity chromatography in an excess, the washing steps prolonged up to 10-times to remove the whole proteome of the cells. Moreover, different experimental setups with incubation time of Rapamycin either alone or with HEK293T simultaneously were evaluated in the experimental design. For HEK293T lysate equilibration buffer was exchanged to NETN buffer. For FK[4.3.1]-16h competitive experimental setup, FK[4.3.1]-16h was added onto the column after 8 washing steps utilized in 5-10 equivalents to Rapamycin (sample

JK; **Suppl. 1**). To remove remaining FK[4.3.1]-16h or potentially ternary complexes, the resin bed was washed 2 times with equilibration buffer (sample JKW) (**Figure 13**).

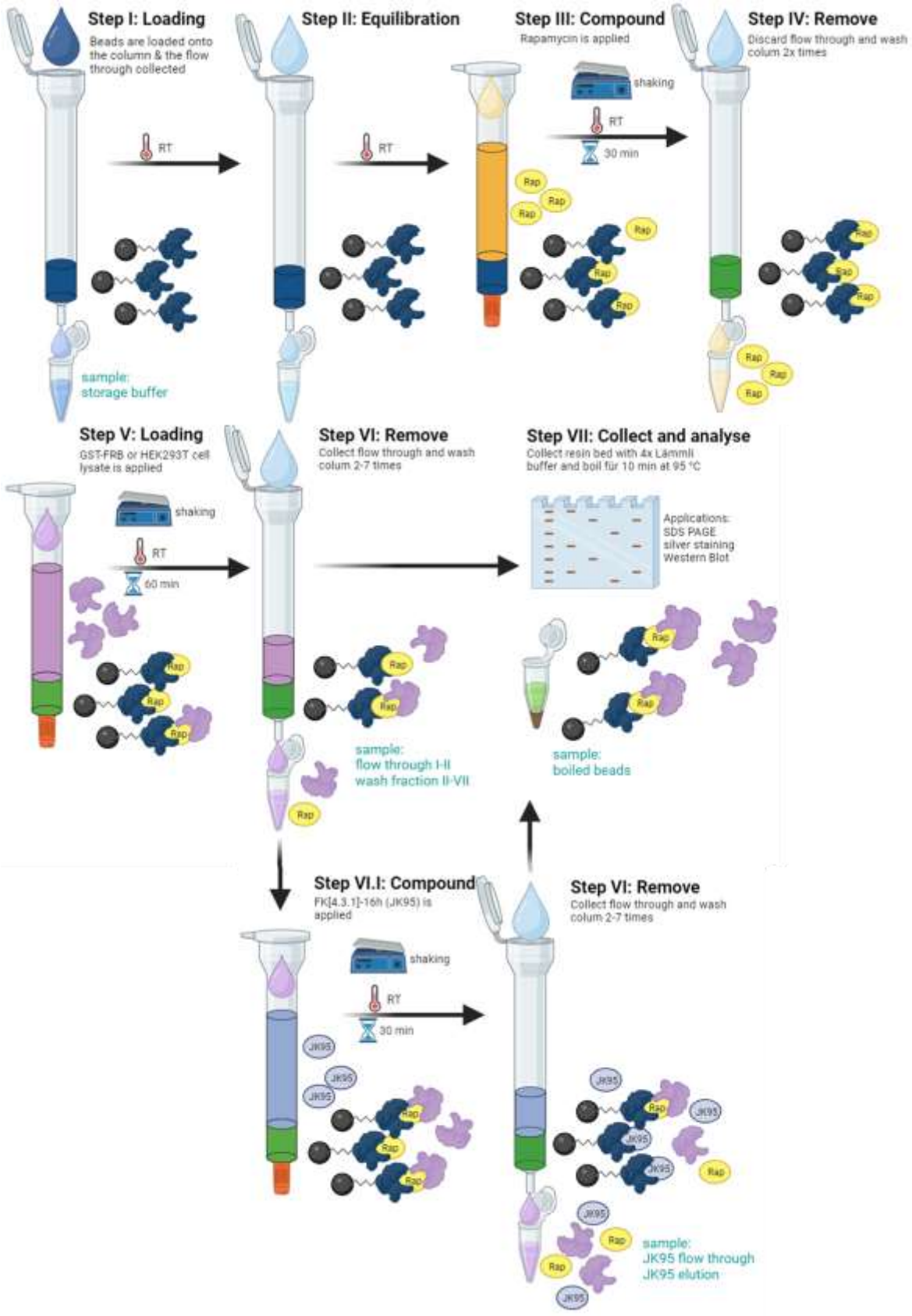

Figure 13: Experimental setup of affinity chromatography utilizing covalent coupled FKBP-bait proteins or the mock control as resin bed. Figure prepared by Biorender.com.

6.2.5 Sodium-dodecyl sulfate – polyacrylamide gel electrophoresis (SDS PAGE)

SDS PAGE is a useful tool to separate proteins based on their molecular weight. SDS binds to proteins and denature them, resulting in a negative charge by which proteins can be separated discontinuously in an electric field. Denatured proteins migrate through the SDS gel to the anode. Proteins with lower molecular weight migrate faster than those with high molecular weight [213]. The SDS gel was cast in 12-well empty cassettes (Bio-Rad). First, the separation gel was added into the cassette and isopropanol was added to remove air bubbles on top and prevent the separation gel from oxygen in the air and undesired reactions with the separation gel buffer. When the separation gel was dried, isopropanol was removed and stacking gel was prepared and added onto the separation gel (**Table 24**). Subsequently a comb was inserted, and the gel was allowed to try for at least 2 hours or overnight in a fume hood.

Table 24: Recipe for SDS PAGE gel. For example, separation gel (10%) is listed as well as stacking gel (4 %) for two gels.

Separation Gel (10%)		Stacking Gel (4 %)	
H_2O	4.1 mL	H_2O	6.1 mL
Acrylamide/bis (30% 37.5:1)	3.3 mL	Acrylamide/bis (30%, 37.5:1)	1.3 mL
Tris–HCl (1.5 M, pH 8.8)	2.5 mL	Tris–HCl (0.5 M, pH 6.8)	2.5 mL
SDS, 10%	100 µL	SDS, 10%	100 µL
N,N,N',N'-tetramethylethylene-diamine (TEMED)	10 µL	TEMED	10 µL
Ammonium persulfate (APS), 10%	32 µL	Ammonium persulfate (APS), 10%	100 µL

N,N,N',N'-tetramethylethylene-diamine (TEMED) and Ammonium persulfate (APS, 10%) were added at last as they induce radical formation and therefore starting the polymerization of the SDS gel.
Samples were boiled in a 1.5 ml reaction tube with 4x Lämmli buffer in a ratio 1:4 at 95 °C for 10 min to denature proteins. Reaction tubes were spinned down and samples were loaded onto the SDS gel after the comb was removed. The proteins were separated in Bio-Rad Chamber dings at 120 V, 400 mA and 100 W for 45-60 min. SDS gels were then further utilized for Western Blotting or Coomassie staining or silver staining.

6.2.6 Colloidal Coomassie staining

After gel electrophoresis, SDS gel is transferred into a tray and covered with colloidal Coomassie staining solution. SDS gel is incubated on a shaking device for at least 30 min or overnight. The gel is then washed with destain solution until protein bands were visualized and colouration is achieved. For storage, gels were transferred into a new tray with distilled H_2O. Buffers were prepared according to **Table 25**.

Table 25: Recipe for colloidal Coomassie staining solution and destain solution.

Colloidal Coomassie staining solution	Destain solution
0.1 % Coomassie R-250 (w/v)	10 % ethanol (v/v)
40 % ethanol (v/v)	7.5 % acetic acid (v/v)
10 % acetic acid (v/v)	

6.2.7 Short silver nitrate staining

Compared to colloidal Coomassie staining, silver nitrate staining is less fast when dying proteins, but it is 50-fold more sensitive. Silver nitrate staining can detect proteins in low nanomolar concentrations. Silver nitrate staining is also compatible with mass spectrometry (MS) and can therefore be a useful tool to detect protein-protein interactions in nanomolar concentration [214]. Buffers required for successful silver nitrate staining are listed in **Table 26**.

Table 26: Buffers required for short silver nitrate staining.

Fixation solution	Wash solution	Sensitizing solution (fresh)
30 % (v/v) ethanol 10 % (v/v) acetic acid	20 % (v/v) ethanol	0.8 nM $Na_2S_2O_3$ in MQ H_2O (Use 0.02 % (w/v) if Na-sulfate pentahydrate is used)
Impregnation solution (fresh)	Developer solution (fresh) 100 ml	Stop solution (fresh)
12 mM $AgNO^3$ in MQ H_2O	3 % (w/v) K_2CO_3 25 µL formalin 12.5 µL 10 % (w/v) $Na_2S_2O_3$ (dilute before use)	4 % (w/v) TRIS HCl 2 % (w/v) acetic acid

After electrophoresis, proteins in the SDS gel are fixed for 30 min in fixation solution. Next, SDS gel is rinsed with wash solution twice for 10 min. The gel was then transferred to MQ H_2O to remove the wash solution. To prepare fixed proteins for sensitization, the SDS gel was incubated for 1 min in Sensitizing solution and rinsed with MQ H_2O. For impregnation, one gel per tray was covered with impregnation solution for 20 min up to maximal two hours. The gel was then transferred to a new tray and developer solution is added. In this step, silver nitrate will be precipitated at the proteins surface. The precipitation as brown or grey colour. It should be ensured that the gels are shaking slightly on a shaking device otherwise a particular surface background will deposit the gel. To stop the precipitation process, the gel is transferred to a tray with stop solution for 30 min up to 2 hours. The stop solution removes excess silver nitrate ions and therefore ends the development before excessive background formation occurs.

6.2.8 Western Blot

Western Blot is a technique to transfer and immobilize proteins from SDS gels to nitro cellulose (NC) or polyvinylidene difluoride (PDFV) membranes by electrophoretic transfer. First, Whatman paper (2 mm) and nitro cellulose membranes were soaked in 1x Turbo Blot buffer (**Table 27**) for 5 min. Whatman paper is placed into the case of the Turbo Blot blotting chamber which act as cathode and nitro cellulose membrane is placed on top. Air bubbles were removed by help of a roller and SDS gel was transferred onto the nitro cellulose membrane. To cover and protect the SDS gel, another Whatman paper is placed between the gel and the lid, which function as anode. Proteins were blotted in a TurboBlot Blotter (Bio-

Rad) by 25 Volt, 1.2 A for 10-25 min depending on the size of proteins which should be blotted. Smaller proteins require less blotting time, than larger proteins.

Table 27: Buffer conditions for Semi dry Western Blot. Arrangement of Whatman paper, membrane and SDS gel in the Turbo Blot tray.

1x Turbo Blot buffer
5.8 g/L glycerine
5.8 g/L TRIS HCl
0.02 % (w/v) SDS
20 % (v/v) ethanol

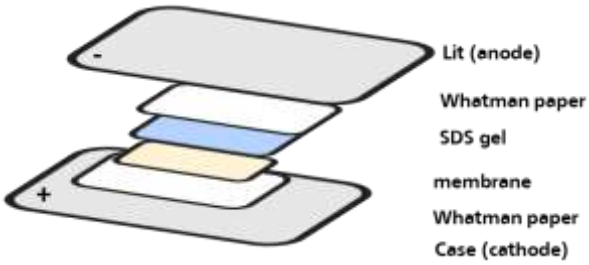

6.2.9 Immunostaining

Ponceau S solution: 0.02 % (w/v) Ponceau S, 3 % (v/v) acetic acid

The technique is used to determine the identity, size, and abundance of proteins after Western blotting. To investigate successful transfer and immobilization of proteins the membrane was incubated for 2 min in Ponceau S solution and then destained in distilled H_2O to an appropriate degree. When the transfer was successful, the membrane was further destained until Ponceau S was almost removed completely. The membrane is then blocked in 5 % milk powder (w/v) in 1x TBS overnight in a tray for at least 30 min or overnight at room temperature on a shaking device. To stain proteins with desired antibodies, either 5 ml of 5 % milk powder (w/v) in 1x TBS or 5 % BSA (w/v) in 1x TBS were utilized depending on the requirements of the antibodies. The membrane was incubated with primary antibodies at least 2 hours at room temperature or overnight. If secondary antibodies were used, the membrane was first removed from the primary antibody solution and placed into a new 50 ml falcon tube. Staining was performed over night at 4 °C on a rolling device.

Standard incubation concentration (or according to the manufacturer's protocol)

Primary antibodies: 5 ml antibody solution ratio 1:5000

Secondary antibodies: 5 ml antibody solution ratio 1:1000

6.2.10 Determination of protein concentrations by UV absorption

Amino acids tyrosine, phenylalanine and tryptophan are aromatic ring systems which have high electron density. When protein samples are irradiated with UV at a wavelength of 280 nm, proteins display absorption. The concentration of proteins can be calculated by Law of Lambert-Beer according to formula:

$A = \varepsilon * c * d$

A : absorption at 280 nm
ε : extinction coefficient e.g., of desired protein
c : path length (cuvette) in cm
d : protein concentration in M

To determine protein concentration extinction coefficient can be calculated based on the protein sequences, by using the web tool Expasy (https://web.expasy.org/protparam/).

6.2.11 Determination of protein concentrations by Bicinchoninic acid (BCA) Assay

A BCA assay is a colorimetric assay which relies on the formation of a Cu^{2+}-protein complex in a basic solution. The amount of Cu^{2+} reduced to Cu^{+} is proportional to the number of proteins which is present in the solution. Two molecules of BCA chelate to a Cu+ ion whereas the colour is changed from green to purple [215; 216]. The manufacturer Thermo fisher scientific indicates an assay range from 20 μg/ml to 2.000 μg/ml.

BCA protein assay as well as Rapid gold BCA protein assay was utilized to determine protein concentration. Rapid gold BCA protein assay is 100-fold times more sensitive than the traditional BCA protein assay. Samples were prepared following the manufacturer's instructions. The incubation time and measurement of absorbance differs in both assays.

BCA protein assay: Incubation 30 min at 37 °C, Absorbance 562 nm

Rapid gold BCA protein assay: Incubation 5 min at room temperature, Absorbance 480 nm

6.3 Protein assays

6.3.1 Active site titration (AST)

Salty FP assay buffer: 20 mM HEPES, 0.002 % Triton-X100, 150 mM NaCl, pH 8.0
Plate: corning (3575) black, 384 well flat bottom
Tracer: MTQ238 (bicyclic FKBP ligand and labelled with fluorophore 5-Tamra; **Suppl. 1**)

To investigate if purified FKBPs were folded correctly with an intact binding pocket of the FK1 domain for compound binding, an active site titration was performed utilizing fluorophore-containing tracer MTQ238. The binding of the tracer was determined by fluorescence polarization (FP) and the half-maximum of tracer bound to the FK1 domain.

The concentration of the protein stock solution was determined by UV concentration and diluted in salty FP assay buffer to a start concentration of 2 μM to 5 μM. 60 μl of protein solution was added in the 1st well of a 384-well assay plate in triplicate and dilution series of 1:1 was performed in 15 steps with salty FP-assay buffer (volume 30 μl). 10 μl of 4x tracer solution (200 nM) was added in each well with a final concentration of 50 nM. As control, salty FP-assay buffer was utilized. The 384-well assay plate was incubated for 15 min at room temperature slightly shaking on a mono shaker.

The fluorescence was measured with a TECAN GENios Pro or TECAN SPARK (Excitation 535 nm, Emission 590 nm, Gain optimum, integration time 40 μs, lag time 0 μs). EC50 and Hillslope were determined by sigmoidal, 4PL, X is log (concentration) in Graph Pad Prismn (https://www.graphpad.com/guides/prism/8/curve-fitting/REG_DR_stim_variable.htm).

The active-site concentration was then determined with following equation:

$$cAST = \left(\frac{cUV}{EC50}\right) * [\frac{cfinal(Tracer)}{2} + Kd(Tracer)]$$

cAST: Active site concentration of desired protein
cUV: Protein concentration determined by UV absorption at 280 nm
EC50: half maximal effective concentration of MTQ238
cfinal(Tracer): 50 nM
Kd(Tracer): Dissociation constant

6.4 Cell biological methods and cell-based assays

6.4.1 Cell lines and growth conditions

HEK293T wildtype and HEK293T FKBP12 knock-out cells were kept at 37 °C and 5 % CO_2 in a humidified incubator. Adherent cells were grown in TC 10 cm petri dishes in 1x DMEM supplemented with 10 % fetal calf serum (FBS) and 1 % penicillin-streptomycin (PS).

6.4.2 Maintenance of cells

When cells reached confluency, the cell culture was split. DMEM medium was removed from HEK293T cells and subsequently cells were washed with 1x PBS. After 1x PBS was removed, 1 ml trypsin/EDTA 0.02 % solution was added, and cells were incubated for 5 minutes at 37 °C. When cells were detached from TC petri dish, 10 ml 1x DMEM medium was utilized to resuspend and transfer cells into a 15 ml Falcon tube. The cell solution was centrifuged for 5 min at 2000 rpm and the supernatant was removed to get rid of the remaining trypsin/EDTA solution. Cells were resuspended in 5 ml 1x DMEM medium (10 % FBS/ 1 % PS) and counted with a Neubauer chamber to determine number of cells. For Maintenance, 200 μl cell solution was placed into a new TC petri dish with 10 ml fresh 1x DMEM (10 % FBS/ 1 % PS).

6.4.3 Cell counting

To set up an experiment, cells were counted in a Neubauer counting chamber (Marienfeld) after resuspension in 1x DMEM. 10 μl of cell suspension was mixed in a ratio of 1:1 with trypan blue. 10 μl was transferred to the Neubauer counting chamber and cells which were not coloured in blue were counted in 4 quadrants equal to 5.000 cells/ml cell suspension.

6.4.4 Cryopreservation of cell lines

For long term storage of cell lines, DMSO was utilized for cryopreservation. DMSO reduces damage to cells at freezing temperatures as the cryoprotectant migrates into the cells and avoids intracellular icing. 1x DMEM medium was supplemented with 10 % (v/v) sterile DMSO. Cells were transferred (1-5x10^5 cells/ml) into Cryo tubes and slowly frozen in a 1 °C cryo container which was filled with isopropanol to slowly cool down cell suspensions at -80 °C. After 48 h cryo tubes were stored in a liquid nitrogen tank.

When new cell culture is prepared, cells are thawed at 37 °C in a water bath. Cells are resuspended in 5 ml 1x DMEM (10 % FBS/ 1 % PS) and centrifuged for 3 min at 1500 g. The supernatant was discarded to get rid of the DMSO excess. Cells were then seeded in 10 ml fresh culture medium in a 10 cm TC petri dish.

6.4.5 Coating of cell culture dishes

Prior transfection, HEK293T cells were seeded into TC containing cell culture dishes for adherent cells in an appropriate number of cells. TC containing cell culture dishes were coated with poly-L-lysine solution (1:1000 in MQ H_2O) and incubated at least for 1 h or overnight at 37 °C and 5 % CO_2 in a humidified incubator. The solution was removed, and cell culture dishes were dried under a sterile fume hood and stored at 4 °C for further experiments.

6.4.6 Cell transfection

6.4.6.1 Transfection with Lipofectamine 2000 reagent

To introduce plasmid expressing mammalian proteins in HEK293T cells, lipofectamine as transfection agent was utilized. Lipofectamine packs plasmid DNA into lipid vesicles which then fuse with the phospholipid bilayer of eukaryotic cells. This procedure allows effective delivery of DNA into the cells as lipofectamine consists of polycationic lipids. According to the manufacturer's protocol, cells were transfected with plasmid DNA listed in **Table 28**.

Table 28: Required conditions for transfection of HEK293T cells with lipofectamine 2000 reagent according to the manufacturer's protocol (Thermo Fisher scientific)

	Surface area (cm²)	Cell number	1xDMEM medium	Plasmid DNA
10 cm petri dish	58.08	1.200.000	9 ml	8 µg
6-well cell culture plate	9.6	180.000	2.5 ml	2 µg
12-well cell culture plate	3.5	80.000	1 ml	800 ng
24-well cell culture plate	1.9	60.000	500 µl	400 ng

Plasmid DNA was solved in OptiMEM medium (100 ng/μl) and mixed in a ratio of 1:1 with lipofectamine solution (1/60 reagent in OptiMEM medium) after the solutions were incubated for 5 min at room temperature separately. The transfection mix was incubated for 20 min at room temperature. Initially, 1x DMEM medium was added onto the cells and the transfection mix was added carefully. Cells were incubated at 37 °C and 5 %CO_2 for 24-36 hours to ensure successful transfection and translation of desired proteins.

6.4.6.2 Transfection with polyethyleneimine (PEI)

An alternative reagent to Lipofectamine 2000 for delivering plasmid DNA into host cells is polyethyleneimine (PEI). PEI 'Max' is a stable cationic polymer which condenses DNA into positively chard particles that bind to anionic cell surfaces. The complex is endocytosed by the cells [217]. 1 g PEI is dissolved in 900 ml MQ H_2O and pH is adjusted to 7.0 with 1 M NaOH and solution is filled up to 1 ml. The solution is table up to 9 months at 4 °C. In general, 9 μg PEI 'Max' is diluted in a total volume of 150 μl OptiMEM whereas 3 μg plasmid DNA is utilized. The mixture is incubated for 30 min at room temperature and PEI-DNA mix is added carefully to each well of adherent cells. For a 10 cm TC petri dish, 22.5 μl PEI are utilized while for a 12-well cell culture plate 1.5 μl PEI were used according to the size of the surface area (see **Table 28**).

6.4.7 Incorporation of genetically encoded unnatural amino acids for photo probing *in-vivo*

Photo probing is a widely utilized tool when protein-protein interactions (PPI's) are studied *in-vivo*. By incorporation of non-canonical amino acids, the genetic code possessing 20 canonical aa can be expanded. Pyrrolysine (pyl) derives from the *Methanosarcinacea* family. Those methanogen archaea overwrite the TAG amber stop codon by incorporation of the unnatural amino acid (unAA) into the genetic code [218]. The incorporation of pyrrolysine requires an unique orthogonal tRNA-tRNA synthetase (RS) pair whereas the PylRS possess the corresponding CUA anticodon [219; 220]. 4-*para*-benzoyl-phenylalanine (pBpa) was first investigated for photo probing in e. *coli* DH10B [221; 222]. For incorporation of an unnatural amino acid (unAA) the media is supplemented with either 1 μM pBpa or 3'-azibutyl-*N*-carbamoyl-lysine (AbK) (**Figure 14**).

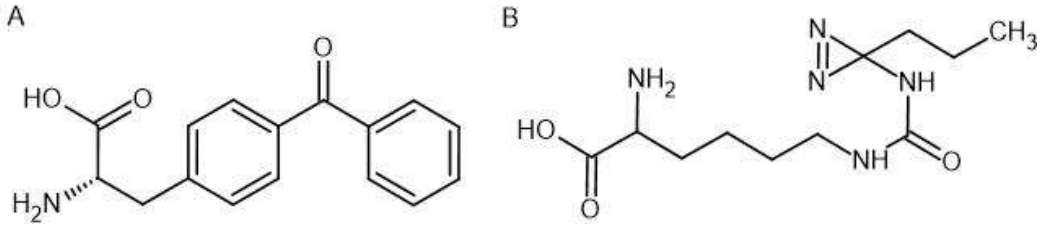

Figure 14: Chemical structure of common utilized photo-crosslinkers **A)** 4-*para*-benzoyl-phenylalanine (pBpa) and **B)** 3'-Azibutyl-*N*-carbamoyl-lysine (AbK).

HEK293T cells were co-transfected with two plasmids containing **(i)** a genetically modified sequence of FKBP51 or FKBP12 and **(ii)** an orthogonal tRNA synthetase according to chapter **6.4.6** in a ratio 1:1 and incubated for 24-36 hours at 37 °C and 5 % CO_2 in a humidified incubator henceforth treatment.

6.4.8 Stimulation, treatment, and lysis of mammalian HEK293T cells

After HEK293T cells were transfected and incubated 24-36 h at 5 % CO_2 in a humidified incubator the media was removed, and cells were washed with 1x PBS. DMEM 1x was supplements with 1 μM Rapamycin, FK506 or Anta B (or DMSO as control) for treatment with the natural products. The supplemented was added and cells were incubated for 30 min at 5 % CO_2 in the humidified incubator. Subsequently, cells were washed with 1x PBS after the medium was removed and either an appropriate volume of NETN buffer or 1x PBS for UV treatment was applied. UV irradiation of cells was performed for 30 min on ice with a VL-215.L UV lamp without the lid. Thereafter, 1x PBS was removed and cells and lysis buffer were added.

Lysis buffer was added, and cells were incubated on-ice slightly shaking up to 1 h to solubilize cellular and nuclear membranes utilizing the detergents Nonident P-40, SDS and sodium deoxycholate depending on either NETN or RIPA buffer. While NETN buffer is widely used for mild conditions, RIPA buffer possess harsher detergents. The lysate was spun down for 3 min at 10.000 g to separate insoluble components. The supernatant was transferred to a 1.5 ml reaction tube and or subsequently utilized as sample for e.g., SDS PAGE and pulldown affinity. Samples were stored at 4 °C in a fridge. For long term storage at -80 °C reaction tubes containing the samples were frozen in liquid nitrogen.

Buffer recipes:

NETN buffer: 100 mM NaCl, 20 mM TRIS-HCl (pH 8.0), 0.5 mM EDTA, 0.5 % (v/v) Nonident P-40.

RIPA buffer: 150 mM NaCl, 50 mM Tris-HCl (pH 8.0), 1 % (v/v) Nonident P-40, 0.1 % (v/v) SDS (10 % w/v), eventually 0.5 % sodium deoxycholate (10 % w/v)

6.4.9 Co-immunoprecipitation with M2 magnetic FLAG® beads

The FLAG tag is a protein modification which allows detection of protein in immunostaining as well as the utilization of the FLAG-tagged protein as bait in pulldown experiments. Magnetic beads are composed of a murine derived anti-FLAG® M2 monoclonal antibody attached to superparamagnetic iron impregnated 4 % agarose beads (manufacturer Sigma Aldrich®; *M8823*). HEK293T cell lysate was applied as recommended by the manufacturer's protocol. 3x FLAG peptide was utilized to compete FLAG tagged proteins from the resin bed (see technical bulletin, Sigma Aldrich®).

6.5 Sample preparation for mass spectrometry analysis

To identify protein-protein interactions mass spectrometry analyses were provided by EMBL Heidelberg (Frank Stein and Per Haberkant) and Dr. Marina Hoffmann in the research group of Prof Dr. Ivan Dikic at the Institute of Biochemistry II (IBC2) of the Medical Faculty of Goethe University Frankfurt.

6.5.1 In-Gel digest of proteins separated by SDS PAGE

For the identification of potential covalently coupled proteins utilizing FKBP51pBpa and FKBP12pBpa mutants in photo probing large scale experiments following magnetic FLAG affinity pulldown were performed. After purification, affinity pulldown and evaporation samples were applied onto a SDS gel and SDS PAGE was performed. Thereafter, the SDS gel was stained with Coomassie brilliant blue (15-20 min). Buffers were prepared with MQ H_2O and SDS gel was protected from direct contact to minimize contamination. As keratin and remaining Coomassie and detergents like SDS can cause problems in proteomic analyses, all tools and surfaces were kept clean. All buffers were set fresh prepared with MS-grade solvents.

The desired protein bands were cut out of the SDS gel and cut into small pieces and subsequently transferred into a LoBind 1.5 ml reaction tube. All samples were shaking on a thermomixer at 37 °C and 500 rpm. The pieces were washed three times for 10 min with 200 μL 50 mM ammonium bicarbonate (ABC)/ 40 % acetonitrile (ACN) until the gel pieces were clear. Subsequently, the pieces were dehydrated for 10 min in 150 μl 100 % ACN. Acetonitrile was removed and pieces were dried for at least 10 min until the gel pieces were white. Trypsin is a serine protease with high cleavage specificity by hydrolysing peptide bonds after a carbonyl group followed by arginine (Arg) or lysine (Lys) which promotes the homogeneity comparing peptide fragmentation spectra against sequence databases [223]. 10 μl trypsin (12.5 ng/μl) in 50 mM ABC was added to the gel pieces continuing swelling the pieces for at least 30 min at 4 °C without shaking allowing trypsin to effectively penetrate the gel pieces. Subsequently 25 μl 50 mM ABC was added and samples were incubated at 37 °C overnight on a thermo shaker. For peptide extraction 50 μl 50 % isopropanol/ 0.5 % TFA was added, and samples were incubated 30 min shaking. The supernatant was transferred into a new protein LoBind tube and 40 μl 50 % isopropanol/ 0.5 % TFA was added. The supernatant was transferred in the LoBind tube and 20 μl isopropanol/ 1 % TFA was added onto the gel pieces for 10 min on a shaker before pooling the supernatant in the new protein LoBind tube.

Protein purification was performed utilizing SDB-RP-StageTips. All centrifugation steps were performed at 4 °C and 3500 g until the sample has passed. When the sample was completely centrifuged, 200 μl ISO/ 1 % TFA was added, centrifugation was repeated. Next, 200 μl 0.2 % TFA in MQ H_2O was added and centrifugation repeated. Proteins were eluted with 50 μl 80 % ACN/ 1.25 % ammonia/H_2O/ACN. Thereafter, samples are evaporated to dryness at 60 °C for approx. 30-40 min. Dried peptides were stored at -20 °C until measurement. Samples were either prepared by tryptic digest or Coomassie stained SDS gels were directly send to EMBL for mass spectrometry and computational analyses.

7 Results and Discussions

7.1 Antascomicin B is acting as a molecular binder for FK506-binding proteins

7.1.1 Fluorescence Polarization assays reveals binding effect of Antascomicin B

Antascomicin B shares the same pipecolate domain as Rapamycin and FK506, which is interacting with the FK506-binding pocket of FKBPs (**Figure 4**) In a fluorescence polarization assay (preparatory work by Wisely Oki Sugiarto, RG Hausch), the interaction of Antascomicin B with the FK506-binding pocket was investigated. Rapamycin as established FKBP-interacting molecule was utilized as control to compare Antascomicin B's effect. The results of the FP assay are described in **Table 29**.

Table 29: Antascomicin B is acting as a molecular binder for FKBPs. The half maximum binding capacity of FKBPs is described as K_D value in nM in a table for FKBP51 FK1, FKBP52 FK1, FKBP12.6 and FKBP12 for each compound, respectively. Fluorescence polarization assay was performed in a triplicate (**Suppl. 2**).

	K_D values in [nM]			
	FKBP12	FKBP12.6	FKBP51FK1	FKBP52FK1
Antascomicin B	0.03 ± 0.006	0.38 ± 0.06	6.7 ± 0.4	1.2 ± 0.1
Rapamycin	0.13 ± 0.02	0.6 ± 0.08	8.5 ± 0.8	12 ± 1.5
FK506	0.20 ± 0.02	1.49 ± 0.34	75.93 ± 4.3	149.7 ± 16.5

Rapamycin is already known to interact as a molecular binder to several FKBPs in nanomolar affinities [139]. Utilizing Antascomicin B revealed lower K_D values for each FKBP in a nanomolar range respectively, while the natural product had a 10-times higher affinity to FKBP52 FK1. As suggested by Fehr *et.* al, Anta B is acting as an antagonist of Rapamycin resulting in a non-immunosuppressive competing effect [116]. To further unravel the mechanism of action of Anta B as molecular binder, the co-crystal structure of FKBP51 FK1 and Anta B was investigated by Andreas Voll and Andreas Bracher.

7.1.2 Co-crystal structure of the FKBP51 FK1 domain and Antascomicin B

Crystallography is an established technique to obtain crystal structures of protein-ligand complexes. Experimental set up and implementation of the co-crystal structure of FKBP51 FK1 and Anta B was performed by the preparatory work of Andreas Voll (RG Hausch) and Andreas Bracher (MPI of Biochemistry, Planegg-Martinsried). Anta B was depicted in white, while the FKBP51 FK1 domain was highlighted in dark red. Involved amino acids are presented in blue (**Figure 15**).

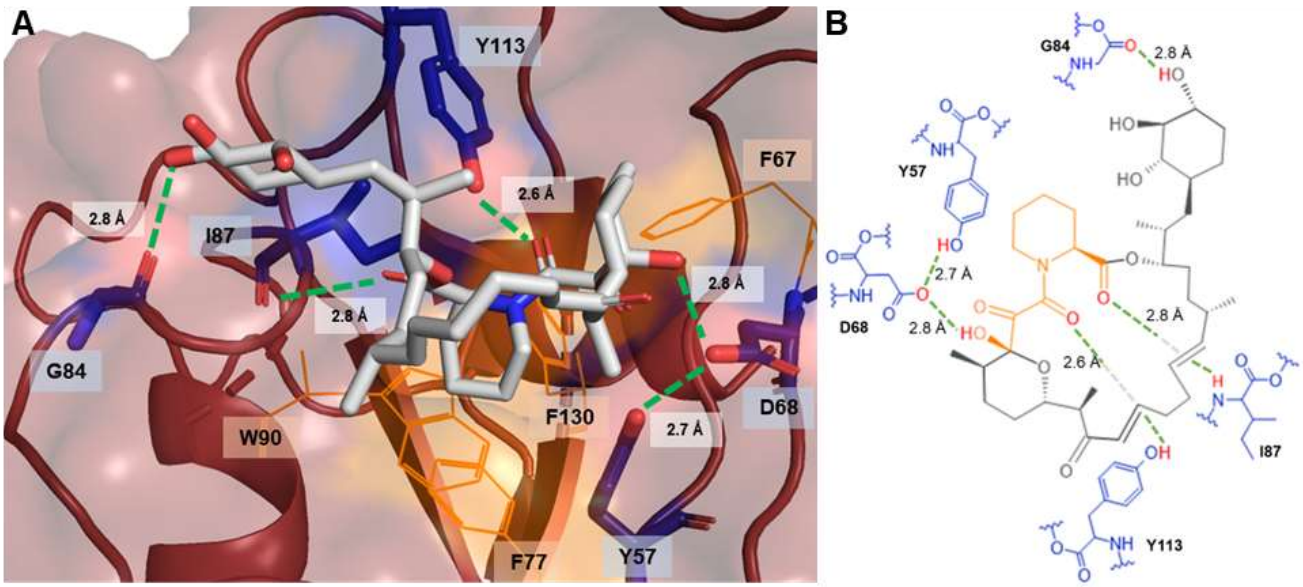

Figure 15: Cocrystal structure of Antascomicin B in complex with FKBP51 (dark red cartoon, PDB: 8r5k). (A) The pipecolate core of Antascomicin B (white sticks) interacts with the hydrophobic pocket of the FK1 domain of FKBP51 (orange lines). The key interacting amino acids are highlighted as blue stick and hydrogen bonds are visualized green dotted lines. **(B)** 2D-scheme of the Antascomicin B-FKBP51. Hydrogen bonding amino acids are shown in blue and hydrogen bonds with the distance between corresponding atoms in Angstrom are represented as green dotted lines.

The hydrophobic pocket consists of three phenylalanine residues, Phe67, Phe77, and Phe130 respectively as well as Trp90 in the centre (**Figure 15A**, depicted in orange) [99] . Amino acid residues Tyr57, Ile87 and Tyr113 stabilize the lactam moiety and adapt the natural product to the FKBP51 FK1 domain with an ideal distance of 2.8 Å. Donor and acceptor of hydrogen bonds normally have a length of 2.6-3.3 Å [224]. As Gly84 forms an additional hydrogen bond to the hydroxyl group of the cyclohexane moiety in the same range, the motif is likely to be more stabilized which may explain lower KD values obtained in the fluorescence polarization assays (**Table 29**). In a 2D-scheme Antascomicin B is shown with involved amino acid residues of FKBP51 FK1 forming hydrogen bonds with the compound (**Figure 15B**). Tyr57 is hydrogen bound to Asp 68, which can then interact with the hydroxyl group of the acetal ring in the macrolide moiety of Antascomicin B with a distance of 2.8 Å. Residues Ile87 and Tyr113 of the FKBP51 FK1 domain also interact with the macrolide moiety in the same range of 2.6-2.8 Å. Amino acid G84 directly interacts with its oxygen residue with a distance of 2.8 Å to the hydroxylated cyclohexane motif of the top group of Antascomicin B. This interaction is not observed in the crystal structure of FKBP51 FK1 and FK506 (**Figure 15B**).

The interaction of Antascomicin B to the FKBP51 FK1 domain was compared to FK506 and Rapamycin as each natural product consist of a pipecolate core which is interacting with hydrophobic amino acids within the binding pocket of the FK1 domain (**Figure 16**). The surrounding amino acids of the FK1 domain which participate in the interaction to the molecular binders were described in **Table 30**.

Table 30: The pipecolate domain of Antascomicin B acts in a similar mechanism of action of hydrophobic interactions with the FK1 domain of FKBP51 compared to Rapamycin and FK506 comparing their distances in Angstrom.

Residue (aa)	Antascomicin B	Rapamycin	FK506
Y57	2.7 Å, to D68	2.8 Å, to D68	2.7 Å, to D68
D68	2.8 Å	2.7 Å	2.7 Å
G84	2.8 Å	2.8 Å	water mediated
Q85	water mediated	2.6 Å	3.5 Å
I87	2.8 Å	2.9 Å	2.9 Å
Y113	2.6 Å	2.6 Å	2.6 Å

According to the co-crystal structure of FKBP51 FK1 and Rapamycin, the molecular glue is interacting with D68, G84, Q85, I87 and Y113 while Y57 serves as hydrogen bond to D68 (**Figure 16A**). Side chains of amino acids are pH sensitive possessing either positive or negative charges dependent on their p*K* value. In case of Y57 the amino acid is positively charged due to a negative inductive effect at the oxygen atom by D68 as tyrosine are likely to be uncharged at a physiological (pH 7), while aspartates are likely to be charged. In general the average of ionizable side chains of amino acids were found to be approx. at 29 % contributing in the stability and function of proteins [225; 226]. When FK506 is interacting with the FKBP51 FK1 domain residue G84 does not engage with the macrolide backbone. Moreover, glutamine at position 85 has a water-mediated distance of 3.5 Å compared to the distance of 2.6 Å of the Rapamycin backbone considering the interaction as Van-der-Waals bond with non-ionic character (**Figure 16B**). Compared to FK506, Antascomicin B shares a hydrogen bond to G84 in the same distance of 2.8 Å as Rapamycin, while the water-mediated interaction to Q85 has not taken place (**Figure 15**; **Table 30**).

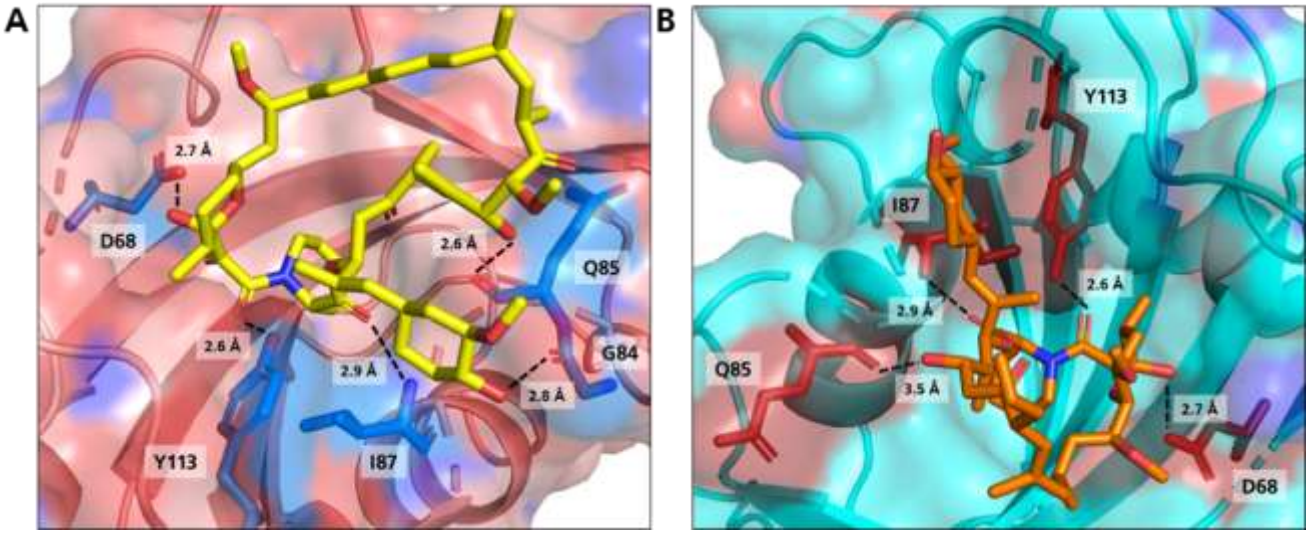

Figure 16: The pipecolate domain of FK506 and Rapamycin is interaction with the hydrophobic pocket of FKBP51 FK1. A) Rapamycin is depicted in yellow and corresponding amino acid residues D68, G84, Q53 I87 and Y113 are highlighted in light blue. Cartoon ribbon of FKBP51 FK1 is coloured in red. Interaction of the amino acid is described in Å (**PDB: 4DRH**, [227]). **B)** FK506 depicted in orange is interacting with amino acid residues D68, I87 and Y113 through hydrogen bonds (coloured in dark red). Residue Q85 has a range of 3.5 Å, which is considered as van der Waals interaction to the oxygen of FK506. Cartoon ribbon of FKBP51 FK1 is depicted in light blue (**PDB: 3O5R**, [19]).

While the interaction of FKBP12 and FK506 to calcineurin is well established, no interaction partner of FKBP51 and FK506 is known so far except that FK506 stimulates the association of FKBP51 with GRβ because of conformational changes within the FK1 domain of FKBP51 [138; 228]. The macrolide moiety of Rapamycin is structurally larger and different compared to FK506 and Antascomicin B. The natural product chemically induces ternary complex formation of either FKBP12 or FKBP51 with the FRB domain of mTOR leading to inhibitory downstream effects of mTORC1 [229]. This can be explained by an alternative stabilization and conformal changes of the PPIase binding pocket of FKBP51 FK1. The macrolide moiety of FK506 and Anta B is more similar compared to Rapamycin (**Figure 17**).

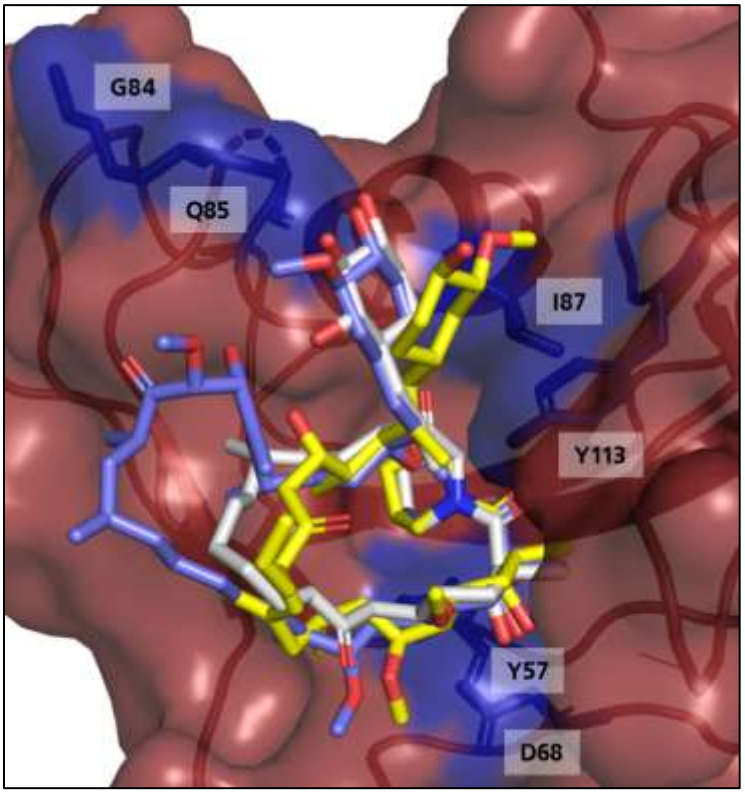

Figure 17: Merged co-crystal structure of the natural products Rapamycin, FK506 and Antascomicin B and FKBP51 FK1. The macrolide moiety of Rapamycin (violet) differs from the structures of FK506 (yellow) and Antascomicin B (white). Corresponding amino acids of the FK1 domain are named and highlighted in blue (Y57, D8, G84, Q85, I87, Y113). Merged structure of PDB 8r5k with 3O5R and 4DRH).

The hydroxylated cyclohexane moiety of FK506 is orientated more likely to residue I87 while the moiety of Anta B and Rapamycin is directed towards G84. As Rapamycin possesses an additional CH_3 group the compound can interact with Q85 while the additional hydroxyl group within the already hydroxylated cyclohexane of Anta B does not induce hydrogen bonds to the surrounding amino acids (**Figure 17**).

Taken together, the binding mechanism of Antascomicin B is more similar with FK506. FK506 shows strong immunosuppressive effects *in-vivo* and it's closely related derivate FK520 (Ascomycin) also requires FKBP12 as a binding partner to inhibit calcineurin. Interestingly, the exchange of an allyl to ethyl group at the C21 position led to lower immunosuppressive effects [230; 231]. As a binding partner for FKBP51 FK506 was found to stimulate the association of FKBP51 and GRβ but it could be suggested that FKBP51:FK506 might address additional target proteins [138; 228]. In case of Antascomicin B no literature is known which describes the potential to chemically induce protein-protein interactions of either FKBP12 or other FKBPs with other cellular proteins. As the natural product is acting as a molecular binder like Rapamycin and FK506 for FKBPs the possibility to function as a molecular glue is given.

7.2 Pulldown experiments with recombinant HsFKBPs to decipher Protein-Protein-interactions (PPI's)

7.2.1 Ternary complex formation of FKBP51 FK1 and FRB domain (mTOR) by Rapamycin utilizing site-specific affinity chromatography

Mono cysteine HsFKBP12 and HsFKBP51FK1 were utilized as bait proteins by iodoacetamide coupling and utilized for affinity chromatography to investigate if a ternary complex of FKBPs and the FRB domain of mTOR can be chemically induced by the natural molecular glue Rapamycin (**Chapter 6.2.3**). In a first attempt, the bait protein FKBP51FK1 and Rapamycin were present in an equimolar amount and purified FRB domain tagged with a GST tag was then added onto the column and allowed to flow through the resin bed. To remove unbound GST-FRB, several washing steps were performed. As the bait protein was covalently coupled, the resin bed was boiled in 4x Lämmli buffer after treatment to remove proteins from the resin bed for further SDS PAGE analysis. To confirm that Rapamycin and GST-FRB were not interacting with unsaturated agarose beads, a mock control was utilized. In this control, the resin bed was only blocked by β-mercaptoethanol, and no specific binding of HsFKBP51 FK1 or the ternary complex was expected (**Figure 18**).

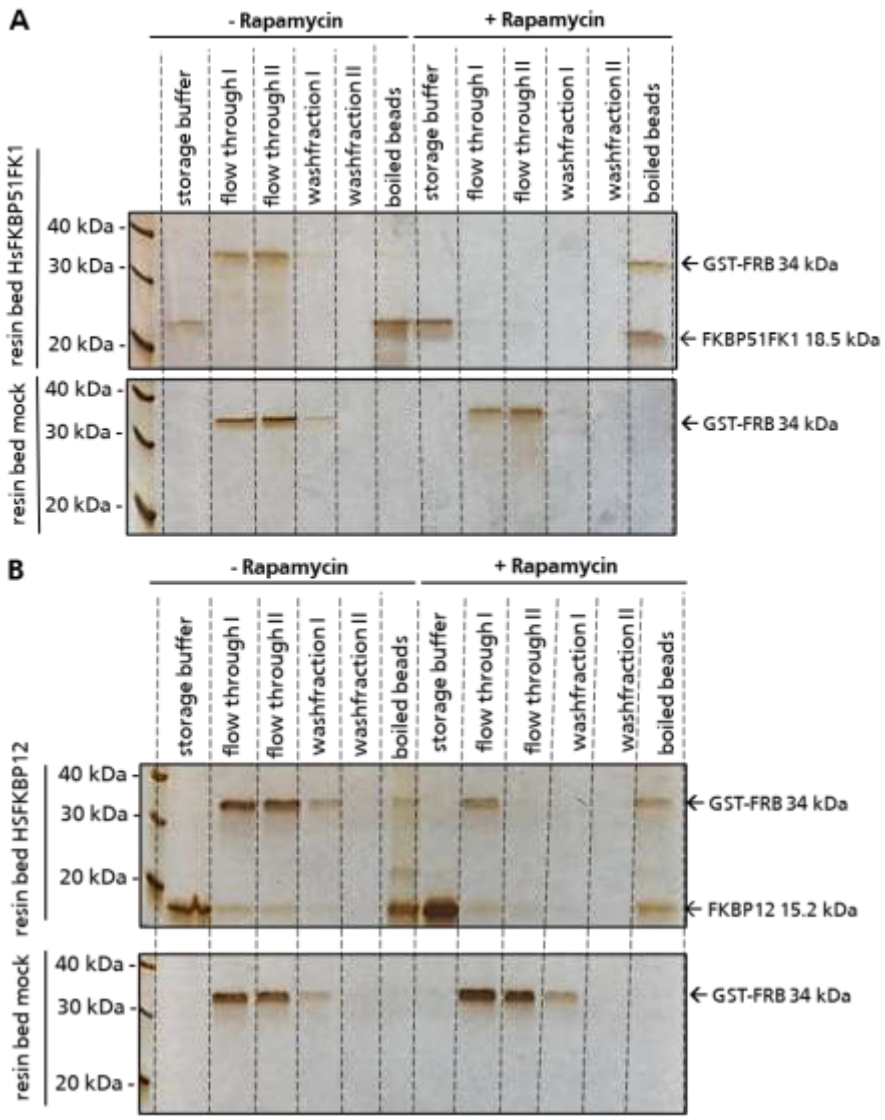

Figure 18: SDS PAGE and silver staining of ternary complex formation of FKBP51 FK1:Rapamycin:GST-FRB. A) Bait protein FKBP51 FK1 and mock control. Storage buffer: FKBP51 FK1 bait protein; flow through I-II: GST-FRB was applied onto the resin bed two times to allow completely saturation of the FKBP51 FK1 bait proteins; wash fraction I-II: uncoupled GST-FRB was removed in several washing steps; boiled beads: FKBP51 FK1 domain bait proteins and the potential ternary complex were boiled in 4x Lämmli buffer. Blocked agarose beads by β-Mercaptoethanol were utilized as resin bed mock control. **B) Bait protein FKBP12 and mock control**. Storage buffer: FKBP12 bait protein; flow through I-II: GST-FRB was applied onto the resin bed two times to allow completely saturation of the FKBP12 bait proteins; wash fraction I-II: uncoupled GST-FRB was removed in several washing steps; boiled beads: FKBP12 domain bait proteins and the potential ternary complex were boiled in 4x Lämmli buffer. Blocked agarose beads by β-Mercaptoethanol were utilized as resin bed mock control.

In the experimental setup, the first lane involved the utilization of FKBP51 FK1 bait protein, which had been stored in a storage buffer. This step ensured that the protein was still present on the resin bed while loss of protein due to the proteins biochemical properties is acceptable. As a control, the resin bed mock control did not exhibit any observable protein. GST-FRB was added to the columns, resulting in flow-through lanes labelled I-II (**Figure 18A**; resin bed HsFKBP51FK1 and resin bed mock). When the resin bed of HsFKBP51FK1 was saturated with Rapamycin, no GST-FRB was detected in the collected flow-through. In contrast, in the absence of Rapamycin treatment or in the resin bed mock control, GST-FRB

completely flowed through the column. Following the addition of GST-FRB onto the column, the resin beds were washed multiple times with a washing buffer to remove any unbound GST-FRB. When the resin bed of HsFKBP51FK1 was treated with Rapamycin, the presence of GST-FRB was clearly observed after boiling the beads, indicating the formation of the ternary complex FKBP51 FK1:Rapamycin:GST-FRB. In contrast, the resin bed mock column did not exhibit any detectable GST-FRB, serving as a control to confirm that the resin bed itself did not interfere with the detection of GST-FRB. When FKBP12 was utilized as bait protein, GST-FRB was found in both lanes of the boiled beads (**Figure 18B**). While GST-FRB was found to be absent in the flow through II lane upon treatment with Rapamycin, the protein was still present in the flow through II or wash fraction I indicating, that FKBP12 as bait protein influences protein-protein interactions as it features 'stickier' surface than FKBP51 FK1. However, the ratio of HsFKBPs and Rapamycin is sufficient to induce ternary complex formation with GST-FRB without loss of protein in the flow through. To investigate, whether site-specific covalent affinity chromatography is a useful tool to investigate unknown protein-protein interactions of FKBPs and POI induced by natural molecular glues, the approach was adapted utilizing HEK293T lysate.

7.2.2 Affinity chromatography of mono Cysteine HsFKBP12 and HsFKBP51 FK1 and HEK293 lysate

To investigate the maximum binding capacity of HsFKBPs and HEK293T lysate, FKBP12 bait proteins were utilized for affinity chromatography considering that the boiled bead fraction was not overloaded by the whole proteome. As HEK293T lysate was utilized, more washing steps with NETN buffer were applied to ensure, that unbound proteins were removed (**Figure 19**).

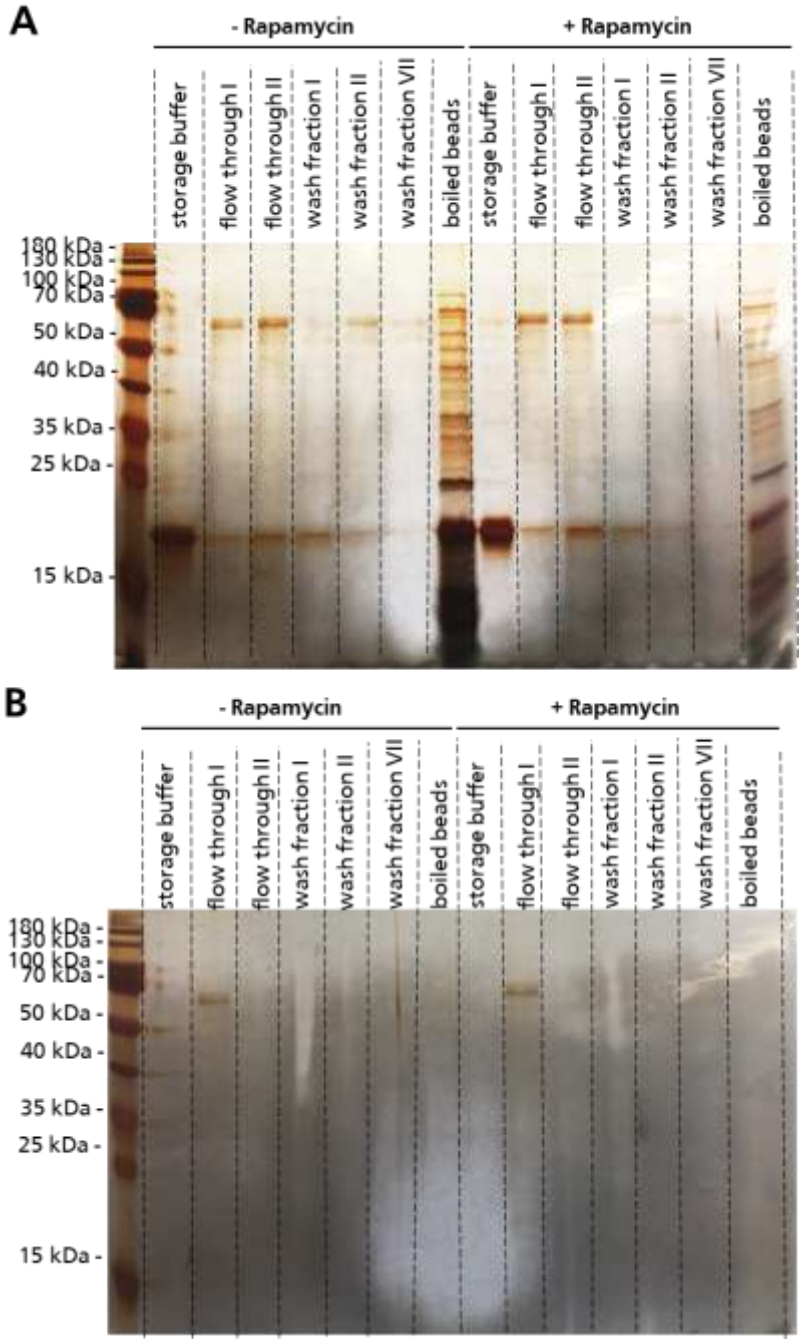

Figure 19: SDS PAGE and silver staining after HEK293T lysate was added onto the resin bed of bait protein HsFKBP12. A) Bait protein FKBP12. Storage buffer: FKBP12 bait protein; flow through I-II: HEK293T cell lysate was applied onto the resinbed two times to allow completely saturation of the FKBP12 bait proteins; wash fraction I-II: unbound proteins of the mammalian proteome were removed in several washing steps; boiled beads: FKBP12 domain bait proteins and the potential ternary complexes were boiled in 4x Lämmli buffer. **B) Blocked agarose beads by β-Mercaptoethanol** were utilized as resin bed mock control and treated as bait protein FKBP12 in A). The number of proteins after pulldown was compared to HEK293T cell lysate and the remaining supernatant in **Suppl. 3**.

Compared to FKBP51 FK1 bait proteins, FKBP12 bait proteins showed a stronger loss of protein when the storage buffer was investigated. This effect also has been observed in the fractions of HEK293T flow through I-II and wash fraction I-VII. However, FKBP12 was still present in a high amount in the lane referred as 'boiled beads'. HEK293T lysate was added onto the column two times after the resin bed was untreated or treated with Rapamycin. At a first glance, no differences between the flow through I-II were observed in both columns. After several washing steps, almost no protein was observed in was fraction VII, indicating that unbound proteins should be removed. Interestingly, in both 'boiled beads' fractions, either untreated or treated with Rapamycin, no difference could have been observed (**Figure 19A**). These results showed, that HEK293T lysate behaves different compared to purified proteins. As purified proteins are normally stored in the same buffer, HEK293T lysate contains the whole proteome of a cell. In aqueous solutions, proteins often aggregate creating so called 'building blocks'. Protein instability is often caused by external additives in lysis buffers or stress response as treatment with Rapamycin increases oxidative stress [232]. This theory was supported when the mock control was analysed as no proteins were found after the beads were boiled (**Figure 19B**). HEK293T cell lysate as well as the supernatant of the 'boiled beads' fraction of the FKBP12 bait proteins were compared. No differences in the protein pattern of either the 'boiled beads' fraction or the corresponding supernatant compared to HEK293T cell lysate could be observed (**Suppl. 3)**.

The main difference between purified proteins and cell lysates in affinity chromatography is the complexity of the sample. As the target protein is well-defined and has a known binding partner, purified protein solutions may only contain less or few closely related proteins. Moreover, when it comes to specificity in affinity chromatography, target proteins or ligands are normally well-characterized and highly selective. Cell lysate contains not only the whole proteome of a cell, it contains lipids, cellular components as well as nucleic acids. The complexity reduces specificity in the interaction of target proteins and ligands resulting in lower yield of the protein of interest. However, affinity chromatography can be utilized to isolate a specific protein from cell lysate for further analysis in proteomics, which does not need purified samples [233–235]. In cells, proteins naturally agglomerate to low or high molecular complexes, e.g., dimers or multimers by hydrophobic interactions, van der Waals forces or even electrostatic interactions. Agglomeration of proteins is an essential function of proteins and can be influenced by changes in pH, temperature, or chemical agents [233; 236]. However, misfolded or denatured proteins can lead to wrong agglomeration resulting in various diseases like Alzheimer [237; 238]. Large macromolecular complexes like ribosomes are highly stable, on the other hand transient interactions like mTOR complexes are common in signalling and regulatory networks [239]. Moreover, chemical agents in lysis buffers such as NETN buffer can have an influence on protein-protein interactions. As observed, loss of bait FKBP12 protein during flow through of HEK293T lysate is probably caused by an exchange of buffer conditions compared to utilized equilibration buffer when purified

proteins are used for affinity chromatography (**Figure 19**, height 15.2 kDa, HsFKBP12). Proteins are sensitive towards pH conditions, while binding affinity to other proteins is decreasing resulting in weaker or even non-specific protein-protein interactions (PPI's) [233; 240]. The most common buffers utilized for whole cell HEK293T cell lysate are NETN and RIPA buffer whereas RIPA has more harsh washing conditions. NETN buffer is relatively mild and is even suitable for the extraction of nuclear proteins while RIPA buffer seems to be more suitable when it comes to total extraction of cellular proteins. Moreover, total volume and flow rate of the lysis buffer can influence binding capacity of the desired proteins to the protein matrix leading to reduced binding efficiency.

To investigate if the total volume of HEK293T cell lysate is required to observe proteins mTOR and Raptor, the experiment was repeated with FKBP12 as bait protein. The cell lysate was collected after flow through and utilized three times to enhance the binding efficiency even in small nanomolar affinities. Samples were analysed by silver staining and the fractions were further utilized in immune staining to observe components of the mTORC1 complex (**Figure 20**).

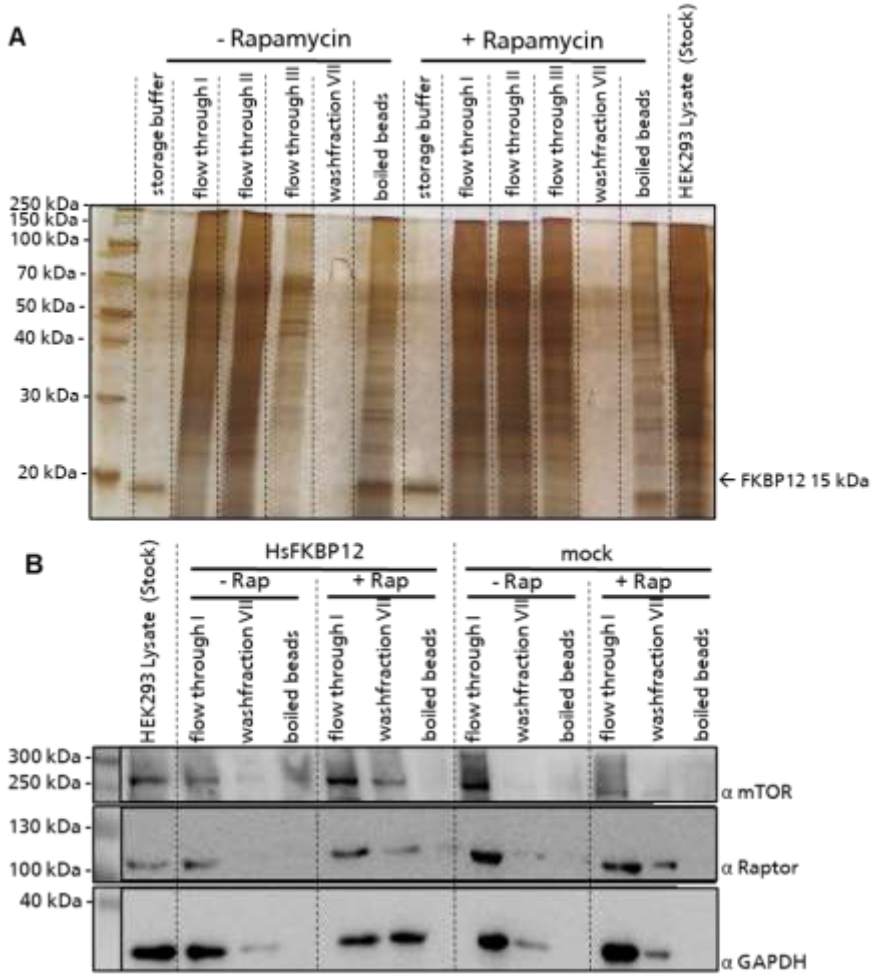

Figure 20: Rapamycin does not induce ternary complex formation of HsFKBP12 and endogenous mTOR by site-specific affinity chromatography. (A) SDS PAGE gel and silver staining after affinity chromatography of bait protein FKBP12 either treated with or without Rapamycin and HEK293T lysate. **(B)** Immunostaining after Western Blotting of mTOR, Raptor and housekeeper GAPDH of HEK293T lysate, flow through, wash fraction, and boiled beads either from HsFKBP12 or mock resin bed.

The SDS-PAGE gel was incubated in the developer solution for an extended duration to enhance the visualization of the boiled beads fraction. Consequently, a diffuse band ("smear") was observed in the lanes corresponding to the flow-through of HEK293T lysate (flow-through I-III). Following seven washing steps, the beads were boiled. As previously described, no noticeable difference in protein bands, irrespective of Rapamycin treatment, was observed between the different protein fractions in the columns (**Figure 20A**). To investigate the amount of endogenous mTOR and Raptor in HEK293T lysate stock solution and respective samples of flow through I, wash fraction VII and the boiled beads fraction, Western Blotting and immunostaining were performed. As control, samples from the mock column were also investigated (silver staining mock column, see **Figure 20B**). The housekeeping protein GAPDH was examined as a control to verify the consistent application of HEK293 lysate onto the columns throughout the experiment. Initially, GAPDH exhibited a consistent pattern in the flow-through I fractions of all four columns, similar to the HEK293T lysate stock solution. The abundance of GAPDH varied after the seventh washing step (wash fraction VII), but no GAPDH signal was observed in the final boiled beads fraction, indicating the success of the washing procedure. In addition to mTOR, the interaction of FKBP12 with Raptor, a component of the mTORC1 complex, was investigated. In the sample of the FKBP12 bait protein without Rapamycin treatment, Raptor was only detected in the flow-through I fraction. However, when the resin bed was treated with Rapamycin, Raptor was identified in wash fraction VII and potentially observed in the boiled beads fraction. The mock column's resin bed was also examined as a control. In the absence of Rapamycin treatment, the mock column exhibited a similar pattern to the untreated FKBP12 column. With the addition of Rapamycin onto the column, Raptor was detected even in wash fraction VII, resembling the observations in the Rapamycin-treated FKBP12 column. However, following the boiling of all four columns' resin beds, no Raptor signal was observed in the boiled beads fraction. Comparatively, mTOR exhibited a similar pattern to Raptor upon immunostaining, indicating the absence of the ternary complex formation during affinity chromatography (**Figure 20B**).

FKBP12 is the smallest member of the FKBP family and often described as a “sticky protein” because of its high binding affinity and specificity to bind e.g. Rapamycin with 0.2 nM [2; 3; 22]. On the other hand FKBP51 has a binding affinity up to 100-fold lower of 25 nM [139]. As FKBP51 is less sticky than his similar family member, it was suggested that less proteins can be observed in the ‘boiled beads’ fraction and therefore less interactions with other proteins are present when utilizing FKBP51 FK1 domain as bait protein. For this, HEK293T cell lysate was applied for affinity chromatography after the resin bed was saturated with Rapamycin. The results were visualized by silver staining as well as immunostaining of mTOR. To investigate if endogenous level of FKBP51 is involved in facilitating ternary complex formation with Rapamycin and mTOR, the samples were analysed for total level of endogenous FKBP51 (**Figure 21**).

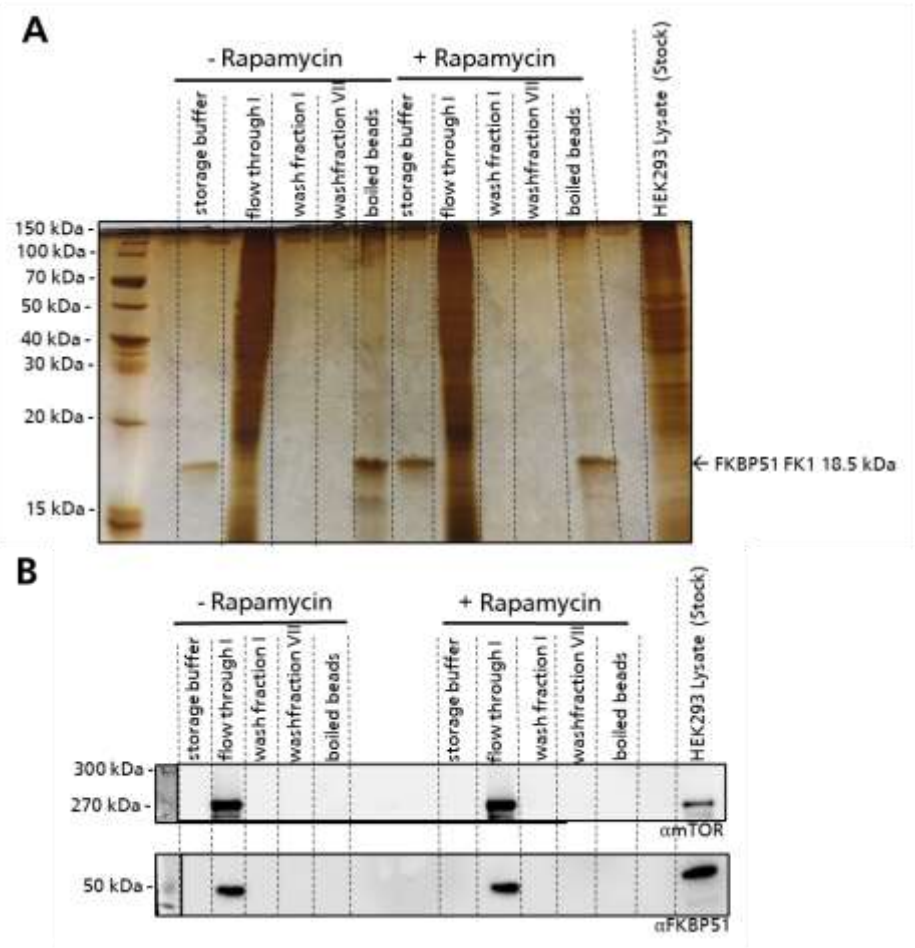

Figure 21: Rapamycin does not induce ternary complex formation of HsFKBP51FK1 and endogenous mTOR of HEK29T lysate in affinity chromatography. **(A)** SDS PAGE and silver staining of the FKBP51 FK1 resin bed, including FKBP51 FK1 in storage buffer; flow through I of HEK293 lysate after applying onto the column and wash fraction I and VII to show, that no proteins, which are unbound to the matrix are left before boiling the resin bed (boiled beads). The silver staining compares FKBP51 FK1 resin bed either untreated or treated with Rapamycin. **(B)** Immunostaining of mTOR and FKBP51 of each sample to investigate the presence or absence of the potential ternary complex of FKBP51 FK1:Rapamycin:mTOR after affinity chromatography.

To enhance the signal of potential protein lanes in the 'boiled beads' fraction, the SDS PAGE gel was incubated for an extended duration in the developer solution. The lanes referred as 'flow through I' were observed as 'smear', which was disappeared already after the first washing step (**Figure 21A**; washing step I). After the resin bed of both columns treated or untreated with Rapamycin were boiled, no differences between both columns were observed in the silver staining ('boiled beads'). Further, no visible protein bands except FKBP51 FK1 could be observed (**Figure 21A**). Compared to bait protein FKBP12, in general less proteins were visible in the washing fractions or in the boiled beads fraction suggesting that FKBP51 FK1 bait protein is less affected of utilizing cell lysis buffer.

Samples of flow through I, wash fraction I and boiled beads fraction were utilized for Western Blotting and Immunostaining (**Figure 21B**). As control, HEK293T lysate stock solution was utilized. Endogenous mTOR was only observed in the flow through I fractions in the same extend as observed in HEK293T lysate. Even after the first wash fraction no mTOR was observed. As the bait protein only consist of the FK1 domain of FKBP51, the samples were also stained against FKBP51 to investigate the level of FKBP51 full length protein which may interfere with the corresponding interaction. This led to the hypothesis, that the endogenous proteins FKBP12 and FKBP51 might be the preferred target of Rapamycin and mTOR as possibly loss of Rapamycin might occur because of high concentrations of the proteome and inappropriate buffer conditions or its volume and flow rate [233–236].

When utilizing FKBP mono cysteine variants for affinity chromatography, the proteins were covalently bound to the matrix. In this scenario, it was not possible to cleave off potential ternary complexes no utilize high affinity agents like biotin for streptavidin matrices to compete the effect of the resin bed. Alternatively, the usage of a competitor might be suitable to elute proteins captured by the FKBP:Rapamycin matrix. FK[4.3.1]-16h (or JK95) is a bicyclic sulfonamide FKBP ligand which can outcompete the effect of Rapamycin upon FKBP binding [241–243] (**Suppl. 1B**).

The bicyclic ligand was applied for affinity chromatography utilizing purified proteins as for HEK293T cell lysate affinity chromatography. For affinity chromatography of purified proteins, FKBP12 as well as FKBP51 FK1 were utilized. Purified GST-FRB was added onto the column after saturation with Rapamycin and after several washing steps the bicyclic FKBP ligand was added in 3-molar excess compared to Rapamycin. Samples were analysed by silver staining (**Figure 22**).

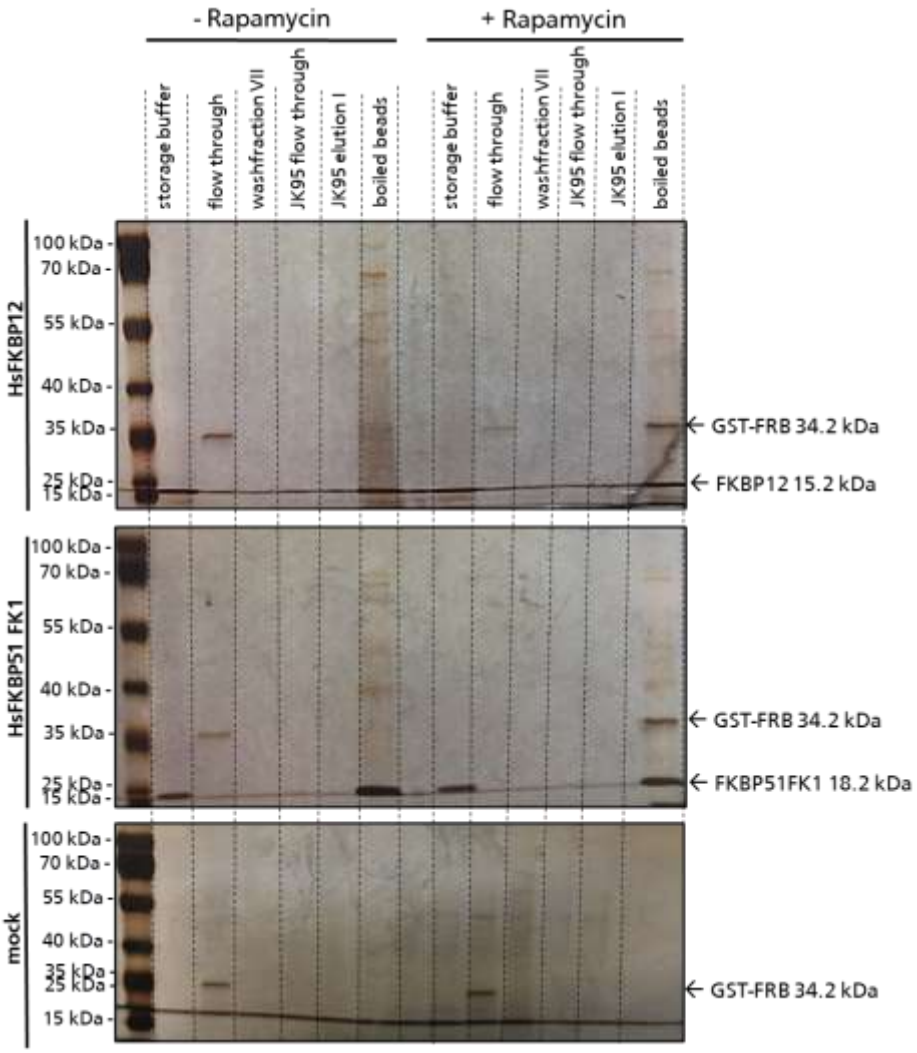

Figure 22: The bicyclic FK[4.3.1]-16h ligand does not compete the effect of Rapamycin when HsFKBP12 or HsFKBP51FK1 were utilized for chemically induced dimerization with GST-FRB by affinity chromatography. As control, blocked beads referred as 'mock' were utilized. Either the resin beds containing mock control, FKBP12 or FKBP51 FK1 one column was treated with Rapamycin. Storage buffer (immobilized FKBP12 or FKBP51 FK1); flow through GST-FRB; wash fraction VII; FK[4.3.1]-16h flow through (FK4.3.1] was added onto the column of 50 µM); FK[4.3.1]-16h elution I (was fraction of FK[4.3.1]); boiled beads fraction.

FKBP12 and FKBP51 FK1 were observed in the storage buffer, compared to the mock control. After treatment with Rapamycin, GST-FRB was added onto the column and the flow through was collected. In general, GST-FRB was added in a higher molar excess to ensure, that FKBP bait proteins and Rapamycin were fully saturated onto the columns. After seven washing steps no GST-FRB was observed in the flow through, suggesting that unbound proteins were removed successfully. Subsequently FK[4.3.1]-16h was added onto the column (FK[4.3.1]-16h flow through). The flow through was collected to investigate if FK[4.3.1]-16h competes the effect of Rapamycin and GST-FRB can be observed in the flow through. After 15 min the resin beds were washed with wash buffer to improve the duration of incubation. However, in both cases, FKBP12 and FKBP51 FK1 were found after the beads were boiled in complex with GST-FRB. FK[4.3.1]-16h was not able to successfully compete the effect of Rapamycin.

Further FK[4.3.1]-16h was utilized for affinity chromatography when HEK293T cell lysate applied onto the FKBP resin bed after treatment with Rapamycin. The ligand was applied, and the column was incubated for 15 min to let the compound settle onto the resin bed and compete the effect of Rapamycin. Thereafter, the columns were washed with washing buffer to investigate if FK[4.3.1]-16h can compete the effect of Rapamycin. As control, the resin bed was boiled, and samples were applied for silver staining. Moreover, immunostaining for mTOR and FKBP12, respectively was performed (**Figure 23**).

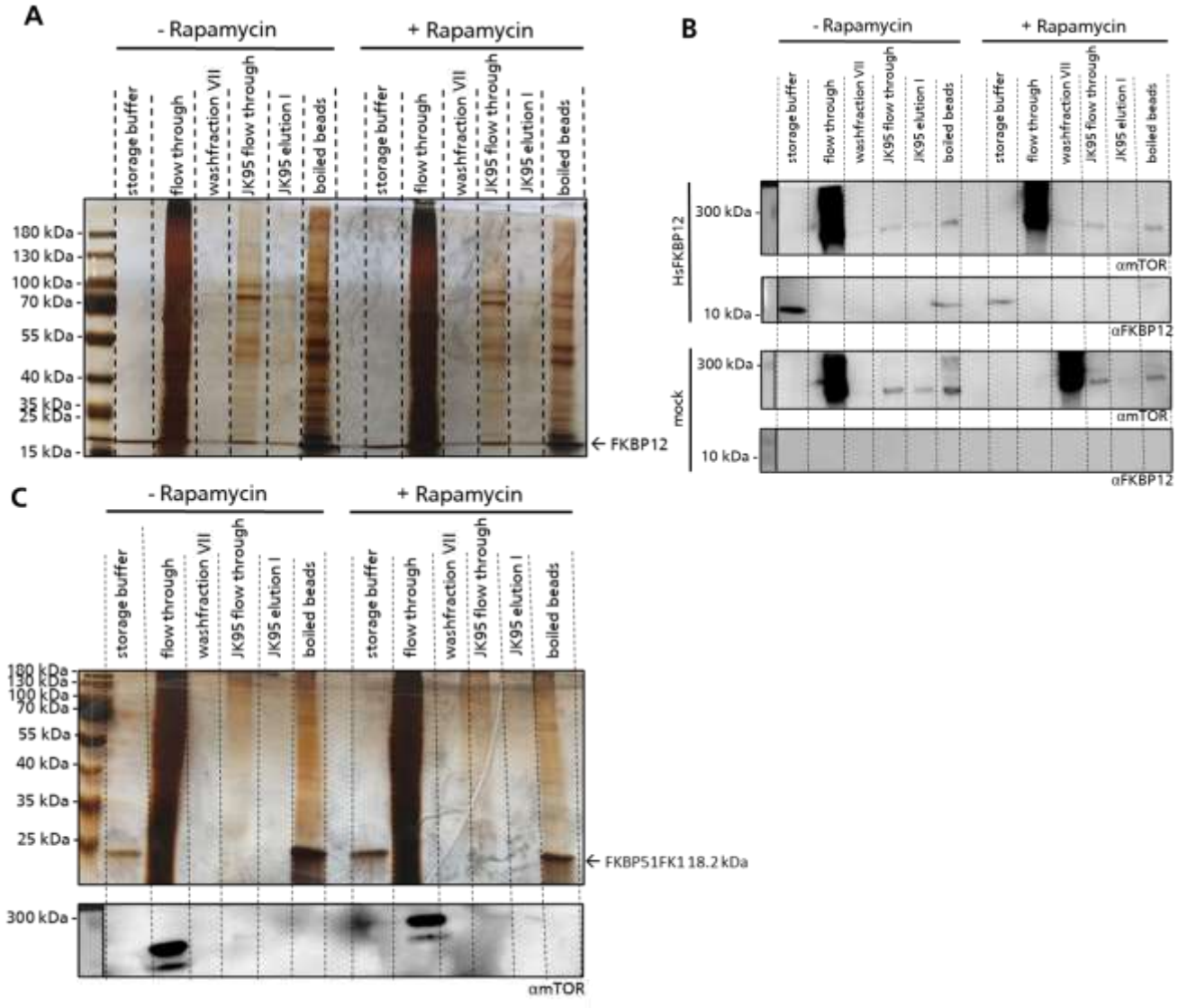

Figure 23: Bicyclic FKBP ligand FK[4.3.1]-16h does not compete the effect of Rapamycin in affinity chromatography utilizing HEK293T cell lysate (A) SDS PAGE and silver staining of FKBP12 resin bed with storage buffer (bait stock); flow through of HEK293T lysate, wash fraction VII to remove unbound proteins, FK[4.3.1]-16h flow through to compete effect of Rapamycin and FK[4.3.1]-16h elution I fraction to wash out the synthetic compound; boiled beads fraction of potential POI's and FKBP12 bait protein. **(B)** Western Blot and Immunostaining of the corresponding samples of Figure A. samples were stained against kinase mTOR and FKBP12. Samples were taken from FKBP12 resin bed columns and mock columns (only blocked beads by β-Mercaptoethanol). **(C)** SDS PAGE and silver staining of FKBP51 FK1 resin bed with storage buffer (bait stock); flow through of HEK293T lysate, wash fraction VII to remove unbound proteins, FK[4.3.1]-16h flow through to compete effect of Rapamycin and FK[4.3.1]-16h elution I fraction to wash out the synthetic compound; boiled beads fraction of potential POI's and FKBP51 FK1 bait protein. The samples were also utilized for Western Blotting and Immunostaining against mTOR kinase. Mock control, see **Suppl. 4**.

In general, bait protein FKBP12 was observed in the flow through of the storage buffer indicating the biological instability of the resin bed and therefore loss of protein and binding efficiency. The SDS gel was exposed with developer solution resulting in a visible 'smear' of the HEK293T lysate flow through. In wash fraction VII no protein was observed, indicating that unbound proteins were rinsed off the column. After 15 min incubation with FK[4.3.1]-16h the flow through was collected. The fraction showed a slight 'smear' indicating that due to FK[4.3.1]-16h solution, some proteins were eluted. However, there was no difference between the columns irrelevant if Rapamycin was present. FK[4.3.1]-16h was diluted in washing buffer to ensure, that the columns still had the same ionic charge and the concentration of DMSO from the stock was less than 2 % (v/v). The FK[4.3.1]-16h flow through fraction nearly showed the same pattern as the boiled bead fraction represented in both columns. When compared the FK[4.3.1]-16h wash fractions to the boiled bead fractions in both columns, significantly amounts of proteins around 100 kDa to 40 kDa were observed indicating that the bicyclic ligand may compete some effects of Rapamycin (**Figure 23A**).

For immunostaining, samples were stained against mTOR kinase and FKBP12, respectively. mTOR kinase was observed in the HEK293T lysate in high doses in all columns. After seven wash steps no mTOR was observed in any of the samples, irrelevant if FKBP12 resin bed or mock resin bed was used. After FK[4.3.1]-16h was added onto the columns, mTOR was observed in the FK[4.3.1]-16h flow through fraction. However, irrelevant if FKBP12 bait protein or mock control were treated or untreated with Rapamycin, mTOR was observed in every column indicating that the resin bed was cluttered with cellular proteins and protein agglomeration was likely to occur. After the resin bed was washed with washing buffer to remove mostly all the synthetic compound, mTOR was also found in fraction FK[4.3.1]-16h elution I. When comparing immunostaining of mTOR to FKBP12 in the treated and untreated column, no FKBP12 was observed. As the idea was to remove proteins of interest by competing the effect of Rapamycin, the idea worked out. But however, mTOR was found in every column, irrelevant if treated with Rapamycin or the mock control. Moreover, as the beads were boiled, mTOR was observed in the columns of bait protein FKBP12 treated or untreated with Rapamycin. Regarding the mock columns, mTOR was also found after the beads were boiled (**Figure 23B**). Overload of the resin bed with HEK293T lysate might be a reason, why mTOR was found after beads were boiled. Another idea was, that the concentration of FK[4.3.1]-16h (50 μM) supported agglomeration of proteins and therefore, washing procedure or buffer conditions were not suitable for this experiment.

When FKBP51FK1 was utilized as bait protein, a 'smear' was observed when FK[4.3.1]-16h was applied onto the column to compete the effect of Rapamycin. In general, FKBP51 FK1 resin bed appeared to be less 'sticky' than utilizing FKBP12 as bait protein. No clear visible protein lane was observed after the flow through of FK[4.3.1]-16h was investigated neither after the column was washed with washing buffer. After boiling the beads, protein lanes were visible after silver staining but no difference between the resin bed treated with Rapamycin and the untreated pendant was observed. The samples were then analysed by immunostaining of mTOR. As expected, mTOR was only found in the HEK293T lysate flow through. Eventually, mTOR was observed after FK[4.3.1]-16h was added onto the columns (FK[4.3.1]-16h flow through), irrelevant if the resin bed was treated with Rapamycin. After the beads were boiled, no mTOR Kinase was observed (**Figure 23C**).

As a consequence, the induction of the ternary complex was investigated in HEK293T cells directly. For this purpose, HEK293 cells were transfected with either FKBP12 or FKBP51. Both proteins contained a Twin-Strep-FLAG tag, which should be utilized in further experiments to allow higher and better purification of ternary complexes by affinity chromatography. The experiment was performed in duplicate and after co-immunoprecipitation ternary complex formation of FKBPs and mTOR were investigated by immunostaining (**Figure 24**).

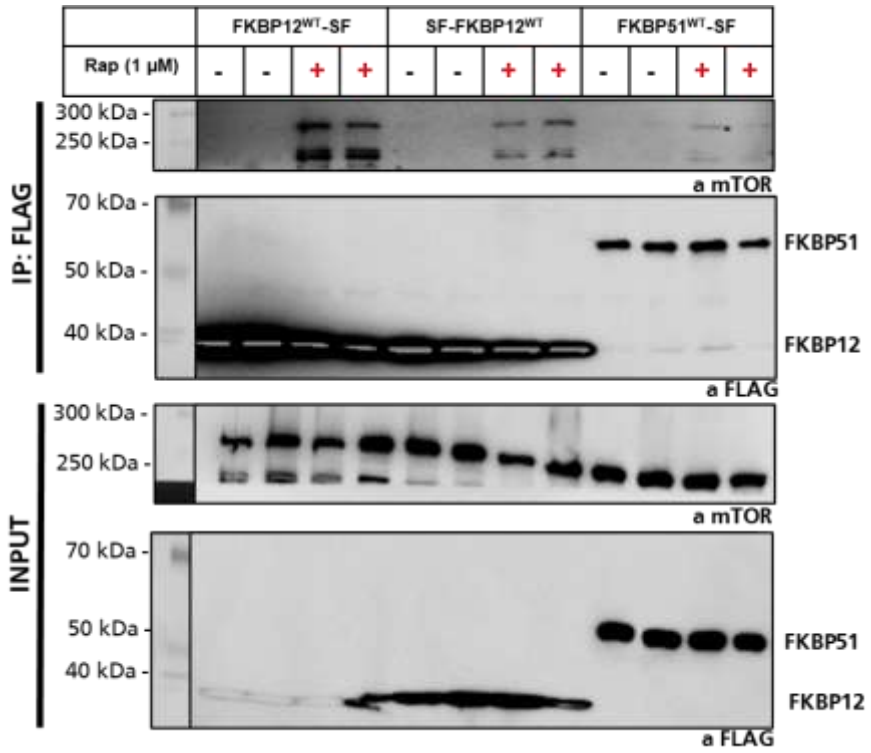

Figure 24: The ternary complex of FKBP:Rapamycin:mTOR can be visualized after transfection of HEK293T cells with FKBP-Twin-Strep-II-FLAG tag constructs. FKBP12 or FKBP51 wildtype were expressed in HEK293T cells with an either N- or C- terminal Twin-Strep FLAG tag (**SF**). Cells were treated with Rapamycin and co-immunoprecipitation was performed utilizing the FLAG tag of FKBPs for pulldown. Immunostaining was performed to investigate ternary complex formation of FKBP12 or FKBP51 and endogenous mTOR after treatment with Rapamycin.

Co-immunoprecipitation was performed utilizing the FLAG tag of FKBP12 and FKBP51. Samples of HEK293T lysate, referred as 'INPUT' were utilized as control, to test if the expression of FKBP constructs was equal and successful in every experiment. Moreover, mTOR was visualized to assess the endogenous level of the kinase. When cells were previously treated with Rapamycin mTOR was found to be present after co-immunoprecipitation (**Figure 24**).

Pulldown of FKBP12 with C-terminal Twin-StrepII-FLAG tag revealed an almost identical amount of endogenous level mTOR involved in ternary complex formation after cells were treated with Rapamycin. The N-terminal variant was only able to precipitate the half maximum after treatment with Rapamycin, suggesting that FKBP12 carrying a C-terminal tag is more suitable for experiments in mammalian cell culture. As the affinity for FKBP51 is lower than FKBP12 for Rapamycin, less mTOR was observed after pulldown. In conclusion, FKBP12 with a C-terminal Twin-StrepII-FLAG tag is preferred for chemically induced ternary complex formation of FKBP12 and mTOR by Rapamycin, whereas only a small amount of mTOR can be observed when FKBP51 wildtype is utilized.

7.2.3 Rapamycin does not induce ternary complex formation of covalently coupled FKBPs as matrix baits in affinity chromatography and mTOR

Affinity chromatography is a widespread and powerful technique, e.g. allowing the purification of recombinantly expressed proteins from bacterial origin. Purification often involves metal ion affinity chromatography by utilizing a hexahistidin tag for the desired protein under mild and nondenaturing conditions [244–246]. The expression and purification of HsFKBPs from *E. coli* BL21 DE3 is a cheap and scalable method to generate excessive amounts of the desired proteins, which then can be purified in a highly specific manner due to their His tag leading to high purity of the protein stock. When coupling mono cysteine FKBPs by iodoacetamide to the silica matrix, reducing agents like dithiothreithole (DTT) were added during the coupling reaction of FKBPs and the resin bed to avoid oxidation of the mono cysteine residue. This step was crucial as oxidation often led to loss of protein during the coupling reaction. However, successful coupling to the silica matrix did not prevent HsFKBPs from denaturation as the biggest disadvantage of proteins utilized as bait in affinity chromatography is their biochemical properties. Proteins are highly sensitive to temperature, pH values and buffer additives which often leads to denaturation or even agglomeration of the proteins [233–236]. Loss of active proteins or agglomeration decreases the ability of the matrix to interact with other proteins resulting in lower yields or unspecific binding.

Storage of proteins requires buffers with physiological conditions at mild pH (7.4) and salts like HEPES and NaCl as the ionic strength of the buffer can affect protein binding. Higher salt concentrations can disrupt electrostatic interactions while low salt conditions can promote those interactions and therefore agglomeration. Often, the buffers are chosen by the protein which is going to be analysed [233; 234]. Mono cysteine FKBP12 and FKBP51 FK1 were stored in the same buffer conditions as purified GST-FRB supporting an equal environment for protein-protein interactions. Rapamycin was diluted in DMSO with a concentration of 1 mM (w/v). DMSO can affect the stability and functionality of proteins. The normal concentration of DMSO in an assay is 0.1 % up to 5 % (v/v) while the lower concentration does have less influences in stabilizing or denaturizing proteins. At 1 % DMSO proteins are already unfolding and starting to aggregate which is increased at higher temperatures [247]. Thus, it was relevant to dilute the Rapamycin stock in equilibration buffer (1:1000) until the DMSO concentration was 0.01 % (v/v) to prevent proteins from chemical instability. The ternary complex formation of HsFKBP12 or HsFKBP51 FK1 domain and GST-FRB was successful when the resin bed was incubated with Rapamycin.

One of the advantages when covalently coupled proteins are used as baits is the stability of the protein itself. They tend to be more stable and less prone to leaching off the matrix compared to those which can be displaced by chemical agents. However, the resin bed had to be boiled to further analyse ternary complex formation of FKBP:Rapamycin:GST-FRB. This procedure tended to be not suitable as boiling the beads twice showed, that either FKBPs or the whole complex was still present in the fraction resulting in loss of yield of the sample. Affinity tags are often used for protein purification [248]. For example, a SUMO tag (small ubiquitin like modifier) is utilized to cleave of the purified protein from its hexahistidin tag and the matrix. However, as the mono cysteine is present on the surface of the HsFKBPs on the opposite of the PPIase domain, introducing a tag would have led to various orientations of the proteins leading to less binding capacity and efficiency when investigating ternary complexes in affinity chromatography.

HEK293T lysate possess the whole proteome of millions of cells whereas proteins prone to form complexes with other proteins aggregating to large molecular protein complexes or even with itself when misfolded or denatured [238; 239]. Buffer conditions can influence transient protein interactions based upon electrostatic dependencies, temperature, or pH value. NETN and RIPA buffer are well known for cell lysis of mammalian cells. While NETN is required for mild conditions, RIPA buffer contain detergents, which allows harsher washing procedures. RIPA buffer was utilized to influence the stability of proteins and their interactions. However, no difference was observed between both buffers and no ternary complex formation of bait FKBPs and endogenous mTOR was observed when the resin bed was treated with Rapamycin.

Next to buffer additives, the experimental procedure was varied. As the lysate was allowed to flow through the resin bed, in other experiments, the columns were incubated on a rolling device for up to one hour to enhance the interaction of endogenous mTOR with the bait proteins. Additionally, HEK293T lysate was supplemented with Rapamycin in different concentrations directly either by incubating on a rolling device or allowing to rinse through the column. In any case, no ternary complex formation was observed.

One limiting step can be protein degradation in cell lysate. It was suggested that the complex protein mix might be degraded when utilized as protein sample during affinity chromatography as the experimental design tended to be time consuming as the lysate was either allowed to flow through the column or the resin bed was incubated with the lysate on a rolling device. Therefore, additives like Phenylmethylsulfonyl fluoride (PMSF) and bovine serum albumin (BSA) were utilized to prevent degradation of proteins in the complex cellular mix. PMSF is an inhibitor for serine proteases preventing the proteome after cell lysis from degradation [249; 250]. BSA is the major component of bovine serum, which is supplemented in cell culture media to inhibit generation of reactive oxygen species (ROS) by EGCG (epigallocatechin gallate), involved in induced cytotoxic cell death [251]. Compared to NETN buffer which was utilized without any additives as usual, no difference was observed in silver staining nor immunostaining against endogenous level of mTOR.

Taken together, the utilization of purified GST-FRB in affinity chromatography experiments employing FKBP proteins as bait proteins resulted in the successful formation of a ternary complex induced by Rapamycin. This formation was visually confirmed through silver staining of SDS gels, as the bait protein was covalently bound to the silica matrix. Boiling the resin bed to investigate ternary complex formation was mandatory in this experimental setup. When HEK293T cell lysate was employed, the flow-through fraction contained the entire proteome of approximately 1x 10^7 cells. The concentration of HEK293T lysate applied during affinity chromatography varied from an equilibrium with bait FKBPs or high molar excess. Variation on applying HEK293T lysate in affinity chromatography did not change the outcome. Consequently, no endogenous mTOR was observed when the resin bed was boiled. Furthermore, even with variations in the incubation time or adjustments in the experimental setup, no ternary complex involving FKBP proteins and mTOR was observed when the resin bed was treated with Rapamycin. Moreover, the choice of lysis buffer and additional additives did not yield any noticeable alterations in the results obtained.

Affinity chromatography has been widely utilized for protein purification from bacterial origin because of its high specificity. When proteins possess a tag, it binds to the matrix with high affinity allowing purification under mild and physiological buffer conditions resulting in high purity of the sample. The approach is easy to be scaled up allowing time-efficient and excellent purification of the desired protein. Moreover, the approach is also utilized to study protein-protein interactions or identification of binding partners. If the protein partner is known, the buffer compositions can be easily adopted to enhance the specificity of the protein partner. Less interactions occur when purified proteins are utilized.

Deciphering an interaction between a protein and an unknown partner is accomplished by affinity chromatography following probing, e.g., mass spectrometry (MS). This can be achieved by TMT labelling, SILAC or non-labelled measurements (LFQ), when the eluate or a defined protein lane excised from SDS gel, are utilized. Silver staining is more sensitive compared to Coomassie staining but the biggest disadvantage is to remove precipitated silver ions from proteins after staining. This procedure is very intense compared to colloidal staining and can influence the sample quality for further measurements.

The covalent captured affinity method utilizing FKBP proteins as bait molecules proves to be unsuitable for the identification of unknown protein interactors within HEK293T cell lysate. The cost of producing FKBP proteins can be high, and their susceptibility to natural protein denaturation exacerbates the issue, resulting in limited specificity and reduced binding capacity of affinity chromatography. One of the most critical bottlenecks in this approach is the availability of the natural product Antascomicin B. Antascomicin B is known to be expressed in only 1 out of every 12,000 soil bacteria strains, and its synthetic production is exceptionally challenging [116; 141]. Moreover, no optimization of the polyketide synthesis of Antascomicins was described in the world so far.

Regarding the fact that the natural compound Antascomicin B has a rare availability, Rapamycin was utilized in pulldown experiments in HEK293T cells. The stock solution of Rapamycin was only 1 μM, while stock solutions for large scale affinities were up to 30 μM. Moreover, ternary complex formation of FKBPs and endogenous mTOR were directly observed after the FLAG epitope was utilized for affinity pulldown. The FKBP12:Rapamycin:mTOR complex is well described in literature and was considered as stable and reliable tool, to investigate the affinity chromatography methodical approach. As HEK293T cells are living systems it is also possible, that other proteins are required to facilitate the protein-protein interaction of FKBPs, natural molecular glues and their unknown interaction partners. To investigate if Antascomicin B has a molecular glue effect on the human proteome, site-specific photo-crosslinking was utilized in further experiments.

7.3 Amber suppression-mediated site-specific photo-crosslinking induces ternary complexes of FKBP51 after Treatment with natural molecular glues

7.3.1 Utilizing unnatural amino acids of the FKBP51 FK1 domain for site-specific photo-crosslinking

Amber suppression-mediated site-specific photo-crosslinking is an effective method to investigate protein-protein interactions *in-vitro*. This method can be a useful tool to investigate the effects of natural molecular glues in protein-protein interactions [252]. As full length FKBP51 consists of 462 amino acids and natural compounds like Rapamycin and FK506 are interfering with its FK1 domain inducing ternary complex formation with other proteins, 21 surface exposed amino acids residues in total were utilized for site-specific photo-crosslinking. To enable amber suppression, a TAG codon for each amino acid was inserted by site directed mutagenesis and HEK293T cells were supplemented with the unnatural amino acid 4-*para*-benzoylphenylalaine (pBpa), which is incorporated by an orthogonal tRNA synthetase (RS) (**Figure 25**).

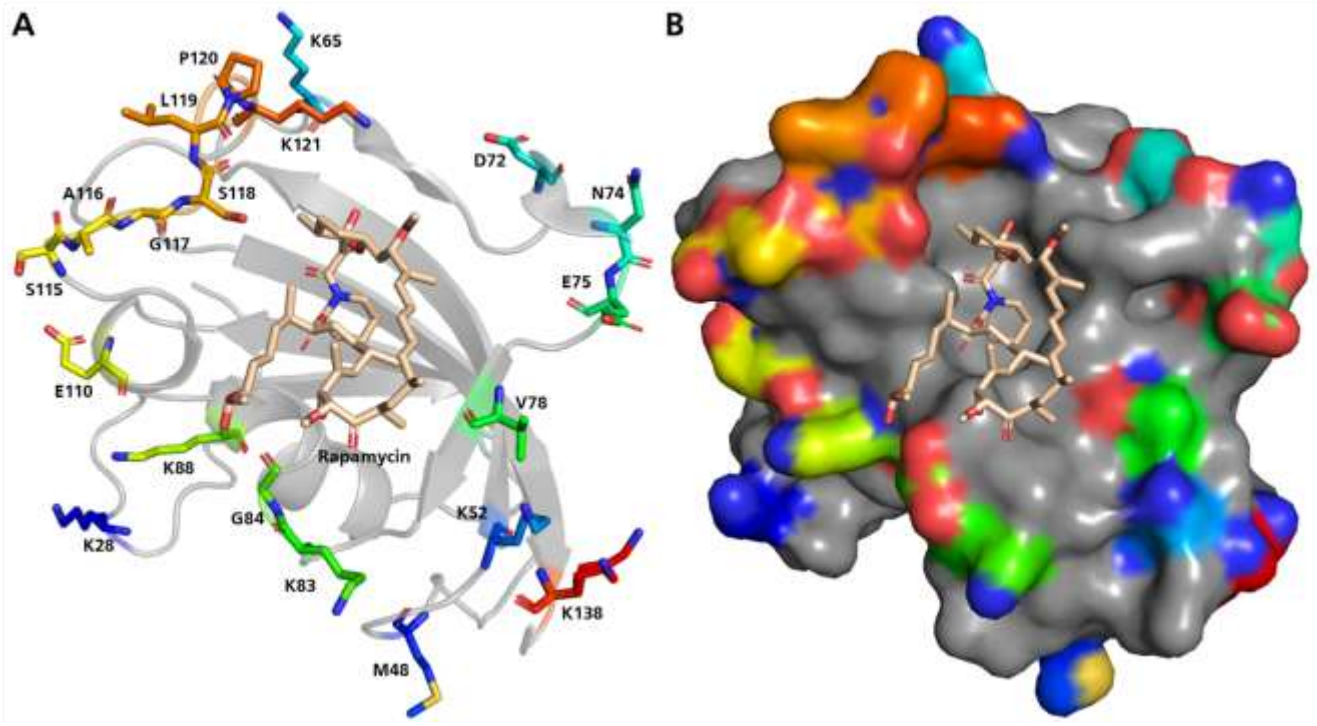

Figure 25: Map of surface amino acids of FKBP51 FK1 domain which are utilized for site-specific photo-crosslinking in HEK293T cells. **(A)** Amino acids located on the surface of the FK1 domain are illustrated in a colour spectrum to delineate each amino acid respectively. **(B)** Figure of the FKBP51 FK1 protein surface structure. Rapamycin is located in the binding pocket of the FK1 PPIase domain surrounded by 21 selected amino acids in total (**PDB: 4DRI**)

7.3.2 Introducing pBpa as photo-crosslinker for ternary complex formation of FKBP51 and natural molecular glues

HEK293T cells were co-transfected with RS aminoacyl tRNA synthetase and FKBP51 WT as control to investigate whether compound treatment or UV irradiation have an influence on expression level of FKBP51 WT or if potentially photo-crosslinks can be observed (**Figure 26A**). Moreover, HEK293T cells were co-transfected with FKBP51 mutants containing an amber suppression codon and RS aminoacyl tRNA synthetase (**Figure 26B**).

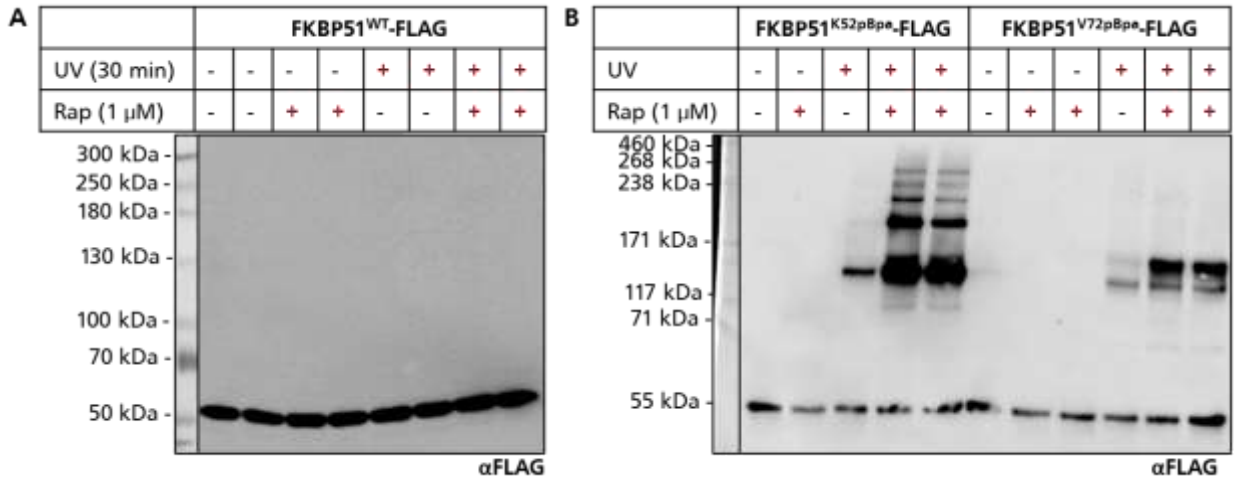

Figure 26: Amber suppression-based site-specific photo-crosslinking of FKBP51^{K52pBpa}/FKBP51^{V72pBpa} after treatment with Rapamycin compared to FKBP51 WT revealed a strong photo-crosslink at 125 kDa. HEK293T cells were transfected with RS-synthetase and either FKBP51 WT or FKBP51$^{K52pBpa/V72pBpa}$. **(A)** No photo-crosslinks were observed when FKBP51 WT expressing cells were treated with Rapamycin or UV light. **(B)** HEK293T cells expressing mutants FKBP51$^{K52pBpa/V72pBpa}$. Without treatment no photo-crosslinks were observed. When HEK293T cells were treated with UV irradiation independently if treated previously with Rapamycin, photo-crosslink bands occurred. While FKBP51^{V72pBpa} only showed photo-crosslinks at around 120-150 kDa, mutant FKBP51^{K52pBpa} showed multiple photo-crosslinks in a range of 120-270 kDa.

Immunostaining analysis of FKBP51 wild-type (WT) protein demonstrated that treatment with Rapamycin or exposure to UV light (365 nm) did not exert any noticeable influence on the expression levels of FKBP51 WT. Furthermore, no photo-crosslinks were observed (**Figure 26A**). Upon the incorporation of the unnatural amino acid (unAA) pBpa into FKBP51 at position K52 or V72 UV induced photo-crosslinks were detected at a molecular weight of approx. 120/125 kDa. Additionally, when cells were treated with Rapamycin, novel photo-crosslinks were observed in comparison to the UV-exposed samples in the absence of compounds. The signal intensity of the photo-crosslink at 120/125 kDa was increased in both mutants upon Rapamycin treatment. While mutant FKBP51^{V72pBpa} displayed the increased 120/125 kDa photo-crosslink upon Rapamycin treatment, mutant FKBP51^{K52pBpa} exhibited additional photo-crosslinks at different molecular weights ranging from 180-270 kDa (**Figure 26B**). The expression level of FKBP51 WT and FKBP51 mutants was not affected by UV irradiation. Moreover, when pBpa was introduced as unnatural amino acid upon UV treatment, photo-crosslinks were observed. Utilizing Rapamycin as molecular glue revealed additional photo-crosslinks after treatment with UV light

whereas further FKBP51 mutants were utilized in a screening. Next to position K52, position E75 in the β3 sheet and positions A116-K121 in the flexible loop of the FKBP51 FK1 domain appeared to induce multiple photo-crosslinks. When mutants were treated with UV light, a similar pattern as previously described was observed. Additionally, mutants were treated with Rapamycin, FK506 and Antascomicin B resulting in new or increased photo-crosslinks represented in **Figure 27**.

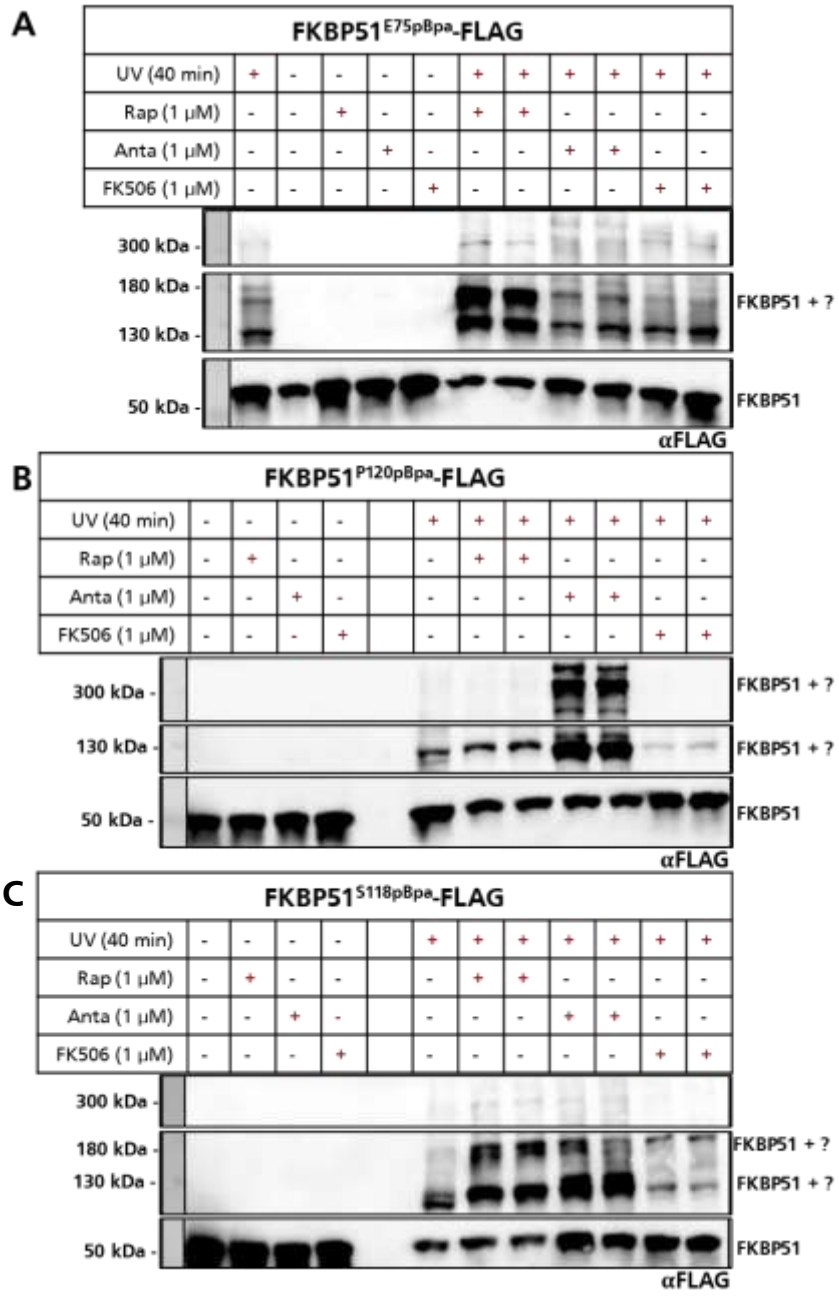

Figure 27: Treatment of different FKBP51 mutants with Rapamycin, Antascomicin B, and FK506 reveal different intensities and arrangements of photo-crosslinks after UV irradiation. A) Immunostaining of FKBP51^{E75pBpa}. When cells were irradiated, several weak photo-crosslinks were observed at different heights, whereas the photo-crosslink at 125 kDa was most prominent in each sample. **B)** Immunostaining of FKBP51^{P120pBpa}. Most prominent photo-crosslinks occurred at 125 kDa and 180 kDa. When samples were treated with Antascomicin B photo-crosslink at 125 kDa was enhanced and further photo-crosslinks were observed at around 270 kDa. **C)**. Immunostaining of FKBP51^{S118pBpa}. As previously observed, prominent photo-crosslinks at 125 kDa and 180 kDa were observed. When cells were treated with Rapamycin or Antascomicin B these photo-crosslinks were enhanced.

When cells expressing mutant FKBP51^{E75pBpa} were treated with Rapamycin, an increased photo-crosslink at around 180 kDa and a slightly increased photo-crosslink at 125 kDa were observed. Treatment with Antascomicin B or FK506 did not show any differences to the irradiated sample without compound treatment (**Figure 27A**).

Upon treatment of mutant FKBP51^{P120pBpa} with Antascomicin B, it became evident that this natural compound notably intensified and induced photo-crosslinks at approximately 125 kDa and 270 kDa, in stark contrast to the effects of Rapamycin or FK506. As observed in the FKBP51^{E75pBpa} sample, Rapamycin slightly enhanced the photo-crosslink at 120 kDa. Rapamycin and FK506 displayed minimal disparities compared to the sample exclusively exposed to UV light with FKBP51^{P120pBpa} (**Figure 27B**).

The effect of Antascomicin B was smaller when mutant FKBP51S^{118pBpa} was treated with the natural compound and no photo-crosslink at 270 kDa was observed. In contrast, Rapamycin augmented the photo-crosslink at 125 kDa, while Antascomicin B appeared to induce a second photo-crosslink at nearly the same molecular weight. As previously observed, samples treated with FK506 did not exhibit any differences to the irradiated sample without the natural product (**Figure 27C**).

The most conspicuous photo-crosslinks were observed with a molecular weight range of 120-180 kDa among all FKBP51 mutants. The impact on these photo-crosslinks was increased when cells were pretreated with molecular glues prior to UV irradiation. A majority of the photo-crosslinks observed in the UV-irradiated sample were also detected in the compound-treated samples. In general, photo-crosslinks at 130 kDa and 150 kDa appeared irrespective of compound treatment. The number of photo-crosslinks was increased within the β4-β5 loop, corresponding to amino acid residues S115-K121 and N74 and E75. In contrast, within the β2-β3a loop, the substitution of K52 with pBpa notably enhanced the efficiency of photo-inducible crosslinks, too.

The results of the corresponding photo-crosslinks of each FKBP51 mutant of the FK1 domain utilized for pretreatment with Rapamycin, Antascomicin B or FK506 prior UV irradiation were summarized in **Figure 28**. The most prominent photo-crosslinks after pretreatment with molecular glues were labelled in red, while photo-crosslinks, which disappeared were highlighted in blue. Moreover, amino acid residues, which were exchanged by pBpa were visualized in the illustration of the FKBP51 FK1 domain. Residues, which only exhibited the 130 kDa and 150 kDa photo-crosslinks were highlighted in salmon, while amino acid residues with additional photo-crosslinks at 180-200 kDa were labelled in orange. The most interesting residues when FKBP51 mutants when pretreated with natural molecular glues were presented in dark red compared to the UV irradiated sample (**Figure 29**).

Mutant	UV irradiation only	Rapamycin	Antascomicin B	FK506
FKBP51^{K28pBpa}	none	120,130,150,270	100	120
FKBP51^{M40pBpa}	120,150	120,150	100,120	none
FKBP51^{K52pBpa}	130,180	**120**,**130**,150,180,200,240,270	**130**,180,200,270	130,180
FKBP51^{K65pBpa}	none	70	**70**,120,130	70,130,150,180
FKBP51^{D72pBpa}	90,100,130,150	90,100,**130**,150	130,180	90,130,150
FKBP51^{N74pBpa}	130,150,180,200,250	120,**130**,**150**,180,200	90,**130**,**150**,180,200,**270**	130,170,180,200,250
FKBP51^{E75pBpa}	100,130,150,180,200,250	100,**120**,**130**,150,180,250	100,130	100,130,150,180,200,250
FKBP51^{V78pBpa}	120,130	120,130	120,150	120,130
FKBP51^{K83pBpa}	130,150	130,150,240	130,150	130,150
FKBP51^{G84pBpa}	130,150	130,150,240	130,150	130,150
FKBP51^{K88pBpa}	130,150	130,150	130,150	130,150
FKBP51^{E110pBpa}	130,150	130,150	130,150	130,150
FKBP51^{S115pBpa}	90,120,130,150	90,120,130,150,180	90,120,130,150	90,120,130,150
FKBP51^{A116pBpa}	90,120,130,150	90,**120**,**130**,150,180,200,240,270	90,**120**,**125**,130,150,200,240,270	90,**120**,130,150,180,**300**
FKBP51^{G117pBpa}	90,100,120,130,150,180	90,100,120,130,150,180	70,120,125,130,150,250,270	130,180
FKBP51^{S118pBpa}	90,120,130,150,180,250,270	**120**,**130**,150,180,250,300	90,120,130,150,180,250,300	90,120,130
FKBP51^{L119pBpa}	90,130,150,180	90,120,130,150,300	90,120,150,250,300	90,130,150,180,**270**
FKBP51^{P120pBpa}	90,100,120,130,150,180,250	90,100,130,150,180	90,100,**120**,**130**,140,200,250,**270**,**400**	100,120,**130**,150,180
FKBP51^{K121pBpa}	90,100,120,130,150,180	90,100,120,130,150,180,250	80,120,130,200	100,120,**130**,150,180
FKBP51^{E136pBpa}	120,130,150,200	120,130,150,200	120,130,150,200	120,130,150,200

Figure 28: Summary of molecular glue-based screening of UV light-inducible photo-crosslinks of FKBP51 mutants. After compound treatment photo-crosslinks, which were enhanced were marked in red, while crosslinks, which disappeared were, marked in blue. FKBP51 mutants, which showed enhanced inducible photo-crosslinks, were highlighted in orange.

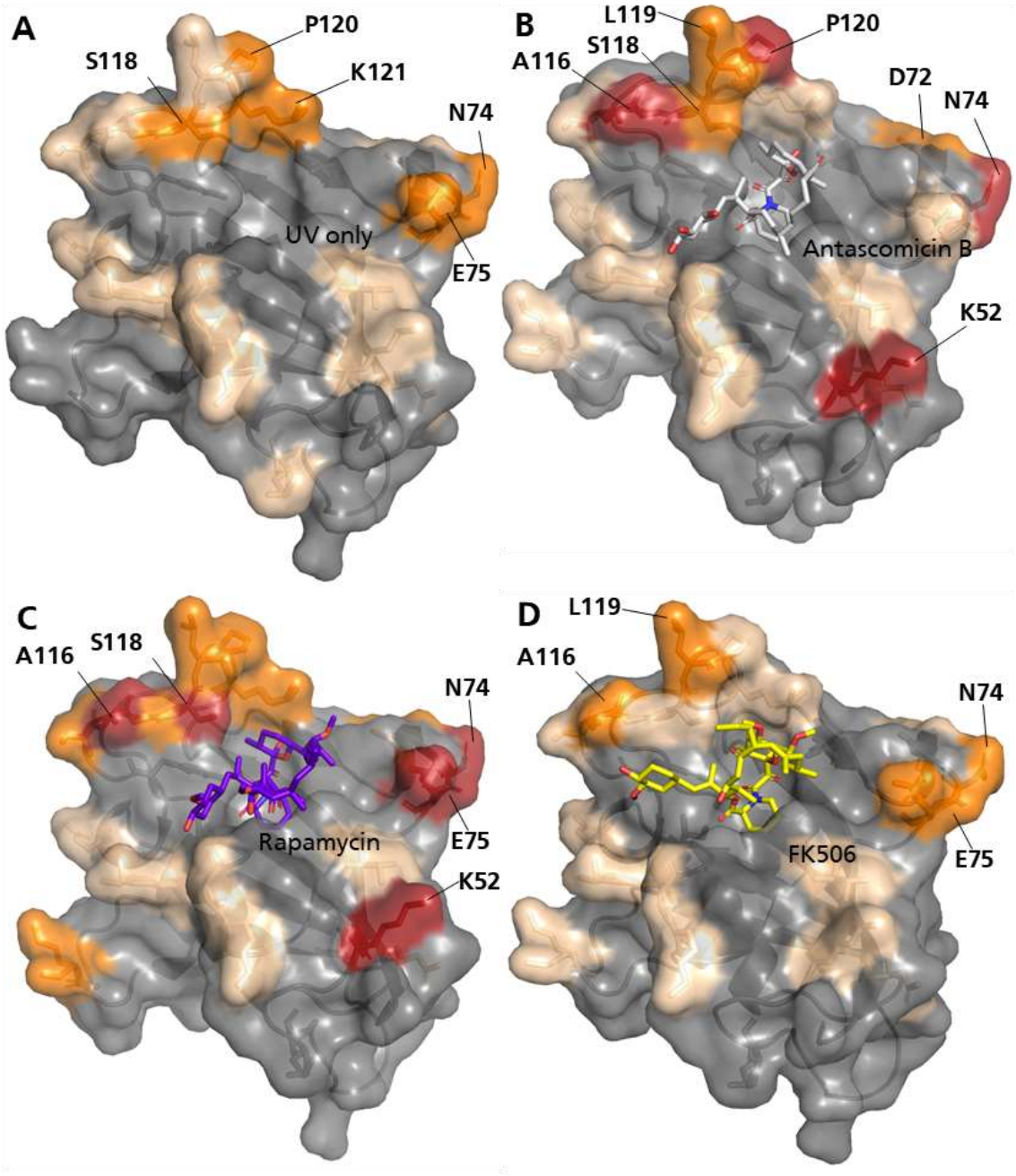

Figure 29: Occurrence of photo-crosslinks after pretreatment of FKBP51 mutants with natural molecular glues prior to UV irradiation. Based on their observed photo-crosslinking reactivity, positions of FKBP51-pBpa were highlighted in a color-coded scheme. Compared to the **A)** only UV irradiated sample (**PDB: 8r5k**), partially occurring photo-crosslinks after pretreatment with molecular glues are represented in salmon and enhanced photo-crosslinks were marked in orange. Residues labelled in dark red indicated new or interesting photo-crosslinks. **B)** structure of FKBP51 FK1 and Antascomicin B. Residues K52, D72, N74, A116, S118, P120 are labelled in dark red (**PDB: 8r5k)**.**C)** Structure of FKBP51 FK1 with Rapamycin and residues K52, N74, E75, A116, S118, highlighted in dark red (**PDB: 4DRI**). **D)** FKBP51 FK1 and FK506 with highlighted residues N74, E75, A116, L119 in orange (**PDB: 3O5R).**

The screening of FKBP51-FK1^{pBpa} mutants revealed a preferential reactivity at specific amino acid residue positions. In general, photo-crosslinks were observed when HEK293T cells were exposed to UV light. The pattern was affected when samples were pretreated with natural molecular glues Rapamycin, Antascomicin B or FK506 resulting in increased or new photo-crosslinks. Notably, most interesting

photo-crosslink patterns occurred at positions K52, N74, E75, S118, P120 and K121, when replaced by the unAA pBpa. Compared to FK506, Rapamycin and Antascomicin B displayed increasingly photo-crosslinks at 120-150 kDa at K52 and A116 (highlighted in dark red), respectively. Additionally, some positions revealed a distinct pattern dependent on the molecular glue. It was also noticed that some photo-crosslinks disappeared at positions A116-K121 when cells were pretreated with FK506 (**Figure 28**).

The abundance of photo-crosslinks after pretreatment with natural molecular glues compared to the UV irradiated results were highlighted in the co-crystal structure of FKBP51 FK1. In the presence of Rapamycin, increased or newly formed photo-crosslinks were observed when pBpa was incorporated at positions N74, E75, P120 and K121 (**Figure 29A**). FKBP51 mutants K52, N74 and E75 possessing pBpa in the β2 or β3b sheet showed increased photo-crosslinks at molecular weights of 120 kDa and 180 kDa. In general, mutants in the flexible loop of β4-β5 showed enhanced photo-crosslinking activity, whereas positions P120 and K121 induced the most interesting photo-crosslinks upon FKBP51 FK1 pretreated with Rapamycin.

Compared to Rapamycin, only a slight increase in photo-crosslinking reactivity was observed when cells were pretreated with FK506 (**Figure 29B**). At position K52, no difference compared to the UV irradiated sample was observed. Furthermore, the activity of photo-crosslinking was decreased among all other positions suggesting that FK506 led to a more rigid binding surface of FKBP51 FK1. Evaluating the positions in the flexible loop β4-β5 revealed, that position A116, P120 and K121 led to a disappearance of the 120/130 kDa photo-crosslink compared to the UV irradiated sample (**Figure 28**).

The photo-crosslinking pattern after pretreated with Antascomicin B revealed a similar pattern as observed for Rapamycin was utilized (**Figure 29C**). An increased photo-crosslink activity was observed at position N74 in the β3b loop as well as in the flexible loop β4-β5 of positions A116-K121. The most favoured position after pretreatment of Antascomicin B was position P120, inducing a strong increase of the photo-crosslink at around 125 kDa and induce an intense photo-crosslink at around 270 kDa. Moreover, the strong increase of the 125 kDa photo-crosslink was also observed when position K52 at the beginning of the β2 sheet was analysed (**Figure 28**).

The positions were unique and highly specific when cells were pretreated with Antascomicin B leading to the hypothesis that these positions can be utilized to further identify potential PPIs of FKBP51 and Antascomicin B *in vitro*. When analysed the positions where amino acids were replaced by pBpa, positions were found to be in the flexible regions between beta sheets 2-5 in the crystal structure of FKBP51 FK1 in **Figure 30**.

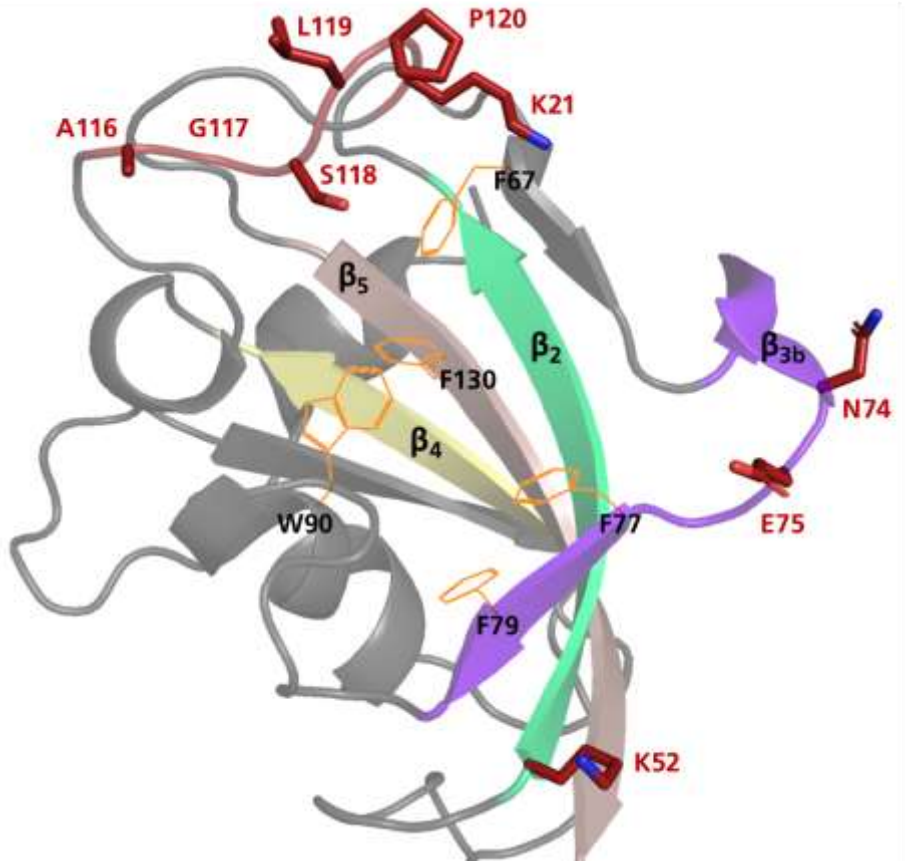

Figure 30: Highly effective photo-crosslink positions after incorporation of pBpa in FKBP51 were found in disordered regions of the FK1 domain. The hydrophobic pocket of FKBP51 FK1 is aligned by amino acid residues F67, F77, F79, W90 and F130 (depicted as orange lines) while the positions for incorporation of pBpa are highlighted in dark red as sticks. For clarification beta sheets were coloured in pale green (β2), purple (β3b), pale yellow (β4) and salmon (β5) (**PDB: 3ORE**, modified [99; 76]).

In summary, pretreatment with Rapamycin and Antascomicin B revealed an increased photo-crosslink efficiency in the positions K52, N74, E75, S118, P120 and K121. When cells were pretreated with FK506, less photo-crosslinks were observed especially at position K52 (**Figure 29**). In general, binding of natural products to the PPIase domain of FKBPs leaded to changes in the binding surface of the FK1 domain. This effect can be underlined when Rapamycin or FK506 are utilized as immunosuppressive substances for FKBP12 targeting either mTOR kinase or calcineurin B [126; 2; 139; 3; 253]. Next to small molecules, the incorporation of unAA as photo-crosslinkers may induce conformational changes which also can alter the interaction interfaces of proteins but is a highly sensitive tool when protein-protein interactions are studied in cells [254; 255].

7.4 Antascomicin B promotes the formation of FKBP51-Kinase protein complexes

7.4.1 Antascomicin B promotes ternary protein complex formation of FKBP51 and Akt1

In previous studies, FKBP51 was identified to interact with the kinase Akt, which is involved in several signalling pathways of cell growth and cell survival [208]. As the molecular weight of Akt is around 65 kDa, the 120/125 kDa photo-crosslink of FKBP51^{P120pBpa} after pretreatment with Antascomicin B could be potentially a promoted ternary complex of FKBP51 and Akt. To test this hypothesis, HEK293T cells were co-transfected with FKBP51^{K52pBpa} or FKBP51^{P120pBpa} and HA-Akt1 construct. The photo-crosslink was observed in HEK293T lysate and co-immunoprecipitation was performed (**Figure 31**).

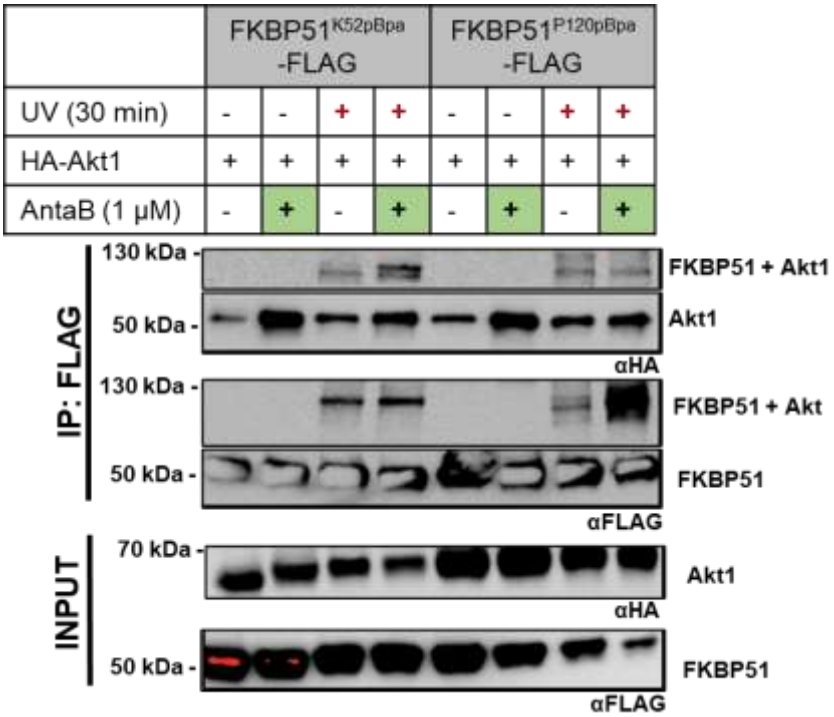

Figure 31: Antascomicin B enhances the protein-protein interaction of FKBP51 and kinase Akt1. Co-immunoprecipitation of FKBP51^{P120pBpa} or FKBP51^{K52pBpa} with HA-Akt1 WT after treatment with Antascomicin B and UV irradiation to investigate ternary complex formation. When samples were treated with Antascomicin B and UV irradiation, an increased amount of photo-crosslink at 120/125 kDa was observed suggesting that Antascomicin B enhances protein-protein interaction of FKBP51 and Akt1. When Antascomicin B was utilized for treatment higher protein level of Akt1 was observed after co-immunoprecipitation, irrespective of UV irradiation.

Pretreatment of Antascomicin B utilizing FKBP51^{P120pBpa} exhibited a photo-crosslink at 120/125 kDa compared to DMSO control or other natural compounds (**Figure 27**). After coIP (co-immunoprecipitation) HA-Akt1 was observed in higher abundance after pretreatment with Antascomicin B (Anta B) when HA tag was utilized for immunostaining (see, IP: FLAG 65 kDa αHA, **Figure 31**). Moreover, when cells were treated by UV light, a photo-crosslink was observed at 120/125 kDa. When samples were stained with αAkt (pan) the pattern was similar to HA tagged staining or FLAG tagged staining. The level of Akt was increased after coIP and the photo-crosslink at 120/125 kDa was enhanced (**Figure 31**).

Antascomicin B promoted ternary complex formation of FKBP51^{K52pBpa} or FKBP51^{P120pBpa} and HA-Akt1 construct. Notably, most of HA-Akt1 construct was not captured by FKBP51 mutants upon UV irradiation which further leaded to the question if the incorporation of the unAA pBpa has an influence on the structure of FKBP51 FK1 domain and therefore lesser binding capacity. Additional FKBP51 mutants were utilized for co-transfection with HA-Akt1 WT in HEK293T cells to investigate if the position of the incorporated pBpa has an influence on photo-crosslink efficiency to Akt1 after co-immunoprecipitation (**Figure 32**).

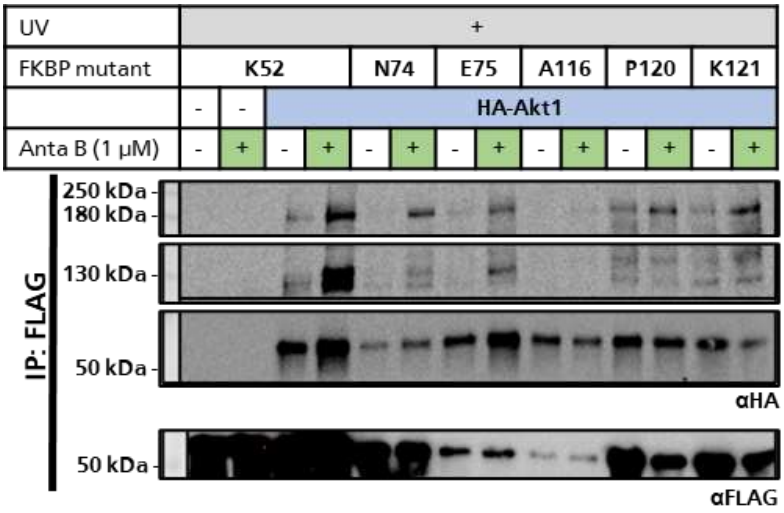

Figure 32: Several FKBP51 pBpa-mutants report an increased photo-crosslink at 125 kDa of Akt1 WT after HEK293T cells were pretreated with Antascomicin B upon UV irradiation. Co-immunoprecipitation of FKBP51 mutants and HA-Akt1 WT. After treatment with Antascomicin B photo-crosslink at 125 kDa was enhanced or induced. An additional photo-crosslink occurred at 180 kDa when cells were treated with Antascomicin B.

When different FKBP51 mutants were pretreated with Antascomicin B prior UV irradiation an enhanced photo-crosslink was found among most mutants (**Figure 32**). When HA-Akt1 construct was utilized for co-transfection a weak photo-crosslink was observed at 125 kDa in FKBP51 mutants K52, P120 and K121 (see IP:FLAG, αHA, 125 kDa). This photo-crosslink was promoted when cells were pretreated with Anta B upon UV irradiation. Additionally, the yield of HA-Akt1 construct was enhanced when the natural product was present (**Figure 32**). FKBP51^{K52pBpa} treated with Antascomicin B had a high impact on the photo-crosslink at 120/125 kDa. The photo-crosslink was strongly increased when cells were treated with the natural product. The incorporation of pBpa at different positions of FKBP51 did not affect the interaction between HA-Akt1 construct and FKBP51 but some positions were more effective.

As only partially photo-crosslinked ternary complexes were identified, FKBP51 wildtype was utilized to investigate the capacity of Antascomicin B to promote protein-protein interactions of FKBP51 and Akt1. Furthermore, FKBP51 lacking a functional TPR domain was utilized to investigate if binding to Hsp90 is required to facilitate the interaction to Akt1 upon Anta B treatment (**Figure 33**).

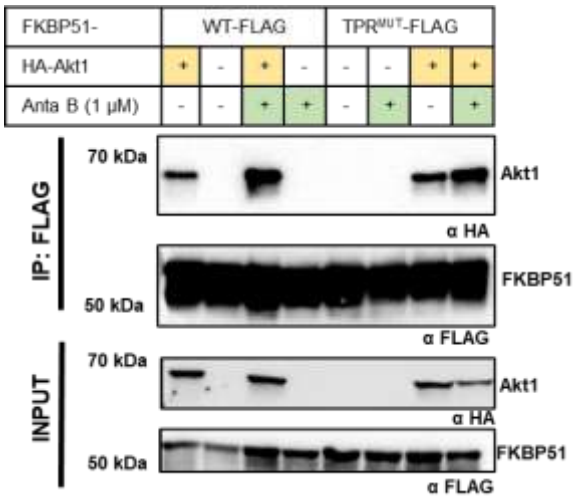

Figure 33: Pulldown experiment of FKBP51 WT and FKBP51 lacking a functional TPR domain revealed increased interaction with Akt1 when HEK293T cells were treated with Antascomicin B. HEK293T cells were co-transfected with either FKBP51 or FKBP51TPRmut (Mutation K352A/R356A) and HA-Akt1 construct and treated with Antascomicin B. Treatment with Antascomicin B increased the interaction of FKBP51 WT and HA-Akt1 WT.

Affinity pulldown of FKBP51 WT and HA-Akt1 construct revealed, that upon treatment with Antascomicin B, the interaction of the protein-protein interaction was increased resulting in a stronger ECL signal (**Figure 33**). When FKBP51TPR mutant was utilized in pulldown experiments, a slight increase of HA-Akt1 was observed in the sample. In conclusion, Antascomicin B promotes the protein-protein interaction of FKBP51 and Akt1. When mutants FKBP51^{K52pBpa} and FKBP51^{P120pBpa} were utilized for *in vitro* photo-crosslinking an increased photo-crosslink at around 125 kDa was observed after treatment with Anta B. This effect was also confirmed, when several FKBP51 mutants were utilized in a screening to investigate if the incorporation of pBpa at different positions of the FKBP51 FK1 domain has an influence upon binding surface of the protein. Notably, after the CoIP HA-Akt1 construct was found to be increased without photo-crosslinking when cells were treated with Anta B. These results indicated that Akt1 construct is only partially photo-crosslinked upon UV irradiation. When FKBP51 wildtype was utilized for pulldown experiments, Anta B also promoted ternary complex formation of FKBP51 and Akt1.

As the efficiency of FKBP51 capturing the HA-Akt1 construct is weak, the proximity of FKBP51 and Akt1 may play a crucial role when samples were irradiated with UV light. First, incorporation of pBpa at positions K52 and P120 in FKBP51 seemed to increase the interaction to Akt1 and second the efficiency of incorporation of pBpa is limited. When FKBP51 and Akt1 are not in close proximity, significant information might be lost as the unAA is rather short and rigid with steric hindrances of the aromatic groups [256]. In general, photo-crosslinkers give insights into the proximity of amino acid residues or protein domains whereas the molecular height of the photo-crosslinks can differ in immunostaining or gels as the samples were analysed via denaturing SDS PAGE [257].

However, the increased photo-crosslink at 125 kDa was present among several FKBP51 mutants including pBpa at positions K52 and P120. Even if the photo-crosslinking efficiency to Akt in general was lowered, other proteins may be involved in the formation of the 125 kDa photo-crosslink. To investigate the hypothesis, MS was utilized to identify additional proteins which might be influenced by protein-protein interactions with FKBP51 promoted by Antascomicin B.

7.4.2 The 125 kDa photo-crosslink may not exclusively be kinase Akt1

For MS, FKBP51^{P120pBpa} was expressed in HEK293T cells in a large-scale approach and treated with Antascomicin B prior to UV irradiation. In a second approach HEK293T FKBP12 knock-out cells were utilized to increase the bioavailability of Anta B within the cells as the natural product preferably binds to FKBP12 with a lower K_D. After CoIP, samples were loaded onto a SDS gel and stained with Coomassie blue to obtain the 125 kDa photo-crosslink for further analysis by MS at EMBL Heidelberg (**Figure 34**).

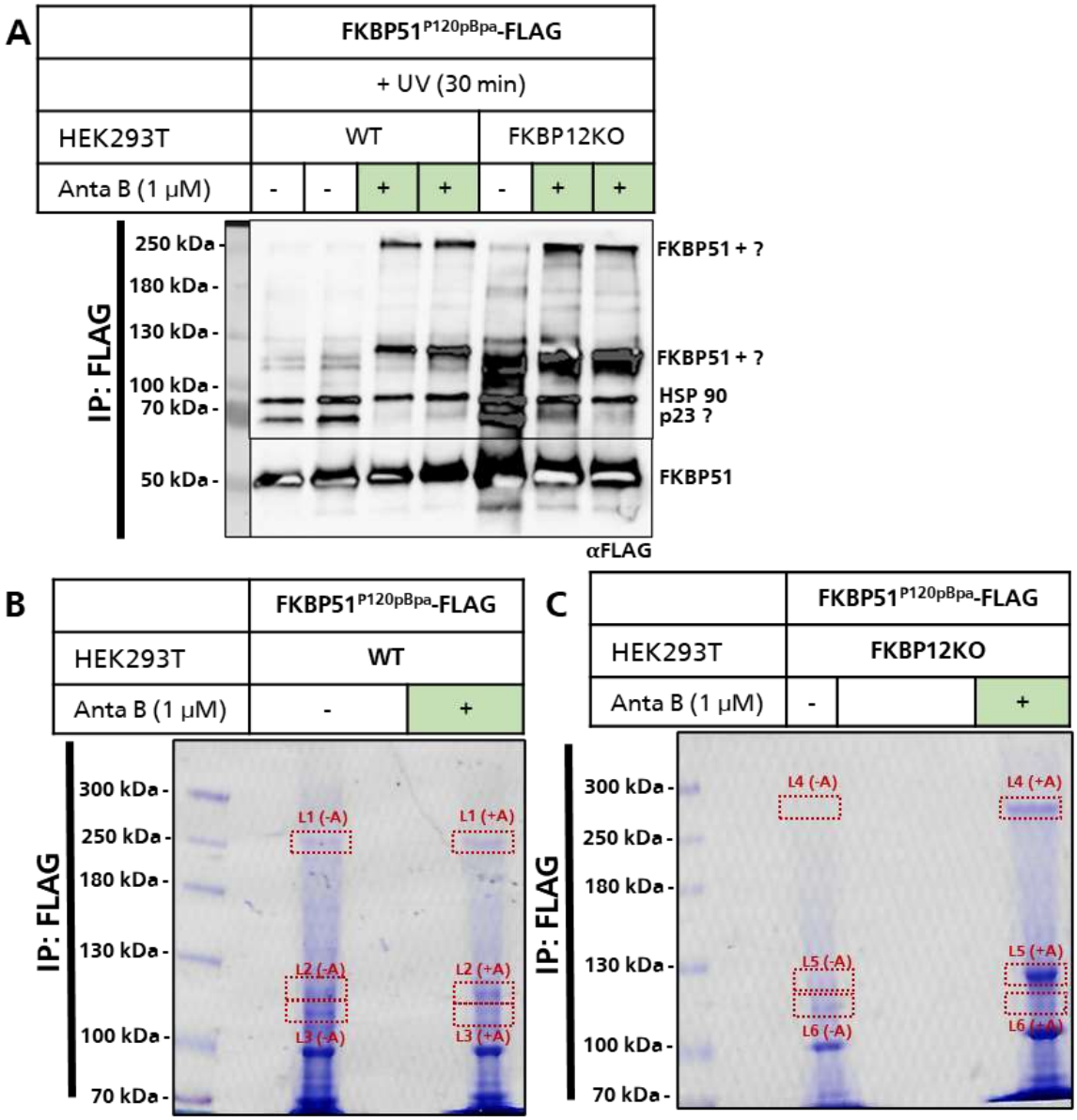

Figure 34: Large scale expression of FKBP51^{P120pBpa} in HEK293T WT and HEK293T FKBP12 knock out cells induced photo-crosslinks at 125 kDa and 300 kDa upon treatment with Antascomicin B and UV irradiation. A) Immunostaining by FLAG of cell lysate from HEK293T WT and HEK293 FKBP12 knock out irradiated with UV light and either treated with Antascomicin B or not. When cells were treated with Antascomicin B prior to UV irradiation, the 125 kDa as well as 300 kDa photo-crosslink occurred, whereas the photo-crosslink was enhanced when HEK293T FKBP12 knock out cells were utilized. **B)** Coomassie staining after pulldown of FKBP51^{P120pBpa} from HEK293T WT lysate. L1 = 300 kDa photo-crosslink, L2 = 125 kDa photo-crosslink, L3 = 110 kDa photo-crosslink, which is only induced upon UV irradiation. **C)** Coomassie staining after pulldown of FKBP51^{P120pBpa} from HEK293T FKBP12 Knock out lysate. L4 = 300 kDa photo-crosslink, L5 = 125 kDa photo-crosslink, L6 = 110 kDa photo-crosslink which only occurs upon UV irradiation. In general, photo-crosslinks at 300 kDa and 125 kDa were enhanced when knock out cells were utilized.

Immunostaining showed an enhanced photo-crosslink at 125 kDa and an induced photo-crosslink at around 250-270 kDa when cells expressing FKBP51^{P120pBpa} were pretreated with Anta B upon UV irradiation (**Figure 34A**). When HEK293T FKBP12 Knock-out cells were utilized, the photo-crosslinks were found to be enhanced compared to the wild type cells. Moreover, without treatment of Anta B an additional photo-crosslink was observed at around 70 kDa, which was suggested to be p23 which is part of the Hsp90 machinery in former analysis in mass spectrometry by Baischew & Engel [84; 210].

Samples were analysed by SDS PAGE. The photo-crosslinks of each approach were marked with red arrows, respectively. For wildtype MS analysis the 250 kDa photo-crosslink was depicted as lane 1 (L1), the 125 kDa photo-crosslink as lane 2 (L2). Moreover, the sample without Anta B possessed a photo-crosslink at around 100 kDa, which was described as lane 3 (L3) (**Figure 34B**). Photo-crosslinks, which were observed after pretreatment of Anta B in HEK293T FKBp12 knock-out cells were highlighted equally (**Figure 34C**).

The gels were sent to the proteomics core facility of the EMBL in Heidelberg whereas samples were prepared by cutting out the photo-crosslinks of the gel. The samples were digested with trypsin and analysed with a mass spectrometer. The results of the measurement were compared between both samples and corresponding protein lanes in **Table 31**.

Table 31: Proteins which were identified in mass spectrometry of protein lanes L1-L6 of FKBP51^{P120pBpa} mutant after treatment with Rapamycin and UV light. Proteins identified were described with **gene name**, **protein ID** and **description**. Additionally, the molecular weight (**mw**) was indicated as well as the results of MS analysis represented in **ssm** (spectra mapping, assignment of protein peptides), **total score** (with mascot, the higher the more reliable), **top3** (abundance of protein in the sample, log10), and **sequence coverage** in %. **A)** FK506-binding proteins found in all samples including FKBP51^{P120pBpa} mutant. **B)** protein kinases which were identified after Antascomicin B and UV treatment with a corresponding mw of around 50 kDa. **C)** Phosphatases which were identified after treatment with Antascomicin B and UV irradiation. **D)** Serendipitous proteins with a corresponding mw of around 50 kDa. Expanded protein table in **Suppl. 5**. Prominent proteins which were described in the following section were highlighted bold and red.

Gene name	Protein ID	Description	Mw (kDa)	Top3	ssm	total score	Seq. cov	Lane (+/- Anta B)
A) FK506-binding proteins								
FKBP5	Q13451	FKBP51-P120pBpa	52.25	7.79	96	147	66.7 %	L1 (-A)
		FKBP51-P120pBpa	**52.25**	**7.03**	**307**	**131**	**79.0 %**	**L1 (+A)**
		FKBP51-P120pBpa	52.25	8.41	173	138	71.7 %	L2 (-A)
		FKBP51-P120pBpa	**52.25**	**7.30**	**346**	**150**	**81.3 %**	**L2 (+A)**
		FKBP51-P120pBpa	52.25	8.39	153	153	68.7 %	L3 (-A)
		FKBP51-P120pBpa	52.25	7.01	160	150	73.0 %	L3 (+A)
		FKBP51-P120pBpa	52.25	7.77	264	144	48.5 %	L4 (+A)
		FKBP51-P120pBpa	52.25	8.34	179	133	49.8 %	L5 (-A)
		FKBP51-P120pBpa	52.25	7.81	248	117	50.2 %	L5 (+A)
		FKBP51-P120pBpa	52.25	8.62	157	128	48.7 %	L6 (-A)
		FKBP51-P120pBpa	52.25	7.42	193	120	50.2 %	L6 (+A)
		Peptidyl-Prolyl cis-trans isomerase FKBP5 (endogenous)	**51.12**	**5.97**	**169**	**2583**	**49.3 %**	**L6 (+A)**
B) Kinases								
AURKA	O14965	AURKA_HUMAN Aurora kinase A	45.81	5.30	3	106	6.4 %	L2 (+A)
AURKB	Q96GD4	AURKB_HUMAN Aurora kinase B	39.31	6.21	4	228	13.6 %	L3 (+A)
CHEK1	**O14757**	**Serine/threonine-protein kinase Chk1**	**54.43**	**6.21**	**6**	**361**	**16.1 %**	**L2 (+A)**
				6.36	**2**	**145**	**5.0 %**	**L5 (+A)**
ILK	Q13418	Integrin-Linked protein kinase	51.42	5.76	4	127	8.8 %	L2 (+A)

PGK1	P00558	Phosphoglycerate kinase 1	44.61	5.47	3	140	12.3 %	L3 (+A)
C) Phosphatases								
PPP4R3A	Q6IN85	Serine/threonine-protein phosphatase 4 regulatory subunit 3A	95.36	5.66	6	210	6.6 %	L3 (+A)
				6.11	4	170	4.8 %	L6 (+A)
D) Serendipitous proteins in Antascomicin B and UV irradiation samples								
ILF2	Q12905	Interleukin enhancer-binding factor 2	43.06	5.43	5	204	15.3 %	L2 (+A)
				5.38	2	142	9.6 %	L3 (+A)
				5.61	3	108	3.0 %	L3 (+A)
NR3C1	**P04150**	**Glucocorticoid receptor**	**85.67**	**5.65**	**3**	**191**	**6.6 %**	**L2 (+A)**
				5.67	**7**	**360**	**10.9 %**	**L3 (+A)**
				5.88	**2**	**142**	**4.2 %**	**L5 (+A)**
				5.77	**3**	**183**	**4.2 %**	**L6 (+A)**

MASCOT is a protein sequence database to analyse ion spectra from MS, utilized by EMBL [258]. Proteins were analysed by label-free quantification (LFQ), whereas the value Top3 describes the calculated mean of the three highest peptide areas measured for each protein [259; 260]. MASCOT utilized probability-based scoring where the total score is the probability that the observed match is a random event but encompassing a wide range of magnitudes leading to false positive events [261]. Therefore, single peptide mapping (ssm) and sequence coverage were also depicted to investigate peptide probabilities within the samples during this thesis.

MS revealed that FKBP51^{P120pBpa} was found to be involved in every lane (L1-6). However, when lane 4 without Anta B of HEK293T FKBP12 knock-out cells were analysed, no proteins were found in the sample (**Figure 34C**). The highest probability of FKBP51^{P120pBpa} was found in samples L1 (+A) and L2 (+A) with 307 or 346 single peptides found, respectively (**Table 31A**, highlighted in red). The sequence coverage fluctuated between 48.5 % and 81.3 %. Depending on the total score and Top3 value, FKBP51^{P120pBpa} was likely to be found in all samples. FKBP51 wildtype was also described to be found in sample L6 (+A) with a total score of 2583 and a lower Top3 value of 5.97 indicating that single peptides found in the sample may also be repeated peptide sequences from FKBP51^{P120pBpa} mutant (**Table 31A**, highlighted in red). The highest sequence coverage and ssm was observed in samples L1 (+A) and L2 (+A) of HEK29T WT as well as L4 (+A) and L5 (+A) of HEK293T FKBP12 knock-out cells indicating that Antascomicin B promotes efficiency of photo-crosslinking events in the cells.

The results were analysed based upon different protein families as well as serendipitous proteins which were only found to be present upon pretreatment with Anta B and UV irradiation. Additionally, proteins which were only observed after UV treatment as well as ubiquitous proteins among all samples were listed in supplementary **Table 32**. In all samples Hsp90, Hsp70 as well as Hsp105 were likely to be found which were already observed in previous studies. Heat shock proteins are often found in mass

spectrometry analysis and were already shown to be captured by photo-crosslinking when pBpa is incorporated in photo probing for FKBP51 [84; 210]. Therefore, those proteins were neglected in further analysis of the effect of Antascomicin B on protein-protein interactions.

The human kinome possess 538 kinases which are involved in essential functions of signalling pathways including in protein phosphorylation [151]. Kinases are structurally related and highly conserved among its kinase domains but may vary in additional structures [262]. As Antascomicin B promotes ternary complex formation of FKBP51 and Akt1, other additional kinases were identified after the results of mass spectrometry. The molecular weight of the kinases ranged from 39.31 kDa to 54.43 kDa. Notably, the largest number single peptide sequences of kinases were found in sample L2 (+A) (**Table 31B**). In general, all kinases were found with a similar Top3 value of endogenous FKBP51 described above. Moreover, kinases single peptide sequences varied from 2 to 6 units leading to a poorly sequence coverage. However, the predictability represented by the total score led to the hypothesis, that the results are reliable. In lane L2 (+A) Aurora kinase A (AurA) was found with 3 single peptide sequences in total, while Aurora kinase B (AurB) was observed in sample L3 (+A). Aurora kinases regulate chromosomal alignment and segregation during mitosis and meiosis [73]. Normally, AurA is present in the nucleus but there is evidence that the kinase is involved in regulation of energy metabolism with the mitochondrial ATP synthase and cell death [263–265]. Another kinase involved in cell cycle progression is the Checkpoint kinase 1 (Chk1/CHEK1) (**Table 31B**, highlighted in red). The kinase was observed in sample L2 (+A) of HEK293T WT treatment and sample L5 (+A) of HEK293T FKBP12 knock-out treatment with a higher abundance in ssm for the WT approach (6 ssm) respectively. Chk1 is involved in triggering cell cycle arrest at the G2/M checkpoint and is regulating DNA damage repair and gene transcription [266–268]. While Chk1 is primarily localized in the cytoplasm to regulate cell cycle checkpoint response, Aurora kinases are found within the nuclear compartment but there is evidence that Aurora kinase A localises to mitochondria controlling the fusion of interconnected organelles to control ATP production [269; 270].

Next to Chk1 and AurA and AurB, integrin-linked protein kinase (ILK) and phosphoglycerate kinase 1 (PGK1) were observed in sample L3 (+A). The values of both kinases were in the same range as observed for kinases involved in cell cycle progression. ILK is a member of the TKL serine-threonine protein kinase family tree and involved in a myriad of signalling pathways including the PI3K/Akt pathway. Moreover, ILK is involved in cell-matrix interactions, cell adhesion and function as an anchor in cell growth. [154; 271]. The protein kinase ILK is suggested to contribute in Akt-dependent cell survival by regulating SER^{473} phosphorylation as PIP3 recruits ILK to the cell membrane next to PDK1 and Akt itself [272–275]. Moreover, ILK is one of the upstream components in SGK1 signal transduction [274; 276]. The serum- and glucocorticoid-regulated kinase 1 (SGK1) is also known as second Akt and part of the AGC kinase

family [277]. PGK1 serves as an ATP-producing glycolytic enzyme controlling ATP and 3-phosphoglycerate levels to coordinate energy production [278; 279]. As a serine-threonine protein kinase its key role is in cell survival and autophagy. The kinase is known to phosphorylate PRAS40 (Akt1S1), which promotes tumorigenesis. Moreover, PRAS40 is known as Akt substrate and is involved in the regulating mTOR complex [280; 281].

All five protein kinases were observed in samples L2 (+A) and L3 (+A) sharing a similar molecular weight with a higher predictability in the total score (**Table 31B**). AurA and AurB are involved in cell cycle processes in the nucleus while ILK and PGK1 are involved in phosphorylation of several pathways including the PI3K/Akt/mTOR signalling pathway. One of the downstream targets is Chk1, which function is to maximize cell survival in facilitating DNA repair [282]. Interleukin enhancer-binding factor 2 (ILF2; see **Table 31D**) as well as serine-threonine protein phosphatase 4 (PPP4R3A; see **Table 31C**) are proteins involved in cellular stress response. In response to DNA damage, ILF2 localizes in the cytoplasm to interact with the spliceosome [283]. Moreover, PPP4R3A in a heterotrimer complex is also involved in DNA damage response (DDR) [284]. Both proteins were found within several samples of L2-L5 (+A) with similar Top3 values and single peptide mappings (ssm). In general proteins involved in DDR are likely to be found upon treatment of samples by UV irradiation, but the higher predictability led to the discussion if those proteins may be influenced upon treatment of Antascomicin B.

The Glucocorticoid (GR) receptor is a well-known target for FKBP51 in the mechanism of the Hsp90 machinery. Previous studies successfully mapped the binding interface of FKBP51 and GR by utilizing pBpa in photo-probing [84; 210]. The receptor was observed in the samples L2-L3 and L5-L6 pretreated with Anta B with similar Top3 values and single peptide mapping (ssm) leading to a sequence coverage of 4.2-10.9 % (**Table 31D**). However, no GR was observed in the corresponding samples without Antascomicin B. As the single peptide mapping (ssm) value is low, the efficiency of the photo-crosslink between FKBP51^{P120pBpa} and GR may vary without Antascomicin B. This could indicate that Antascomicin B has an influence on the binding surface of FKBP51^{P120pBpa} and GR. FKBP51^{P120pBpa} and FKBP51^{A398pBpa} were already investigated in previous studies, where FKBP51^{P120pBpa} was shown to induce photo-crosslinks with GR upon UV irradiation. Moreover, FKBP51^{A398pBpa} does not initiate a photo-crosslink when GR expressed in HEK293T cells [210]. The FKBP51 mutants were utilized for co-transfection with a HA-GR construct to evaluate the influence of Antascomicin B on the binding interface of both proteins after affinity pulldown (**Figure 35**).

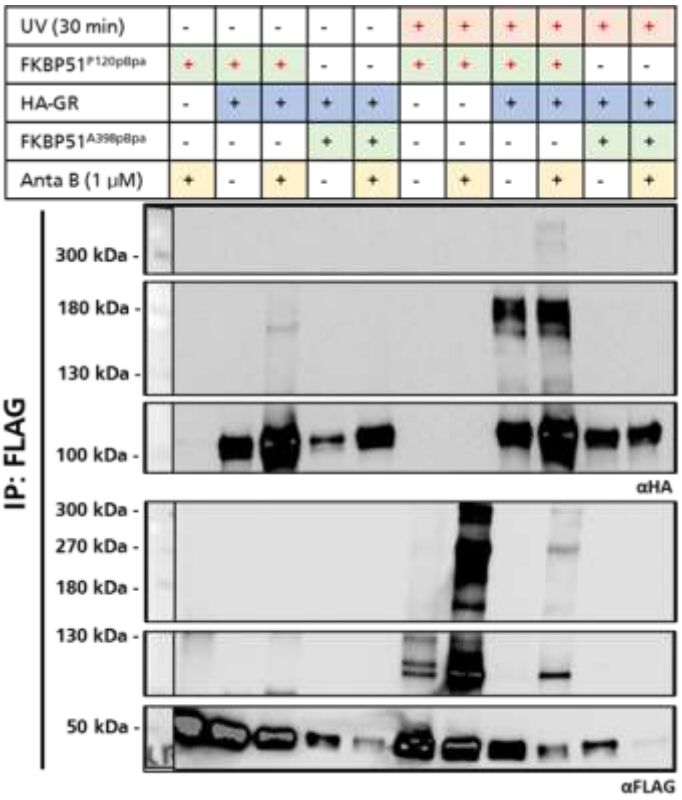

Figure 35: Antascomicin B does not influence the protein-protein interaction of FKBP51 and GR. HEK293T cells were co-transfected with FKBP51^{P120pBpa} or FKBP51^{A398pBpa} and HA-GR construct. Cells were pretreated with Anta B upon UV irradiation. After UV irradiation photo-crosslinks induced by Antascomicin B were observed at 125 kDa, 180 kDa and around 270/300 kDa at FKBP51^{P120pBpa}. When FKBP51^{A398pBpa} was utilized no photo-crosslinks were observed.

When cells expressing FKBP51^{P120pBpa} were treated with Anta B upon UV irradiation, induced photo-crosslinks at 125 kDa, 180 kDa and 270/300 kDa were observed. The 125 kDa photo-crosslink was also observed without the effect of Anta B (see IP: FLAG, 130 kDa, αFLAG; **Figure 35**). The effect on photo-crosslinking efficiency was lowered when HA-GR was co-expressed in HEK293T cells. Utilizing FKBP51^{A398pBpa} resulted in the absence of photo-crosslinks (see IP:FLAG, αFLAG lane 10-11) [210]. When samples were investigated for the presence of HA-GR, it was found, that the amount of HA-GR was increased when cells were treated with Anta B (see IP:FLAG, 100 kDa, αHA; **Figure 35**). Immunostaining by FLAG revealed an increased photo-crosslink at around 180 kDa, which might be consistent with the 180 kDa photo-crosslink observed in the FLAG immunostaining indicating proximity of FKBP51 and GR [84].

Notably, the pattern of FLAG and HA immunostaining differed. As previously samples L2-L3 (+A) and L5-L6 (+A) were investigated for mass spectrometry, the corresponding molecular height of the desired photo-crosslink was at 100-125 kDa (**Table 31**; **Figure 34**). The single peptide sequences were only found in the Anta B treated samples, which is consistent with the increased yield of HA-GR observed after treatment with Anta B (**Figure 35**). In conclusion, higher yields of GR were observed when cells

were pretreated with Antascomicin B. As the natural product is closely related to FK506 which is modulating GR activity upon binding to FKBP51 an identical influence of Antascomicin B is possible while the GR is not the primary target of the FKBP51:AntaB complex [19]. Moreover, so far, no ternary complex formation of FKBP51 and GR upon treatment with FK506 was found. The glucocorticoid receptor resides in the cytoplasm in complex with FKBP51 and FKBP52, maintaining the receptor in a transcriptionally inactive state. The classic signalling pathway of the GR is mediated by transcriptional responses, but kinases like Akt appeared to be additionally involved in signalling events of the GR [285]. In general, the activation of GR gene expression is a multistep event which requires translocation of the GR to the nucleus. Akt1 is found to directly phosphorylate S134 in the GR. When Akt was inhibited by MK2206, the phosphorylation site was found to be decreased. Piovan *et. al* demonstrated that mutant NR3C1 S134A showed an increased nuclear localization to the nucleus compared to the wild type NR3C1 comparable with treatment of dexamethasone [286]. Hypothetically, the phosphorylation at S134 of the GR is lowered as Akt1 is in complex with FKBP51 and Antascomicin B resulting in an increased localization to the nucleus whereas the GR could upregulate its NR3C1 genes. As FKBP51 and GR are naturally interacting with each other, higher yields of the GR could be then found after affinity pulldown with FKBP51-FLAG tagged protein. Higher yields of the GR after pulldown were then suggested to be a side effect of the ternary complex of FKBP51:Anta B:Akt1.

However, Akt1 was not detected in MS analysis. The identification of kinases in MS analysis is an ongoing field as kinases are fundamental and highly conserved among the human kinome [151]. The kinome is one of the largest superfamilies of homologous proteins with over 500 kinases and divided in eight typical and 13 atypical families [149]. Kinases are often expressed at low cellular levels which can affect the detection in the whole cellular proteome [287]. Therefore, identification of kinases in MS is a challenging field, as kinases are present in different phosphorylation states as well as isoforms. Additionally, they share a high sequence similarity which can affect detection in mass spectrometry [149]. In mass spectrometry, kinases Chk1, AurA, AurB, ILK and PGK1 were observed with a relatively stable predictability even if their ssm and sequence coverage were lower. This can be explained by lower cellular expression levels. It was suggested that in addition to Akt1 other kinases could be also addressed by the complex of FKBP51 and Antascomicin B due to their high sequence homology. Moreover, as previously observed in the immunostaining of αFLAG, the Antascomicin B induced 125 kDa photo-crosslink is not exclusively the kinase Akt1 (**Figure 31**). Depending on the molecular weight compared to Akt1 (56 kDa), Chk1 has a similar molecular weight of 54 kDa. If Antascomicin B induces a ternary complex of FKBP51^{P120pBpa} and Chk1, an induced photo-crosslink would be also observable at around 125 kDa.

Moreover, it occurred that only a small percentage of Chk1 could stably be associated with Hsp90 [288]. This could also indicate, that FKBP51 participates in transient interactions or chaperoning of Chk1 whereas the interaction of both proteins was enhanced when cells were pretreated with Antascomicin B. Comparing Akt1 and Chk1, both kinases are members of different kinase families. While Chk1 belongs to the CAMK (Ca^{2+}/calmodulin-dependent protein kinase) Akt1 is part of the AGC (related to cAMP-dependent protein kinase PKA) family. In the dendrogram, both kinase families are closely related based upon their primary sequence compared to the other six large kinase families [149]. Comparing protein structures of Akt1 and Chk1, the nucleic kinase only possesses 26 % sequence identity. The template modelling score of Chk1 to Akt was 0.69 utilizing RCSB PDB pairwise structure alignment where a TM-score of 1 indicates a perfect match between 3D-structures. Both kinases have the same protein fold as shown in **Figure 36**.

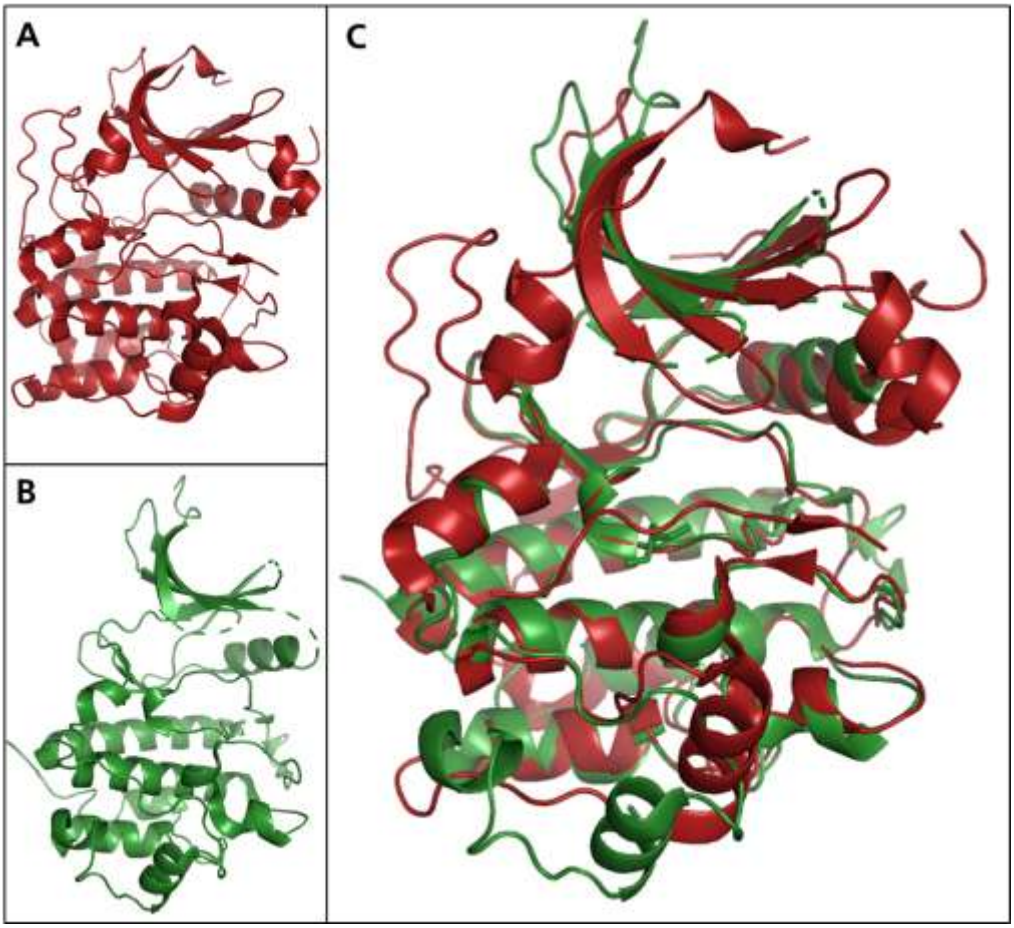

Figure 36: Akt1 and Chk1 share high sequence homology. A) Akt1 is coloured in dark red (**PDB: 1O6L**) **B)** Chk1 is marked in dark green (**PDB: 4FTO**). **C)** 3D-structure alignment of Akt1 and Chk1 showed that upon 1D-sequcence identify the protein fold of the two kinases are homologous.

Chk1 participates in DNA damage response (DDR) signalling cascades leading to cell cycle arrest and DNA repair. Chk1 is part of the ATR complex which is activated downstream of 4EBP1 and elF4E. 4EBP1 is a downstream target of the mTORC1 complex which is regulated by AKT activation [289]. Thus, FKBP51 and Chk1 are not direct interaction partners in signalling pathways regarding cell cycle arrest. As FKBP51 is known as co-chaperone of Hsp90, Chk1 is a transient binding partner as the kinase is activated within the Hsp90 machinery [288]. It was reasonable, that Chk1 was found to co-immunoprecipitate with FKBP51. The interaction of FKBP51 and Chk1 was promoted by Antascomicin B, which was also observed as UV inducible photo-crosslink (**Supp. 6**).

7.5 The interaction of FKBP51 and Akt1 promoted by Antascomicin B does not require a specific phosphorylation state of the kinase

Kinases are major key players in cell signalling pathways. Ordinary they have different isoforms as well as additional splicing variants within the proteome [149; 290]. Activation and therefore downstream signalling of kinases requires phosphorylation which is a posttranslational modification. Posttranslational modification leads to transient activation states of kinases resulting in changes of their conformation. Each kinase consists of a C- and N-lobe as well as a regulatory and catalytic spine. Both spines are anchored to the hydrophobic F-helix which is the organizing element of the kinase core [291]. Regulation of kinases involves a dynamic reorganization of the molecule, which is typically complex and highly regulated [292; 293].

As kinases possess different activation states, it was suggested that Antascomicin B might promote ternary complex formation with FKBP51 when Akt1 and other kinases harbour a specific activation state. As Akt1 regulates the mTORC pathway, resulting in regulation of cell cycle arrest, different Akt1 mutants possessing several transient activation states were elucidated. Phosphorylation sites might have an influence on the ternary complex of FKBP51:Anta B:Akt1. Alanine (A) mimics the inactive form, while exchange of the corresponding amino acid to glutamine (D) mimics the active form of the kinase. Wildtype Akt1 was utilized as control to compare photo-crosslink efficiency of $FKBP51^{K52pBpa}$ and Akt1 mutants promoted by Antascomicin B (**Figure 37**).

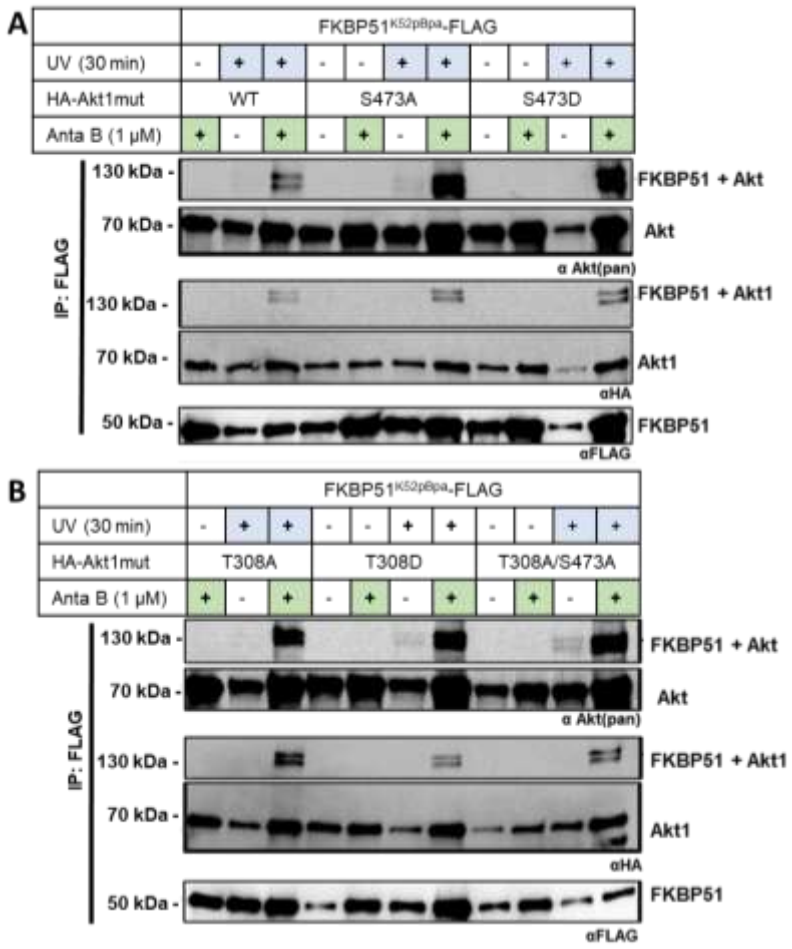

Figure 37: The interaction of FKBP51 and Akt1 does not require a specific activation state of the kinase. Mimicking different activation states of Akt1 by introducing Alanine (A) or Glutamine (D) on phosphorylation sites S473 and T308 did not promote the ternary complex formation of FKBP51:Anta B:Akt1. Antascomicin B promotes photo-crosslinking efficiency of the ternary complex at 120/125 kDa despite the activation state of the kinase.

When FKBP51^{K52pBpa} was treated with Antascomicin B, the yield of HA-Akt1 constructs was increased after affinity pulldown in each sample, irrelevant of UV treatment (IP:FLAG, αAkt(pan) 70 kDa; **Figure 37**). When samples were treated with Antascomicin B and UV irradiation, at 120-125 kDa a double photo-crosslink was observed among all HA-Akt1 variants. In none of the cases, a specific form of HA-Akt1 was suggested to be favoured upon Antascomicin B treatment. This indicated that phosphorylation states of Akt1, which are required for full activation by phosphorylation of residues T308 and S473, are not necessary. The ternary complex formation of FKBP51:Anta B:Akt1 is independent of the phosphorylation state and therefore activity of the kinase [294].

Additionally, 20 other residues of Akt1 have been identified to be phosphorylated so far in mass spectrometry [295]. Some residues like Thr305, Thr312 and Tyr474 were shown to contribute in optimal Akt1 activation while other residues like Thr72 or Ser246 are suggested to be auto phosphorylated in trans or residues Thr34, Thr450 and Tyr176 appeared to be mediated by upstream kinases [296–298]. Most of the phosphorylation sites have not been characterized until today and their function is unknown so far, as well as the influence on signalling pathways within the cell. Ternary complex formation of FKBP51 and Akt1 by Anta B does not require a specific phosphorylation state of Thr308 or Ser473, but the natural compound could support additional posttranslational modifications of Akt1 and other kinases. In general, posttranslational modifications may have an influence on conformation, stability, activity, subcellular localization or protein-protein interactions whereas phosphorylation is crucial for regulation of signal transduction pathways [299].

It was suggested that Antascomicin B addresses additional signalling pathways such as its related natural compounds Rapamycin and FK506. Phosphoproteomics in mass spectrometry may help to investigate and identify activated signalling networks which are influenced by Antascomicin B allowing conclusions, which FKBP51:Anta B:kinase complex has an important impact in cellular signalling pathways. In general, phosphorylation is a transient and reversible posttranslational modification which is highly dynamic on the seconds-to minutes time scale [299; 300]. Another experimental setup would be surface plasmon resonance (SPR) which is an optical technique to measure molecular interactions in real time by help of Kretschmann configuration utilizing a gold film at the interface of two dielectric media [301]. The experimental setup could contain the immobilized FKBP51:Anta B complex on the metal surface of the SPR transducer. If kinases will interact with the immobilized complex, the solution refractive index at the interface changes which then leads to a different angle in the SPR revealing information about the binding amount, the association and dissociation rate constants as well as the apparent association [302].

The ternary complex formation rate of FKBP51 and Akt1 or Chk1 is not in a ratio of 1:1 suggesting that different activation states or isoforms are responsible to interact with FKBP51 upon Antascomicin B treatment. Quantitative real-time PCR (qRT-PCR) or next-generation sequencing could be utilized to further elucidate the influence of the FKBP51:Anta B:kinase complexes on the genomic level of the cell. Transcription and translation of proteins required in e.g., apoptosis or immune response are driven by upstream signalling pathways. As Akt1 and Chk1 are major key proteins in signal transduction in many essential pathways like apoptosis, cell cycle progression or immune response, transcription and translation of downstream genes could lead to further insights which signalling pathway is affected by Antascomicin B. Moreover, protein stabilization is often widely utilized to study protein-protein interactions. As kinases are dynamic and undergo conformational changes upon activation due to

phosphorylation at specific residues a defined conformation could be utilized to further elucidate the affinity of the FKBP51:Anta B complex to interact with the corresponding kinase. As Akt1 is involved in various protein-protein interactions, tendencies with other proteins may influence the interaction interface between FKBP51:Anta B and Akt1 [167; 303]. Chk1 and Akt are known to interact with Hsp90 which has co-chaperoning and therefore an activating function of kinases within the cell [288; 303]. The capability of Antascomicin B to induce ternary complex formation of FKBP51 and Akt1 was lowered when FKBP51 lacking a functional TPR domain was utilized (**Figure 33**). The TPR domain is required to interact with the Hsp90 machinery but the interaction of FKBP51 to Akt1 seems to be Hsp90 independent. However, lack of data could not completely exclude the influence of Hsp90. If a stabilized isoform of Akt1 and Chk1 would be utilized, the interaction with Hsp90 could also be abandoned, leading to further insights into the interaction of FKBP51 and kinases.

To increase the interaction between FKBP51 and Antascomicin B, HEK293T FKBP12 knock-out cells were utilized in mass spectrometry (**Figure 34**). Mass spectrometry analysis revealed that in either WT cells or knock-out cells Chk1 and corresponding kinases were present in the 125 kDa photo-crosslink. However, the absence of FKBP12 led to changes upon transcription or translation of various other proteins suggesting that utilizing FKBP12 knock-out cell lines were not suitable to further validate the influence of Antascomicin B by ternary complex formation or downstream signalling.

While Antascomicin B was found to interact with the binding pocket of FKBP51 FK1 domain with a nanomolar affinity of 6.7 nM, the compound was found to interact with FKBP12.6 (0.6 nM) and FKBP12 with a KD of 0.03 nM (**Table 29**). FKBP12 was thought to be involved in additional ternary complexes when cells were treated with Antascomicin B. For this purpose, SDM was utilized to generate FKBP12 mutants which incorporate pBpa for further photo-crosslinking experiments.

7.6 Amber suppression-mediated site-specific photo-crosslinking of FKBP12 mutants upon treatment with natural molecular glues

7.6.1 Incorporation of pBpa in FKBP12 mutants is less efficient for *in vitro* photo-crosslinking

FKBP12 contains 108 amino acid residues and is the smallest member of the FKBP family. The protein is well known to interact with the FRB domain of the mammalian target of Rapamycin (mTOR) [126]. The protein-protein interaction is induced by Rapamycin resulting in an inhibition of mTORC1 modulating signalling pathways involved in immune response [304–306]. To investigate potential protein-protein interactions with natural compounds, pBpa was introduced in FKBP12 during translation. In total, 23 amino acid residues were utilized for site-specific in-cell photo-crosslinking (**Figure 38**).

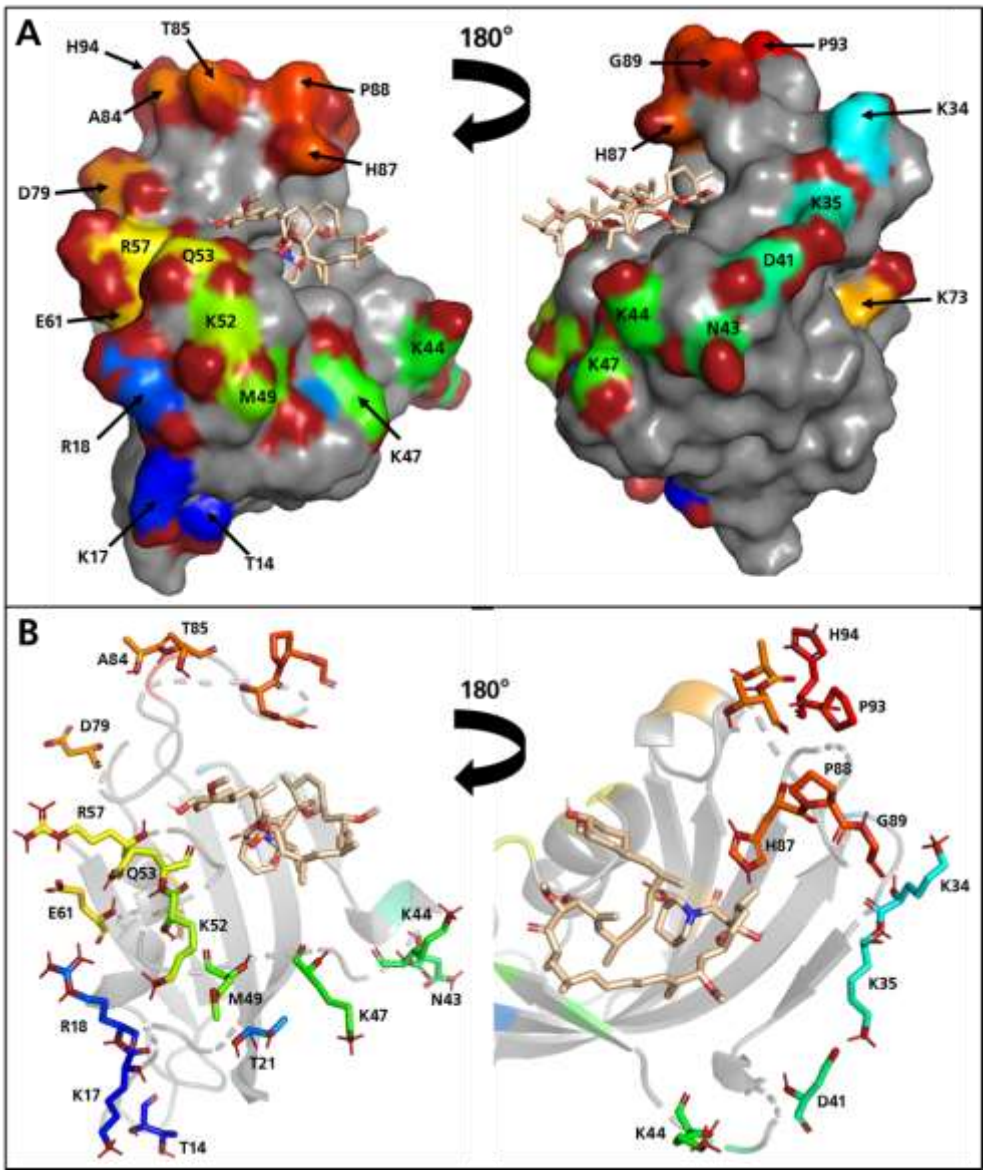

Figure 38: Map of surface amino acids of FKBP12, which are utilized for site-specific photo-crosslinking in HEK293T cells. (A) Amino acids located on the surface of the FKBP12 domain are illustrated in a colour spectrum to delineate each amino acid, respectively. **(B)** Figure of the FKBP12 protein surface structure. Rapamycin is located in the binding pocket of the PPIase domain surrounded by 23 selected amino acids in total (**PDB: 1FAP**)

First, Twin-Strep FLAG plasmids containing FKBP12 WT and FKBP12^{K47pBPa} were utilized to investigate if UV irradiation induces site-effects. Rapamycin was utilized as a molecular glue as the compound is known to induce the FKBP12:Rapamycin:mTOR complex (**Figure 39**).

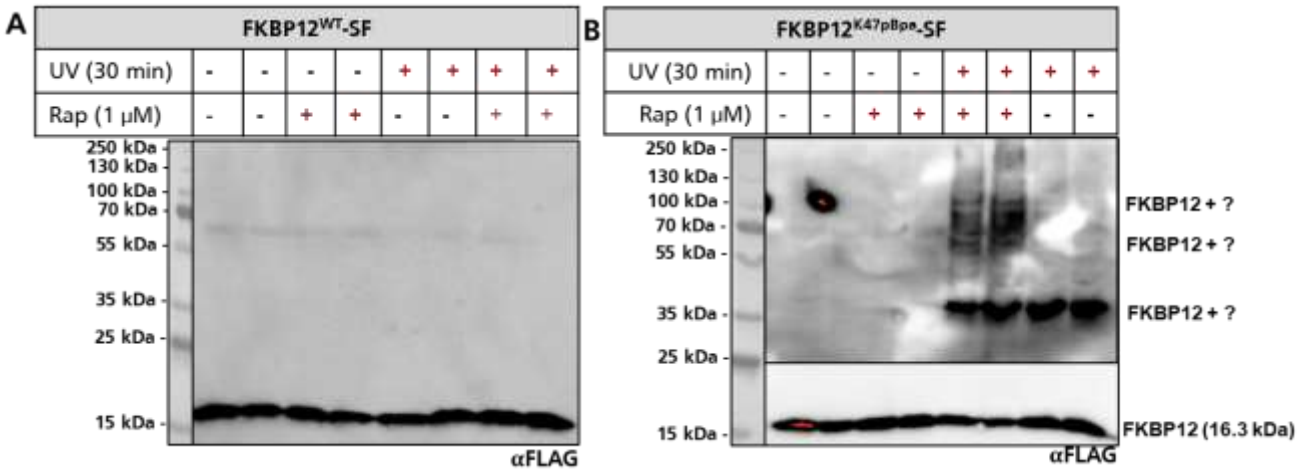

Figure 39: The incorporation of pBpa in FKBP12^{K47pBpa} induces photo-crosslinks while FKBP12WT is unaffected upon UV irradiation in HEK293T cells. A) Expression of FKBP12 WT is not affected upon treatment with Rapamycin prior to UV irradiation. **B)** Expression of FKBP12^{K47pBpa} was observed as in FKBP12 WT cells. Upon UV irradiation and Rapamycin treatment, several photo-crosslinks were observed at 55-130 kDa, while a strong photo-crosslink at 35 kDa was observed by Rapamycin and UV irradiation.

No photo-crosslinks upon UV irradiation of HEK293T WT cells expressing FKBP12 WT were observed after immunostaining. The expression level of FKBP12 WT was unaffected in cells that treated with UV irradiation or with Rapamycin (**Figure 39A**). When cells expressing FKBP12^{K47pBpa} were treated by UV light; a strong photo-crosslink was observed at 35 kDa. Moreover, when cells were treated with Rapamycin, several photo-crosslinks at a molecular height of 35-130 kDa additionally occurred (**Figure 39B**).

However, no photo-crosslink at around 280-300 kDa was observed. Full length mTOR as well as its isoforms were expected to initiate a photo-crosslink at above 200 kDa as Rapamycin induces ternary complex formation with FKBP12 [307]. Regarding position K47, it was suggested that pBpa incorporated at other positions within the FKBP12 sequence might be more effective in capturing mTOR. Additionally, it was investigated if the 35 kDa photo-crosslink could also be observed when additional positions were utilized and if Rapamycin has an influence on the photo-crosslink efficiency (**Figure 40**).

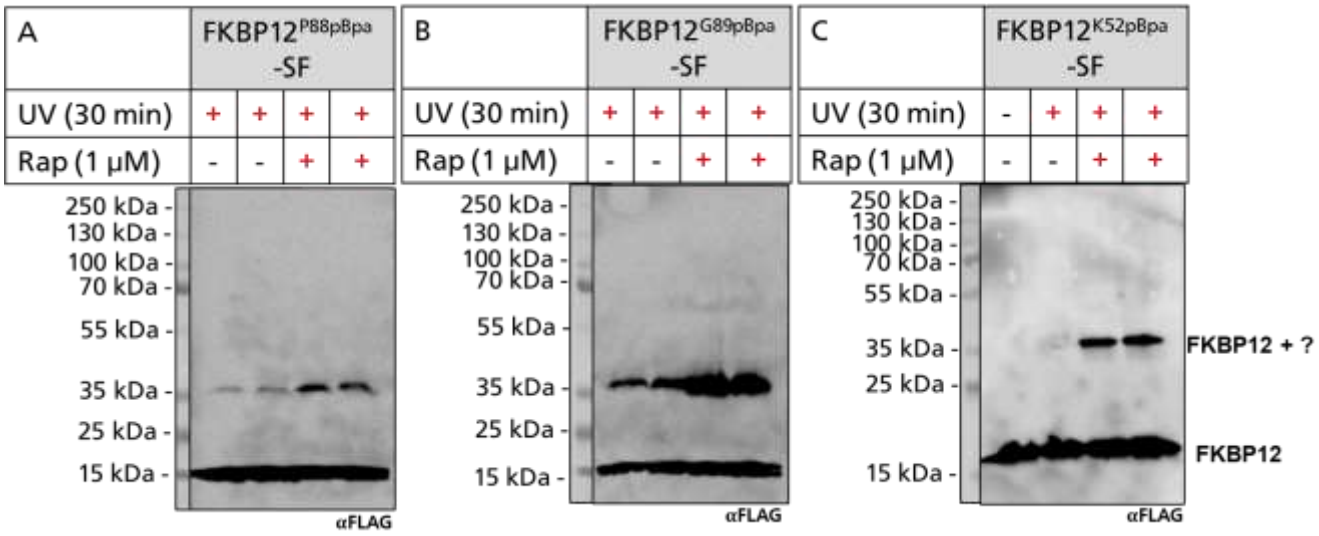

Figure 40: The 35 kDa photo-crosslink after treatment of FKBP12 mutants with Rapamycin is induced at several FKBP12 mutants. The 35 kDa photo-crosslink appeared when FKBP12^{P88pBpa}, FKBP12^{G89pBpa} and FKBP12^{K52pBpa} were treated with UV light (365 nm). When samples were treated additionally with Rapamycin, the photo-crosslink was enhanced.

The 35 kDa photo-crosslink was observed within several FKBP12 mutants after UV irradiation. When FKBP12 mutants P88, G89 and K52 were treated additionally with Rapamycin, the photo-crosslink was enhanced (**Figure 40**). Among all FKBP12 mutants in the flexible loop, FKBP12^{G89pBpa} showed the most increasing effect on the 35 kDa photo-crosslink after treatment with Rapamycin (**Figure 40B**). Interestingly, the 35 kDa photo-crosslink was only partially observed when mutant FKBP12^{K52pBpa} were irradiated with UV light (**Figure 40C**). The photo-crosslink was strongly increased after HEK293T WT cells were treated with Rapamycin. Among several FKBP12 mutants the 35 kDa photo-crosslink was found to be either induced upon UV irradiation or enhanced when cells were previously treated with Rapamycin.

FKBP12 is also known to interact with the phosphatase calcineurin when FK506 is utilized as natural molecular glue resulting in inhibition of the phosphatase and nuclear factor of activated T cells (NFAT) [23; 308; 309]. As FKBP12^{K52pBpa} was suggested to induce steric hindrance to mTOR, FKBP12^{Q53pBpa} was further utilized. To compare the effect of FK506 to Rapamycin, both natural compounds were utilized in HEK293T FKBP12 knock-out cells before UV irradiation (**Figure 41**).

By utilizing HEK293T FKBP12 knock-out cells it should have been prevented, that FK506 and Rapamycin are likely to interact with endogenous FKBP12 which then was thought to be capable to induce ternary complex formation with either mTOR or calcineurin.

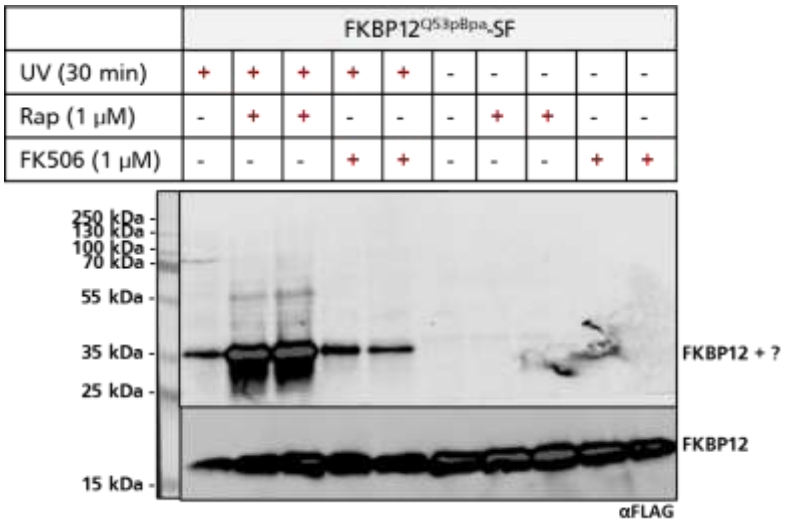

Figure 41: FK506 does have no influence on the 35 kDa photo-crosslink of FKBp12^{Q53pBpa} compared to Rapamycin. HEK293T cells were treated with either Rapamycin or FK506 prior to UV irradiation. FKBP12^{Q53pBpa} was observed at 16.2 kDa. The 35 kDa photo-crosslink was observed when samples were treated with UV light. Treatment of HEK293T cells with Rapamycin resulted in increase of the 35 kDa photo-crosslink, while treatment with FK506 did not show any differences to the UV irradiated sample alone.

After UV irradiation, the 35 kDa photo-crosslink was observed in every sample, independently of the utilized molecular glues. Utilizing HEK293T FKBP12 knock-out cells led to an increased photo-crosslinking pattern. UV irradiation was found to induce a slight photo-crosslink at around 70 kDa while treatment with Rapamycin resulted in a strong increase of the 35 kDa photo-crosslink. Rapamycin-dependent photo-crosslinks were also observed at around 55 kDa. On the other hand, FK506 was observed to have no influence on the intensity of the 35 kDa photo-crosslink suggesting that the enrichment is only influenced by Rapamycin (**Figure 41**). However, no photo-crosslinks indicating ternary complex formation of FKBP12:Rapamycin:mTOR (> 200 kDa) or FKBP12:FK506:calcineurin (approx. 80 kDa) were observed. To validate if the incorporation of pBpa resulted in an incorrect folding of FKBP12 and conformational changes, FKBP12 WT and several mutants were utilized in pulldown experiments. It was investigated if Rapamycin was still able to induce ternary complex formation of FKBP12 and mTOR (**Figure 42**).

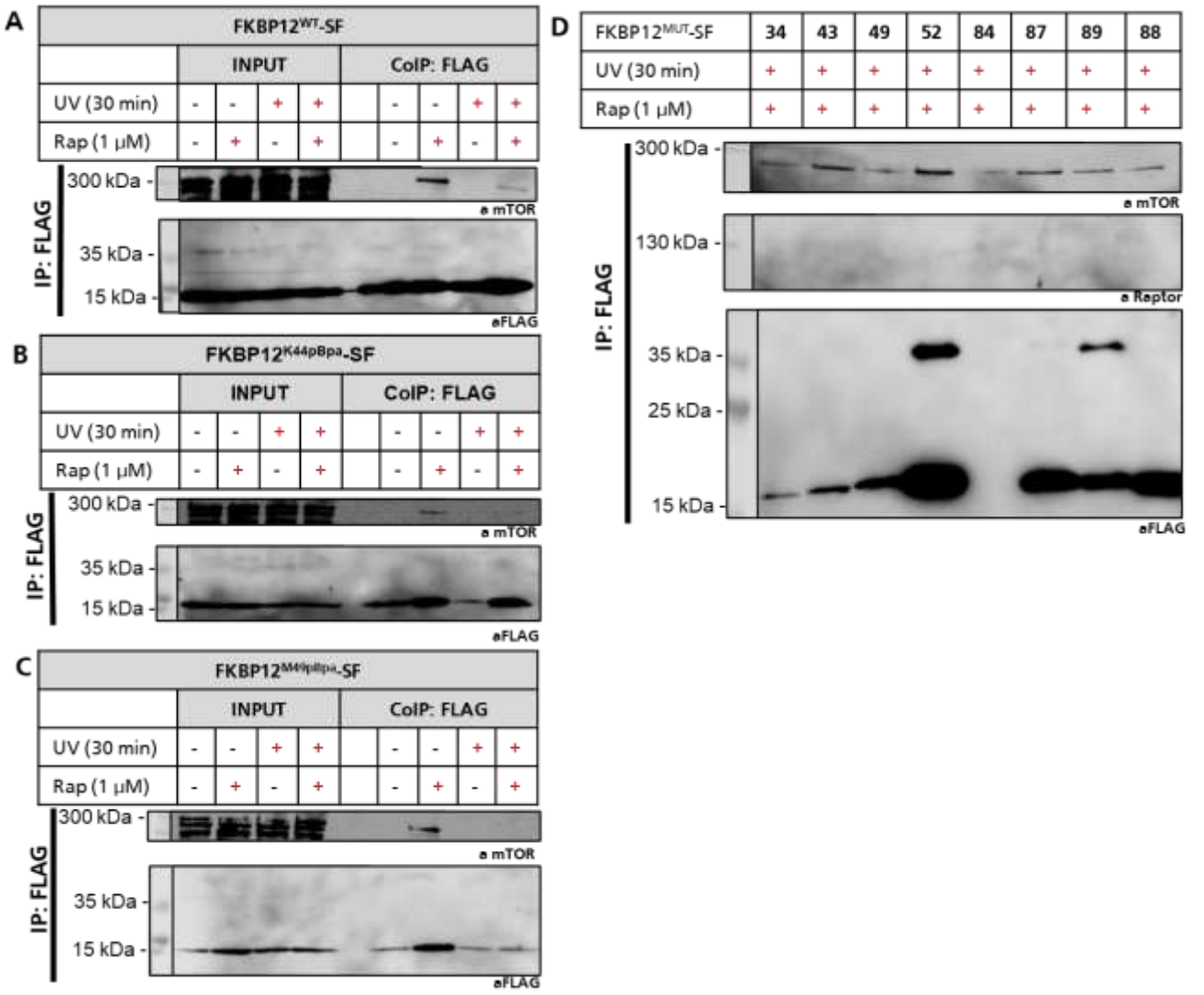

Figure 42: CoIP experiments of FKBP12 and mTOR after treatment with UV irradiation and Rapamycin. HEK293T FKBP12 knock-out cells were transfected with FKBP12 wildtype or mutants. After cells were treated with Rapamycin, UV irradiation was performed. **A)** CoIP experiment of FKBP12 wildtype. Left: lysate, right: Co-immunoprecipitation of FKBP12:Rapamycin:mTOR complex. **B)** CoIP experiment of $FKBP12^{K44pBpa}$. Left: lysate as input; right: Co-immunoprecipitation of $FKBP12^{K44pBpa}$:Rapamycin:mTOR. **C)** CoIP experiment of $FKBP12^{M49pBpa}$. Left: lysate as input; right: Co-immunoprecipitation of $FKBP12^{M49pBpa}$:Rapamycin:mTOR. **D)** Only UV and Rapamycin treated samples were utilized to investigate amount of endogenous mTOR when different FKBP12 mutants were utilized. Moreover, immunostaining of αRaptor was utilized to identify if Raptor is also present after co-immunoprecipitation.

Utilizing FKBP12 as bait protein in FLAG affinity pulldown revealed an induced PPI of FKBP12 and mTOR by Rapamycin. The effect was lower when cells were additionally irradiated by UV light suggesting that mTOR is UV sensitive (**Figure 42A**). Further, mutant $FKBP12^{K44pBpa}$ was used to investigate if mTOR could be observed in CoIP. In general, less mTOR was observed after CoIP compared to FKBP12 WT samples in the sample only treated with Rapamycin. Upon UV irradiation almost no mTOR was observed (**Figure 42B**). Equal results were obtained when mutant $FKBP12^{M49pBpa}$ was treated with Rapamycin. The amount of mTOR which was observed after pulldown was suggested to be larger compared to the mutant $FKBP12^{K44pBpa}$ sample. After UV irradiation no mTOR was observed in the pulldown experiment (**Figure 42C**).

To compare the capability of different FKBP12 mutants to binding to mTOR after treatment with Rapamycin and UV irradiation, samples of large-scale experiments were pooled and applied for immunostaining. The 35 kDa photo-crosslink was only observed at $FKBP12^{K52pBpa}$ and $FKBP12^{G89pBpa}$ after CoIP while no photo-crosslinks above >200 kDa were found to be involved in ternary complex formation of FKBP12 and mTOR (**Figure 42D**). Despite the absence of photo-crosslinks, mTOR was found to be present in each sample respectively suggesting that FKBP12 possess almost no photo-crosslink efficiency against kinase mTOR. As Raptor is a component of the mTORC1 complex it was further investigated if the protein could be observed after pulldown. The component of the mTORC1 was not observed after pulldown suggesting that the activity of mTOR on its downstream targets p70 S6K and 4E BP1 is inhibited upon dimerization with FKBP12:Rapamycin [310].

Taken together, the expression level of FKBP12 WT and its mutants was not affected upon UV irradiation. Notably, among several mutants a 35 kDa photo-crosslink occurred after UV irradiation which was enhanced when FKBP12 mutants at position K52 and G89 were treated with Rapamycin before UV irradiation. Those positions were found to remain after CoIP experiments suggesting that the 35 kDa photo-crosslink observed in HEK293T lysate might indicate transient dimerization of FKBP12. Indeed, FKBP12 is capable of reversible dimerization within the 80's loop (Pro90) in *Aspergillus fumigatus* indicating different dimer strengths [230]. Moreover, recombinant FKBP12 was found to form dimers or even multimers by help of Cys23 and Phe36 [311].

However, so far, no photo-crosslinks indicated a dimerization of FKBP12:Rapamycin:mTOR despite the kinase was observed after pulldown experiments. To investigate the photo-crosslinking efficiency of FKBP12 mutants and Rapamycin to mTOR the FKBP-Rapamycin-binding domain (FRB) possessing a HA tag was utilized for co-transfection in HEK293T WT cells (**Figure 43**).

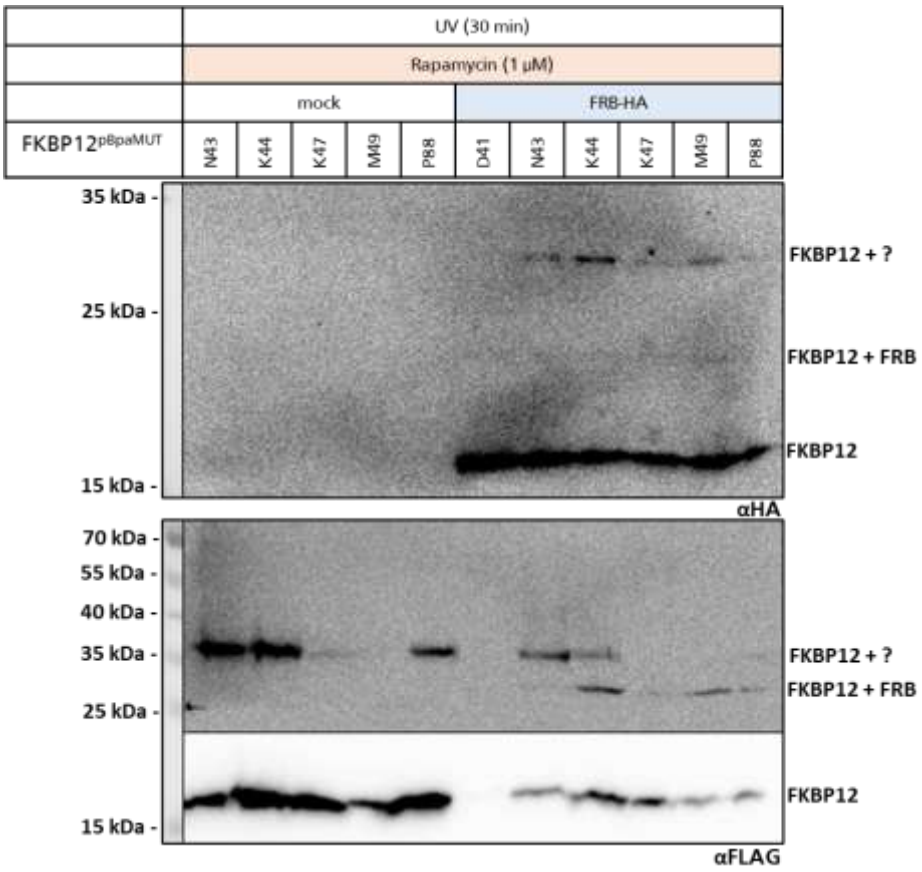

Figure 43: Rapamycin induces photo-crosslinks between HA-FRB and FKBP12 mutants in HEK293T FKBP12 k.o. cells. As control, mock plasmid was utilized. Upon treatment with UV irradiation and Rapamycin treatment, 35 kDa photo-crosslink occurred at FKBP12pBpa mutants N43, K44 and P88. Cells co-expressing HA-FRB and FKBP12pBpa mutants N43, K44, M49 induced photo-crosslink at around 25 kDa.

When HEK293T cells only expressing FKBP12pBpa mutants were treated with Rapamycin and UV irradiated, the 35 kDa photo-crosslink was observed, especially when pBpa was incorporated at positions N43, K44 and P88. Only a small amount of the 35 kDa photo-crosslink was observed when FKBP12^{K47pBpa} was utilized and position M49 did not show this photo-crosslink (**Figure 43**; αFLAG). When cells were co-transfected with HA-FRB and FKBP12 mutants, expression level was found to be lowered compared to the pCDNA3.0 mock plasmid control. However, the 35 kDa photo-crosslink was observed within the same FKBP12 mutants as previously described. Moreover, a 25 kDa photo-crosslink occurred. The photo-crosslink was enhanced when FKBP12^{K44pBpa}, FKBP12^{M49pBpa} and FKBP12^{P88pBpa} were utilized whereas FKBP12^{N43pBpa} and FKBP12^{K47pBpa} only showed less photo-crosslinking efficiency. In general, the intensity of the photo-crosslink was lower compared to the 35 kDa photo-crosslink. After immunostaining of HA, weak photo-crosslinks at around 25 kDa were observed (**Figure 43**; αHA). FKBP12^{K44pBpa} and FKBP12^{M49pBpa} were observed to induce stronger ternary complex formation compared to other FKBP12 mutants. This led to the hypothesis, that some pBpa positions within the FKBP12 protein might be favoured.

FKBP12 is the smallest member of the immunophilin family with a molecular weight of 12 kDa which interacts with the FRB domain of mTOR upon binding to Rapamycin [126; 306]. As depicted in **Figure 44**, co-crystal structure of the mTORC1 (depicted in green) and the FRB domain of mTOR (yellow) with FKBP12 (orange) and Rapamycin (blue) shows, that the binding interface of FKBP12 and FRB is mainly induced by Rapamycin binding in the hydrophobic pocket of FKBP12 and FRB.

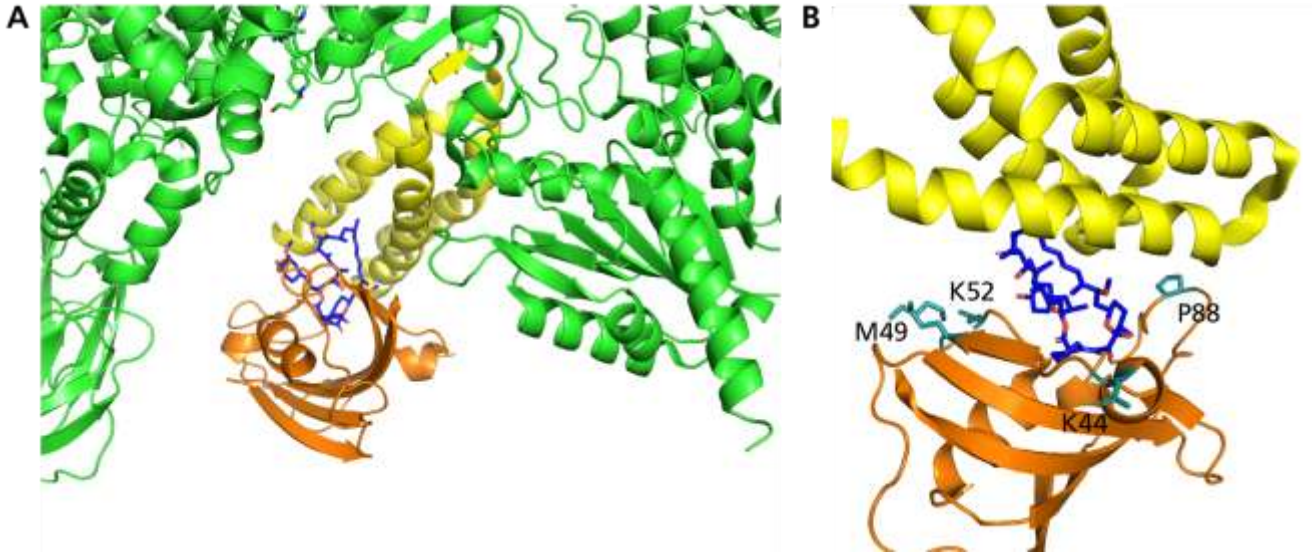

Figure 44: Co-crystal structure of mTORC1 and FKBP12:Rapamycin. **A)** mTORC1 is represented in green as the FRB domain of mTOR is highlighted in yellow. Rapamycin is depicted in blue while in complex with FKBP12 (orange). **B)** Rapamycin depicted in blue interacts with the hydrophobic pocket of FKBP12 (orange). FKBP12 mutants are highlighted in pale blue and labelled with the amino acid positions K44, M49, K52 and P88.

Rapamycin covers approx. 50 % of the interface between both proteins, while amino acid residues Trp59, Tyr26, Phe46 and Phe99 of FKBP12 participate in hydrophobic contacts to Rapamycin and Gly86 and Arg42 are responsible for hydrogen bonds to Arg2042 and Asp2102 of FRB. Calculation of the binding free energy showed that apart from Gly86/Arg2042 and Arg42/Asp2012 only very limited interactions were observed between FKBP12 and FRB [312]. Further structural characterization by photo-affinity labelling (PAL) of diazirine-based photo-Rapamycin at C40-OH revealed a distance to $FKBP12^{D79}$ of 4.5 Å and 5.0 Å to FRB^{E18} [313]. Upon UV irradiation, 4-*para*-benzoyl phenylalanine (pBpa) forms a diradical undergoing an insertion preferably into C-H bonds of close proximity proteins while glycine and methionine are also preferred as contact site in photo-crosslinking of pBpa and can enlarge the radius [314; 315]. Taken together, the activity radius of pBpa and the inflexibility of its benzophenone group was suggested to decrease crosslinking efficiency towards kinase mTOR as well as HA-FRB. Diazirine containing photo-crosslinkers are known for their higher reactivity compared to benzophenone photo-crosslinkers due to their carbene group. Moreover, diazirine photo-crosslinkers possesses high flexibility due to the variable side chain. The incorporation of diazirine containing photo-crosslinkers is provided

by the pyrrolysyl tRNA synthetase. Photo-crosslinkers like DiZPK, AbK or TmdZlys were developed with a reactivity radius of 14-15 Å and are more efficient in capturing transient PPIs irrelevant if acting as wide or short-range photo-crosslinker [316; 317; 257]. 3'-Azibutyl-N-carbamoyl-lysine (AbK) containing a reactive diazirine was utilized for amber-suppression-mediated expression of FKBP51^{E75pBpa} and FKBP51^{S118pBpa} as well as FKBP12^{K52pBpa} in HEK293T FKBP12 knock-out cells. Rapamycin was utilized for treatment for UV irradiation. As control, no unAA was incorporated while the photo-crosslinking efficiency of pBpa and AbK were compared (**Figure 45**).

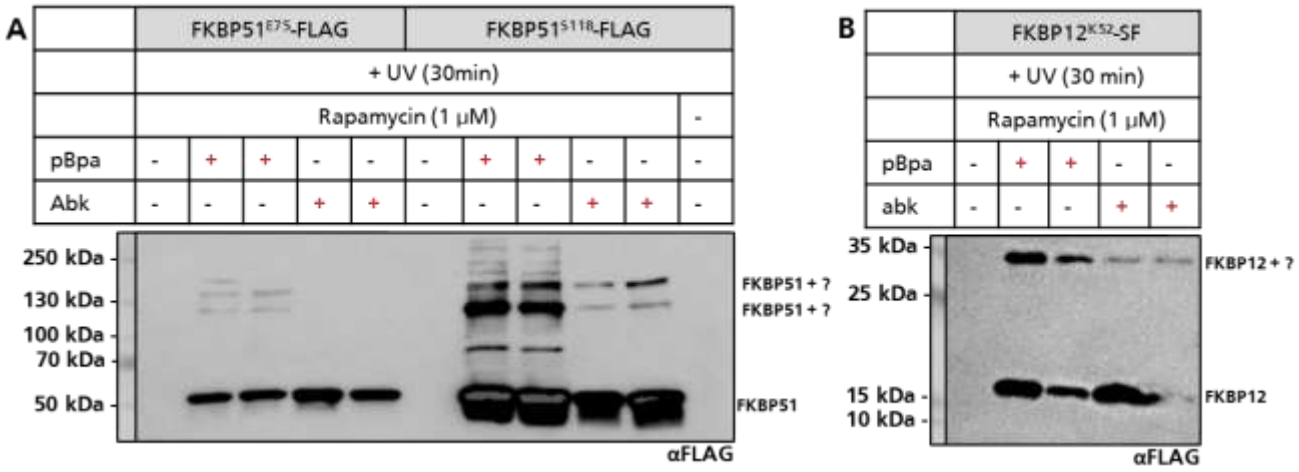

Figure 45: 3'-Azibutyl-N-carbamoyl-lysine (AbK) showed less photo-crosslinking efficiency compared to pBpa. A) Incorporation of either pBpa or AbK in FKBP51^{E75pBpa} and FKBP51^{S118pBpa} in HEK293T FKBP12 knock-out cells revealed less photo crosslinking efficiency by AbK. **B)** Incorporation of either pBpa or AbK in FKBP12^{K52pBpa} resulted in less photo-crosslinking efficiency at 35 kDa photo-crosslink and no additional photo-crosslinks were observed.

The expression levels of FKBP51E75pBpa and FKBP51E75AbK did not differ upon incorporation of the unAA photo-crosslinkers. Mutant FKBP51E75pBpa induced weak photo-crosslinks in a range of 120-180 kDa while utilizing FKBP51E75AbK resulted in the absence of any detectable photo-crosslinks (**Figure 45A**). When FKBP51S118pBpa and FKBP51S118AbK were treated with Rapamycin upon UV irradiation less photo-crosslinks upon incorporation of AbK were observed. Only photo-crosslinks at 120 kDa and 150 kDa were observed but compared to FKBP51 mutants with incorporated pBpa the photo-crosslink at 120 kDa remained relatively weak compared to the pBpa-induced photo-crosslinks. Interestingly, the intensities of the 150 kDa photo-crosslink bands were stronger than the 120kDa photo-crosslink band for the AbK mutant. This was different to the the pBpa mutants (**Figure 45A**). When similarly, the 35 kDa photo-crosslinks were stronger for FKBP12^{K52pBpa} treated with Rapamycin compared to only UV irradiated FKBP12^{K52pBpa} sample (**Figure 45B**).

In conclusion, 3'-Azibutyl-N-carbamoyl-lysine (AbK) decreased the photo-crosslinking efficiency of either FKBP51 mutants or FKBP12^{K52pBpa}. The incorporation of AbK had taken place in the same range as incorporation of pBpa which can be assessed by the expression level of each mutant. However, FKBP51^{E75AbK} did not induce photo-crosslinks while FKBP51^{S118AbK} induced photo-crosslinks at 120 kDa and 150 kDa. These photo-crosslinks were suggested to reflect photo-crosslinks to Hsp90 or the GR as observed in previous studies [84]. Utilizing AbK as photo-crosslinker might require additional positions within the FKBP51 sequence as incorporation of the unAA in the FK1 domain might be inefficient because no precise orientation has taken place [318; 257; 319]. In general, molecules containing a diazirine are highly sensitive to light and therefore often contain minor impurities which can affect the efficiency of photo-crosslinking *in-vivo* [320].

Initially it was thought that incorporation of an alternative photo-crosslinker might enhance the photo-crosslinking efficiency of FKBP12 mutants to kinase mTOR. However, the efficiency of the 35 kDa photo-crosslink was lower and no additional photo-crosslinks were observed. Moreover, FKBP12 mutant contains a Twin-Strep-II-FLAG tag, which constitutes of approx. 40 % of the recombinant FKBP12 protein. The tag might also affect photo-crosslinking efficiency in cells whereas other FKBP12 variants with either FLAG or HA Tag could be utilized to avoid steric effects. Further analyses are required to investigate the photo-crosslinking efficiency of FKBP12 in cells.

7.6.2 Mass spectrometry analyses of the Rapamycin-induced 35 kDa photo-crosslink

As the 35 kDa photo-crosslink was very prominent among most of the FKBP12 mutants, the potential protein-protein interaction was utilized in large scale experiments for MS. First, an affinity pulldown was utilized to gain a higher concentration of the 35 kDa complex. Mutant FKBP12^{K52pBpa} was treated with Rapamycin upon UV irradiation. For comparison, FKBP12^{K52pBpa} was only treated with Rapamycin (**Figure 46**).

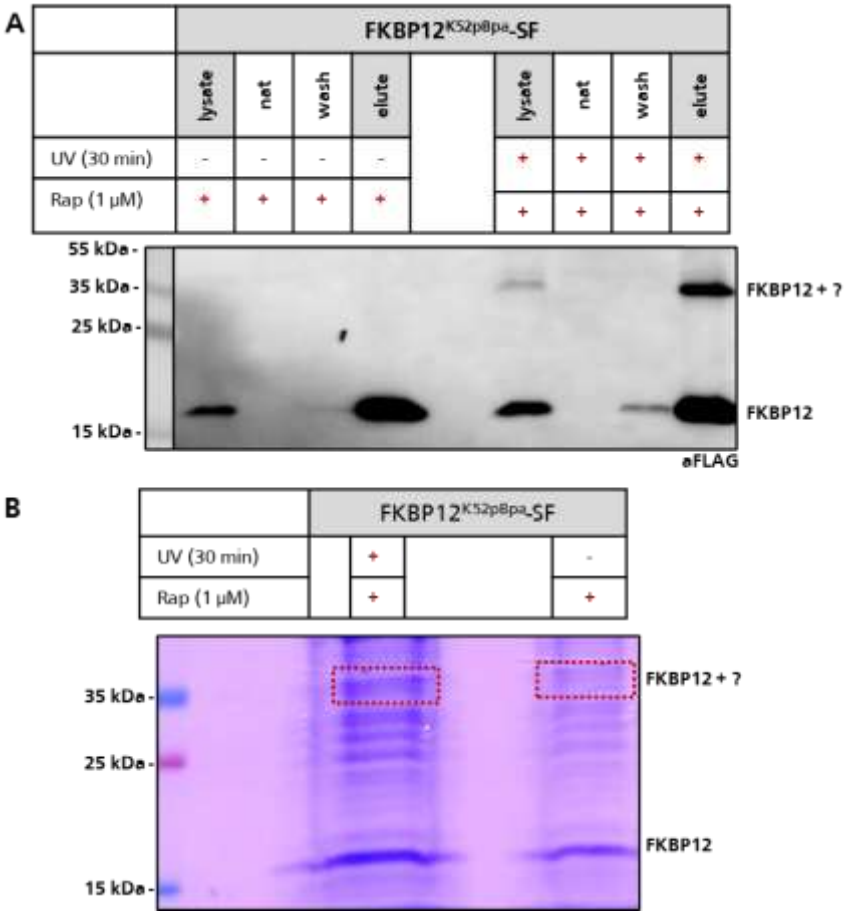

Figure 46: Rapamycin and UV induce the 35 kDa photo-crosslink utilizing mutant FKBP12^{K52pBpa} for mass spectrometry. A) Affinity pulldown of the 35 kDa photo-crosslink after FKBP12^{K52pBpa} was treated with Rapamycin following UV irradiation. Samples of the supernatant (nat) as well as the wash fraction (wash) were presented compared to the samples of lysate and elution fraction (elute). Samples were either only treated with Rapamycin or additional treated with UV light. **B)** Coomassie staining of concentrated eluate fraction for mass spectrometry. The 35 kDa photo-crosslink was highlighted with a black bar. FKBP12^{K52pBpa} was observed at around 15 kDa.

Without UV irradiation, no photo-crosslink was observed when cells expressing FKBP12K52pBpa were treated with Rapamycin. When UV additionally irradiated cells the 35 kDa photo-crosslink was observed within the lysate (**Figure 46A**). After pulldown, the samples were enriched within the elution fraction (elute). No loss of the 35 kDa photo-crosslink complex was observed within the supernatant (Nat) as well as in the wash fraction (wash). Samples were further concentrated by evaporation and applied onto an SDS gel. After SDS PAGE, the gel was stained by Coomassie Blue to visualize the proteins (**Figure 46B**). The 35 kDa photo-crosslink was cut out with a knife as well as the corresponding -UV sample and sent to EMBL Heidelberg for further analysis by mass spectrometry (**Table 32**).

Table 32: Proteins which were identified in MS of the 35 kDa photo-crosslink of FKBP12^{K52pBpa} mutant after treatment with Rapamycin and UV light. Proteins identified were described with **gene name**, **protein ID** and **description**. Additionally, the molecular weight (**mw**) was indicated as well as the results of MSMS analysis represented in **ssm** (spectra mapping, assignment of protein peptides), **max score** (with mascot, the higher the more reliable), **top3** (abundance of protein in the sample, log10), and **sequence coverage** in % (**Suppl. 7**).

gene name	protein ID	description	mw (kDa)	Top3	ssm	total score	seq. cov
FKBP1A	P62942	FKBP12-K52pBpa (FKBP12 WT modified)	16.52	7.31	78	129	94.2 %
NACA	F8VZJ2	Nascent polypeptide-associated complex subunit alpha	15.01	6.97	34	140	81.8 %
NME2	P22392	Nucleoside diphosphate kinase B	17.29	6.37	4	197	35.9 %
NME2P1	O60361	NDK8_HUMAN Putative nucleoside diphosphate kinase	15.52	6.37	4	197	39.9 %
POLR3H	Q9Y535	RPC8_HUMAN DNA-directed RNA polymerase III subunit RPC8	22.91	6.19	3	183	26.3 %
TPD52L2	O43399-6	TPD54 (7 isoforms in total)	17.47	6.24	2	111	15.2 %
TRA2A	Q13595-4	Transformer-2 protein homolog alpha	20.59	7.02	15	481	55.8 %
WBP2	Q969T9	WW domain-binding protein 2	18.22	6.57	2	155	14.3 %

The cut-off was set in a range of 16.52 kDa to 22.91 kDa. It was suggested that the photo-crosslink involves the FKBP12 mutant and a protein resulting in a total molecular weight of around 35 kDa. In the UV treated sample, FKBP12^{K52pBpa} was found with a sequence coverage of 94.2 % and with the highest Top3 value of 7.31. 78 peptides (ssm) were assigned to the protein sequence. In the UV untreated sample, no FKBP12^{K52pBpa} was observed. Proteins which are listed in **Table 32** were only identified in the UV treated sample. The highest Top3 value as well as ssm was represented by genes NACA and TRA2A. Moreover, the sequence coverage of NACA with 81.8 % was higher compared to TRA2A (55.8 %), while the max score for TRA2A was determined with 481. For both proteins, several isoforms were detected. As isoforms often share a high sequence similarity, several entries from the same gene were found even if the protein ID originally differs from the main protein. The NACA gene codes for the nascent polypeptide associated complex subunit alpha protein which in general is a ribosome-associated protein biogenesis factor and is suggested to have a proposed function to act as a co-translational molecular chaperone [321–323]. The gene TRA2A encodes for the transformer-2 protein homolog alpha which is a nuclear protein consisting of several RNA recognition motifs playing an important role in the regulation of pre-mRNA-splicing [324]. All proteins, which were listed in **Table 32**, participate in ribosomal RNA signalling. Notably, none of the proteins were found in literature to directly interact with FKBP12. In general, no FKBP12 interacting proteins after mass spectrometry could be observed. Further analyses are required to elucidate the composition of the 35 kDa photo-crosslink upon treatment of FKBP12^{K52pBpa} by Rapamycin. Samples could be either prepared in triplicate as previously performed with FKBP51P120pBpa. Moreover, utilizing HEK293T WT cells next to knock-out cells could give a glue which proteins might be affected.

In conclusion, the expression level of FKBP12 mutants compared to FKBP51 mutants was lowered in general as well as inducible photo-crosslinks upon UV irradiation. The most commonly observed photo-crosslinks were observed within a molecular range of 35-100 kDa (**Figure 39**). Only a small amount of the utilized FKBP12 mutants were found to induce additional photo-crosslinks compared to the 35 kDa photo-crosslink. The 35 kDa photo-crosslink was very prominent within several FKBP12 mutants while the intensity increased when cells were treated with Rapamycin prior UV irradiation.

Apart from Rapamycin, FK506 and Antascomicin B were utilized as molecular glues for FKBP12 mutants. However, no additional photo-crosslinks than the 35 kDa photo-crosslink were observed despite weak photo-crosslinks at 55 kDa when FK506 or Antascomicin B were utilized (**Figure 41**). As calcineurin possess a molecular weight of around 60 kDa it was thought that FKBP12^{pBpa}:FK506 was not able to address the phosphatase. Moreover, no photo-crosslinks which indicate ternary complex formation of FKBP12:Rapamycin:mTOR were observed while mTOR was observed after pulldown experiments (**Figure 42**). As no Raptor was observed it could be suggested that mTOR was addressed by the FKBP12^{pBpa}:Rapamycin complex.

To optimize the photo-crosslinking efficiency of FKBP12 mutants, HEK293T FKBP12 knock-out cells were utilized. This was based on the hyphthesis that Rapamycin might additionally bind to endogenous FKBP12. However, no differences were observed between both cell lines. As FKBP12 mutants possessed a Twin-Strep-II-FLAG tag which was initially thought for being utilized for better purification of a potential PPI it was thought that the length of the tag might induce steric hindrance upon FKBP12-protein interactions. Compared to FKBP12 which consist of 106 amino acids, the tag comprises 46 amino acids in total which is approx. 40 % of the recombinant protein. To avoid steric hindrance, a single FLAG tag could be utilized as affinity pulldown of FLAG-tagged proteins is thought to be sufficient for enrichment by magnetic beads.

The unAA AbK was thought to increase photo-crosslinking efficiency of FKBP12 mutants as it possesses a diazirine linker which widens the potential distance of capturing POI upon UV irradiation up to 14-15 Å [316; 317; 257]. However, the photo-crosslinking efficiency decreased compared to incorporation of pBpa in FKBP12 mutants. Diazirine containing molecules are highly light-sensitive (**Figure 45**). To confirm the purity of AbK in further experiments, the unAA could be analysed via HPLC as reacted diazirines differs in their spectra [320]. Moreover, additional unAA could be utilized to further optimize the orientation of the unAA within the FKBP12 sequence. In case of diazirines, the intensity of UV irradiation should be considered. In case of pBpa the irradiation took place within 30 minutes, while diazirines might be more efficient, possibly allowing short irradiation times.

As mTOR was not observed within photo-crosslinking experiments upon treatment with Rapamycin, HA-FRB was utilized to further analyse if the FKBP12 mutants can induce photo-crosslinks to the FK506-binding site of mTOR (**Figure 42**). Notably, an additional photo-crosslink of 25 kDa was observed after FKBP12 mutants co-expressed in HEK293T cells were treated with Rapamycin. The photo-crosslink was identified as ternary complex of FKBP12:Rapamycin:FRB (**Figure 43**).

Furthermore the 35 kDa photo-crosslink was investigated by mass spectrometry as the photo-crosslink was very prominent among all FKBP12 mutants. However, so far only proteins involved in ribosomal RNA biosynthesis were observed (**Table 32**). The results were not significant enough to allow any solid statements. Further studies are required to elucidate the identity and composition of the 35 kDa photo-crosslink.

FKBP12 is often investigated as fusion protein in combination with FRB for selectively targeting proteins as the FKBP12:Rapamycin:FRB complex has high affinity and high specificity [325]. The ternary complex can be also applied to precisely capture proteins within several compartments of the cell [326]. Previous studies already indicated that labelling endogenous FKBP12 requires further investigation. In a case study of Tamura *et.* al. an optimized piperazine linker was successfully utilized to label the protein by ligand-directed tosyl (LDT) chemistry. In a large linker screening they finally were able to demonstrate a successful labelling of FKBP12 as well as UV-induced covalent photo-crosslinking to the HA-FRB when Rapamycin was utilized [327]. Hypothetically, incorporation of an unAA might lead to different secondary structures while ligand-directed chemistry could be an additional tool in FKBP12 modifications. As FKBP51 possess an additional TPR domain, the incorporation of pBpa might not show high impact. On the other hand, FKBP12 only consist of the FK1 domain with 106 amino acids, respectively, suggesting that minor changes upon its secondary structure might influence its binding capacity to FRB upon binding to Rapamycin.

8 Summary

Antascomicin B was discovered in the late 90's along with other natural products from bacterial origin. Based on its FKBP12-binding properties similar to the related compounds Rapamycin and FK506 that possess immunosuppressive effects in humans, Antascomicin B as well as other so called 'orphan' molecular glues lack immunosuppressive effects but antagonize the effects of Rapamycin and FK506. Fluorescence polarization assays revealed higher affinity of Antascomicin B to several FKBPs compared to Rapamycin confirming the natural product as an antagonist. The interaction of Anta B with the hydrophobic binding pocket of the FK1 domain of FKBP51 was elucidated in a co-crystal structure. Large scale affinity chromatography utilizing FKBP12 or FKBP51 FK1 as bait protein were successfully applied when purified GST-FRB was utilized as protein target in the presence of Rapamycin. However, no endogenous mTOR was detected when utilizing HEK293T cell lysate in this approach. Further adjustment of buffers and conditions did not have an influence on the ternary complex as well as competitive experiments with ligand FK[4.3.1]-16h. Therefore, potential interaction partners of the FKBP51:AntaB complex were further analysed in cells by photo-probing utilizing the unnatural amino acid 4-*para*-benzoyl-phenylalanine (pBpa). High photo-crosslink efficiency was observed when pBpa was incorporated at positions K52, N74, E75, A116-K121 within the FK1 domain of FKBP51. Prominent results were obtained utilizing FKBP51^{K52pBpa} and FKBP51^{P120pBpa} for expression in HEK293T cells upon treatment with Anta B and UV irradiation. An intensive photo-crosslink at 120/125 kDa was observed, while FKBP51^{P120pBpa} developed additional photo-crosslinks at around 270 kDa. The basal interaction of FKBP51 and Akt1 was enhanced when Antascomicin B was utilized as molecular binder in photo-probing experiments. To confirm a ternary complex formation of FKBP51:AntaB:Akt1 mass spectrometry analyses were performed revealing the kinase Chk1 as an additional target of FKBP51:AntaB. Western Blot analysis confirmed the interaction of the complex to Chk1 suggesting that other kinases might also interact with FKBP51:AntaB due to their highly homologous secondary structure. The phosphorylation state at S473 and T308 of Akt1 did not affect the binding capacity of the kinase to FKBP51 when cells were treated with Antascomicin B and UV irradiation. Further studies by SPR or qRT-PCR of downstream targets of both kinases might be necessary to investigate which kinase might be favoured by the natural product.

Compared to FKBP51, incorporation of pBpa in FKBP12 resulted in less photo-crosslinking efficiency, where a 35 kDa photo-crosslink was prominent among all mutants with and without different molecular binders. When cells were treated with Rapamycin before UV irradiation, no photo-crosslinks indicating a FKBP12:Rapamycin:mTOR complex were observed at around 290-300 kDa. CoIP experiments revealed the presence of mTOR in the eluate after treatment of FKBP12^{pBpa} mutants expressing cells with Rapamycin before UV irradiation. This led to the conclusion that the FKBP12:Rapamycin complex is

functional with no photo-crosslinking efficiency to the kinase. Moreover, several FKBP12 mutants were able to induce a ternary complex to HA-FRB upon treatment with Rapamycin. However, the photo-crosslinking efficiency suggested that the Twin-Strep-II-FLAG tag might affected the interaction of the FKBP12^{pBpa} mutants and mTOR. Incorporation of the diazirine containing 3'-Azibutyl-*N*-carbamoyl-*L*-lysine resulted in loss of photo-crosslinking efficiency indicating that further studies of additional photo-probes must be applied. Mass spectrometry analysis of the 35 kDa photo-crosslink revealed different proteins with a molecular range of approx. 15-22 kDa which participate in ribosomal RNA synthesis. While incorporation of pBpa within FKBP51 is sufficient for identification of potential protein-protein interactions *in vivo*, further optimization of FKBP12 is required to unravel its full potential as accessory protein for Antascomicin B.

9 Appendix

9.1 Chemical structure of MTQ238 and FK[4.3.1]-16h

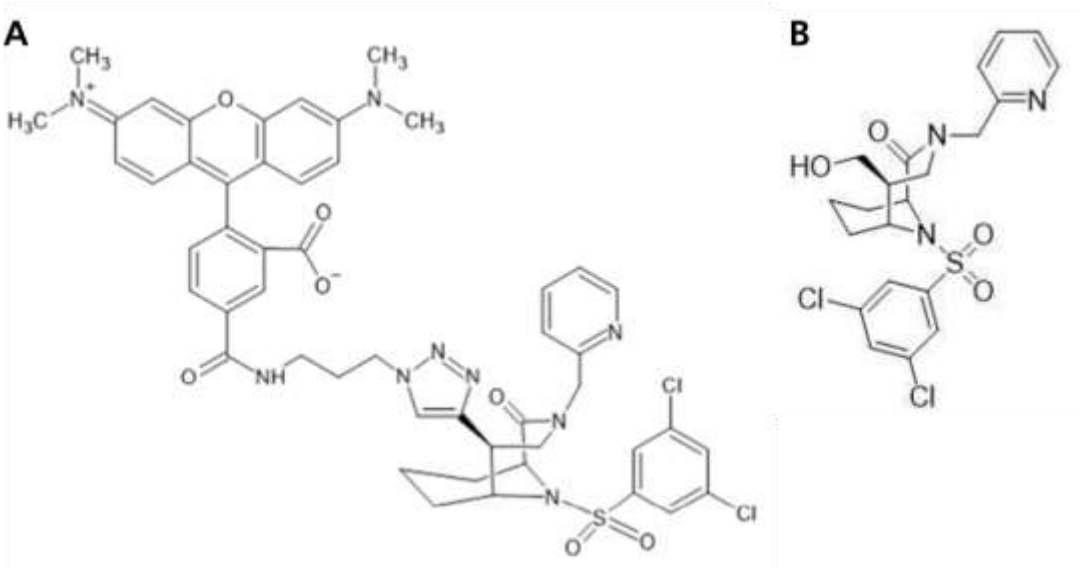

Suppl. 1: Chemical structure of **A)** MTQ238 and **B)** FK[4.3.1]-16h

MTQ238 was provided by Tianqi Mao [328] as equivalent of FTSP11 [329]. FK[4.3.1]-16h (JK95) was synthesised by Dr. Jürgen Kolos [330] and investigated in a NanoBRET-Binding assay as FKBP-ligand [331].

9.2 Antascomicin B acts as a molecular binder for FK-506 binding proteins

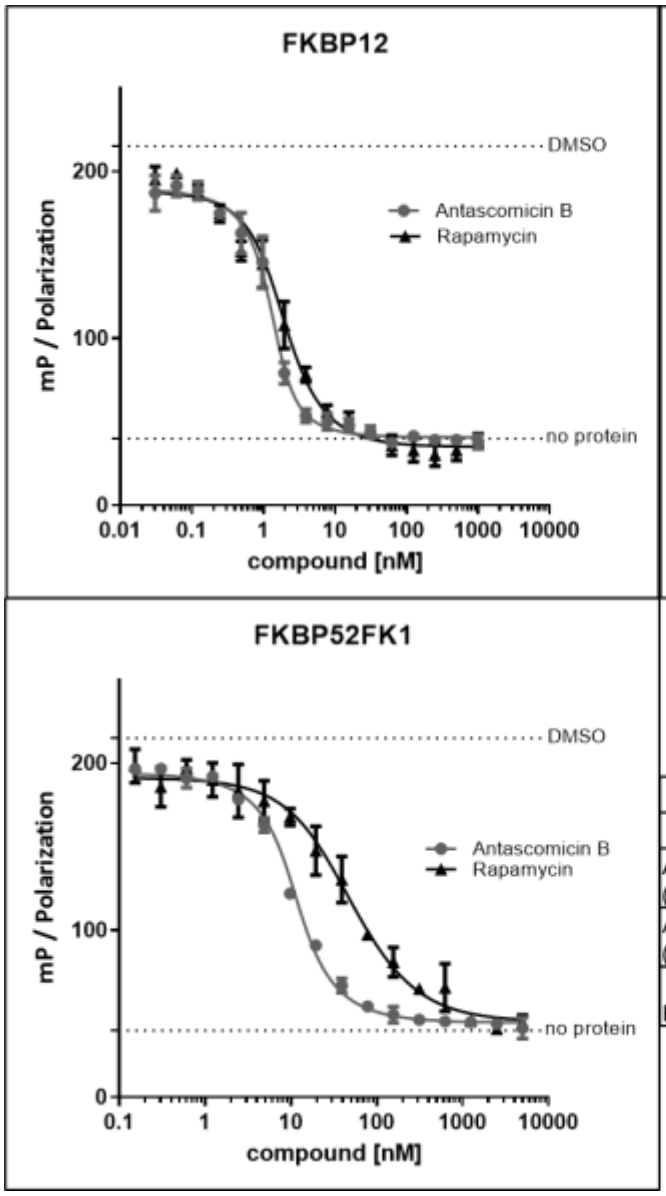

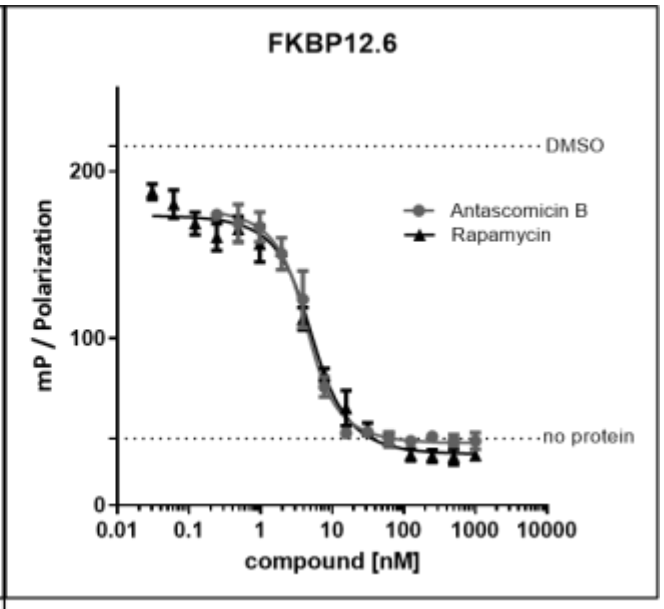

	KD values in [nM]			
	FKBP51FK1	FKBP52FK1	FKBP12.6	FKBP12
Antascomicin B (synthetic)	6.7 ± 0.4	1.2 ± 0.1	0.38 ± 0.06	0.03 ± 0.006
Antascimcin B (Biosynthetic)	12.5 ± 0.5	1.5 ± 0.2	2.2 ± 0.4	0.32 ± 0.04
Rapamycin	8.5 ± 0.8	12 ± 1.5	0.6 ± 0.08	0.13 ± 0.02

Suppl. 2: Antascomicin B is acting as a molecular binder for FKBP12, FKBP12.6, FKBP51 FK1 and FKBP52 FK1. Biosynthetic Antascomicin B was received from TU Tübingen and was utilized for pre-experiments to save synthetic Antascomicin B from Stephen Ley. Biosynthetic Antascomicin B is thought to be a mix of with derivates and bacterial waste. The FP Assay was performed by Wisely Oki Sugiarto as preparatory work.

9.3 Pulldown experiments with recombinant HsFKBPs to decipher Protein-Protein-interactions (PPI's)

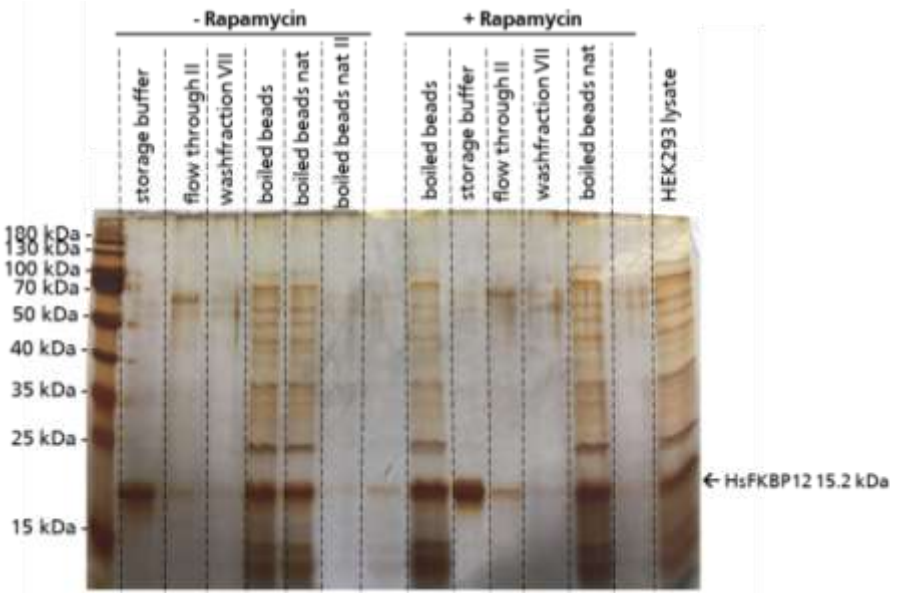

Suppl. 3: SDS PAGE and silver staining after HEK293T lysate was added onto the resin bed of bait protein HsFKBP12. Bait protein FKBP12. Storage buffer: FKBP12 bait protein; flow through II: HEK293T cell lysate was applied onto the resinbed two times to allow completely saturation of the FKBP12 bait proteins; wash fraction VII: unbound proteins of the mammalian proteome were removed in several washing steps; boiled beads: FKBP12 domain bait proteins and the potential ternary complexes were boiled in 4x Lämmli buffer; boiled beads nat: After boiling the beads with 4x Lämmli, the supernatant was removed und applied as 'boiled beads' fraction while the remaining beads were boiled with 4x Lämmli again; boiled beads nat II: The supernatant in which FKBP12-bait proteins were collected was applied for SDS PAGE.

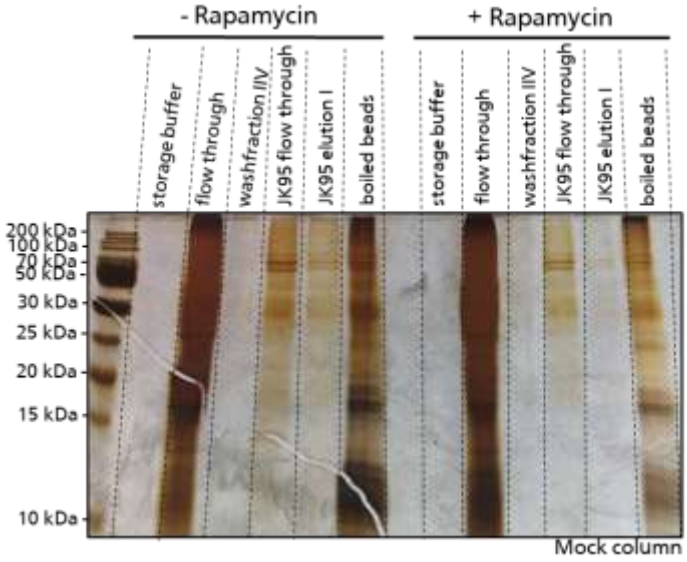

Suppl. 4: Bicyclic FKBP ligand FK[4.3.1]-16h does not compete the effect of Rapamycin in affinity chromatography utilizing HEK293T cell lysate (A) SDS PAGE and silver staining of mock resin bed with storage buffer (bait stock); flow through of HEK293T lysate, wash fraction VII to remove unbound proteins, FK[4.3.1]-16h flow through to compete effect of Rapamycin and FK[4.3.1]-16h elution I fraction to wash out the synthetic compound; boiled beads fraction of potential POI's and FKBP12 bait protein.

9.4 The 125 kDa photo-crosslink may not exclusively be kinase Akt1

Suppl. 5: Proteins which were identified in MS of protein lanes L1-L6 of FKBP51^{P120pBpa} mutant after treatment with Rapamycin and UV light. Proteins identified were described with **gene name**, **protein ID** and **description**. Additionally, the molecular weight (**mw**) was indicated as well as the results of MSMS analysis represented in **ssm** (spectra mapping, assignment of protein peptides), **total score** (with mascot, the higher the more reliable), **top3** (abundance of protein in the sample, log10), and **sequence coverage** in %. **A)** FK506-binding proteins found in all samples including FKBP51^{P120pBpa} mutant. **B)** protein kinases which were identified after Antascomicin B and UV treatment with a corresponding mw of around 50 kDa. **C)** Phosphatases which were identified after treatment with Antascomicin B and UV irradiation. **D)** Serendipitous proteins with a corresponding mw of around 50 kDa. Prominent proteins which were described in the following section were highlighted bold and red.

Gene name	Protein ID	Description	Mw (kDa)	Top3	ssm	total score	Seq. cov	Lane (+/- Anta B)
A) FK506-binding proteins								
FKBP5	Q13451	FKBP51-P120pBpa	52.25	7.79	96	147	66.7 %	L1 (-A)
		FKBP51-P120pBpa	**52.25**	**7.03**	**307**	**131**	**79.0 %**	**L1 (+A)**
		FKBP51-P120pBpa	52.25	8.41	173	138	71.7 %	L2 (-A)
		FKBP51-P120pBpa	**52.25**	**7.30**	**346**	**150**	**81.3 %**	**L2 (+A)**
		FKBP51-P120pBpa	52.25	8.39	153	153	68.7 %	L3 (-A)
		FKBP51-P120pBpa	52.25	7.01	160	150	73.0 %	L3 (+A)
		FKBP51-P120pBpa	52.25	7.77	264	144	48.5 %	L4 (+A)
		FKBP51-P120pBpa	52.25	8.34	179	133	49.8 %	L5 (-A)
		FKBP51-P120pBpa	52.25	7.81	248	117	50.2 %	L5 (+A)
		FKBP51-P120pBpa	52.25	8.62	157	128	48.7 %	L6 (-A)
		FKBP51-P120pBpa	52.25	7.42	193	120	50.2 %	L6 (+A)
		Peptidyl-prolyl cis-trans isomerase FKBP5 (endogenous)	**51.12**	**5.97**	**169**	**2583**	**49.3 %**	**L6 (+A)**
FKBP4	Q02790	Peptidyl-prolyl cis-trans isomerase FKBP4 (endogenous)	51.80	6.11	6	144	13.3 %	L2 (-A)
				5.51	6	166	10.2 %	L2 (+A)
				6.42	4	243	6.4 %	L3 (+A)
				5.84	15	341	19.8 %	L5 (-A)
B) Kinases								
AKAP11	Q9UKA4	AKA11_HUMAN A-kinase anchor protein 11	210.05	5.81	3	165	2.2 %	L1 (-A)
				5.60	4	124	2.4 %	L1 (+A)
AKAP12	Q02952	AKA12_HUMAN A-kinase anchor protein 12 (FL and isoforms 2; 3)	191.48	5.93	11	124	7.8 %	L1 (-A)
				5.59	4	68	3.3 %	L1 (+A)
AURKA	**O14965**	**AURKA_HUMAN Aurora kinase A**	**45.81**	**5.30**	**3**	**106**	**6.4 %**	**L2 (+A)**
AURKB	**Q96GD4**	**AURKB_HUMAN Aurora kinase B**	**39.31**	**6.21**	**4**	**228**	**13.6 %**	**L3 (+A)**
BUB1B	O60566	Mitotic checkpoint serine/threonine-protein kinase BUB1 beta (FL and isoforms 2; 3)	119.5	6.12	7	303	7.9 %	L2 (-A)
				6.70	6	250	4.2 %	L2 (+A)
CDK11B	P21127	Cyclin-dependent kinase 11B (FL and isoforms 2, 8, SV1, SV5)	92.70	6.93	20	844	22.6 %	L2 (-A)
				6.75	10	439	13.8 %	L2 (+A)
				6.76	8	445	10.9 %	L3 (-A)
CHEK1	**O14757**	**Serine/threonine-protein kinase Chk1 (FL and isoforms 2; 3)**	**54.43**	**6.21**	**6**	**361**	**16.1 %**	**L2 (+A)**
				6.36	**2**	**145**	**5.0 %**	**L5 (+A)**

DGKQ	P52824	Diacylglycerol kinase theta	101.15	5.77	4	266	6.4 %	L3 (+A)
HGS	O14964	Hepatocyte growth factor-regulated tyrosine kinase substrate	86.19	6.55	11	455	9.8 %	L2 (-A)
				6.49	8	363	9.8 %	L2 (+A)
				6.76	15	577	13.0 %	L3 (-A)
				6.38	9	354	11.7 %	L3 (+A)
HK1	P19367	Hexokinase-1 (FL and isoforms 2,3,4)	102.48	7.53	48	1908	38.3 %	L2 (-A)
				6.98	38	1502	32.4 %	L2 (+A)
				6.19	6	345	8.3 %	L3 (-A)
				6.12	8	399	8.6 %	L3 (+A)
				6.64	8	354	7.3 %	L5 (-A)
				5.89	5	221	4.5 %	L5 (+A)
HK2	P52789	Hexokinase-2	102.38	6.85	41	1813	34.9 %	L2 (-A)
				6.93	30	1530	30.3 %	L2 (+A)
				6.25	11	495	13.0 %	L3 (-A)
				5.77	8	346	10.0 %	L3 (+A)
				6.76	11	496	10.0 %	L5 (-A)
				6.69	9	414	9.3 %	L5 (+A)
				5.57	2	108	2.5 %	L6 (-A)
ILK	**Q13418**	**Integrin-Linked protein kinase**	**51.42**	**5.76**	**4**	**127**	**8.8 %**	**L2 (+A)**
MARCKS	P29966	HUMAN Myristoylated alanine-rich C-kinase substrate	31.59	5.91	5	341	20.8 %	L3 (-A)
MASTL	Q96GX5	Serine/threonine-protein kinase greatwall	97.32	5.93	5	286	6.1 %	L2 (-A)
				5.90	6	418	8.0 %	L2 (+A)
				5.54	3	119	4.9 %	L5 (+A)
NEK9	Q8TD19	Serine/threonine-protein kinase Nek9	107.17	5.31	3	100	3.9 %	L1 (+A)
				5.99	8	416	8.5 %	L2 (-A)
				5.96	10	437	9.1 %	L2 (+A)
				5.71	4	184	4.7 %	L5 (-A)
PGK1	**P00558**	**Phosphoglycerate kinase 1**	**44.61**	**5.47**	**3**	**140**	**12.3 %**	**L3 (+A)**
C) Phosphatases								
INPP4A	Q96PE3	Type I inositol 3,4-bisphosphate 4-phosphatase	109.95	6.15	2	129	2.8 %	L2 (+A)
				5.57	3	160	3.7 %	L3 (+A)
PHACTR4	Q8IZ21	Phosphatase and actin regulator 4 (FL and isoform 2, 3)	78.21	6.29	7	281	10.8 %	L3 (-A)
				5.81	3	123	7.4 %	L3 (+A)
PPP1R12A	O14974	Protein phosphatase 1 regulatory subunit 12A (FL and isoforms 2, 5)	115.28	5.14	2	137	2.8 %	L2 (-A)
				5.33	2	151	2.8 %	L3 (-A)
PPP4R3A	Q6IN85	Serine/threonine-protein phosphatase 4 regulatory subunit 3A	95.36	5.66	6	210	6.6 %	L3 (+A)
				6.11	4	170	4.8 %	L6 (+A)
D) Serendipitous proteins in Antascomicin B and UV irradiation samples								
DSG1	Q02413	Desmoglein-1	133.74	5.75	5	255	7.1 %	L1 (+A)
ACO1	P21399	Cytoplasmic aconitate hydratase	98.39	6.20	3	106	3.4 %	L6 (+A)
CMTR1	Q8N1G2	Cap-specific mRNA (nucleoside-2'-O-)-methyltransferase 1	95.32	5.69	5	216	7.2 %	L3 (+A)

DDX11	A8MPP1	Probable ATP-dependent DNA helicase DDX11	108.31	6.14	3	216	4.4 %	L6 (+A)
DNA2	P51530	DNA replication ATP-dependent helicase/nuclease DNA2	120.41	6.00	4	264	6.1 %	L2 (+A)
FBOX30	Q8TB52	F-box only protein 30	82.30	6.42	4	243	6.4 %	L3 (+A)
HAUS6	Q7Z4H7	HAUS augmin-like complex subunit 6	91.12	5.71	3	107	4.9 %	L2 (+A)
HDX	Q7Z353	Highly divergent homeobox	77.02	6.09	14	536	20.4 %	L3 (+A)
ILF2	Q12905	Interleukin enhancer-binding factor 2	43.06	5.43	5	204	15.3 %	L2 (+A)
				5.38	2	142	9.6 %	L3 (+A)
MAN2C1	Q9NTJ4	Alpha-Mannosidase 2C1	115.84	6.21	3	143	2.8 %	L2 (+A)
				5.61	3	108	3.0 %	L3 (+A)
NR3C1	**P04150**	**Glucocortioid receptor**	**85.67**	**5.65**	**3**	**191**	**6.6 %**	**L2 (+A)**
				5.67	**7**	**360**	**10.9 %**	**L3 (+A)**
				5.88	**2**	**142**	**4.2 %**	**L5 (+A)**
				5.77	**3**	**183**	**4.2 %**	**L6 (+A)**
PCBP1	Q15365	Poly(rC)-binding protein 1	37.49	6.39	8	192	29.1 %	L3 (+A)
				9.97	5	192	10.4 %	L6 (+A)
PSMC6	P62333	26s protease regulatory subunit 10B	44.17	5.87	2	116	7.4 %	L2 (+A)
WDR47	O94967	WD repeat-containing protein 47	101.95	5.68	3	147	33.6 %	L2 (+A)
E) Serendipitous proteins in only UV irradiated samples								
ALCAM	Q13740	CD166 antigen	65.10	6.30	8	411	11.5 %	L3 (-A)
ANXA11	P50995	Annexin A11	54.39	5.87	3	144	7.3 %	L5 (-A)
CBS	P22681	Cystathionine beta-synthase	60.58	5.5	3	163	5.6 %	L5 (-A)
CTAGE5	O15320	cTAGE family member 5	90.99	6.38	8	423	13.4 %	L2 (-A)
DDHD1	Q8NEL9	Phospholipase DDHD1	100.43	6.14	4	146	3.8 %	L2 (-A)
ECE1	P42892	Endothelin-converting enzyme 1	87.16	5.81	4	134	5.6 %	L2 (-A)
MTOR	P42345	Serine/threonine-protein kinase mTOR	288.89	6.24	17	797	7.5 %	L1 (-A)
TKT	P29401	Transketolase	67.87	6.31	3	142	4.8 %	L5 (-A)
F) Ubiquitous proteins in all samples								
HSP0AA1	P07900	Heat shock protein HSP 90-alpha (FL and isoform 2)	84.66	6.73	40	1619	33.2 %	L1 (-A)
				6.85	49	1855	35.3 %	L1 (+A)
				7.14	42	1883	39.2 %	L2 (-A)
				6.92	39	1740	38.6 %	L2 (+A)
				7.15	51	2029	39.7 %	L3 (-A)
				6.91	41	1683	34.9 %	L3 (+A)
				6.84	26	740	15.3 %	L4 (+A)
				7.12	26	953	21.0 %	L5 (-A)
				6.39	18	491	12.8 %	L5 (+A)
				6.71	27	842	17.3 %	L6 (-A)
				6.53	21	603	12.4 %	L6 (+A)
HSP90AB1	P08238	Heat shock protein HSP 90-beta	83.26	6.96	48	1797	36.0 %	L1 (-A)
				7.04	69	2375	44.6 %	L1 (+A)
				7.14	50	2142	45.4 %	L2 (-A)
				7.24	48	2140	44.3 %	L2 (+A)

				7.33	56	2195	41.8 %	L3 (-A)
				7.37	61	2130	40.3 %	L3 (+A)
				7.48	35	996	18.8 %	L4 (+A)
				7.19	30	1032	19.2 %	L5 (-A)
				6.86	23	793	16.4 %	L5 (+A)
				7.30	36	1039	19.9 %	L6 (-A)
				7.70	33	981	19.4 %	L6 (+A)
HSPA1A	P0DMV8	Heat shock 70 kDa protein 1A	70.05	6.78	19	874	26.5 %	L1 (-A)
				6.32	25	1129	32.2 %	L1 (+A)
				6.67	18	880	28.5 %	L2 (-A)
				6.64	18	841	27.4 %	L2 (+A)
				6.71	17	805	27.7 %	L3 (-A)
				6.61	16	809	25.9 %	L3 (+A)
				6.53	9	387	11.4 %	L4 (+A)
				6.71	11	449	13.2 %	L5 (-A)
				6.06	7	289	9.5 %	L6 (-A)
				6.24	5	207	8.3 %	L6 (+A)
HSPA1B	P0DMV9	Heat shock 70 kDa protein 1B	70.05	6.78	19	874	26.5 %	L1 (-A)
				6.71	17	805	27.7 %	L3 (-A)
				6.71	11	449	13.2 %	L5 (-A)
				6.67	18	880	28.5 %	L2 (-A)
				6.64	18	841	27.4 %	L2 (+A)
				6.61	16	809	25.9 %	L3 (+A)
				6.53	9	387	11.4 %	L4 (+A)
				6.32	25	1129	32.2 %	L1 (+A)
				6.24	5	207	8.3 %	L6 (+A)
				6.06	7	289	9.5 %	L6 (-A)
HSPA4	P34932	Heat shock 70 kDa protein 4	94.33	7.87	151	3909	66.8 %	L2 (-A)
				7.59	111	3445	64.0 %	L2 (+A)
				7.07	76	2723	58.7 %	L3 (-A)
				6.62	45	1820	48.3 %	L3 (+A)
				5.78	5	159	4.9 %	L4 (+A)
				6.86	55	1445	28.1 %	L5 (-A)
				7.14	53	1432	29.4 %	L5 (+A)
				6.51	27	746	21.9 %	L6 (-A)
				6.73	25	722	19.6 %	L6 (+A)
HSPA8	P11142	Heat shock cognate 71 kDa protein	70.89	5.54	7	322	13.4 %	L1 (-A)
				5.89	9	380	16.2 %	L1 (+A)
				6.56	8	411	14.4 %	L2 (-A)
				6.28	10	449	17.5 %	L2 (+A)
				6.47	8	354	10.4 %	L4 (+A)
				6.70	17	639	18.1 %	L5 (-A)
				6.22	7	244	9.1 %	L5 (+A)

				6.46	8	320	11.7 %	L6 (-A)
HSPD1	P10809	Heat schock protein 60 kDa protein, mitochondrial	61.05	6.03	4	209	7.0 %	L1 (-A)
				5.85	4	168	6.3 %	L1 (+A)
				6.59	12	712	23.3 %	L2 (-A)
				6.50	7	387	13.6 %	L2 (+A)
				6.39	8	472	17.2 %	L3 (-A)
				6.09	7	411	13.8 %	L3 (+A)
				6.44	4	198	6.6 %	L5 (-A)
				6.39	3	131	4.4 %	L6 (-A)
				6.13	2	101	4.2 %	L6 (+A)
HSPH1	Q92598	Heat shock protein 105 kDa	96.86	7.65	95	3257	55.2 %	L2 (-A)
				7.45	65	2652	52.9 %	L2 (+A)
				7.12	48	1754	42.7 %	L3 (-A)
				7.06	27	1144	24.4 %	L3 (+A)
				7.09	32	891	16.4 %	L5 (-A)
				7.02	30	806	13.7 %	L5 (+A)
				6.68	16	498	10.8 %	L6 (-A)
				6.82	14	446	9.3 %	L6 (+A)
STIP1	P31948	Stress-induced-phosphoprotein 1	62.64	6.18	8	247	13.1 %	L1 (-A)
				6.09	12	447	20.6 %	L1 (+A)
				7.12	47	1769	52.2 %	L2 (-A)
				6.75	39	1451	44.9 %	L2 (+A)
				6.69	9	309	16.2 %	L3 (-A)
				6.14	5	220	9.9 %	L3 (+A)
				6.32	17	578	24.8 %	L4 (+A)
				6.96	63	1805	41.5 %	L5 (-A)
				6.60	27	908	30.0 %	L5 (+A)
				6.42	23	815	25.2 %	L6 (-A)
				6.65	8	372	16.2 %	L6 (+A)

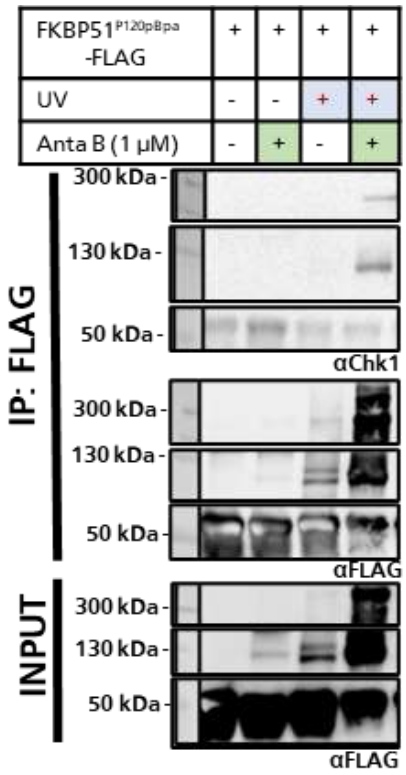

Suppl. 6: The Checkpoint kinase 1 (Chk1) was found to co-immunoprecipitate with FKBP51. Upon UV irradiation and treatment with Antascomicin B, an induced photo-crosslink at around 120-125 kDa and 270 kDa was observed.

gene_name	protein_id	description	mw	top3	ssm	usm	upm	max_score	total_score	sequence_coverage
sp|P1920_FKB	P1920_FKBP1A	P1920_FKBP1A_52FpBPA	16521,3599	7,3132525	78	13	13	129	1012	94,2
NACA	E9PAV3-2	NACAM_HUMAN Isoform 2 of Nascent polypeptide-associated complex subunit alpha, muscle-specific form	94680,8031	6,97271474	34	10	8	140	869	12,1
NACA	E9PAV3	NACAM_HUMAN Nascent polypeptide-associated complex subunit alpha, muscle-specific form	205421,522	6,97271474	34	10	8	140	869	5,4
NACA	Q13765	NACA_HUMAN Nascent polypeptide-associated complex subunit alpha	23383,8993	6,97271474	34	10	8	140	869	51,9
NACA	H0YHX9	H0YHX9_HUMAN Nascent polypeptide-associated complex subunit alpha (Fragment)	22943,5173	6,97271474	34	10	8	140	869	52,3
NACA	F8VZI2	F8VZI2_HUMAN Nascent polypeptide-associated complex subunit alpha	15016,0102	6,97271474	34	10	8	140	869	81,8
NME2	P22392-2	NDKB_HUMAN Isoform 3 of Nucleoside diphosphate kinase B	30137,0743	6,37603481	4	4	4	97	197	20,5
NME2	P22392	NDKB_HUMAN Nucleoside diphosphate kinase B	17298,0356	6,37603481	4	4	4	97	197	35,9
NME2P1	O60361	NDK8_HUMAN Putative nucleoside diphosphate kinase	15529,0608	6,37603481	4	4	4	97	197	39,9
POLR3H	Q9Y535-2	RPC8_HUMAN Isoform 2 of DNA-directed RNA polymerase III subunit RPC8	19658,0492	6,19334279	3	3	3	91	183	30,7
POLR3H	Q9Y535	RPC8_HUMAN DNA-directed RNA polymerase III subunit RPC8	22917,9299	6,19334279	3	3	3	91	183	26,3
TPD52L2	O43399-7	TPD54_HUMAN Isoform 7 of Tumor protein D54	24853,6977	6,24751666	2	2	2	56	111	10,9
TPD52L2	O43399-5	TPD54_HUMAN Isoform 5 of Tumor protein D54	23786,5229	6,24751666	2	2	2	56	111	11,3
TPD52L2	O43399-3	TPD54_HUMAN Isoform 3 of Tumor protein D54	22517,1141	6,24751666	2	2	2	56	111	11,9
TPD52L2	O43399-4	TPD54_HUMAN Isoform 4 of Tumor protein D54	21449,9393	6,24751666	2	2	2	56	111	12,4
TPD52L2	O43399-2	TPD54_HUMAN Isoform 2 of Tumor protein D54	19901,1442	6,24751666	2	2	2	56	111	13,4
TPD52L2	O43399-6	TPD54_HUMAN Isoform 6 of Tumor protein D54	17473,4788	6,24751666	2	2	2	56	111	15,2
TPD52L2	A0A087WYR3	A0A087WYR3_HUMAN Tumor protein D54	23764,7645	6,24751666	2	2	2	56	111	11,2
TPD52L2	O43399	TPD54_HUMAN Tumor protein D54	22237,7278	6,24751666	2	2	2	56	111	12,1
TRA2A	Q13595-3	TRA2A_HUMAN Isoform 3 of Transformer-2 protein homolog alpha	20745,7328	7,02434163	15	11	8	92	481	55,5
TRA2A	Q13595-4	TRA2A_HUMAN Isoform 4 of Transformer-2 protein homolog alpha	20589,5453	7,02434163	15	11	8	92	481	55,8
TRA2A	Q13595	TRA2A_HUMAN Transformer-2 protein homolog alpha	32688,626	7,02434163	15	11	8	92	481	35,7
TRA2A	Q13595	TRA2A_HUMAN Transformer-2 protein homolog alpha	32688,626	5,89560719	18	10	7	83	444	28,6
WBP2	Q969T9	WBP2_HUMAN WW domain-binding protein 2	28086,9492	6,5788672	2	2	2	94	155	9,2
WBP2	K7EMC9	K7EMC9_HUMAN WW domain-binding protein 2	27550,3644	6,5788672	2	2	2	94	155	9,3
WBP2	A6NG10	A6NG10_HUMAN WW domain-binding protein 2	25807,3964	6,5788672	2	2	2	94	155	10
WBP2	K7ENL2	K7ENL2_HUMAN WW domain-binding protein 2	24710,2887	6,5788672	2	2	2	94	155	10,3
WBP2	K7EIJ0	K7EIJ0_HUMAN WW domain-binding protein 2 (Fragment)	18223,9378	6,5788672	2	2	2	94	155	14,3
WBP2	K7ESN4	K7ESN4_HUMAN WW domain-binding protein 2 (Fragment)	16142,4919	6,5788672	2	2	2	94	155	15,7
WBP2	K7EIN1	K7EIN1_HUMAN WW domain-binding protein 2 (Fragment)	11966,6327	6,5788672	2	2	2	94	155	20,9
WBSCR22	O43709	WBS22_HUMAN Probable 18S rRNA (guanine-N(7))-methyltransferase	31880,3708	6,62047973	11	7	7	75	353	34,4

Suppl. 7: Proteins which were identified in MS of the 35 kDa photo-crosslink of FKBP12^{K52pBpa} mutant after treatment with Rapamycin and UV light. Proteins identified were described with **gene name**, **protein ID** and **description**. Additionally, the molecular weight (**mw**) was indicated as well as the results of MSMS analysis represented in **ssm** (spectra mapping, assignment of protein peptides), **max score** (with mascot, the higher the more reliable), **top3** (abundance of protein in the sample, log10), and **sequence coverage** in %.

10 Abbreviations

° C	degree Celsius
(w/v)	weight per volume
(v/v)	volume per volume
Å	Ångström
A	ampere
aa	amino acid
ABC	ammonium bicarbonate
ACN	acetonitrile
AGC kinase	cAMP-dependent, cGMP-dependent and PKC (protein kinase C) kinase
Ala	Alanine (A)
Anta B	Antascomicin B
AP	Alkaline phosphatase
APS	Ammonium peroxydisulfate
approx..	approximately
Arg	Arginine (R)
Asn	Aspartate (D)
Asp	Asparagine (N)
AST	Active site titration
ATP	Adenosine-5'-triphosphate
bp	Base pair(s)
BCA	Bicinchoninic acid
BSA	Bovine serum albumin
CAA	chloroacetic acid
cm	centimetres
cm^2	square centimetres
CO_2	carbon dioxide
CV	column volume
Cys	Cysteine (C)
d	day
Da	Dalton
DMSO	dimethyl sulfoxide
DNA	deoxyribonucleic acid
dNTPs	deoxynucleotide triphosphates
dsDNA	Double stranded DNA
DTT	dithiothreitol
EC_{50}	half maximal effective concentration
e. *coli*	*Escherichia coli*
EDTA	Ethylendiamine-tetraacetic acid
e.g.,	exempli gratia
EtOH	Ethanol
FBS	Fetal bovine serum
FKBP	FK506-binding protein
FP	Fluorescence polarization
FRB	FKBP12-Rapamycin binding site of mTOR
fwd	forward
g	gram(s)
Glu	glutamate (E)
Gln	glutamine (Q)
Gly	glycine (G)
GR	glucocorticoid receptor
GST	glutathione S-transferase
h	hour(s)
HEPES	4-(2-hydroxyethyl)-1-piperazineethanesulfonic acid
His	Histidin (H)

HRP	Horseradish peroxidase
Hs	Homo sapiens
HSP70	Heat-shock protein 70
Hsp90	Heat-shock protein 90
Ile	Isoleucine (I)
IP	Immunoprecipitation
IPTG	Isopropyl-β-D-1-thiogalactopyranoside
kb	kilo base pair
K_D	dissociation constant
kDa	kilo Dalton
KO	knock-out
LB medium	Luria-Broth medium
Leu	Leucine (L)
Lys	Lysine (K)
M	molar
m^2	square meter
mA	milliampere
MCS	multiple cloning site
MeOH	methanol
Met	Methionine (M)
mg	milligrams
min	minutes
ml	millilitres
Mm	milli meter
mM	millimolar
MS	mass spectrometry
NaCl	sodium chloride
NaOH	sodium hydroxide
NC	nitrocellulose
NETN buffer	nuclear and cytoplasmatic extraction buffer
Ni-NTA	nitrilotriacetic acid
nm	nano meter
mTOR	mammalian/mechanical target of Rapamycin
µg	micrograms
µl	microlitres
µM	micromolar
µs	microseconds
OD	optical density
PAGE	polyacrylamide gel electrophoresis
PEI	polyethyleneimine
PPI	protein-protein interaction(s)
pBpa	4-*para*-benzoyl-phenylalanine
PBS	phosphate buffered saline
PCR	polymerase chain reaction
pH	potential hydrogen
Phe	Phenylalanine (F)
Pro	Proline (P)
PS	penicillin-streptomycin
pyl	pyrrolysine
rap	Rapamycin
rev	revers
RIPA	radioimmunoprecipitation assay buffer
rpm	rounds per minute
SDM	site directed mutagenesis
SDS	sodium dodecyl sulfate
sec	seconds

Ser	Serine (S)
TBS	Tris-buffered saline
TEMED	N,N,N′,N′ -Tetramethylethylenediamine
TEV	tobacco etch virus
TFA	trifluoroacetic acid
Thr	Threonine (T)
Trp	Tryptophan (W)
Tyr	Tyrosine (Y)
TUM	Technical university Munich
TUD	Technical university Darmstadt
unAA	unatural amino acid
UV	ultraviolet light
V	volt
W	watt
WT	wildtype

11 Bibliography

[1] C. Schiene-Fischer, T. Aumüller und G. Fischer, *Topics in current chemistry* **2013**, *328,* 35–67, DOI: 10.1007/128_2011_151.

[2] J. J. Siekierka, S. H. Y. Hung, M. Poe, C. S. Lin und N. H. Sigal, *Nature* **1989**, *341,* 755–757, DOI: 10.1038/341755a0.

[3] M. W. Harding, A. Galat, D. E. Uehling und S. L. Schreiber, *Nature* **1989**, *341,* 758–760, DOI: 10.1038/341758a0.

[4] G. D. van Duyne, R. F. Standaert, P. A. Karplus, S. L. Schreiber und J. Clardy, *Science (New York, N.Y.)* **1991**, *252,* 839–842, DOI: 10.1126/science.1709302.

[5] S. W. Michnick, M. K. Rosen, T. J. Wandless, M. Karplus und S. L. Schreiber, *Science (New York, N.Y.)* **1991**, *252,* 836–839, DOI: 10.1126/science.1709301.

[6] A. P. Timerman, T. Jayaraman, G. Wiederrecht, H. Onoue, A. R. Marks und S. Fleischer, *Biochemical and biophysical research communications* **1994**, *198,* 701–706, DOI: 10.1006/bbrc.1994.1101.

[7] G. Fischer, *Angewandte Chemie International Edition in English* **1994**, *33,* 1415–1436, DOI: 10.1002/anie.199414151.

[8] M. S. Weiss, A. Jabs und R. Hilgenfeld, *Nature structural biology* **1998**, *5,* 676, DOI: 10.1038/1368.

[9] W. J. Wedemeyer, E. Welker und H. A. Scheraga, *Biochemistry* **2002**, *41,* 14637–14644, DOI: 10.1021/bi020574b.

[10] S. Fischer, S. Michnick und M. Karplus, *Biochemistry* **1993**, *32,* 13830–13837, DOI: 10.1021/bi00213a011.

[11] C. B. Kang, Y. Hong, S. Dhe-Paganon und H. S. Yoon, *Neuro-Signals* **2008**, *16,* 318–325, DOI: 10.1159/000123041.

[12] A. Galat, *Current topics in medicinal chemistry* **2003**, *3,* 1315–1347, DOI: 10.2174/1568026033451862.

[13] G. M. Rubin, M. D. Yandell, J. R. Wortman, G. L. Gabor Miklos, C. R. Nelson, I. K. Hariharan, M. E. Fortini, P. W. Li, R. Apweiler, W. Fleischmann, J. M. Cherry, S. Henikoff, M. P. Skupski, S. Misra, M. Ashburner, E. Birney, M. S. Boguski, T. Brody, P. Brokstein, S. E. Celniker, S. A. Chervitz, D. Coates, A. Cravchik, A. Gabrielian, R. F. Galle, W. M. Gelbart, R. A. George, L. S. Goldstein, F. Gong, P. Guan, N. L. Harris, B. A. Hay, R. A. Hoskins, J. Li, Z. Li, R. O. Hynes, S. J. Jones, P. M. Kuehl, B. Lemaitre, J. T. Littleton, D. K. Morrison, C. Mungall, P. H. O'Farrell, O. K. Pickeral, C. Shue, L. B. Vosshall, J. Zhang, Q. Zhao, X. H. Zheng und S. Lewis, *Science (New York, N.Y.)* **2000**, *287,* 2204–2215, DOI: 10.1126/science.287.5461.2204.

[14] J. C. Ahn, D.-W. Kim, Y. N. You, M. S. Seok, J. M. Park, H. Hwang, B.-G. Kim, S. Luan, H.-S. Park und H. S. Cho, *BMC plant biology* **2010**, *10,* 253, DOI: 10.1186/1471-2229-10-253.

[15] P. J. Gollan und M. Bhave, *Plant molecular biology* **2010**, *72,* 1–16, DOI: 10.1007/s11103-009-9547-1.

[16] Mingming Tong und Yu Jiang.

[17] S. L. Rulten, R. A. Kinloch, H. Tateossian, C. Robinson, L. Gettins und J. E. Kay, *Mammalian genome : official journal of the International Mammalian Genome Society* **2006**, *17,* 322–331, DOI: 10.1007/s00335-005-0127-7.

[18] M. Shirane und K. I. Nakayama, *Nature cell biology* **2003**, *5,* 28–37, DOI: 10.1038/ncb894.

[19] C. R. Sinars, J. Cheung-Flynn, R. A. Rimerman, J. G. Scammell, D. F. Smith und J. Clardy, *Proceedings of the National Academy of Sciences of the United States of America* **2003**, *100,* 868–873, DOI: 10.1073/pnas.0231020100.

[20] E. Lam, M. Martin und G. Wiederrecht, *Gene* **1995**, *160,* 297–302, DOI: 10.1016/0378-1119(95)00216-s.

[21] B. Wu, P. Li, Y. Liu, Z. Lou, Y. Ding, C. Shu, S. Ye, M. Bartlam, B. Shen und Z. Rao, *Proceedings of the National Academy of Sciences of the United States of America* **2004**, *101,* 8348–8353, DOI: 10.1073/pnas.0305969101.

[22] B. E. Bierer, P. S. Mattila, R. F. Standaert, L. A. Herzenberg, S. J. Burakoff, G. Crabtree und S. L. Schreiber, *Proceedings of the National Academy of Sciences of the United States of America* **1990**, *87,* 9231–9235, DOI: 10.1073/pnas.87.23.9231.
[23] C. R. Kissinger, H. E. Parge, D. R. Knighton, C. T. Lewis, L. A. Pelletier, A. Tempczyk, V. J. Kalish, K. D. Tucker, R. E. Showalter, E. W. Moomaw, L. N. Gastinel, N. Habuka, X. Chen, F. Maldonado, J. E. Barker, R. Bacquet und J. E. Villafranca, *Nature* **1995**, *378,* 641–644, DOI: 10.1038/378641a0.
[24] J. P. Griffith, J. L. Kim, E. E. Kim, M. D. Sintchak, J. A. Thomson, M. J. Fitzgibbon, M. A. Fleming, P. R. Caron, K. Hsiao und M. A. Navia, *Cell* **1995**, *82,* 507–522, DOI: 10.1016/0092-8674(95)90439-5.
[25] S. L. Schreiber und G. R. Crabtree, *Immunology today* **1992**, *13,* 136–142, DOI: 10.1016/0167-5699(92)90111-J.
[26] S. L. Schreiber, *Cell* **1992**, *70,* 365–368, DOI: 10.1016/0092-8674(92)90158-9.
[27] A. B. Brillantes, K. Ondrias, A. Scott, E. Kobrinsky, E. Ondriasová, M. C. Moschella, T. Jayaraman, M. Landers, B. E. Ehrlich und A. R. Marks, *Cell* **1994**, *77,* 513–523, DOI: 10.1016/0092-8674(94)90214-3.
[28] M. Carmody, J. J. Mackrill, V. Sorrentino und C. O'Neill, *FEBS letters* **2001**, *505,* 97–102, DOI: 10.1016/s0014-5793(01)02787-9.
[29] T. Ikura und N. Ito, *Protein science : a publication of the Protein Society* **2007**, *16,* 2618–2625, DOI: 10.1110/ps.073203707.
[30] T. Jayaraman, A. M. Brillantes, A. P. Timerman, S. Fleischer, H. Erdjument-Bromage, P. Tempst und A. R. Marks, *The Journal of biological chemistry* **1992**, *267,* 9474–9477.
[31] M. Samsó, X. Shen und P. D. Allen, *Journal of molecular biology* **2006**, *356,* 917–927, DOI: 10.1016/j.jmb.2005.12.023.
[32] E. Lam, M. M. Martin, A. P. Timerman, C. Sabers, S. Fleischer, T. Lukas, R. T. Abraham, S. J. O'Keefe, E. A. O'Neill und G. J. Wiederrecht, *The Journal of biological chemistry* **1995**, *270,* 26511–26522, DOI: 10.1074/jbc.270.44.26511.
[33] H. B. Xin, K. Rogers, Y. Qi, T. Kanematsu und S. Fleischer, *The Journal of biological chemistry* **1999**, *274,* 15315–15319, DOI: 10.1074/jbc.274.22.15315.
[34] A. P. Timerman, E. Ogunbumni, E. Freund, G. Wiederrecht, A. R. Marks und S. Fleischer, *The Journal of biological chemistry* **1993**, *268,* 22992–22999.
[35] R. L. Patterson, D. Boehning und S. H. Snyder, *Annual review of biochemistry* **2004**, *73,* 437–465, DOI: 10.1146/annurev.biochem.73.071403.161303.
[36] A. M. Cameron, J. P. Steiner, D. M. Sabatini, A. I. Kaplin, L. D. Walensky und S. H. Snyder, *Proceedings of the National Academy of Sciences of the United States of America* **1995**, *92,* 1784–1788, DOI: 10.1073/pnas.92.5.1784.
[37] Y. G. Chen, F. Liu und J. Massague, *The EMBO journal* **1997**, *16,* 3866–3876, DOI: 10.1093/emboj/16.13.3866.
[38] T. Wang, P. K. Donahoe und A. S. Zervos, *Science (New York, N.Y.)* **1994**, *265,* 674–676, DOI: 10.1126/science.7518616.
[39] M. Kawabata, T. Imamura und K. Miyazono, *Cytokine & growth factor reviews* **1998**, *9,* 49–61, DOI: 10.1016/s1359-6101(97)00036-1.
[40] M. J. Macias, P. Martin-Malpartida und J. Massagué, *Trends in biochemical sciences* **2015**, *40,* 296–308, DOI: 10.1016/j.tibs.2015.03.012.
[41] C. Kawamura, M. Kizaki, K. Yamato, H. Uchida, Y. Fukuchi, Y. Hattori, T. Koseki, T. Nishihara und Y. Ikeda, *Blood* **2000**, *96,* 2005–2011.
[42] T. Holien, T. K. Våtsveen, H. Hella, C. Rampa, G. Brede, L. A. G. Grøseth, M. Rekvig, M. Børset, T. Standal, A. Waage und A. Sundan, *Leukemia* **2012**, *26,* 1073–1080, DOI: 10.1038/leu.2011.263.
[43] O. E. Olsen, K. F. Wader, K. Misund, T. K. Våtsveen, T. B. Rø, A. K. Mylin, I. Turesson, B. F. Størdal, S. H. Moen, T. Standal, A. Waage, A. Sundan und T. Holien, *Blood cancer journal* **2014**, *4,* e196, DOI: 10.1038/bcj.2014.16.

[44] T. B. Ro, R. U. Holt, A.-T. Brenne, H. Hjorth-Hansen, A. Waage, O. Hjertner, A. Sundan und M. Borset, *Oncogene* **2004**, *23,* 3024–3032, DOI: 10.1038/sj.onc.1207386.
[45] I. Quist-Løkken, C. Andersson-Rusch, M. H. Kastnes, J. M. Kolos, J. Jatzlau, H. Hella, O. E. Olsen, A. Sundan, P. Knaus, F. Hausch und T. Holien, *Cell communication and signaling : CCS* **2023**, *21,* 25, DOI: 10.1186/s12964-022-01033-9.
[46] F.-L. Liu, P.-H. Liu, H.-W. Shao und F.-L. Kung, *Biochemical and biophysical research communications* **2006**, *350,* 472–477, DOI: 10.1016/j.bbrc.2006.09.073.
[47] H. Sugata, K. Matsuo, T. Nakagawa, M. Takahashi, H. Mukai, Y. Ono, K. Maeda, H. Akiyama und T. Kawamata, *Neuroscience letters* **2009**, *459,* 96–99, DOI: 10.1016/j.neulet.2009.04.062.
[48] L. Jiang, P. Chakraborty, L. Zhang, M. Wong, S. E. Hill, C. J. Webber, J. Libera, L. J. Blair, B. Wolozin und M. Zweckstetter, *Science advances* **2023**, *9,* eadd9789, DOI: 10.1126/sciadv.add9789.
[49] K. Nakamura, A. Greenwood, L. Binder, E. H. Bigio, S. Denial, L. Nicholson, X. Z. Zhou und K. P. Lu, *Cell* **2012**, *149,* 232–244, DOI: 10.1016/j.cell.2012.02.016.
[50] C. A. Hoeffer, W. Tang, H. Wong, A. Santillan, R. J. Patterson, L. A. Martinez, M. V. Tejada-Simon, R. Paylor, S. L. Hamilton und E. Klann, *Neuron* **2008**, *60,* 832–845, DOI: 10.1016/j.neuron.2008.09.037.
[51] L. J. Blair, B. A. Nordhues, S. E. Hill, K. M. Scaglione, J. C. 3. O'Leary, S. N. Fontaine, L. Breydo, B. Zhang, P. Li, L. Wang, C. Cotman, H. L. Paulson, M. Muschol, V. N. Uversky, T. Klengel, E. B. Binder, R. Kayed, T. E. Golde, N. Berchtold und C. A. Dickey, *The Journal of clinical investigation* **2013**, *123,* 4158–4169, DOI: 10.1172/JCI69003.
[52] T. Ikura und N. Ito, *Protein engineering, design & selection : PEDS* **2013**, *26,* 539–546, DOI: 10.1093/protein/gzt033.
[53] J. 3. Koren, U. K. Jinwal, Z. Davey, J. Kiray, K. Arulselvam und C. A. Dickey, *Molecular neurobiology* **2011**, *44,* 65–70, DOI: 10.1007/s12035-011-8182-4.
[54] L. B. Shelton, J. 3. Koren und L. J. Blair, *Frontiers in neuroscience* **2017**, *11,* 724, DOI: 10.3389/fnins.2017.00724.
[55] D. F. Smith, B. A. Baggenstoss, T. N. Marion und R. A. Rimerman, *The Journal of biological chemistry* **1993**, *268,* 18365–18371.
[56] T. H. Davies, Y.-M. Ning und E. R. Sánchez, *The Journal of biological chemistry* **2002**, *277,* 4597–4600, DOI: 10.1074/jbc.C100531200.
[57] F. Pirkl und J. Buchner, *Journal of molecular biology* **2001**, *308,* 795–806, DOI: 10.1006/jmbi.2001.4595.
[58] R. L. Barent, S. C. Nair, D. C. Carr, Y. Ruan, R. A. Rimerman, J. Fulton, Y. Zhang und D. F. Smith, *Molecular endocrinology (Baltimore, Md.)* **1998**, *12,* 342–354, DOI: 10.1210/mend.12.3.0075.
[59] G. Baughman, G. J. Wiederrecht, N. F. Campbell, M. M. Martin und S. Bourgeois, *Molecular and cellular biology* **1995**, *15,* 4395–4402, DOI: 10.1128/MCB.15.8.4395.
[60] P. G. Febbo, M. Lowenberg, A. R. Thorner, M. Brown, M. Loda und T. R. Golub, *The Journal of urology* **2005**, *173,* 1772–1777, DOI: 10.1097/01.ju.0000155845.44729.ba.
[61] S. Periyasamy, T. Hinds, JR, L. Shemshedini, W. Shou und E. R. Sanchez, *Oncogene* **2010**, *29,* 1691–1701, DOI: 10.1038/onc.2009.458.
[62] L. Ni, C.-S. Yang, D. Gioeli, H. Frierson, D. O. Toft und B. M. Paschal, *Molecular and cellular biology* **2010**, *30,* 1243–1253, DOI: 10.1128/MCB.01891-08.
[63] P. D. Reynolds, Y. Ruan, D. F. Smith und J. G. Scammell, *The Journal of clinical endocrinology and metabolism* **1999**, *84,* 663–669, DOI: 10.1210/jcem.84.2.5429.
[64] J. Cheung-Flynn, V. Prapapanich, M. B. Cox, D. L. Riggs, C. Suarez-Quian und D. F. Smith, *Molecular endocrinology (Baltimore, Md.)* **2005**, *19,* 1654–1666, DOI: 10.1210/me.2005-0071.
[65] D. L. Riggs, P. J. Roberts, S. C. Chirillo, J. Cheung-Flynn, V. Prapapanich, T. Ratajczak, R. Gaber, D. Picard und D. F. Smith, *The EMBO journal* **2003**, *22,* 1158–1167, DOI: 10.1093/emboj/cdg108.
[66] Susanne Tranguch, Joyce Cheung-Flynn, Takiko Daikoku, Viravan Prapapanich, Marc B. Cox, Huirong Xie, Haibin Wang, Sanjoy K. Das, David F. Smith und Sudhansu K. Dey, *Proceedings of the National Academy of Sciences* **2005**, *102,* 14326–14331, DOI: 10.1073/pnas.0505775102.

[67] L. C. Amler, D. B. Agus, C. LeDuc, M. L. Sapinoso, W. D. Fox, S. Kern, D. Lee, V. Wang, M. Leysens, B. Higgins, J. Martin, W. Gerald, N. Dracopoli, C. Cordon-Cardo, H. I. Scher und G. M. Hampton, *Cancer research* **2000**, *60,* 6134–6141.
[68] J. A. Magee, L. Chang, G. D. Stormo und J. Milbrandt, *Endocrinology* **2006**, *147,* 590–598, DOI: 10.1210/en.2005-1001.
[69] K. Maeda, M. Habara, M. Kawaguchi, H. Matsumoto, S. Hanaki, T. Masaki, Y. Sato, H. Matsuyama, K. Kunieda, H. Nakagawa und M. Shimada, *Molecular oncology* **2022**, *16,* 940–956, DOI: 10.1002/1878-0261.13030.
[70] R. L. Barent, S. C. Nair, D. C. Carr, Y. Ruan, R. A. Rimerman, J. Fulton, Y. Zhang und D. F. Smith, *Molecular endocrinology (Baltimore, Md.)* **1998**, *12,* 342–354, DOI: 10.1210/mend.12.3.0075.
[71] J. C. Young, W. M. Obermann und F. U. Hartl, *The Journal of biological chemistry* **1998**, *273,* 18007–18010, DOI: 10.1074/jbc.273.29.18007.
[72] C. L. Storer, C. A. Dickey, M. D. Galigniana, T. Rein und M. B. Cox, *Trends in endocrinology and metabolism: TEM* **2011**, *22,* 481–490, DOI: 10.1016/j.tem.2011.08.001.
[73] A. Baischew, S. Engel, T. M. Geiger, M. C. Taubert und F. Hausch, *Journal of cellular biochemistry* **2023, DOI:** 10.1002/jcb.30384.
[74] A. Banerjee, S. Periyasamy, I. M. Wolf, T. D. Hinds, JR, W. Yong, W. Shou und E. R. Sanchez, *Biochemistry* **2008**, *47,* 10471–10480, DOI: 10.1021/bi8011862.
[75] A. M. Silverstein, M. D. Galigniana, K. C. Kanelakis, C. Radanyi, J. M. Renoir und W. B. Pratt, *The Journal of biological chemistry* **1999**, *274,* 36980–36986, DOI: 10.1074/jbc.274.52.36980.
[76] A. Bracher, C. Kozany, A. K. Thost und F. Hausch, *Acta crystallographica. Section D, Biological crystallography* **2011**, *67,* 549–559, DOI: 10.1107/S0907444911013862.
[77] W. B. Denny, D. L. Valentine, P. D. Reynolds, D. F. Smith und J. G. Scammell, *Endocrinology* **2000**, *141,* 4107–4113, DOI: 10.1210/endo.141.11.7785.
[78] E. Kirschke, D. Goswami, D. Southworth, P. R. Griffin und D. A. Agard, *Cell* **2014**, *157,* 1685–1697, DOI: 10.1016/j.cell.2014.04.038.
[79] W. B. Pratt und D. O. Toft, *Endocrine reviews* **1997**, *18,* 306–360, DOI: 10.1210/edrv.18.3.0303.
[80] H. Vermeer, B. I. Hendriks-Stegeman, D. van Suylekom, G. T. Rijkers, S. C. van Buul-Offers und M. Jansen, *Molecular and cellular endocrinology* **2004**, *218,* 49–55, DOI: 10.1016/j.mce.2003.12.011.
[81] J. Cheung und D. F. Smith, *Molecular endocrinology (Baltimore, Md.)* **2000**, *14,* 939–946, DOI: 10.1210/mend.14.7.0489.
[82] T. R. Hubler, W. B. Denny, D. L. Valentine, J. Cheung-Flynn, D. F. Smith und J. G. Scammell, *Endocrinology* **2003**, *144,* 2380–2387, DOI: 10.1210/en.2003-0092.
[83] C. M. Noddings, J. L. Johnson und D. A. Agard, *Nature Structural & Molecular Biology* **2023, DOI:** 10.1038/s41594-023-01128-y.
[84] A. Baischew, S. Engel, M. C. Taubert, T. M. Geiger und F. Hausch, *Nature Structural & Molecular Biology* **2023**, *30,* 1857–1866, DOI: 10.1038/s41594-023-01098-1.
[85] G. M. Wochnik, J. Rüegg, G. A. Abel, U. Schmidt, F. Holsboer und T. Rein, *The Journal of biological chemistry* **2005**, *280,* 4609–4616, DOI: 10.1074/jbc.M407498200.
[86] G. Baughman, G. J. Wiederrecht, F. Chang, M. M. Martin und S. Bourgeois, *Biochemical and biophysical research communications* **1997**, *232,* 437–443, DOI: 10.1006/bbrc.1997.6307.
[87] E. B. Binder, D. Salyakina, P. Lichtner, G. M. Wochnik, M. Ising, B. Pütz, S. Papiol, S. Seaman, S. Lucae, M. A. Kohli, T. Nickel, H. E. Künzel, B. Fuchs, M. Majer, A. Pfennig, N. Kern, J. Brunner, S. Modell, T. Baghai, T. Deiml, P. Zill, B. Bondy, R. Rupprecht, T. Messer, O. Köhnlein, H. Dabitz, T. Brückl, N. Müller, H. Pfister, R. Lieb, J. C. Mueller, E. Lõhmussaar, T. M. Strom, T. Bettecken, T. Meitinger, M. Uhr, T. Rein, F. Holsboer und B. Muller-Myhsok, *Nature genetics* **2004**, *36,* 1319–1325, DOI: 10.1038/ng1479.
[88] K. A. Ellsworth, I. Moon, B. W. Eckloff, B. L. Fridley, G. D. Jenkins, A. Batzler, J. M. Biernacka, R. Abo, A. Brisbin, Y. Ji, S. Hebbring, E. D. Wieben, D. A. Mrazek, R. M. Weinshilboum und L. Wang, *Pharmacogenetics and genomics* **2013**, *23,* 156–166, DOI: 10.1097/FPC.0b013e32835dc133.

[89] Y.-F. Zou, F. Wang, X.-L. Feng, W.-F. Li, J.-H. Tao, F.-M. Pan, F. Huang und H. Su, *Neuroscience letters* **2010**, *484,* 56–61, DOI: 10.1016/j.neulet.2010.08.019.
[90] G. Balsevich, A. S. Häusl, C. W. Meyer, S. Karamihalev, X. Feng, M. L. Pöhlmann, C. Dournes, A. Uribe-Marino, S. Santarelli, C. Labermaier, K. Hafner, T. Mao, M. Breitsamer, M. Theodoropoulou, C. Namendorf, M. Uhr, M. Paez-Pereda, G. Winter, F. Hausch, A. Chen, M. H. Tschöp, T. Rein, N. C. Gassen und M. V. Schmidt, *Nature communications* **2017**, *8,* 1725, DOI: 10.1038/s41467-017-01783-y.
[91] M. Maiarù, K. K. Tochiki, M. B. Cox, L. V. Annan, C. G. Bell, X. Feng, F. Hausch und S. M. Géranton, *Science translational medicine* **2016**, *8,* 325ra19, DOI: 10.1126/scitranslmed.aab3376.
[92] M. V. Schmidt, M. Paez-Pereda, F. Holsboer und F. Hausch, *ChemMedChem* **2012**, *7,* 1351–1359, DOI: 10.1002/cmdc.201200137.
[93] O'Leary, III, John C. AND Dharia, Sheetal AND Blair, Laura J. AND Brady, Sarah AND Johnson, Amelia G. AND Peters, Melinda AND Cheung-Flynn, Joyce AND Cox, Marc B. AND de Erausquin, Gabriel AND Weeber, Edwin J. AND Jinwal, Umesh K. AND Dickey, Chad A., *PloS one* **2011**, *6,* 1–9, DOI: 10.1371/journal.pone.0024840.
[94] C. Touma, N. C. Gassen, L. Herrmann, J. Cheung-Flynn, D. R. Büll, I. A. Ionescu, J.-M. Heinzmann, A. Knapman, A. Siebertz, A.-M. Depping, J. Hartmann, F. Hausch, M. V. Schmidt, F. Holsboer, M. Ising, M. B. Cox, U. Schmidt und T. Rein, *Biological psychiatry* **2011**, *70,* 928–936, DOI: 10.1016/j.biopsych.2011.07.023.
[95] Jakob Hartmann, Klaus V. Wagner, Claudia Liebl, Sebastian H. Scharf, Xiao-Dong Wang, Miriam Wolf, Felix Hausch, Theo Rein, Ulrike Schmidt, Chadi Touma, Joyce Cheung-Flynn, Marc B. Cox, David F. Smith, Florian Holsboer, Marianne B. Müller und Mathias V. Schmidt, *Neuropharmacology* **2012**, *62,* 332–339, DOI: 10.1016/j.neuropharm.2011.07.041.
[96] S. Albu, C. P. N. Romanowski, M. Letizia Curzi, V. Jakubcakova, C. Flachskamm, N. C. Gassen, J. Hartmann, M. V. Schmidt, U. Schmidt, T. Rein, F. Holsboer, F. Hausch, M. Paez-Pereda und M. Kimura, *Journal of Sleep Research* **2014**, *23,* 176–185, DOI: 10.1111/jsr.12112.
[97] L. A. Stechschulte, B. Qiu, M. Warrier, Hinds, Terry D., Jr., M. Zhang, H. Gu, Y. Xu, S. S. Khuder, L. Russo, S. M. Najjar, B. Lecka-Czernik, W. Yong und E. R. Sanchez, *Endocrinology* **2016**, *157,* 3888–3900, DOI: 10.1210/en.2015-1996.
[98] G. Baida, P. Bhalla, A. Yemelyanov, L. A. Stechschulte, W. Shou, B. Readhead, J. T. Dudley, E. R. Sánchez und I. Budunova, *Oncotarget* **2018**, *9,* 34772–34783, DOI: 10.18632/oncotarget.26194.
[99] A. Hähle, S. Merz, C. Meyners und F. Hausch, *Biomolecules* **2019**, *9, DOI:* 10.3390/biom9010035.
[100] S. Gaali, A. Kirschner, S. Cuboni, J. Hartmann, C. Kozany, G. Balsevich, C. Namendorf, P. Fernandez-Vizarra, C. Sippel, A. S. Zannas, R. Draenert, E. B. Binder, O. F. X. Almeida, G. Rühter, M. Uhr, M. V. Schmidt, C. Touma, A. Bracher und F. Hausch, *Nature chemical biology* **2015**, *11,* 33–37, DOI: 10.1038/nchembio.1699.
[101] M. L. Pöhlmann, A. S. Häusl, D. Harbich, G. Balsevich, C. Engelhardt, X. Feng, M. Breitsamer, F. Hausch, G. Winter und M. V. Schmidt, *Frontiers in behavioral neuroscience* **2018**, *12,* 262, DOI: 10.3389/fnbeh.2018.00262.
[102] G. Cildir, K. C. Low und V. Tergaonkar, *Trends in Molecular Medicine* **2016**, *22,* 414–429, DOI: 10.1016/j.molmed.2016.03.002.
[103] S. Mitchell, J. Vargas und A. Hoffmann, *WIREs Systems Biology and Medicine* **2016**, *8,* 227–241, DOI: 10.1002/wsbm.1331.
[104] Q. Zhang, M. J. Lenardo und D. Baltimore, *Cell* **2017**, *168,* 37–57, DOI: 10.1016/j.cell.2016.12.012.
[105] S. Romano, A. D'Angelillo, R. Pacelli, S. Staibano, E. de Luna, R. Bisogni, E.-L. Eskelinen, M. Mascolo, G. Calì, C. Arra und M. F. Romano, *Cell death and differentiation* **2010**, *17,* 145–157, DOI: 10.1038/cdd.2009.115.
[106] M. Kästle, B. Kistler, T. Lamla, T. Bretschneider, D. Lamb, P. Nicklin und D. Wyatt, *European journal of immunology* **2018**, *48,* 1904–1914, DOI: 10.1002/eji.201847699.
[107] K. Luo, Y. Li, Y. Yin, L. Li, C. Wu, Y. Chen, S. Nowsheen, Q. Hu, L. Zhang, Z. Lou und J. Yuan, *The EMBO journal* **2017**, *36,* 1434–1446, DOI: 10.15252/embj.201695669.

[108] H. Pei, L. Li, B. L. Fridley, G. D. Jenkins, K. R. Kalari, W. Lingle, G. Petersen, Z. Lou und L. Wang, *Cancer cell* **2009**, *16,* 259–266, DOI: 10.1016/j.ccr.2009.07.016.
[109] A.-K. Fabian, A. März, S. Neimanis, R. M. Biondi, C. Kozany und F. Hausch, *PloS one* **2013**, *8,* e57508, DOI: 10.1371/journal.pone.0057508.
[110] J. Yu, B. Qin, F. Wu, S. Qin, S. Nowsheen, S. Shan, J. Zayas, H. Pei, Z. Lou und L. Wang, *Cell reports* **2017**, *18,* 1229–1240, DOI: 10.1016/j.celrep.2017.01.009.
[111] N. C. Gassen, J. Hartmann, J. Zschocke, J. Stepan, K. Hafner, A. Zellner, T. Kirmeier, L. Kollmannsberger, K. V. Wagner, N. Dedic, G. Balsevich, J. M. Deussing, S. Kloiber, S. Lucae, F. Holsboer, M. Eder, M. Uhr, M. Ising, M. V. Schmidt und T. Rein, *PLoS medicine* **2014**, *11,* e1001755, DOI: 10.1371/journal.pmed.1001755.
[112] R. E. Handschumacher, M. W. Harding, J. Rice, R. J. Drugge und D. W. Speicher, *Science (New York, N.Y.)* **1984**, *226,* 544–547, DOI: 10.1126/science.6238408.
[113] J. F. Borel, C. Feurer, H. U. Gubler und H. Stähelin, *Agents and actions* **1976**, *6,* 468–475, DOI: 10.1007/BF01973261.
[114] J. Liu, J. D. Farmer, JR, W. S. Lane, J. Friedman, I. Weissman und S. L. Schreiber, *Cell* **1991**, *66,* 807–815, DOI: 10.1016/0092-8674(91)90124-h.
[115] Q. Huai, H.-Y. Kim, Y. Liu, Y. Zhao, A. Mondragon, J. O. Liu und H. Ke, *Proceedings of the National Academy of Sciences of the United States of America* **2002**, *99,* 12037–12042, DOI: 10.1073/pnas.192206699.
[116] T. Fehr, J. J. Sanglier, W. Schuler, L. Gschwind, M. Ponelle, W. Schilling und C. Wioland, *The Journal of antibiotics* **1996**, *49,* 230–233, DOI: 10.7164/antibiotics.49.230.
[117] Gino M. Salituro, Deborah L. Zink, Arlene Dahl, Jennifer Nielsen, Elizabeth Wu, Leeyuan Huang, Carolyn Kastner und Francis J. Dumont, *Tetrahedron Letters* **1995**, *36,* 997–1000, DOI: 10.1016/0040-4039(94)02425-B.
[118] M. Y. Summers, M. Leighton, D. Liu, K. Pong und E. I. Graziani, *The Journal of antibiotics* **2006**, *59,* 184–189, DOI: 10.1038/ja.2006.26.
[119] Satoshi Matsuda und Shigeo Koyasu, *Immunopharmacology* **2000**, *47,* 119–125, DOI: 10.1016/S0162-3109(00)00192-2.
[120] T. H. Tung, *Hand (New York, N.Y.)* **2010**, *5,* 1–8, DOI: 10.1007/s11552-009-9193-8.
[121] C. Vézina, A. Kudelski und S. N. Sehgal, *The Journal of antibiotics* **1975**, *28,* 721–726, DOI: 10.7164/antibiotics.28.721.
[122] S. N. Sehgal, H. Baker und C. Vézina, *The Journal of antibiotics* **1975**, *28,* 727–732, DOI: 10.7164/antibiotics.28.727.
[123] H. Baker, A. Sidorowicz, S. N. Sehgal und C. Vézina, *The Journal of antibiotics* **1978**, *31,* 539–545, DOI: 10.7164/antibiotics.31.539.
[124] D. P. Houchens, A. A. Ovejera, S. M. Riblet und D. E. Slagel, *European journal of cancer & clinical oncology* **1983**, *19,* 799–805, DOI: 10.1016/0277-5379(83)90012-3.
[125] R. R. Martel, J. Klicius und S. Galet, *Canadian journal of physiology and pharmacology* **1977**, *55,* 48–51, DOI: 10.1139/y77-007.
[126] L. A. Banaszynski, C. W. Liu und T. J. Wandless, *Journal of the American Chemical Society* **2005**, *127,* 4715–4721, DOI: 10.1021/ja043277y.
[127] J. Choi, J. Chen, S. L. Schreiber und J. Clardy, *Science (New York, N.Y.)* **1996**, *273,* 239–242, DOI: 10.1126/science.273.5272.239.
[128] A. M. März, A.-K. Fabian, C. Kozany, A. Bracher und F. Hausch, *Molecular and cellular biology* **2013**, *33,* 1357–1367, DOI: 10.1128/MCB.00678-12.
[129] F. Hausch, C. Kozany, M. Theodoropoulou und A.-K. Fabian, *Cell Cycle* **2013**, *12,* 2366–2370, DOI: 10.4161/cc.25508.
[130] K. H. Schreiber, S. I. Arriola Apelo, D. Yu, J. A. Brinkman, M. C. Velarde, F. A. Syed, C.-Y. Liao, E. L. Baar, K. A. Carbajal, D. S. Sherman, D. Ortiz, R. Brunauer, S. E. Yang, S. T. Tzannis, B. K. Kennedy und D. W. Lamming, *Nature communications* **2019**, *10,* 3194, DOI: 10.1038/s41467-019-11174-0.

[131] V. S. Rodrik-Outmezguine, M. Okaniwa, Z. Yao, C. J. Novotny, C. McWhirter, A. Banaji, H. Won, W. Wong, M. Berger, E. de Stanchina, D. G. Barratt, S. Cosulich, T. Klinowska, N. Rosen und K. M. Shokat, *Nature* **2016**, *534,* 272–276, DOI: 10.1038/nature17963.
[132] B. J. Lee, J. A. Boyer, G. L. Burnett, A. P. Thottumkara, N. Tibrewal, S. L. Wilson, T. Hsieh, A. Marquez, E. G. Lorenzana, J. W. Evans, L. Hulea, G. Kiss, H. Liu, D. Lee, O. Larsson, S. McLaughlan, I. Topisirovic, Z. Wang, Z. Wang, Y. Zhao, D. Wildes, J. B. Aggen, M. Singh, A. L. Gill, J. A. M. Smith und N. Rosen, *Nature chemical biology* **2021**, *17,* 1065–1074, DOI: 10.1038/s41589-021-00813-7.
[133] Z. Zhang, Q. Fan, X. Luo, K. Lou, W. A. Weiss und K. M. Shokat, *Nature* **2022**, *609,* 822–828, DOI: 10.1038/s41586-022-05213-y.
[134] Y. Ehinger, Z. Zhang, K. Phamluong, D. Soneja, K. M. Shokat und D. Ron, *Nature communications* **2021**, *12,* 4407, DOI: 10.1038/s41467-021-24567-x.
[135] Michael J. Hoy, Eunchong Park, Hyunji Lee, Won Young Lim, D. Christopher Cole, Nicholas D. DeBouver, Benjamin G. Bobay, Phillip G. Pierce, David Fox, Maria Ciofani, Praveen R. Juvvadi, William Steinbach, Jiyong Hong und Joseph Heitman, *mBio* **2022**, *13,* e01049-22, DOI: 10.1128/mbio.01049-22.
[136] T. H. Davies, Y.-M. Ning und E. R. Sánchez, *Biochemistry* **2005**, *44,* 2030–2038, DOI: 10.1021/bi048503v.
[137] J. M. Westberry, P. W. Sadosky, T. R. Hubler, K. L. Gross und J. G. Scammell, *The Journal of steroid biochemistry and molecular biology* **2006**, *100,* 34–41, DOI: 10.1016/j.jsbmb.2006.03.004.
[138] X. Zhang, A. F. Clark und T. Yorio, *Investigative ophthalmology & visual science* **2008**, *49,* 1037–1047, DOI: 10.1167/iovs.07-1279.
[139] A. M. März, A.-K. Fabian, C. Kozany, A. Bracher und F. Hausch, *Molecular and cellular biology* **2013**, *33,* 1357–1367, DOI: 10.1128/MCB.00678-12.
[140] M. He, B. Haltli, M. Summers, X. Feng und J. Hucul, *Gene* **2006**, *377,* 109–118, DOI: 10.1016/j.gene.2006.03.021.
[141] D. E. A. Brittain, C. M. Griffiths-Jones, M. R. Linder, M. D. Smith, C. McCusker, J. S. Barlow, R. Akiyama, K. Yasuda und S. V. Ley, *Angewandte Chemie (International ed. in English)* **2005**, *44,* 2732–2737, DOI: 10.1002/anie.200500174.
[142] J. M. Hutchison, A. S. Gibson, D. T. Williams und M. C. McIntosh, *Tetrahedron Letters* **2011**, *52,* 6349–6351, DOI: 10.1016/j.tetlet.2011.09.027.
[143] W. Qi und M. C. McIntosh, *Tetrahedron* **2008**, *64,* 7021–7025, DOI: 10.1016/j.tet.2008.05.070.
[144] FEHR THEODOR (CH), SANGLIER JEAN-JACQUES (CH) und SCHULER WALTER (DE), *RAPAMYCIN-LIKE MACROLIDE AND A NEW STRAIN OF STREPTOMYCES WHICH PRODUCES IT,* https://www.sumobrain.com/patents/WO1994018207A1.html, **1994**.
[145] K. P. Wilson, M. M. Yamashita, M. D. Sintchak, S. H. Rotstein, M. A. Murcko, J. Boger, J. A. Thomson, M. J. Fitzgibbon, J. R. Black und M. A. Navia, *Acta crystallographica. Section D, Biological crystallography* **1995**, *51,* 511–521, DOI: 10.1107/S0907444994014514.
[146] T. Schwecke, J. F. Aparicio, I. Molnár, A. König, L. E. Khaw, S. F. Haydock, M. Oliynyk, P. Caffrey, J. Cortés und J. B. Lester, *Proceedings of the National Academy of Sciences of the United States of America* **1995**, *92,* 7839–7843, DOI: 10.1073/pnas.92.17.7839.
[147] U. K. Shigdel, S.-J. Lee, M. E. Sowa, B. R. Bowman, K. Robison, M. Zhou, K. H. Pua, D. T. Stiles, J. A. V. Blodgett, D. W. Udwary, A. T. Rajczewski, A. S. Mann, S. Mostafavi, T. Hardy, S. Arya, Z. Weng, M. Stewart, K. Kenyon, J. P. Morgenstern, E. Pan, D. C. Gray, R. M. Pollock, A. M. Fry, R. D. Klausner, S. A. Townson und G. L. Verdine, *Proceedings of the National Academy of Sciences of the United States of America* **2020**, *117,* 17195–17203, DOI: 10.1073/pnas.2006560117.
[148] D. Kubota, K. Gocho, S. Kikuchi, K. Akeo, M. Miura, K. Yamaki, H. Takahashi und S. Kameya, *Ophthalmic genetics* **2018**, *39,* 500–507, DOI: 10.1080/13816810.2018.1466338.
[149] G. Manning, D. B. Whyte, R. Martinez, T. Hunter und S. Sudarsanam, *Science (New York, N.Y.)* **2002**, *298,* 1912–1934, DOI: 10.1126/science.1075762.
[150] Tony Hunter und Bartholomew M. Sefton, *Proceedings of the National Academy of Sciences* **1980**, *77,* 1311–1315, DOI: 10.1073/pnas.77.3.1311.

[151] H. Zhang, X. Cao, M. Tang, G. Zhong, Y. Si, H. Li, F. Zhu, Q. Liao, L. Li, J. Zhao, J. Feng, S. Li, C. Wang, M. Kaulich, F. Wang, L. Chen, L. Li, Z. Xia, T. Liang, H. Lu, X.-H. Feng und B. Zhao, *eLife* **2021**, *10, DOI:* 10.7554/eLife.64943.
[152] P. Cohen, *Nature cell biology* **2002**, *4,* E127-E130, DOI: 10.1038/ncb0502-e127.
[153] G. Manning, G. D. Plowman, T. Hunter und S. Sudarsanam, *Trends in biochemical sciences* **2002**, *27,* 514–520, DOI: 10.1016/S0968-0004(02)02179-5.
[154] S. Eid, S. Turk, A. Volkamer, F. Rippmann und S. Fulle, *BMC bioinformatics* **2017**, *18,* 16, DOI: 10.1186/s12859-016-1433-7.
[155] Daniel R. Knighton, Jianhua Zheng, Lynn F. Ten Eyck, Victor A. Ashford, Nguyen-Huu Xuong, Susan S. Taylor und Janusz M. Sowadski, *Science (New York, N.Y.)* **1991**, *253,* 407–414, DOI: 10.1126/science.1862342.
[156] G. K. Kanev, C. de Graaf, I. J. P. de Esch, R. Leurs, T. Würdinger, B. A. Westerman und A. J. Kooistra, *Trends in pharmacological sciences* **2019**, *40,* 818–832, DOI: 10.1016/j.tips.2019.09.002.
[157] C. Arter, L. Trask, S. Ward, S. Yeoh und R. Bayliss, *The Journal of biological chemistry* **2022**, *298,* 102247, DOI: 10.1016/j.jbc.2022.102247.
[158] J. A. Endicott, M. E. Noble und L. N. Johnson, *Annual review of biochemistry* **2012**, *81,* 587–613, DOI: 10.1146/annurev-biochem-052410-090317.
[159] Nicholas R. Brown, Martin E.M. Noble, Alison M. Lawrie, May C. Morris, Paul Tunnah, Gilles Divita, Louise N. Johnson und Jane A. Endicott, *Journal of Biological Chemistry* **1999**, *274,* 8746–8756, DOI: 10.1074/jbc.274.13.8746.
[160] Natalia Jura, Xuewu Zhang, NicholasÂ F. Endres, MarkusÂ A. Seeliger, Thomas Schindler und John Kuriyan, *Molecular cell* **2011**, *42,* 9–22, DOI: 10.1016/j.molcel.2011.03.004.
[161] P. D. Jeffrey, A. A. Russo, K. Polyak, E. Gibbs, J. Hurwitz, J. Massagué und N. P. Pavletich, *Nature* **1995**, *376,* 313–320, DOI: 10.1038/376313a0.
[162] B. Farrell und A. L. Breeze, *Biochemical Society Transactions* **2018**, *46,* 1753–1770, DOI: 10.1042/BST20180004.
[163] W. Yeung, Z. Ruan und N. Kannan, *IUBMB Life* **2020**, *72,* 1189–1202, DOI: 10.1002/iub.2253.
[164] Vivek Modi und Roland L. Dunbrack, *Proceedings of the National Academy of Sciences* **2019**, *116,* 6818–6827, DOI: 10.1073/pnas.1814279116.
[165] D. Essegian, R. Khurana, V. Stathias und S. C. Schürer, *Cell reports. Medicine* **2020**, *1,* 100128, DOI: 10.1016/j.xcrm.2020.100128.
[166] Alejandro E. Leroux, JÃ¶rg O. Schulze und Ricardo M. Biondi, *Seminars in cancer biology* **2018**, *48,* 1–17, DOI: 10.1016/j.semcancer.2017.05.011.
[167] R. W. Matheny und M. L. Adamo, *Experimental biology and medicine (Maywood, N.J.)* **2009**, *234,* 1264–1270, DOI: 10.3181/0904-MR-138.
[168] A. Mora, D. Komander, van Aalten, Daan M F und D. R. Alessi, *Seminars in cell & developmental biology* **2004**, *15,* 161–170, DOI: 10.1016/j.semcdb.2003.12.022.
[169] D. R. Alessi, M. Andjelkovic, B. Caudwell, P. Cron, N. Morrice, P. Cohen und B. A. Hemmings, *The EMBO journal* **1996**, *15,* 6541–6551.
[170] V. Calleja, D. Alcor, M. Laguerre, J. Park, B. Vojnovic, B. A. Hemmings, J. Downward, P. J. Parker und B. Larijani, *PLOS Biology* **2007**, *5,* e95, DOI: 10.1371/journal.pbio.0050095.
[171] R. A. Currie, K. S. Walker, A. Gray, M. Deak, A. Casamayor, C. P. Downes, P. Cohen, D. R. Alessi und J. Lucocq, *The Biochemical journal* **1999**, *337 (Pt 3),* 575–583.
[172] C. C. Milburn, M. Deak, S. M. Kelly, N. C. Price, D. R. Alessi und van Aalten, Daan M F, *The Biochemical journal* **2003**, *375,* 531–538, DOI: 10.1042/BJ20031229.
[173] D. Stokoe, L. R. Stephens, T. Copeland, P. R. Gaffney, C. B. Reese, G. F. Painter, A. B. Holmes, F. McCormick und P. T. Hawkins, *Science (New York, N.Y.)* **1997**, *277,* 567–570, DOI: 10.1126/science.277.5325.567.
[174] J. M. García-Martínez und D. R. Alessi, *The Biochemical journal* **2008**, *416,* 375–385, DOI: 10.1042/BJ20081668.
[175] D. D. Sarbassov, D. A. Guertin, S. M. Ali und D. M. Sabatini, *Science (New York, N.Y.)* **2005**, *307,* 1098–1101, DOI: 10.1126/science.1106148.
[176] B. D. Manning und A. Toker, *Cell* **2017**, *169,* 381–405, DOI: 10.1016/j.cell.2017.04.001.

[177] B. A. Hemmings und D. F. Restuccia, *Cold Spring Harbor perspectives in biology* **2012**, *4,* a011189, DOI: 10.1101/cshperspect.a011189.
[178] D. A. Altomare und J. R. Testa, *Oncogene* **2005**, *24,* 7455–7464, DOI: 10.1038/sj.onc.1209085.
[179] E. Vander Haar, S.-I. Lee, S. Bandhakavi, T. J. Griffin und D.-H. Kim, *Nature cell biology* **2007**, *9,* 316–323, DOI: 10.1038/ncb1547.
[180] S. Romano, A. D'Angelillo, S. Staibano, G. Ilardi und M. F. Romano, *Cell death & disease* **2010**, *1,* e55, DOI: 10.1038/cddis.2010.32.
[181] J. Yu, B. Qin, F. Wu, S. Qin, S. Nowsheen, S. Shan, J. Zayas, H. Pei, Z. Lou und L. Wang, *Cell reports* **2017**, *18,* 1229–1240, DOI: 10.1016/j.celrep.2017.01.009.
[182] M. Tufano, L. Marrone, C. D'Ambrosio, V. Di Giacomo, S. Urzini, Y. Xiao, M. Matuozzo, A. Scaloni, M. F. Romano und S. Romano, *Cell death & disease* **2023**, *14,* 116, DOI: 10.1038/s41419-023-05629-y.
[183] L. Carrassa und G. Damia, *Cancer Treatment Reviews* **2017**, *60,* 139–151, DOI: 10.1016/j.ctrv.2017.08.013.
[184] Y. Zhang und T. Hunter, *International journal of cancer* **2014**, *134,* 1013–1023, DOI: 10.1002/ijc.28226.
[185] C. Ronco, A. R. Martin, L. Demange und R. Benhida, *MedChemComm* **2017**, *8,* 295–319, DOI: 10.1039/c6md00439c.
[186] A. M. Weber und A. J. Ryan, *Pharmacology & therapeutics* **2015**, *149,* 124–138, DOI: 10.1016/j.pharmthera.2014.12.001.
[187] S. D. Zabludoff, C. Deng, M. R. Grondine, A. M. Sheehy, S. Ashwell, B. L. Caleb, S. Green, H. R. Haye, C. L. Horn, J. W. Janetka, D. Liu, E. Mouchet, S. Ready, J. L. Rosenthal, C. Queva, G. K. Schwartz, K. J. Taylor, A. N. Tse, G. E. Walker und A. M. White, *Molecular Cancer Therapeutics* **2008**, *7,* 2955–2966, DOI: 10.1158/1535-7163.MCT-08-0492.
[188] Fiifi Neizer-Ashun und Resham Bhattacharya, *Cancer Letters* **2021**, *497,* 202–211, DOI: 10.1016/j.canlet.2020.09.016.
[189] N. Xu, S. Libertini, Y. Zhang und D. A. Gillespie, *Biochemical and biophysical research communications* **2011**, *413,* 465–470, DOI: 10.1016/j.bbrc.2011.08.119.
[190] E. Shtivelman, J. Sussman und D. Stokoe, *Current biology : CB* **2002**, *12,* 919–924, DOI: 10.1016/s0960-9822(02)00843-6.
[191] F. W. King, J. Skeen, N. Hay und E. Shtivelman, *Cell Cycle* **2004**, *3,* 634–637.
[192] E. S. Kandel, J. Skeen, N. Majewski, A. Di Cristofano, P. P. Pandolfi, C. S. Feliciano, A. Gartel und N. Hay, *Molecular and cellular biology* **2002**, *22,* 7831–7841, DOI: 10.1128/MCB.22.22.7831-7841.2002.
[193] P. Cohen, D. Cross und P. A. Jänne, *Nature reviews. Drug discovery* **2021**, *20,* 551–569, DOI: 10.1038/s41573-021-00195-4.
[194] D. S. Krause und R. A. van Etten, *The New England journal of medicine* **2005**, *353,* 172–187, DOI: 10.1056/NEJMra044389.
[195] H. Daub, *Nature chemical biology* **2010**, *6,* 249–250, DOI: 10.1038/nchembio.336.
[196] M. A. Fabian, W. H. 3. Biggs, D. K. Treiber, C. E. Atteridge, M. D. Azimioara, M. G. Benedetti, T. A. Carter, P. Ciceri, P. T. Edeen, M. Floyd, J. M. Ford, M. Galvin, J. L. Gerlach, R. M. Grotzfeld, S. Herrgard, D. E. Insko, M. A. Insko, A. G. Lai, J.-M. Lélias, S. A. Mehta, Z. V. Milanov, A. M. Velasco, L. M. Wodicka, H. K. Patel, P. P. Zarrinkar und D. J. Lockhart, *Nature biotechnology* **2005**, *23,* 329–336, DOI: 10.1038/nbt1068.
[197] M. W. Karaman, S. Herrgard, D. K. Treiber, P. Gallant, C. E. Atteridge, B. T. Campbell, K. W. Chan, P. Ciceri, M. I. Davis, P. T. Edeen, R. Faraoni, M. Floyd, J. P. Hunt, D. J. Lockhart, Z. V. Milanov, M. J. Morrison, G. Pallares, H. K. Patel, S. Pritchard, L. M. Wodicka und P. P. Zarrinkar, *Nature biotechnology* **2008**, *26,* 127–132, DOI: 10.1038/nbt1358.
[198] M. B. Lodish, *The Journal of clinical endocrinology and metabolism* **2013**, *98,* 1333–1342, DOI: 10.1210/jc.2012-4085.
[199] M. M. Attwood, D. Fabbro, A. V. Sokolov, S. Knapp und H. B. Schiöth, *Nature Reviews Drug Discovery* **2021**, *20,* 839–861, DOI: 10.1038/s41573-021-00252-y.

[200] Li Xing, Jacquelyn Klug-Mcleod, Brajesh Rai und Elizabeth A. Lunney, *Bioorganic & Medicinal Chemistry* **2015**, *23,* 6520–6527, DOI: 10.1016/j.bmc.2015.08.006.
[201] V. Sharma und M. Gupta, *Chemical Biology & Drug Design* **2022**, *100,* 968–980, DOI: 10.1111/cbdd.14024.
[202] S. Chan, *British journal of cancer* **2004**, *91,* 1420–1424, DOI: 10.1038/sj.bjc.6602162.
[203] H. Modjtahedi, B. C. Cho, M. C. Michel und F. Solca, *Naunyn-Schmiedeberg's Archives of Pharmacology* **2014**, *387,* 505–521, DOI: 10.1007/s00210-014-0967-3.
[204] B. Anderson, P. Rosston, H. W. Ong, M. A. Hossain, Z. W. Davis-Gilbert und D. H. Drewry, *The Biochemical journal* **2023**, *480,* 1331–1363, DOI: 10.1042/BCJ20220217.
[205] C. J. Gloeckner, K. Boldt, A. Schumacher und M. Ueffing, *Methods in molecular biology (Clifton, N.J.)* **2009**, *564,* 359–372, DOI: 10.1007/978-1-60761-157-8_21.
[206] G. M. Wochnik, J. Rüegg, G. A. Abel, U. Schmidt, F. Holsboer und T. Rein, *The Journal of biological chemistry* **2005**, *280,* 4609–4616, DOI: 10.1074/jbc.M407498200.
[207] Wochnik Gabriela Monika.
[208] A.-K. Fabian.
[209] H. Pei, L. Li, B. L. Fridley, G. D. Jenkins, K. R. Kalari, W. Lingle, G. Petersen, Z. Lou und L. Wang, *Cancer cell* **2009**, *16,* 259–266, DOI: 10.1016/j.ccr.2009.07.016.
[210] Asat Baischew, *In-cell analysis of FK506 binding protein 51-glucocorticoid receptorheat shock protein 90 interaction at single residue resolution,* Darmstadt, **2023**.
[211] B. J. Peiffer, Le Qi, A. R. Ahmadi, Y. Wang, Z. Guo, H. Peng, Z. Sun und J. O. Liu, *Cell chemical biology* **2019**, *26,* 652-661.e4, DOI: 10.1016/j.chembiol.2019.01.011.
[212] O. Edelheit, A. Hanukoglu und I. Hanukoglu, *BMC biotechnology* **2009**, *9,* 61, DOI: 10.1186/1472-6750-9-61.
[213] David E. Garfin, in: *Guide to Protein Purification* (Hrsg.: Murray P. Deutscher), Academic Press, **1990,** 425–441.
[214] M. Chevallet, S. Luche und T. Rabilloud, *Nature protocols* **2006**, *1,* 1852–1858, DOI: 10.1038/nprot.2006.288.
[215] K. J. Wiechelman, R. D. Braun und J. D. Fitzpatrick, *Analytical biochemistry* **1988**, *175,* 231–237, DOI: 10.1016/0003-2697(88)90383-1.
[216] P. K. Smith, R. I. Krohn, G. T. Hermanson, A. K. Mallia, F. H. Gartner, M. D. Provenzano, E. K. Fujimoto, N. M. Goeke, B. J. Olson und D. C. Klenk, *Analytical biochemistry* **1985**, *150,* 76–85, DOI: 10.1016/0003-2697(85)90442-7.
[217] P. A. Longo, J. M. Kavran, M.-S. Kim und D. J. Leahy, *Methods in enzymology* **2013**, *529,* 227–240, DOI: 10.1016/B978-0-12-418687-3.00018-5.
[218] B. Hao, W. Gong, T. K. Ferguson, C. M. James, J. A. Krzycki und M. K. Chan, *Science (New York, N.Y.)* **2002**, *296,* 1462–1466, DOI: 10.1126/science.1069556.
[219] T. Hohsaka und M. Sisido, *Current opinion in chemical biology* **2002**, *6,* 809–815, DOI: 10.1016/s1367-5931(02)00376-9.
[220] J. M. Kavran, S. Gundllapalli, P. O'Donoghue, M. Englert, D. Söll und T. A. Steitz, *Proceedings of the National Academy of Sciences of the United States of America* **2007**, *104,* 11268–11273, DOI: 10.1073/pnas.0704769104.
[221] I. S. Farrell, R. Toroney, J. L. Hazen, R. A. Mehl und J. W. Chin, *Nature Methods* **2005**, *2,* 377–384, DOI: 10.1038/nmeth0505-377.
[222] J. W. Chin, A. B. Martin, D. S. King, L. Wang und P. G. Schultz, *Proceedings of the National Academy of Sciences of the United States of America* **2002**, *99,* 11020–11024, DOI: 10.1073/pnas.172226299.
[223] Jesper V. Olsen, Shao-En Ong und Matthias Mann, *Molecular & Cellular Proteomics* **2004**, *3,* 608–614, DOI: 10.1074/mcp.T400003-MCP200.
[224] R. E. Hubbard und M. Kamran Haider, in: *Encyclopedia of Life Sciences,* John Wiley & Sons, Ltd, **2010**.
[225] C. N. Pace, G. R. Grimsley und J. M. Scholtz, *The Journal of biological chemistry* **2009**, *284,* 13285–13289, DOI: 10.1074/jbc.R800080200.

[226] I. K. Jordan, F. A. Kondrashov, I. A. Adzhubei, Y. I. Wolf, E. V. Koonin, A. S. Kondrashov und S. Sunyaev, *Nature* **2005**, *433,* 633–638, DOI: 10.1038/nature03306.
[227] A. Bracher, C. Kozany, A. K. Thost und F. Hausch, *Acta crystallographica. Section D, Biological crystallography* **2011**, *67,* 549–559, DOI: 10.1107/S0907444911013862.
[228] J. F. Dumont, *Current Medicinal Chemistry* **2000**, *7,* 731–748, DOI: 10.2174/0929867003374723.
[229] J. Li, S. G. Kim und J. Blenis, *Cell metabolism* **2014**, *19,* 373–379, DOI: 10.1016/j.cmet.2014.01.001.
[230] P. R. Juvvadi, B. G. Bobay, S. M. C. Gobeil, D. C. Cole, R. A. Venters, J. Heitman, L. D. Spicer und W. J. Steinbach, *Biochemical and biophysical research communications* **2020**, *526,* 48–54, DOI: 10.1016/j.bbrc.2020.03.062.
[231] A. Rivera und J. Heitman, *PLoS pathogens* **2023**, *19,* e1011056, DOI: 10.1371/journal.ppat.1011056.
[232] Amber E. Kofman, Margeaux R. McGraw, and Christopher J. Payne, *AGING* **2012, DOI:** 10.18632/aging.100451.
[233] D. S. Hage und J. Cazes, *Handbook of Affinity Chromatography,* CRC Press, **2005**.
[234] S. Vunnum, G. Vedantham und B. Hubbard, in: *Process Scale Purification of Antibodies,* John Wiley & Sons, Ltd, **2017,** 113–133.
[235] M.A Firer, *Journal of Biochemical and Biophysical Methods* **2001**, *49,* 433–442, DOI: 10.1016/S0165-022X(01)00211-1.
[236] S Jones und J M Thornton, *Proceedings of the National Academy of Sciences* **1996**, *93,* 13–20, DOI: 10.1073/pnas.93.1.13.
[237] H. Garcia-Seisdedos, J. A. Villegas und E. D. Levy, *Angewandte Chemie International Edition* **2019**, *58,* 5514–5531, DOI: 10.1002/anie.201806092.
[238] M. Stefani und C. M. Dobson, *Journal of molecular medicine (Berlin, Germany)* **2003**, *81,* 678–699, DOI: 10.1007/s00109-003-0464-5.
[239] S. E. Acuner Ozbabacan, H. B. Engin, A. Gursoy und O. Keskin, *Protein engineering, design & selection : PEDS* **2011**, *24,* 635–648, DOI: 10.1093/protein/gzr025.
[240] I. M. Nooren und J. M. Thornton, *The EMBO journal* **2003**, *22,* 3486–3492, DOI: 10.1093/emboj/cdg359.
[241] J. M. Kolos, S. Pomplun, S. Jung, B. Rieß, P. L. Purder, A. M. Voll, S. Merz, M. Gnatzy, T. M. Geiger, I. Quist-Løkken, J. Jatzlau, P. Knaus, T. Holien, A. Bracher, C. Meyners, P. Czodrowski, V. Krewald und F. Hausch, *Chemical science* **2021**, *12,* 14758–14765, DOI: 10.1039/d1sc04638a.
[242] S. Pomplun, C. Sippel, A. Hähle, D. Tay, K. Shima, A. Klages, C. M. Ünal, B. Rieß, H. T. Toh, G. Hansen, H. S. Yoon, A. Bracher, P. Preiser, J. Rupp, M. Steinert und F. Hausch, *Journal of medicinal chemistry* **2018**, *61,* 3660–3673, DOI: 10.1021/acs.jmedchem.8b00137.
[243] R. C. E. Deutscher, M. Safa Karagöz, P. L. Purder, J. M. Kolos, C. Meyners, W. Oki Sugiarto, P. Krajczy, F. Tebbe, T. M. Geiger, C. Ünal, U. A. Hellmich, M. Steinert und F. Hausch, *Chembiochem : a European journal of chemical biology* **2023,** e202300442, DOI: 10.1002/cbic.202300442.
[244] Jerker Porath, *Protein Expression and Purification* **1992**, *3,* 263–281, DOI: 10.1016/1046-5928(92)90001-D.
[245] T.-T. Yip und T. W. Hutchens, *Molecular Biotechnology* **1994**, *1,* 151–164, DOI: 10.1007/BF02921556.
[246] F. H. Arnold, *Bio/Technology* **1991**, *9,* 151–156, DOI: 10.1038/nbt0291-151.
[247] A. Tjernberg, N. Markova, W. J. Griffiths und D. Hallén, *Journal of biomolecular screening* **2006**, *11,* 131–137, DOI: 10.1177/1087057105284218.
[248] M. E. Kimple, A. L. Brill und R. L. Pasker, *Current protocols in protein science* **2013**, *73,* 9.9.1-9.9.23, DOI: 10.1002/0471140864.ps0909s73.
[249] K. Charov und M. D. Burkart, *ACS infectious diseases* **2019**, *5,* 1518–1523, DOI: 10.1021/acsinfecdis.9b00150.
[250] R. L. Lundblad, *Biochemistry* **1971**, *10,* 2501–2506, DOI: 10.1021/bi00789a012.
[251] Y. Zhang, Y.-Y. Xu, W.-J. Sun, M.-H. Zhang, Y.-F. Zheng, H.-M. Shen, J. Yang und X.-Q. Zhu, *BioMed research international* **2016**, *2016,* 5013409, DOI: 10.1155/2016/5013409.

[252] R. Serfling und I. Coin, *Methods in enzymology* **2016**, *580,* 89–107, DOI: 10.1016/bs.mie.2016.05.003.
[253] J. Liu, Farmer, Jesse D., Jr., W. S. Lane, J. Friedman, I. Weissman und S. L. Schreiber, *Cell* **1991**, *66,* 807–815, DOI: 10.1016/0092-8674(91)90124-H.
[254] N. D. Pham, R. B. Parker und J. J. Kohler, *Current opinion in chemical biology* **2013**, *17,* 90–101, DOI: 10.1016/j.cbpa.2012.10.034.
[255] W. Wang, J. K. Takimoto, G. V. Louie, T. J. Baiga, J. P. Noel, K.-F. Lee, P. A. Slesinger und L. Wang, *Nature Neuroscience* **2007**, *10,* 1063–1072, DOI: 10.1038/nn1932.
[256] M. Zhang, S. Lin, X. Song, J. Liu, Y. Fu, X. Ge, X. Fu, Z. Chang und P. R. Chen, *Nature chemical biology* **2011**, *7,* 671–677, DOI: 10.1038/nchembio.644.
[257] H. Ai, W. Shen, A. Sagi, P. R. Chen und P. G. Schultz, *Chembiochem : a European journal of chemical biology* **2011**, *12,* 1854–1857, DOI: 10.1002/cbic.201100194.
[258] T. Koenig, B. H. Menze, M. Kirchner, F. Monigatti, K. C. Parker, T. Patterson, J. J. Steen, F. A. Hamprecht und H. Steen, *Journal of proteome research* **2008**, *7,* 3708–3717, DOI: 10.1021/pr700859x.
[259] B. Fabre, T. Lambour, D. Bouyssié, T. Menneteau, B. Monsarrat, O. Burlet-Schiltz und M.-P. Bousquet-Dubouch, *EuPA Open Proteomics* **2014**, *4,* 82–86, DOI: 10.1016/j.euprot.2014.06.001.
[260] J. C. Silva, M. V. Gorenstein, G.-Z. Li, J. P. Vissers und S. J. Geromanos, *Molecular & Cellular Proteomics* **2006**, *5,* 144–156, DOI: 10.1074/mcp.M500230-MCP200.
[261] Matrix science, *Mascot: The trusted reference standard for protein identification by mass spectrometry for 25 years,* https://www.matrixscience.com/.
[262] V. Modi und R. L. Dunbrack, *Scientific reports* **2019**, *9,* 19790, DOI: 10.1038/s41598-019-56499-4.
[263] R. K. Sharma, A. Chafik und G. Bertolin, *Cell death discovery* **2023**, *9,* 203, DOI: 10.1038/s41420-023-01501-2.
[264] E. Willems, M. Dedobbeleer, M. Digregorio, A. Lombard, P. N. Lumapat und B. Rogister, *Cell division* **2018**, *13,* 7, DOI: 10.1186/s13008-018-0040-6.
[265] B. Goldenson und J. D. Crispino, *Oncogene* **2015**, *34,* 537–545, DOI: 10.1038/onc.2014.14.
[266] Q. Liu, S. Guntuku, X. S. Cui, S. Matsuoka, D. Cortez, K. Tamai, G. Luo, S. Carattini-Rivera, F. DeMayo, A. Bradley, L. A. Donehower und S. J. Elledge, *Genes & development* **2000**, *14,* 1448–1459.
[267] M. Shimada, H. Niida, D. H. Zineldeen, H. Tagami, M. Tanaka, H. Saito und M. Nakanishi, *Cell* **2008**, *132,* 221–232, DOI: 10.1016/j.cell.2007.12.013.
[268] C. S. Sørensen, L. T. Hansen, J. Dziegielewski, R. G. Syljuåsen, C. Lundin, J. Bartek und T. Helleday, *Nature cell biology* **2005**, *7,* 195–201, DOI: 10.1038/ncb1212.
[269] G. Bertolin, A.-L. Bulteau, M.-C. Alves-Guerra, A. Burel, M.-T. Lavault, O. Gavard, S. Le Bras, J.-P. Gagné, G. G. Poirier, R. Le Borgne, C. Prigent und M. Tramier, *eLife* **2018**, *7, DOI:* 10.7554/eLife.38111.
[270] G. Bertolin, M.-C. Alves-Guerra, A. Cheron, A. Burel, C. Prigent, R. Le Borgne und M. Tramier, *Life science alliance* **2021**, *4, DOI:* 10.26508/lsa.202000806.
[271] A. Górska und A. J. Mazur, *Cellular and molecular life sciences : CMLS* **2022**, *79,* 100, DOI: 10.1007/s00018-021-04104-1.
[272] I. U. Ali, L. M. Schriml und M. Dean, *Journal of the National Cancer Institute* **1999**, *91,* 1922–1932, DOI: 10.1093/jnci/91.22.1922.
[273] R. Amaravadi und C. B. Thompson, *The Journal of clinical investigation* **2005**, *115,* 2618–2624, DOI: 10.1172/JCI26273.
[274] J. Chun und S. S. Kang, *Integrative Biosciences* **2005**, *9,* 161–171, DOI: 10.1080/17386357.2005.9647267.
[275] S. Persad, S. Attwell, V. Gray, N. Mawji, J. T. Deng, D. Leung, J. Yan, J. Sanghera, M. P. Walsh und S. Dedhar, *The Journal of biological chemistry* **2001**, *276,* 27462–27469, DOI: 10.1074/jbc.M102940200.
[276] I. Guerriero, G. Monaco, V. Coppola und A. Orlacchio, *Pharmaceuticals (Basel, Switzerland)* **2020**, *13, DOI:* 10.3390/ph13110413.

[277] V. Dattilo, R. Amato, N. Perrotti und M. Gennarelli, *Frontiers in genetics* **2020**, *11,* 826, DOI: 10.3389/fgene.2020.00826.
[278] S. Wang, B. Jiang, T. Zhang, L. Liu, Y. Wang, Y. Wang, X. Chen, H. Lin, L. Zhou, Y. Xia, L. Chen, C. Yang, Y. Xiong, D. Ye und K.-L. Guan, *PLOS Biology* **2015**, *13,* e1002243, DOI: 10.1371/journal.pbio.1002243.
[279] H. Hu, W. Zhu, J. Qin, M. Chen, L. Gong, L. Li, X. Liu, Y. Tao, H. Yin, H. Zhou, L. Zhou, D. Ye, Q. Ye und D. Gao, *Hepatology (Baltimore, Md.)* **2017**, *65,* 515–528, DOI: 10.1002/hep.28887.
[280] T. Zhang, Y. Wang, H. Yu, T. Zhang, L. Guo, J. Xu, X. Wei, N. Wang, Y. Wu, X. Wang und L. Huang, *Cell death & disease* **2022**, *13,* 68, DOI: 10.1038/s41419-022-04499-0.
[281] K. Zhang, L. Sun und Y. Kang, *Cell communication and signaling : CCS* **2023**, *21,* 240, DOI: 10.1186/s12964-023-01256-4.
[282] X. Zhou, W. Liu, X. Hu, A. Dorrance, R. Garzon, P. J. Houghton und C. Shen, *Scientific reports* **2017**, *7,* 1535, DOI: 10.1038/s41598-017-01729-w.
[283] M. Marchesini, Y. Ogoti, E. Fiorini, A. Aktas Samur, L. Nezi, M. D'Anca, P. Storti, M. K. Samur, I. Ganan-Gomez, M. T. Fulciniti, N. Mistry, S. Jiang, N. Bao, V. Marchica, A. Neri, C. Bueso-Ramos, C.-J. Wu, L. Zhang, H. Liang, X. Peng, N. Giuliani, G. Draetta, K. Clise-Dwyer, H. Kantarjian, N. Munshi, R. Orlowski, G. Garcia-Manero, R. A. DePinho und S. Colla, *Cancer cell* **2017**, *32,* 88-100.e6, DOI: 10.1016/j.ccell.2017.05.011.
[284] D. Chowdhury, X. Xu, X. Zhong, F. Ahmed, J. Zhong, J. Liao, D. M. Dykxhoorn, D. M. Weinstock, G. P. Pfeifer und J. Lieberman, *Molecular cell* **2008**, *31,* 33–46, DOI: 10.1016/j.molcel.2008.05.016.
[285] R. H. Oakley und J. A. Cidlowski, *The Journal of allergy and clinical immunology* **2013**, *132,* 1033–1044, DOI: 10.1016/j.jaci.2013.09.007.
[286] E. Piovan, J. Yu, V. Tosello, D. Herranz, A. Ambesi-Impiombato, A. C. Da Silva, M. Sanchez-Martin, A. Perez-Garcia, I. Rigo, M. Castillo, S. Indraccolo, J. R. Cross, E. de Stanchina, E. Paietta, J. Racevskis, J. M. Rowe, M. S. Tallman, G. Basso, J. P. Meijerink, C. Cordon-Cardo, A. Califano und A. A. Ferrando, *Cancer cell* **2013**, *24,* 766–776, DOI: 10.1016/j.ccr.2013.10.022.
[287] F. S. Oppermann, F. Gnad, J. V. Olsen, R. Hornberger, Z. Greff, G. Kéri, M. Mann und H. Daub, *Molecular & cellular proteomics : MCP* **2009**, *8,* 1751–1764, DOI: 10.1074/mcp.M800588-MCP200.
[288] Y. Miyata, *Cellular and molecular life sciences : CMLS* **2009**, *66,* 1840–1849, DOI: 10.1007/s00018-009-9152-0.
[289] M. I. Khalil und A. de Benedetti, *Cancer drug resistance (Alhambra, Calif.)* **2022**, *5,* 93–101, DOI: 10.20517/cdr.2021.109.
[290] D. Fabbro, S. W. Cowan-Jacob und H. Moebitz, *British journal of pharmacology* **2015**, *172,* 2675–2700, DOI: 10.1111/bph.13096.
[291] S. S. Taylor und A. P. Kornev, *Trends in biochemical sciences* **2011**, *36,* 65–77, DOI: 10.1016/j.tibs.2010.09.006.
[292] J. A. Adams, *Biochemistry* **2003**, *42,* 601–607, DOI: 10.1021/bi020617o.
[293] M. Huse und J. Kuriyan, *Cell* **2002**, *109,* 275–282, DOI: 10.1016/S0092-8674(02)00741-9.
[294] N. Balasuriya, M. McKenna, X. Liu, S. S. C. Li und P. O'Donoghue, *Genes* **2018**, *9, DOI:* 10.3390/genes9090450.
[295] H. Guo, M. Gao, Y. Lu, J. Liang, P. L. Lorenzi, S. Bai, D. H. Hawke, J. Li, T. Dogruluk, K. L. Scott, E. Jonasch, G. B. Mills und Z. Ding, *Oncogene* **2014**, *33,* 3463–3472, DOI: 10.1038/onc.2013.301.
[296] K. Mahajan, D. Coppola, S. Challa, B. Fang, Y. A. Chen, W. Zhu, A. S. Lopez, J. Koomen, R. W. Engelman, C. Rivera, R. S. Muraoka-Cook, J. Q. Cheng, E. Schönbrunn, S. M. Sebti, H. S. Earp und N. P. Mahajan, *PloS one* **2010**, *5,* e9646, DOI: 10.1371/journal.pone.0009646.
[297] M. Mao, X. Fang, Y. Lu, R. Lapushin, R. C. Bast, JR und G. B. Mills, *The Biochemical journal* **2000**, *352 Pt 2,* 475–482.
[298] D. J. Powell, E. Hajduch, G. Kular und H. S. Hundal, *Molecular and cellular biology* **2003**, *23,* 7794–7808, DOI: 10.1128/MCB.23.21.7794-7808.2003.
[299] J. S. Gerritsen und F. M. White, *Expert review of proteomics* **2021**, *18,* 661–674, DOI: 10.1080/14789450.2021.1976152.

[300] T. Hunter und B. M. Sefton, *Proceedings of the National Academy of Sciences of the United States of America* **1980**, *77,* 1311–1315, DOI: 10.1073/pnas.77.3.1311.
[301] E. Kretschmann, *Optics Communications* **1972**, *6,* 185–187, DOI: 10.1016/0030-4018(72)90224-6.
[302] Y. Tang, X. Zeng und J. Liang, *Journal of chemical education* **2010**, *87,* 742–746, DOI: 10.1021/ed100186y.
[303] A. Paladino, F. Marchetti, L. Ponzoni und G. Colombo, *Journal of chemical theory and computation* **2018**, *14,* 1059–1070, DOI: 10.1021/acs.jctc.7b00997.
[304] Ryan M. Drenan, Xiangyu Liu, Paula G. Bertram und X.F.Steven Zheng, *Journal of Biological Chemistry* **2004**, *279,* 772–778, DOI: 10.1074/jbc.M305912200.
[305] H. Yang, D. G. Rudge, J. D. Koos, B. Vaidialingam, H. J. Yang und N. P. Pavletich, *Nature* **2013**, *497,* 217–223, DOI: 10.1038/nature12122.
[306] N. Oshiro, K. Yoshino, S. Hidayat, C. Tokunaga, K. Hara, S. Eguchi, J. Avruch und K. Yonezawa, *Genes to cells : devoted to molecular & cellular mechanisms* **2004**, *9,* 359–366, DOI: 10.1111/j.1356-9597.2004.00727.x.
[307] G. Panasyuk, I. Nemazanyy, A. Zhyvoloup, V. Filonenko, D. Davies, M. Robson, R. Pedley, M. Waterfield und I. Gout, *The Journal of biological chemistry* **2009**, *284,* 30807–30814, DOI: 10.1074/jbc.M109.056085.
[308] W. M. Flanagan, B. Corthésy, R. J. Bram und G. R. Crabtree, *Nature* **1991**, *352,* 803–807, DOI: 10.1038/352803a0.
[309] C. Luo, K. T. Shaw, A. Raghavan, J. Aramburu, F. Garcia-Cozar, B. A. Perrino, P. G. Hogan und A. Rao, *Proceedings of the National Academy of Sciences of the United States of America* **1996**, *93,* 8907–8912, DOI: 10.1073/pnas.93.17.8907.
[310] K. Hara, Y. Maruki, X. Long, K. Yoshino, N. Oshiro, S. Hidayat, C. Tokunaga, J. Avruch und K. Yonezawa, *Cell* **2002**, *110,* 177–189, DOI: 10.1016/s0092-8674(02)00833-4.
[311] B. Schories, T. E. Nelson und D. C. Sane, *Journal of peptide science : an official publication of the European Peptide Society* **2007**, *13,* 475–480, DOI: 10.1002/psc.871.
[312] S. Chaurasia, S. Pieraccini, R. de Gonda, S. Conti und M. Sironi, *Chemical Physics Letters* **2013**, *587,* 68–74, DOI: 10.1016/j.cplett.2013.09.042.
[313] H. A. Flaxman, C.-F. Chang, H.-Y. Wu, C. H. Nakamoto und C. M. Woo, *Journal of the American Chemical Society* **2019**, *141,* 11759–11764, DOI: 10.1021/jacs.9b03764.
[314] Y. Tanaka, M. R. Bond und J. J. Kohler, *Molecular bioSystems* **2008**, *4,* 473–480, DOI: 10.1039/b803218a.
[315] A. Wittelsberger, B. E. Thomas, D. F. Mierke und M. Rosenblatt, *FEBS letters* **2006**, *580,* 1872–1876, DOI: 10.1016/j.febslet.2006.02.050.
[316] T. Yanagisawa, N. Hino, F. Iraha, T. Mukai, K. Sakamoto und S. Yokoyama, *Mol. BioSyst.* **2012**, *8,* 1131–1135, DOI: 10.1039/C2MB05321G.
[317] M. Zhang, S. Lin, X. Song, J. Liu, Y. Fu, X. Ge, X. Fu, Z. Chang und P. R. Chen, *Nature chemical biology* **2011**, *7,* 671–677, DOI: 10.1038/nchembio.644.
[318] A. Leitner, T. Walzthoeni, A. Kahraman, F. Herzog, O. Rinner, M. Beck und R. Aebersold, *Molecular & cellular proteomics : MCP* **2010**, *9,* 1634–1649, DOI: 10.1074/mcp.R000001-MCP201.
[319] H. Ai, W. Shen, A. Sagi, P. R. Chen und P. G. Schultz, *Chembiochem : a European journal of chemical biology* **2011**, *12,* 1854–1857, DOI: 10.1002/cbic.201100194.
[320] F. Beiroth, T. Koudelka, T. Overath, S. D. Knight, A. Tholey und T. K. Lindhorst, *Beilstein journal of organic chemistry* **2018**, *14,* 1890–1900, DOI: 10.3762/bjoc.14.163.
[321] B. Wiedmann, H. Sakai, T. A. Davis und M. Wiedmann, *Nature* **1994**, *370,* 434–440, DOI: 10.1038/370434a0.
[322] A.-K. Ott, L. Locher, M. Koch und E. Deuerling, *PloS one* **2015**, *10,* e0143457, DOI: 10.1371/journal.pone.0143457.
[323] K. Shen, M. Gamerdinger, R. Chan, K. Gense, E. M. Martin, N. Sachs, P. D. Knight, R. Schlömer, A. N. Calabrese, K. L. Stewart, L. Leiendecker, A. Baghel, S. E. Radford, J. Frydman und E. Deuerling, *Molecular cell* **2019**, *74,* 729-741.e7, DOI: 10.1016/j.molcel.2019.03.012.
[324] J. Xue, T. Ma und X. Zhang, *Heliyon* **2023**, *9,* e15516, DOI: 10.1016/j.heliyon.2023.e15516.

[325] L. C. Kapitein, M. A. Schlager, van der Zwan, Wouter A, P. S. Wulf, N. Keijzer und C. C. Hoogenraad, *Biophysical journal* **2010**, *99,* 2143–2152, DOI: 10.1016/j.bpj.2010.07.055.
[326] P. S. Bosch, J. Pepperl und K. Basler, *G3 (Bethesda, Md.)* **2020**, *10,* 1745–1752, DOI: 10.1534/g3.120.401055.
[327] T. Tamura, S. Tsukiji und I. Hamachi, *J. Am. Chem. Soc.* **2012**, *134,* 2216–2226, DOI: 10.1021/ja209641t.
[328] T. Mao, *Development of Novel Small-Molecule Degraders of FK506-Binding Protein 51,* UNSPECIFIED, **2020**.
[329] S. Pomplun, C. Sippel, A. Hähle, D. Tay, K. Shima, A. Klages, C. M. Ünal, B. Rieß, H. T. Toh, G. Hansen, H. S. Yoon, A. Bracher, P. Preiser, J. Rupp, M. Steinert und F. Hausch, *Journal of medicinal chemistry* **2018**, *61,* 3660–3673, DOI: 10.1021/acs.jmedchem.8b00137.
[330] J. Kolos, *Synthesis of tailor-made bicyclic [4.3.1] aza-amides,* UNSPECIFIED, **2023**.
[331] M. T. Gnatzy, T. M. Geiger, A. Kuehn, N. Gutfreund, M. Walz, J. M. Kolos und F. Hausch, *Chembiochem : a European journal of chemical biology* **2021**, *22,* 2257–2261, DOI: 10.1002/cbic.202100113.

12 Table of figures

13 List of tables

14 Acknowledgement

Foremost, I would like to thank Dr. Felix Hausch for the fantastic opportunity, to complete my PhD thesis under his supervision. The fruitful discussions in our 'Progress Reports' told me, how to analyse data critically and how I could improve ideas and hypotheses in a bigger picture. In tough times, you never forgot the overall objective and you were very patient and supportive which motivated me to move on, except any difficulties on my way to submit this PhD thesis.

I also thank Dr. Katja Schmitz as second examiner of my PhD thesis - I really like the idea being recognized as a woman with a DNA underneath her skin. I also wanted to thank Dr. Cristina Cardoso, for supporting my idea of contributing as a PhD student in the RG Hausch. I feel honoured that you are part of my examination committee!

I would like to thank Wisely Oki Sugiarto for his preparatory work of the FP assay data of FKBP's and natural products. I also thank Dr. Andreas Bracher and Dr. Andreas Voll for the preparatory work of the co-crystal structure of FKBP51 FK1 and Antascomicin B. Andi Voll and Jürgen Kolos were the first 'chemistry' people I met when I started my PhD at the RG Hausch and I still want to drink another 'Laternchen' with you guys! I still kept your Aspirin, Jürgen !

I also would like to thank all of my colleagues who I became friends with in the last 4 years. As we are all in the same boat, I am very thankful, that we all supported each other in the lab so great! ♥

Stephie was incredibly supportive in affinity chromatography as we were working on the same approach. She kept our backs free by organizing tons of lab-related stuff. I also thank Tim for many sarcastic discussions, which always cheered me up while Anna laughingly rolled her eyes. Moreover, Anna was always supportive when I was mourning after I failed another AntaB-weekly-experiment with good vibes!

I also wanted to thank Thomas and Sarah. Sarah is a 'happy' soul, which more than one time lifted my mood in a unique way. Thomas reputation, when it comes to discussions on different experiments, is outstanding. I know you miss the 'Dorf-Stories' – I should create a Blog so that both of you can stay informed – in exchange of self-brewed beer?

Next, I would like to say 'thank you sooo much!' to my 'balcony-partner' Michael. Happy that we met! I really missed you within the last months of my PhD thesis! It was always a great time during our coffee breaks, talking about 'normal life-things', your PROTAC problems or the B in AntaB. I'm 'calculating' with Weinfes.. ähh Markt (you perpetuated it in your acknowledgement!) from now on every year together with Steffen!

Steffen, we know each other since the master's genetic course, you're a hard-working person with a unique sense of humour – take it along and keeps it at you! I am sure your job at the Bundesnachrichtendienst (BND) will surpass everything!

I also would like to thank Max, of course! The Nikyu Nikyu no Mi (paw-paw-fruit - for all who do not understand) has finally pushed 'A.'s phantasy' in its paw-shaped bubble, finally storing it (hopefully) forever. I am happy that we share the same affinity for Memes – Memes can simply be used in every situation – like… sniping centrifuges and stuff… Wish you all the best, FKBP12-TwInStRePfLaG-partner!
I would like to thank my other 'biochemistry' lab mates Martha, Monika, Asat, Christian and Oki. Glad that I had so handsome colleagues as you! I also say thank you to Patrick (PPurdi), Fabi, Robin, and Charles (or Yuxin – spelled like Ju-chin) – the 'chemists'. I wish you all the best – and always joy! I had lot of fun as a member of the Hausch group – we won the Chem Cup (thanks to Trainer ~~Christian~~ Brudi) – what an honour! I enjoyed hiking and skiing (with Min and Marisol) with you in the Kleinwalsertal – I will never forget about the 'Corona-Fahrt' (where Christian and I were still negative hehe) or the summer-hiking route by Komoot (thank you Martha's App!).
I also enjoyed some Hausch SKAT Cups with Johannes, Carlo, Max, Moritz, Horst, and others, I hope I see you around in a while guys, maybe at the next Hausch SKAT Cup (made by either Horst or Moritz)?

I now have **VACANCIES** – what comes up next?

Die letzten Zeilen dieser Dr. Arbeit verfasse ich auf Deutsch. Ich möchte hiermit nämlich all den Menschen danken, die in all dieser Zeit immer an mich geglaubt und unterstützt haben. Dazu gehören vor allem meine längsten und engsten Freunde – Danke das ihr mich ertragen habt (wenn's mal wieder nicht so lief), mir immer zugehört habt und mich immer wieder aufgebaut habt! Ich weiß ich kann ein unglaublicher Dickschädel sein, wenn ich etwas will. Mein Dank geht raus an meine Großcousine Ann-Kathrin (AKK), an Julia, Steffi, Anni & Daniel, Sascha – und Michael. Michael du bist ein wahrer Freund und hast mich während unseren Nachtschichten überhaupt erst motiviert, mich einzuschreiben an der Uni! Danke auch an Meike und die vielen guten philosophischen Gespräche, ich könnte mal wieder einen pisco sour im MiPeru vertragen? 1000 Dank auch an Sha, deine ruhige Art , die Dinge zu sehen hat mir immer sehr gut getan! Das Beste kommt bekanntlich zum Schluss – meine Familie! Ich bin unglaublich dankbar Teil dieser wahnsinnigen Familie zu sein! Ganz besonders danke ich meinem Vater, der in den letzten 9 ½ (keine 10 bitte!) Jahren mich immer unterstützt hat und den ich sogar im Bereich Ökologie und Tierwelt klüger halte als mich studierte Biologin – das ist ein Fakt! Natürlich weiß ich auch jeden anderen von euch zu schätzen – aber der restliche Platz bleibt für meinen größten Fan: meine Oma Anneliese! Seit ich denken kann, hast du mich immer bei meinen Träumen unterstützt. Wenn ich mir etwas vorgenommen habe, hast du versucht – mir zu helfen, auch wenn es nur mental war. Ich bin dir unendlich dankbar, du bist der Mensch, der immer bedingungslos hinter mir gestanden hat und ich widme diese Dr. Arbeit ganz allein Dir.

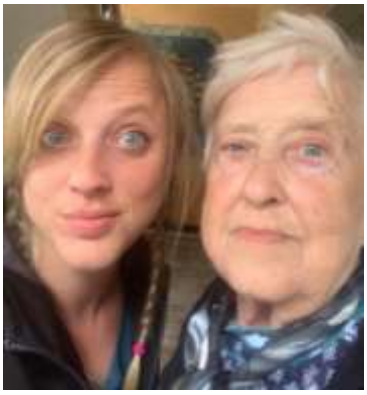

DANKE! ♥